Analytical Assessments in Support of the U.S. Fish and Wildlife Service 3-Bat Species Status Assessment

January 2022

Edited by Bethany R. Straw[1], Jaclyn A. Martin[1], Jonathan D. Reichard[2], and Brian E. Reichert[1]

Prepared in cooperation with the U.S. Geological Survey, United States Fish and Wildlife Service and Bat Conservation International

[1] U.S. Geological Survey, Fort Collins Science Center, Fort Collins, Colorado, 80526, USA
[2] U.S. Fish and Wildlife Service, Ecological Services, Hadley, Massachusetts, 01035, USA

Acknowledgments

We would like to thank Alyssa Bennett, Carl Herzog, Han Li, Joy O'Keefe, Laci Pattavina, Alex Silvis, and Adam Smith for their thoughtful and helpful feedback on earlier versions of the report. We would like to acknowledge Rich Geboy, John JaKa, Jennifer Wong and Jeremy Coleman (U.S. Fish and Wildlife Service) who helped solicit data from state managers for this report. We would also like to acknowledge Dane Smith (U.S. Geological Survey), James Cox (Contractor- U.S. Geological Survey), Ben Gotthold (U.S. Geological Survey), and all others at the North American Bat Monitoring Program (NABat) that assisted in formatting and collating data for this effort. Finally, we would like to acknowledge all the data contributors from the following agencies for their hard work in gathering and contributing these data to NABat and these analyses: Alabama Department of Conservation & Natural Resources, Alberta Environment and Parks, Arkansas Game and Fish Commission, Connecticut Department of Energy & Environmental Protection, Delaware Division of Fish & Wildlife, Florida Fish & Wildlife Conservation Commission, Georgia Department of Natural Resources, Idaho Department of Fish & Game, Illinois Department of Natural Resources, Indiana Department of Natural Resources, Iowa Department of Natural Resources, Kentucky Department of Fish & Wildlife Resources, Louisiana Department of Wildlife and Fisheries, Maine Department of Inland Fisheries & Wildlife, Maryland Department of Natural Resources, Massachusetts Division of Fisheries & Wildlife, Michigan Department of Natural Resources, Minnesota Department of Natural Resources, Mississippi Department of Wildlife, Fisheries & Parks, Missouri Department of Conservation, Montana Natural Heritage Program, New Hampshire Fish & Game, New Jersey Division of Fish and Wildlife - Endangered and Nongame Species Program, New York Department of Environmental Conservation, Newfoundland & Labrador

Department of Fisheries & Land Resources, North Carolina Wildlife Resources Commission, Ohio Department of Natural Resources, Pennsylvania Game Commission, Quebec Ministry of Forests, Wildlife & Parks, Rhode Island Division of Fish & Wildlife, Saint Mary's University, South Carolina Department of Natural Resources, Tennessee Valley Authority, Tennessee Wildlife Resources Agency, Texas Parks & Wildlife, U. S. Fish and Wildlife Service - Ozark Plateau National Wildlife Refuge, U.S. Forest Service, Vermont Fish & Wildlife Department, Virginia Department of Wildlife Resources, West Virginia Division of Natural Resources, Wisconsin Department of Natural Resources, and Wyoming Game & Fish Department. Finally, we thank the U.S. Fish and Wildlife Service Three Bat Species Status Assessment Core Team for their collaboration throughout the process. Any use of trade, firm, or product names is for descriptive purposes only and does not imply endorsement by the U.S. Government. The findings and conclusions in this article are those of the authors and do not necessarily represent the views of the U.S. Fish and Wildlife Service. Funding support provided by the U.S. Geological Survey, U.S. Fish and Wildlife Service, and Bureau of Land Management.

Table of Contents

Abbreviations

AIC	Akaike information criterion
AWS	Adult winter survival
BCI	Bat Conservation International
CCRS	Canada Centre for Remote Sensing
CI	Confidence interval
CONUS	Continental United States
DEM	Digital elevation model
DOY	Day of year
GLMM	Generalized linear mixed model
GRTS	Generalized Random-Tessellation Stratified [survey design]
ID	Identification
MYLU	*Myotis lucifugus,* little brown bat
MYSE	*Myotis septentrionalis*, northern long-eared bat
MCMC	Markov chain Monte Carlo
MDSM	Multiple detection states stie confirmation model
MW	Megawatt
NA	Not applicable
NABat	The North American Bat Monitoring Program
NE	Northeast
NREL	National Renewable Energy Laboratory
NYDEC	New York Department of Environmental Conservation
OC	Observation confirmation
Pd	Pseudogymnoascus destructans
PESU	*Perimyotis subflavus,* tricolored bat
qPCR	Quantitative polymerase chain reaction
RPU	Representation Unit
SSA	Species status assessment
SD	Standard deviation
SE	Standard error
SE	Southeast
SW	Southwest

USFWS	U.S. Fish and Wildlife Service
USGS	U.S. Geological Survey
WNS	White-nose syndrome
YSA	Years since arrival
YSD	Years since detection

Executive Summary

By Brian E. Reichert and Bethany R. Straw

Beginning in February of 2020, researchers and staff of the United States Geological Survey (USGS), Bat Conservation International (BCI), Virginia Polytechnic Institute and State University, and Montana State University associated with the North American Bat Monitoring Program (NABat) collaborated with the United States Fish and Wildlife Service (USFWS) to provide technical assistance in support of the USFWS Three Bat Species Status Assessments (SSA) including the little brown bat (MYLU, *Myotis lucifugus*), northern long-eared bat (MYSE, *Myotis septentrionalis*), and tricolored bat (PESU, *Perimyotis subflavus*). Analytical support for the SSA was not intended to provide interpretive results, which should therefore be considered beyond the scope of this report. Technical assistance for the SSA included facilitating the USFWS data call by educating and working directly with data contributors to manage, submit, and archive a variety of bat monitoring data in the online NABat database[1] using standardized data submission templates accessible through the upload features on the NABat website. Most data collected through the USFWS data call for the SSA were submitted and stored in the NABat database. These represent the efforts of hundreds of partnering organizations across more than 200 individual NABat Partner Portal Projects. A few organizations contributed data for use in these analyses that were not submitted to the NABat database. Records submitted in response to the USFWS data call included bat capture, stationary and mobile acoustic, and internal roost count data (winter and summer). Data collated in the NABat database and used for the analyses

[1] https://sciencebase.usgs.gov/nabat/#/home

described herein are documented[2] (NABat 2020a, NABat 2020b, NABat 2021) and available through the NABat third party request feature[3].

This report documents analyses conducted in support of the SSA. The analyses estimate the historical, current, and future population status and trend for each of the three species, at regional and range-wide scales. A summary of each chapter is provided below. Several chapters refer to "Representation Units" (RPU) for each species. The spatial extent of each unit was defined by the USFWS and is shown in the maps below (Figures 1-3).

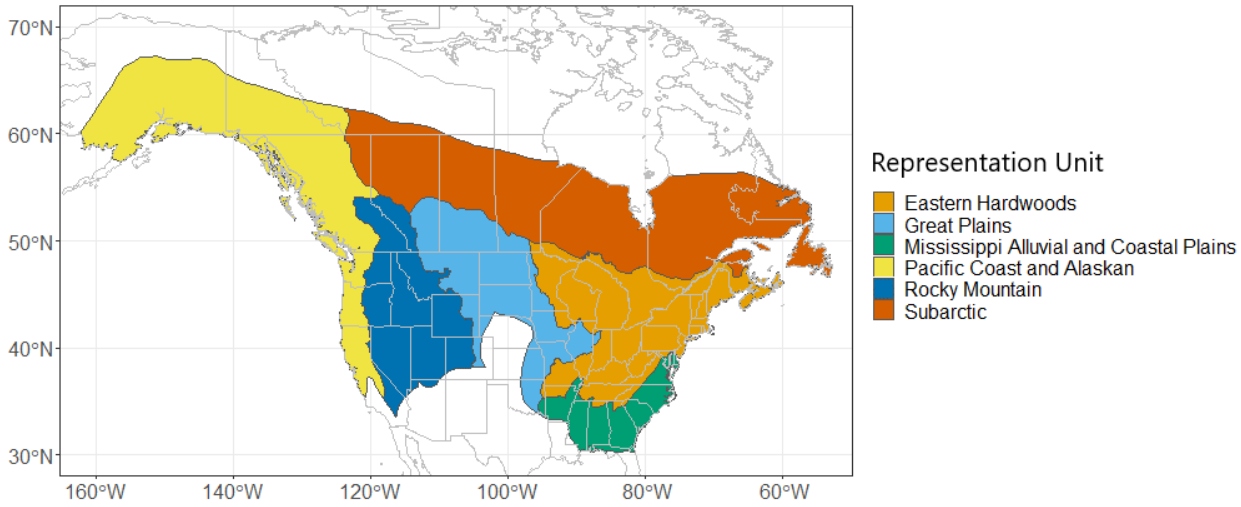

Figure 1. *Myotis lucifugus* Representation Units (RPU) as defined by the USFWS. Subarctic = RPU 1, Eastern Hardwoods = RPU 2, Mississippi Alluvial and Coastal Plains = RPU 3, Great Plains = RPU 4, Rocky Mountain = RPU 5, and Pacific Coast and Alaskan = RPU 6.

[2] https://sciencebase.usgs.gov/nabat/#/data/requests/all
[3] https://sciencebase.usgs.gov/nabat/#/data/inventory

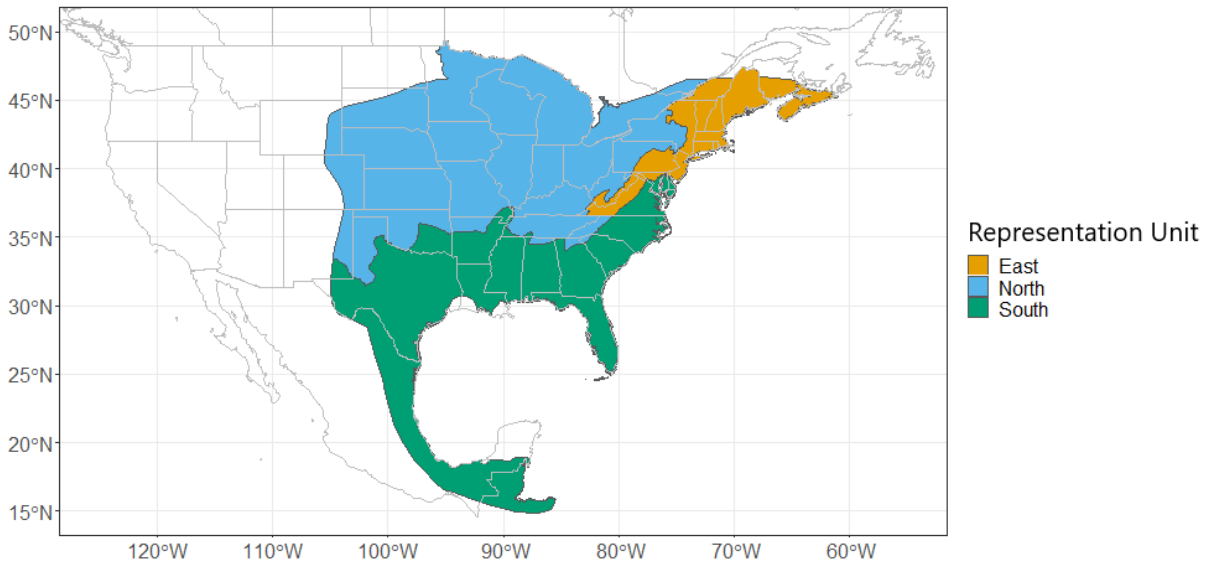

Figure 1. *Perimyotis subflavus* Representation Units (RPU) as defined by the USFWS. North = RPU 1, East = RPU 2, and South = RPU 3.

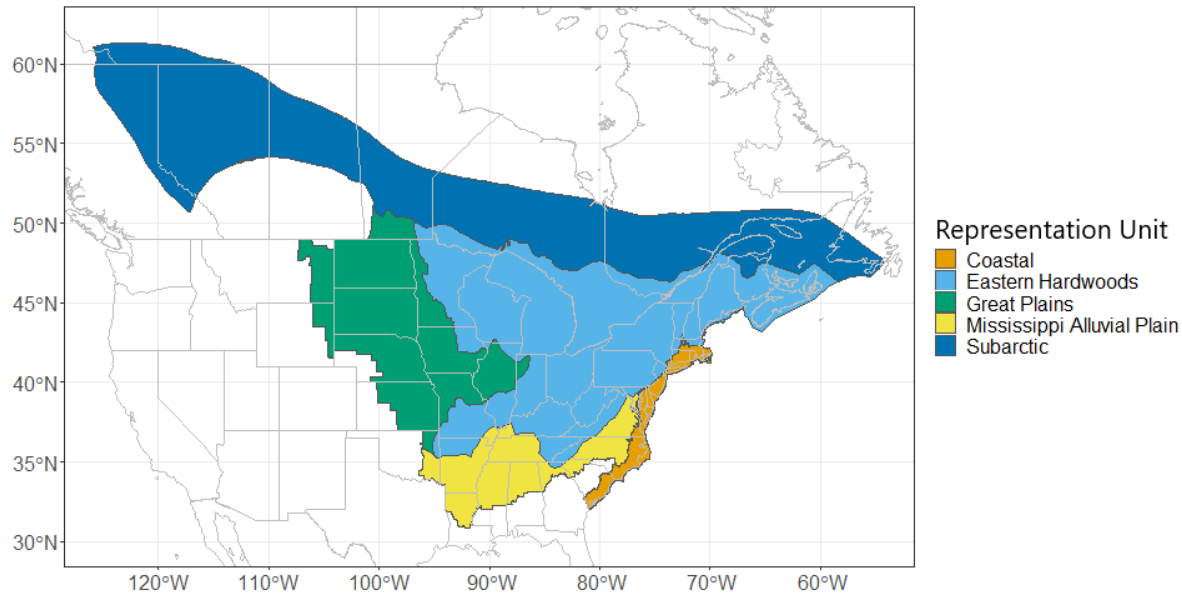

Figure 2. *Myotis septentrionalis* Representation Units (RPU) as defined by the USFWS. Mississippi Alluvial Plan = RPU 1, Eastern Hardwoods = RPU 2, Subarctic = RPU 3, Great Plains = RPU 4, and Coastal = RPU 5.

Chapter A documents analyses using capture data provided by numerous federal, state, and private industry partners and which sought to (1) evaluate population trends for each species of interest; (2) determine whether the number of reproductive females or juveniles for each species of interest has declined since the onset of white-nose syndrome (WNS); and (3) assess the body condition of each species of interest in relation to the years since the arrival of WNS. Results indicate large decreases in the overall and mean number of captures between year since arrival of WNS (YSA) and subsequent years, as well as over time. The mean captures per effort values indicate decreases in the captures of MYLU and MYSE in YSA >0 and high variation based on YSA for PESU. Median predicted rates of capture declined by roughly one half since the arrival of *Pseudogymnoascus destructans* (*P*d*)* for MYLU and MYSE and between 1999 and 2019 for PESU. Summary data indicate large declines in the number of juveniles and reproductive females captured as YSA increases and between subsequent calendar years. However, mean values were somewhat more ambiguous, due to low denominators. There appears to be a large overlap in body conditions between YSA periods, however the largest upper distributions for both mostly appear in the WNS pre-arrival period, regardless of month. Detailed analytical results and model predictions are available through a USGS data release (Deeley and Ford 2021).

Chapter B documents summertime occupancy modeling for all three bat species using automatically identified stationary acoustic calls, manually vetted stationary acoustic calls, automatically identified mobile acoustic calls, manually vetted mobile acoustic calls, and bat capture data. The objectives of the summertime occupancy modeling were to (1) estimate summertime distributions across the entire species range; and (2) provide estimates of population annual rate of change in summertime occupancy λ within RPUs. For all three species, estimated

total change in occupancy (based on sampled NABat grid cells only and model assumptions) declined between 2010 and 2019 across all RPUs with sufficient data.

Results are provided in figures within the chapter. Also provided are shapefiles describing the estimated occupancy probability with uncertainty for every NABat grid cell within each species range and an excel file describing the estimated change in occupancy (λ) with uncertainty for each geopolitical spatial subunit and RPU (provided above) for each species. Detailed analytical results and model predictions are available through a USGS data release (Irvine and Stratton 2021).

Chapter C documents the analyses of mobile acoustic data for all three species which sought to estimate changes in bat populations at four different spatial scales including (1) at locations where mobile acoustic transect sampling was conducted; (2) range-wide but bound by the spatial extent of sampling; (3) within each RPU (provided above), and (4) within each state. Categories of variables to model the count of call sequences along a transect include stressors to populations, spatial variation in activity, and sampling variation. Results show the count of call sequences of MYLU, MYSE, and PESU along mobile transects all declined steeply within 2-4 years of the predicted arrival of *Pd*. Four years after the arrival of *Pd*, decline rates for MYLU and MYSE appear shallower as the predicted number of call sequences per transect approach zero. For PESU, which has higher call sequences per transect, call sequences continue to decline each year. All species exhibited a decline in counts of call sequences with increasing wind energy risk index (a factor of the size, number, and distribution of wind energy installations, as well as species-specific flight distances). The median predicted total decline from 2009-2020 at sampled sites was 62% for MYLU, 83% for MYSE, and 50% for PESU. Across the species range, a decline of 53% is estimated for MYLU, 79% for MYSE, and 53% for PESU. Detailed

analytical results and model predictions are available through a USGS data release (Whitby et al. 2021).

Chapter D documents analysis of count surveys of wintering colonies at hibernacula for all three species which sought to provide annual estimates of the population growth rate (lambda) while taking into account impacts caused by WNS and variation occurring among sites and years. The number of winter surveys by year included in the analyses (after data filtering) varied by year, with the most amount of sampling occurring in the years following the first case of WNS in North America (after 2006), peaking around 2010/2011 for all three species and then declining again. Predicted median counts at a site indicate that populations were most likely stable prior to *Pd* arrival and declined coincident with *Pd* detection for all three species. Declines in estimated colony sizes are most evident in reference to year since *Pd* detection (YSD), but are still evident when summarized by calendar year, even though calendar years since 2007 contain a mixture of sites across the sampled range where *Pd* has and has not yet arrived. Trends in weighted lambda (lambda weighted by the count in that year) for all three species also indicate that populations declined coincident with the arrival of *Pd*. Results indicate moderate declines (36-51%) during *Pd* invasion (YSD 0-1) and increased with each additional stage of WNS progression leading to severe (95-99%) decline compared to pre-arrival of *Pd* for all three species by the endemic stage (YSD > 7). Detailed analytical results and model predictions are available through a USGS data release (Cheng et al. 2021).

Chapter E documents the modeling of population abundance into the future. A statistical analysis of winter colony count data was conducted for all three bat species, modeling population abundance over time and projecting abundance estimates into the future under several different scenarios. These models and projections serve to help characterize and understand

historical, current, and possible future population trends and the impacts of stressors on the three bat species. Datasets for each species were comprised of historical winter colony counts from 1990-2020. A variety of future projection scenarios were explored, characterizing both current and plausible future scenarios with a variety of predicted impacts of WNS and wind energy deployment, as well as baseline scenarios for comparison. Results are provided in figures within the chapter and indicate depressed populations for MYLU, MYSE and PESU through 2060, with variation among plausible scenarios, when compared to historic estimates for all three species. Based on the WNS spread models, future projections of WNS impacts indicated continued sharp declines in bat abundance as WNS reaches all known sites. All species show similar trajectories, but MYSE, which has a smaller known total abundance than MYLU and PESU, reached a total abundance of zero in the future based on our modeling assumptions. Detailed analytical results and model predictions are available through a USGS data release (Wiens et al. 2021).

References Cited

Cheng T., W. Frick, B.E. Reichert, W.E. Thogmartin, B.J. Udell, A.M. Wiens, M. Whitby, J. Reichard, and J. Szymanski. 2021. In Support of the U.S. Fish and Wildlife Service 3-Bat Species Status Assessment: Winter Colony Count Analysis. U.S. Geological Survey data release, https://doi.org/10.5066/P9YG45TG.

Deeley, S.M., and Ford, W.M., 2021, Pre- and post-White-nose Syndrome Bat Capture Models: U.S. Geological Survey data release, https://doi.org/10.5066/P9YDMOMH.

Irvine, K.M. and C. Stratton. 2021. Rangewide summertime model predictions for three bat species (*Myotis lucifugus, Myotis septentrionalis*, and *Perimyotis subflavus*) from acoustic and mist net data 2010 to 2019: US Geological Survey data release, https://doi.org/10.5066/P9XZ8D6N.

North American Bat Monitoring Program (NABat). Database v5.3.11 (Provisional Release): U.S. Geological Survey. Accessed 2020-11-18 a. NABat Request Number 10. https://doi.org/10.5066/P9UXA6CF

North American Bat Monitoring Program (NABat). Database v5.3.11 (Provisional Release): U.S. Geological Survey. Accessed 2020-11-18 b. NABat Request Number 11. https://doi.org/10.5066/P9UXA6CF

North American Bat Monitoring Program (NABat). Database v6.0.12 (Provisional Release): U.S. Geological Survey. Accessed 2021-02-10. NABat Request Number 12. https://doi.org/10.5066/P9UXA6CF.

Whitby, M., B. Udell, A. Wiens, T. Cheng, W. Frick, B.E. Reichert, and J. Reichard. 2021. In Support of the USFWS 3-Species Status Assessment: Summer Mobile Acoustic Transect Analysis. U.S. Geological Survey data release. https://doi.org/10.5066/P9W9OZU0.

Wiens, A., J. Szymanski, and W.E. Thogmartin. 2021. In Support of the U.S. Fish and Wildlife Service 3-Bat Species Status Assessment: Future Projections of Known North American Bat Populations for 3 Species (2020-2060), Processed from NABat Database Winter Colony Counts from 1990-2020, https://doi.org/10.5066/P9NDMY47.

Chapter A. Summary Assessment of USFWS Capture Data for Little Brown, Northern Long-eared and Tricolored Bat Species Status Assessment

By Sabrina Deeley[1], and Mark Ford[2]

Introduction

White-nose syndrome (WNS) is a fungal disease that, at the time these analyses were conducted, had spread to 35 U.S. states and 7 Canadian provinces (U.S. Fish and Wildlife Service 2019). Substantial little brown bat (*Myotis lucifugus*; MYLU), northern long-eared bat (*Myotis septentrionalis*; MYSE), and tricolored bat (*Perimyotis subflavus*; PESU) population decreases have been observed within affected areas since its onset in upstate New York (Ingersoll et al. 2013, Pettit and O'Keefe 2017). Morbidity and mortality impacts are multi-faceted but mostly attributable to depletion of fat reserves stemming from increased arousals and/or dehydration during hibernation along with exposure and/or predation for individuals leaving hibernacula during the winter period (Reeder et al. 2012).

Poor body condition, such as that caused by WNS (Reeder et al. 2012) in female bats may lead to lower reproductive success (Kunz et al. 1998). Regions impacted by WNS have seen declines in the numbers and proportions of reproductive females and juveniles (Francl et al. 2012, Reynolds et al. 2016, Pettit and O'Keefe 2017). Because warmer summer day-roosts allow for faster gestation lengths and juvenile development (Altringham 2011), bats born in more northern latitudes later in the summer may be less likely to survive (Frick et al. 2010). The relationships between summer body condition and populations in WNS-impacted areas are

[1] Department of Fish and Wildlife Conservation, Virginia Polytechnic Institute and State University, Blacksburg, VA 24061
[2] U.S. Geological Survey, Virginia Cooperative Fish and Wildlife Research Unit, Blacksburg, VA 24061

unclear; however, higher winter body fat can increase overwinter survival of WNS (Cheng et al. 2019), as was possibly observed in Kentucky where some WNS-impacted species showed higher body condition metrics than before the onset of WNS (Lacki et al. 2015).

Objectives

1. *Evaluate population trends for each species of interest.* White-nose syndrome impacts have increased the amount of effort required to capture some impacted species, thereby increasing the amount of effort required to detect presence (U.S. Fish and Wildlife Service 2020). Therefore, as the number of years after the onset of WNS increases, we expect that our ability to detect species, even in areas where still present in low numbers, will continue to decrease with active (mist-netting) sampling.
2. *Determine whether the number of reproductive females or juveniles for each species of interest have declined since WNS onset*. If maternity colonies are failing due to population decreases or other WNS impacts, we predict decreases in the numbers of juveniles and reproductive females, especially lactating females.
3. *Assess how years since WNS has impacted the body condition of each species of interest.* It is unknown whether WNS impacts have resulted in large-scale, measurable changes to bat body condition (as a potential surrogate for health).

Methods

Datasets

Capture data were provided by numerous federal, state, and private industry partners. Some data included detailed information about each bat captured (species, age class, sex, location, and capture time) whereas others provided a number per summer, month, or day. Data were collected through a range of methods: mist-netting and harp-trapping of free-flying bats, and mist-netting/harp-trapping maternity colonies.

Additionally, many organizations provided information only for the species of interest. The result is a USFWS-provided dataset with presence data based on the three species of interest. Some absences could be created from site-nights where not all three species were captured, though these absent data would be biased as they exist only due to the presence of other species of interest.

Capture effort (net placement and the number of nets deployed) can greatly impact capture success (U.S. Fish and Wildlife Service 2020). However, within-night catch per unit effort is inconsistently described (e.g., number of net locations and net width and height). Accordingly, inference from analyses should be viewed cautiously. Moreover, a subset of data with historic records (e.g., West Virginia) could not be associated with NABat grid cell identification and/or county information thereby limiting their utility.

To prepare these data, we reviewed comments with the records, removing any data where positive species identifications were in question. We removed instances where comments indicated uncertainty in bat identification. We removed bats that were marked as “escaped from net,” or as “escaped” but had less than one measurement.

We created unique netting events (site-night) from the data provided between May and August 1999-2019. Netting events that contained the results from several nights were excluded when nightly effort was not provided. For each netting event (site-night), we calculated the number of bats of each species that were captured. For each netting event with effort data, we calculated the number of bats of each species per unit effort ([captures per event]/[number of nets]).

We also calculated the number of pregnant, lactating, and juvenile bats of each species captured for each species of interest (e.g. [female captures per event]/[number of nets]). The pregnant and lactating dataset only included site-night events when adult females were documented, to exclude data where sex was not recorded or where only males or juveniles were captured. Similarly, we only included juvenile sampling events where age class data were included.

To assess whether WNS has impacted the body condition of bats, we calculated a body condition metric (weight/forearm) for each adult bat (Pearce et al. 2008). For forearm analysis, we only included adult bats whose forearm measurements fell within USFWS standards, and we only included body condition data where both a bat's forearm and weight fell within USFWS standards. Therefore, we restricted observations to those that were within 3 SD of the mean measurements currently in the USFWS database, to exclude likely-erroneous records.

Covariates

Annual temperature, mean elevation, and annual temperature range were provided by U.S. Geological Survey (2020) at the NABat grid cell level. USFWS Representation Unit (RPU) data were provided by the USFWS (see Executive Summary). Year since arrival (YSA) of

WNS values were based on the year of WNS arrival at the NABat grid cell level as reported/estimated by Wiens et al. (2021). Year of arrival values were rounded down (e.g., 2017.6 became 2017) and subtracted from the sample year to create the YSA used for our analysis. All negative YSA values became 0 YSA. We then created YSA categories, similar to Langwig et. al (2015): Pre-arrival YSA <0, Invasion YSA = 1, Epidemic YSA = 2 – 4, and Established YSA ≥ 5).

We associated RPU and YSA values with each grid cell, or county if grid identification was unavailable, using R package sf (Pebesma 2018). If a cell overlapped two RPU's, it was included in both.

Summary statistics

We calculated the number, mean and standard deviation of the number of captures per sample event, captures by effort, pregnant females per sample event, lactating females per sample event, juveniles per sample event, individual adult forearm measurements, individual adult mass measurements, and individual male adult body condition. These metrics were calculated for each YSA, year of capture, and USFWS Unit. In cases where month would influence the results (e.g., female reproduction, juveniles, and body condition), we also calculated these values based on month for each RPU.

Generalized linear mixed models

We developed negative binomial generalized linear mixed models (GLMMs) to assess changes in effort-adjusted bat capture numbers for each category of interest relative to various predictor variables of interest. We fit all models in R using package glmmTMB (Magnusson et al. 2020, R Core Team 2020). Only datasets with at least 20 samples, 3 years total, and 3 years

since arrival of WNS were modeled. Due to USFWS' primary focus of whether populations have changed over time or since WNS, all models included either YSA or sample year, except the null models. We also included models with up to two YSA or year inflection points. Since sample year was correlated with YSA, models did not include both covariates.

To account for the large numbers of zero responses in the juvenile models, juvenile-specific models included a zero-inflation parameter. We compared models using Akaike information criterion (AIC) values < 5 to evaluate each model set and then used DHARMa in Program R to evaluate the selected model for distribution, dispersion, outliers, and residuals (Florian 2020). When these results were comparable, we selected the most parsimonious model. Statistical significance was set to $p < 0.05$. All models used appropriately scaled and centered covariates.

We conducted two sets of GLMM analyses: one with the entire region of interest, and the other within the discrete USFWS Units. Models based on the entire region only included sampling events with grid cell identifications and covariates provided by USGS. These analyses included month, year, YSA, mean annual temperature, mean elevation, and annual temperature range. We included states and grid cell as random grouping effects.

Representation Unit models included all samples within the RPU range except where sampling events did not include a pregnant, lactating, or juvenile (as appropriate) that occurred prior to the first species of interest being observed in any year. For USFWS Unit analyses, we included as much data as possible, but consequentially had to omit location-specific covariates such as mean annual temperature, mean elevation, and annual temperature range covariates. Additionally, with the assumption that day of year may be more impactful on the fine scale (versus month), Unit models for juveniles included day of year as a covariate.

Kruskal-Wallis

To determine whether statistically significant changes ($p < 0.05$) to forearm length or body condition occurred between different YSA categories, we conducted Kruskal-Wallis tests followed by a pairwise Wilcoxon test with Bonferroni adjustment in Program R (Wilcoxon 1945, Kruskal and Wallis 1952, R Core Team 2020). We conducted these body condition analyses for each month. As various environmental characteristics may impact weight (timing of pregnancy by latitude or elevation and/or environmental productivity, i.e., prey abundance), we also analyzed the results on the state level to provide a partial control. We selected June for these additional analyses based on the timing of lactating female and juvenile bats within the dataset. For a state's Kruskal-Wallis analysis, we selected samples from June and when the state had at least 3 YSA categories and 100 samples. Significance discussed was $p < 0.05$. Additionally, we conducted these tests for all adult males for each month.

Results

Results from the analyses describe herein are available through a USGS data release (Deeley and Ford 2021) and summarized below. Summary statistics are published and available on Dryad (Deeley and Ford 2022).

Objective 1

Between 1999 and 2019, 40,520 MYLU in 7,179 sampling events, 42,955 MYSE in 9,885 sampling events, and 10,489 PESU in 3,290 sampling events were reported. Several USFWS Units had sparse data, especially in later YSA. We calculated 2,713 netting events with effort (number of nets) values (MYLU = 1,105; MYSE= 1,572; PESU = 736).

There were large decreases in the overall number and mean number of captures between YSA 0 and subsequent years, as well as over time (whether YSAs or years) (Deeley and Ford 2022). Some later YSAs had increases in captures and means based on a few samples with large numbers of captures, which is reflected in the large standard deviations for those YSAs/years. These patterns of decline were reflected within the USFWS Units. The mean captures per effort values indicate decreases in the captures of MYLU and MYSE in YSA >0 and high variation based on YSA for PESU (Deeley and Ford 2022).

Regional generalized linear mixed models

Sample year or YSA were significant in all models and indicate declines for all species. Sparse data in later years/YSAs or factors we did not account for may have led to models exhibiting high residuals, or unmodeled heterogeneity (Deeley and Ford 2022). The MYLU model contained 5,911 samples. The most parsimonious model within the model set for MYLU included a quadratic YSA, and random intercepts for state and grid cell GRTS number (Tables A1 and A2, Figure A1). This model explained approximately 40% of deviance, but we note that there were statistically significant outliers and Kolmogorov-Smirnov metrics.

The MYSE model contained 7,793 samples. The most parsimonious model within the model set included a quadratic YSA, annual temperature range, month, and state and grid cell (Tables A1 and A3, Figure A2). Approximately 39% of deviance was explained, but we note that there were statistically significant outliers and Kolmogorov-Smirnov metrics, and overdispersion. Most outliers were from West Virginia and Pennsylvania, and all instances with multiple captures (>15) within one netting event.

The PESU model contained 2,225 samples. The most parsimonious model within the model set included year, annual mean temperature, state and GRTS cell (Tables A1 and A4,

Figure A3). Approximately 43% of deviance was explained, but we note that there were statistically significant outliers, Kolmogorov-Smirnov metrics and overdispersion. Most outliers were from August (n =15) and May (n = 8) within (in descending order of importance) Pennsylvania, Virginia, Georgia, Kentucky, Maryland, North Carolina, and West Virginia. All instances had multiple captures (>9) within one netting event.

Representation Unit Model Results - MYLU

The MYLU RPU 2 model contained 6,683 samples. The most parsimonious model within the model set included quadratic year, month, and state (Tables A5 and A6, Figure A4). Approximately 43% of deviance was explained, but we note a statistically significant Kolmogorov-Smirnov metric.

The MYLU RPU 3 model contained 107 samples. The most parsimonious model within the model set quadratic year and state (Tables A5 and A7, Figure A4). Approximately 54% of deviance was explained, but we note that there were significant quantile deviations.

The MYLU RPU 4 model contained 194 samples. The most parsimonious model within the model set included quadratic YSA (Tables A5 and A8, Figure A4). Approximately 49% of deviance was explained, but we note a significant Kolmogorov-Smirnov metric and overdispersion.

The MYLU RPU 5 model contained 231 samples, but only had two YSAs. Therefore, we did not run the YSA models. However, we ran models with year, and the most parsimonious model within the model set included quadratic year, month, and state, though year was not significant (Tables A5 and A9, Figure A4). Approximately 51% of deviance was explained, but we note that there were significant Kolmogorov-Smirnov metric and quantile deviations.

Representation Unit Model Results - MYSE

The MYSE RPU 1 model contained 235 samples. The most parsimonious model within the model set for MYSE included quadratic year term (Tables A10 and A11, Figure A5). Approximately 48% of deviance was explained, but we note a significant Kolmogorov-Smirnov metric, quantile deviation and overdispersion.

The MYSE RPU 2 model contained 9,465 samples. The most parsimonious model within the model set for MYSE included quadratic year term and state (Tables A10 and A12, Figure A5). Approximately 45% of deviance was explained, but we note a significant Kolmogorov-Smirnov metric, overdispersion, and outliers. Most outliers were from West Virginia and were all instances with multiple captures (>9) within one netting event.

The MYSE RPU 4 model contained 74 samples. The most parsimonious model within the model set for MYSE included quadratic year, and state (Table A10 and A13, Figure A5). Approximately 66% of deviance was explained, but we note a significant Kolmogorov-Smirnov metric and quantile deviation.

The MYSE RPU 5 model contained 211 samples. The most parsimonious model within the model set for MYSE included quadratic year and month (Table A10 and A14, Figure A5). 47% of deviance was explained, but we note that it was overdispersed and there was significant Kolmogorov-Smirnov metric, overdispersion and quantile deviation.

Representation Unit Model Results - PESU

The PESU RPU 1 model contained 2,420 samples. The most parsimonious model within the model set included quadratic year, month, and state (Tables A15 and A16, Figure A6). Approximately 44% of deviance was explained, but we note that it was overdispersed and there

were significant outliers, Kolmogorov-Smirnov metric, and quantile deviations. Outliers were events with high numbers of (captures ≥ 24) and primarily from West Virginia and YSA = 0.

The PESU RPU 2 model contained 1,322 samples. The most parsimonious model within the model set included a quadratic year, month, and state (Tables A15 and A17, Figure A6). 47% of deviance was explained, but we note that there were there were significant outliers, Kolmogorov-Smirnov metric, overdispersion, and quantile deviations. Outliers were events with high numbers of (captures ≥ 16) and primarily from West Virginia.

The PESU RPU 3 model contained 491 samples. The most parsimonious model within the model set included quadratic year (Tables A15 and A18, Figure A6). Forty-nine percent (49%) of deviance was explained, but we note that it was overdispersed and there were significant outliers, Kolmogorov-Smirnov metric, overdispersion, and quantile deviations. All three outliers were events with high numbers of (captures ≥ 16) and all were from before WNS arrival.

Objective 2

Between 1999 and 2019, we documented 6,236 juvenile MYLU in 6,961 sampling events and 3,527 pregnant and 4,468 lactating MYLU in 3,790 events. We documented 5,645 juvenile MYSE in 9,649 sampling events and 5,225 pregnant and 5,853 lactating MYSE in 5,549 events. We documented 1,537 juvenile PESU in 2,975 sampling events and 469 pregnant and 484 lactating PESU in 979 events. Summary data indicate large declines in the number of juveniles and reproductive females based on YSA and year. However, mean values were somewhat more ambiguous, due to low denominators.

Regional Model Results

Zero inflation was an issue for both the MYSE and PESU regional models, therefore we used zero-inflation models for both these species' model sets, which slightly improved zero inflation. Sample year or YSA were significant in many, but not all, juvenile models. A sparsity of data in later years/YSAs or of factors such as variable capture effort which we did not account for with covariates, may have led to models suffering from high residuals and outliers.

The MYLU juvenile model contained 5,734 samples. The most parsimonious model within the model set included YSA, month, elevation, state, and grid cell (Table A19 and A20, Figure A7). Approximately 31% of deviance was explained, but we note a significant Kolmogorov-Smirnov metric.

The MYSE juvenile model contained 7,608 samples. The most parsimonious model within the model set included quadratic YSA, month, mean temperature, and grid cell (Tables A19 and A20, Figure A8). Approximately 30% of deviance was explained, but we note a significant Kolmogorov-Smirnov metric.

The PESU juvenile model contained 1,946 samples. The most parsimonious model within the model set included YSA, month, mean annual temperature, and grid cell, though YSA was not significant (Tables A19 and A22, Figure A9). Approximately 30% of deviance was explained, but we note that there were significant quantile deviations.

Representation Unit Model Results - MYLU

The MYLU RPU 2 juvenile model contained 6,473 samples. The most parsimonious model within the model set included a quadratic YSA, day of year, and state (Tables A23 and

A24, Figure A10). Approximately 30% of deviance was explained, but we note a significant Kolmogorov-Smirnov metric.

The MYLU RPU 3 juvenile model contained 81 samples. The most parsimonious model within the model set included quadratic YSA and state (Tables A23 and A25, Figure A10). Approximately 56% of deviance was explained.

The MYLU RPU 4 juvenile model contained 183 samples but did not have at least 3 YSAs. The most parsimonious model within the model set included quadratic year, month, and state (Tables 23 and 26, Figure 10). Approximately 39% of deviance was explained, but we note that there were significant quantile deviations.

The MYLU RPU 5 juvenile model contained 194 samples but did not have at least 3 YSAs. However, we ran models with year, and found the most parsimonious model within the model set was the null model (Tables A23). However, we are displaying the most parsimonious year model (Table A27 and Figure A10). Approximately 53% of deviance was explained.

Representation Unit Model Results - MYSE

The MYSE RPU 1 juvenile model contained 161 samples. The most parsimonious model within the model set included year and month, however year was not significant (Tables A28 and A29, Figure A11). Approximately 34% of deviance was explained.

The MYSE RPU 2 juvenile model contained 9,248 samples. The most parsimonious model within the model set included quadratic YSA, day of year and state (Tables A28 and A30, Figure A11). Approximately 29% of deviance was explained and there were quantile deviations.

The MYSE RPU 4 juvenile model contained 74 samples. The most parsimonious model within the model set including a quadratic year, day of month and state (Tables A28 and A32, Figure A11). Approximately 43% of deviance was explained, but we note a quantile deviation.

The MYSE RPU 5 juvenile model contained 204 samples. The most parsimonious model within the model set included YSA, day of year, and state but YSA was not significant (Tables A28 and A31, Figure A11). Approximately 37% of deviance was explained, but we note quantile deviation.

Representation Unit Model Results - PESU

The PESU RPU 1 juvenile model contained 2,104 samples. The most parsimonious model within the model set included quadratic YSA, day of year, and state (Tables A33 and A34, Figure A12). Approximately 34% of deviance was explained, but we note that there were significant outliers and was over dispersed. The 8 outliers were from pre-WNS West Virginia, Kentucky, and North Carolina with number of juveniles ≥ 4.

The PESU RPU 2 juvenile model contained 1,159 samples. The most parsimonious model within the model set included YSA and day of year (Tables A33 and A35, Figure A12). Approximately 35% of deviance was explained, but we note that there were significant outliers. The 4 outliers were from pre-WNS West Virginia with number of juveniles ≥ 6.

The PESU RPU 3 juvenile model contained 233 samples. The most parsimonious model within the model set included YSA, day of year, and state, though YSA was not significant (Tables A33 and A36, Figure A12). Approximately 45% of deviance was explained, but we note that there were significant quantile deviations.

Results Objective 3

From 1999 to 2019, 17,904 MYLU; 24,736 MYSE, and 5,877 PESU had forearm measurements falling within the USFWS standards, and 17,493 MYLU; 24,287 MYSE; and 5,803 PESU had appropriate body condition samples. For the month of June, we had 163 MYLU samples from New Jersey; 385 samples in Vermont; 4,033 samples from West Virginia, and 234 samples from Wisconsin. West Virginia was the only state with enough samples for the Kruskal-Wallis for the other two species (MYSE = 10,712 and PESU = 1,677). We had 7,503 adult male MYLU samples (June = 2,709; July = 2,967; August = 1,827), 10,319 adults male MYSE samples (June = 5,273; July = 3,458; August = 1,588), and 4,161 adult male PESU samples (June = 1,712; July = 1,525; August = 924).

Kruskal-Wallis tests

Most Kruskal-Wallis tests identified forearm, body condition, and mass differences between our YSA categories, though the Wilcoxon tests results were mixed as to whether the pre-arrival data was significantly different than the subsequent periods (Tables A37 – 46). The sample distributions indicate overlap for all YSA categories, but often contain a greater number of upper outliers in the pre-arrival dataset (Figures A13 and A14). Though we expected that body condition could be lower in May in the years after the onset of WNS, the data indicated similar or slightly higher body condition values (Figure A13). Though there appears to be a large overlap in all measurements between YSA periods, the largest upper distributions mostly appear in the WNS pre-arrival period, regardless of month (Figures A13 and A14).

Table A1. Generalized linear mixed models with delta Akaike information criterion (AIC) values < 5. Data were based on little brown bat (*Myotis lucifugus*; MYLU), northern long-eared bat (*Myotis septentrionalis*; MYSE), and tricolored bat (*Perimyotis subflavus*; PESU) site-night captures from the continental United States 1999 – 2019. Covariates include GRTS = NABat grid cell priority identification number, month = month of capture, year = year of capture, YSA = years since arrival of white-nose syndrome, state = state of capture, tempR = annual temperature range, and tempM = annual temperature mean, and elev = mean elevation. Bolded models were identified as most parsimonious within the dataset.

Species	ΔAIC	Covariates	AIC
MYLU	0	YSA+ I(YSA^2)+month+(1|State)+(1|GRTS)+elev	29722.25
	0.7746	**YSA+ I(YSA^2)+(1|State)+ (1|GRTS)**	**29723.03**
	0.9636	YSA+ I(YSA^2)+(1|State)+ (1|GRTS)+month	29723.22
	1.5576	YSA+ I(YSA^2)+month+(1|State)+(1|GRTS)+ tempM+elev	29723.81
	1.7438	YSA+ I(YSA^2)+ I(YSA^3)+month+(1|State)+(1|GRTS)+elev	29724
	1.9981	YSA+ I(YSA^2)+month+(1|State)+(1|GRTS)+ tempR+elev	29724.25
	2.0274	YSA+ I(YSA^2)+month+(1|State)+(1|GRTS)+ tempR	29724.28
	2.2751	YSA+ I(YSA^2)+month+(1|State)+(1|GRTS)+ tempM	29724.53
	2.5035	YSA+ I(YSA^2)+ I(YSA^3)+(1|State)+ (1|GRTS)	29724.76
	2.7332	YSA+ I(YSA^2)+ I(YSA^3)+ (1|GRTS)+(1|State)+month	29724.99
	3.2564	YSA+ I(YSA^2)+ I(YSA^3)+month+(1|State)+(1|GRTS)+ tempM+elev	29725.51
	3.7398	YSA+ I(YSA^2)+ I(YSA^3)+month+(1|State)+(1|GRTS)+ tempR+elev	29725.99
	3.7556	YSA+ I(YSA^2)+ I(YSA^3)+month+(1|State)+(1|GRTS)+ tempR	29726.01
	4.0657	YSA+ I(YSA^2)+ I(YSA^3)+month+(1|State)+(1|GRTS)+ tempM	29726.32
MYSE	0	YSA+ I(YSA^2)+ I(YSA^3)+month+(1|State)+(1|GRTS)+ tempR	30267.41
	1.9983	YSA+ I(YSA^2)+ I(YSA^3)+month+(1|State)+(1|GRTS)+ tempR+elev	30269.41
	2.1387	**YSA+ I(YSA^2)+ I(YSA^3)+(1|State)+ (1|GRTS)**	**30269.55**
	2.4744	YSA+ I(YSA^2)+ I(YSA^3)+ (1|GRTS)+(1|State)+month	30269.88
	3.8842	YSA+ I(YSA^2)+ I(YSA^3)+month+(1|State)+(1|GRTS)+ tempM	30271.29
	3.9722	YSA+ I(YSA^2)+ I(YSA^3)+month+(1|State)+(1|GRTS)+elev	30271.38
PESU	0	year+ I(year^2)+month+(1|GRTS)+ tempM	7524.719
	0.8461	**year+month+(1|GRTS)+ tempM**	**7525.565**
	1.3925	year+ I(year^2)+ I(year^3)+month+(1|GRTS)+ tempM	7526.112
	1.4249	year+ I(year^2)+month+(1|GRTS)+ tempM+elev	7526.144
	2.0000	year+ I(year^2)+month+(1|State)+(1|GRTS)+ tempM	7526.719
	2.2934	year+month+(1|GRTS)+ tempM+elev	7527.013
	2.8461	year+month+(1|State)+(1|GRTS)+ tempM	7527.565
	2.9451	year+ I(year^2)+ I(year^3)+month+(1|GRTS)+ tempM+elev	7527.664
	3.3925	year+ I(year^2)+ I(year^3)+month+(1|State)+(1|GRTS)+ tempM	7528.112
	3.4249	year+ I(year^2)+month+(1|State)+(1|GRTS)+ tempM+elev	7528.144
	4.2934	year+month+(1|State)+(1|GRTS)+ tempM+elev	7529.013
	4.9451	year+ I(year^2)+ I(year^3)+month+(1|State)+(1|GRTS)+ tempM+elev	7529.664

Table A2. Model coefficients describing the relationship between generalized linear mixed model covariates and little brown bat (*Myotis lucifugus*) site-night captures from the continental United States, 1999 – 2019. Model coefficients are for centered and scaled covariates. Associated covariates and abbreviations include GRTS = NABat grid cell priority identification number, SD = standard deviation, SE = standard error, YSA = years since arrival of white-nose syndrome, and state = state of capture.

Groups Name		**Variance**	**SD**	
State (Intercept)		0.1850	0.4301	
GRTS (Intercept)		0.3758	0.6130	
	Estimate	**SE**	**z value**	**Pr(>|z|)**
(Intercept)	1.1821	0.0997	11.860	< 0.001
YSA	-0.3165	0.0411	-7.696	< 0.001
I(YSA^2)	0.0376	0.0103	3.643	0.0003

Table A3. Relationship between generalized linear mixed model covariates and northern long-eared bat (*Myotis septentrionalis*) based on site-night captures from the continental United States 1999 – 2019 based on generalized linear mixed models. Covariates and abbreviations include GRTS = NABat grid cell priority identification number, month = month of capture, SD = standard deviation, SE = standard error, tempR = annual temperature range, YSA = years since arrival of white-nose syndrome, and state = state of capture.

Groups Name		**Variance**	**SD**	
State (Intercept)		0.0595	0.2439	
GRTS (Intercept)		0.1168	0.3417	
	Estimate	**SE**	**z value**	**Pr(>|z|)**
(Intercept)	0.8934	0.0660	13.545	< 0.001
YSA	-0.1746	0.0257	-6.795	< 0.001
I(YSA^2)	-0.1170	0.036	-3.254	0.0011
I(YSA^3)	0.0308	0.0097	3.171	0.0015
month	-0.0161	0.0132	-1.218	0.2233
tempR	-0.0471	0.0229	-2.054	0.0340

Table A4. Relationship between generalized linear mixed models covariates and tricolored bat (*Perimyotis subflavus*) based on site-night captures from the continental United States 1999 – 2019 based on generalized linear mixed models. Covariates and abbreviations include GRTS = NABat grid cell priority identification number, month = month of capture, SD = standard deviation, SE = standard error, year = year of capture, and tempM = annual temperature mean.

Groups Name		**Variance**	**SD**	
GRTS (Intercept)		0.1446	0.3802	
	Estimate	**SE**	**z value**	**Pr(>|z|)**
(Intercept)	0.5112	0.0255	20.034	< 0.001
year	-0.1566	0.0216	-7.256	< 0.001
month	0.0416	0.0209	1.994	0.0461
tempM	0.1004	0.0245	4.098	< 0.001

Table A5. Generalized linear mixed models with Akaike information criterion (AIC) values < 5 for each U.S. Fish and Wildlife Service Representation Unit (RPU). Data were based on little brown bat (*Myotis lucifugus*) site-night captures from the continental United States 1999 – 2019 based on generalized linear mixed models. Covariates include month = month of capture, year = year of capture, YSA = years since arrival of white-nose syndrome, and state = state of capture. Bolded models were identified as most parsimonious within the dataset.

RPU	**∆AIC**	**Covariates**	**AIC**
2	**0**	**year+I(year^2)+I(year^3)+(1|State)+month**	**36562.7332**
	0	**year+I(year^2)+I(year^3)+(1|State)**	**596.4855**
	0.4128	year+I(year^2)+I(year^3)+(1|State)+month	596.8983
	1.0868	YSA+I(YSA^2)+I(YSA^3)+(1|State)+month	597.5724
3	1.8658	YSA+I(YSA^2)+I(YSA^3)+(1|State)	598.3513
	3.9308	YSA+I(YSA^2)+(1|State)+month	600.4163
	4.3215	YSA+I(YSA^2)+(1|State)	600.8070
	4.6047	year+I(year^2)+(1|State)	601.0903
	0	YSA+I(YSA^2)+I(YSA^3)+month	1118.3642
4	**0.6504**	**YSA+I(YSA^2)+I(YSA^3)**	**1119.0146**
	2	YSA+I(YSA^2)+I(YSA^3)+(1|State)+month	1120.3642
5	**0**	**year+I(year^2)+I(year^3)+(1|State)+month**	**1339.8308**

Table A6. Relationship between generalized linear mixed model covariates and little brown bat (*Myotis lucifugus*) U.S. Fish and Wildlife Service Representation Unit (RPU) 2 based on site-night captures from the continental United States 1999 – 2019 based on generalized linear mixed models. Covariates and abbreviations include month = month of capture, year = year of capture, SD = standard deviation, SE = standard error, state = state of capture.

Groups Name		**Variance**	**SD**	
State (Intercept)		0.4754	0.6895	
	Estimate	**SE**	**z value**	**Pr(>|z|)**
(Intercept)	1.7179	0.1530	11.226	< 0.001
year	-0.3250	0.0273	-11.903	< 0.001
I(year^2)	-0.0509	0.0097	-5.225	< 0.001
I(year^3)	0.0373	0.0067	5.587	< 0.001
month	0.0463	0.0127	3.640	0.0003

Table A7. Relationship between generalized linear mixed model covariates and little brown bat (*Myotis lucifugus*) site-night captures in U.S. Fish and Wildlife Service Representation Unit (RPU) 3 1999 – 2019. Covariates and abbreviations include SD = standard deviation, SE = standard error, state = state of capture, and year = year of capture.

Groups Name		**Variance**	**SD**	
State (Intercept)		0.8664	0.9308	
	Estimate	**SE**	**z value**	**Pr(>|z|)**
(Intercept)	2.0296	0.4620	4.393	< 0.001
year	0.3075	0.2539	1.211	0.2258
I(year^2)	-0.3983	0.1067	-3.732	0.0002
I(year^3)	-0.2720	0.1055	-2.578	0.010

Table A8. Relationship between generalized linear mixed model covariates and little brown bat (*Myotis lucifugus*) site-night captures in U.S. Fish and Wildlife Service Representation Unit (RPU) from 1999 – 2019. Covariates and abbreviations include SE = standard error and YSA = years since arrival of white-nose syndrome.

	Estimate	**SE**	**z value**	**Pr(>|z|)**
(Intercept)	2.1052	0.1434	14.681	< 0.001
YSA	0.0643	0.2177	0.295	0.7679
I(YSA^2)	-0.6183	0.2292	-2.698	0.007
I(YSA^3)	0.1178	0.0496	2.376	0.0175

Table A9. Relationship between generalized linear mixed model covariates and little brown bat (*Myotis* lucifugus) in U.S. Fish and Wildlife Service Representation Unit (RPU) 5 based on site-night captures 1999 – 2019 based on generalized linear mixed models. Covariates and abbreviations include month = month of capture, SD = standard deviation, SE = standard error, state = state of capture, and year = year of capture.

Groups Name	**Variance**	**SD**	
State (Intercept)	0.2749	0.5243	
	Estimate	**SE**	**z value**	**Pr(>|z|)**
(Intercept)	1.4645	0.4020	3.643	< 0.001
year	-0.3094	0.1877	-1.648	0.0993
I(year^2)	-0.1103	0.0640	-1.723	0.0848
I(year^3)	0.1415	0.0632	2.237	0.0253
month	0.2411	0.0734	3.284	0.0010

Table A10. Generalized linear mixed models with Akaike information criterion (AIC) values < 5 for each U.S. Fish and Wildlife Service Representation Unit (RPU) (1-4). Data were based on northern long-eared bat (*Myotis septentrionalis*) site-night captures from the continental United States 1999 – 2019 based on generalized linear mixed models. Covariates include month = month of capture, state = state of capture, and year = year of capture. Bolded models were identified as most parsimonious within the dataset.

RPU	ΔAIC	Covariates	AIC
1	**0**	**year+I(year^2)**	**910.8559**
	1.2010	year+I(year^2)+I(year^3)	912.0569
	1.9946	year+I(year^2)+month	912.8504
	2.0000	year+I(year^2)+(1|State)	912.8559
2	0	year+I(year^2)+I(year^3)+(1|State)+month	44525.3181
	0.3227	**year+I(year^2)+I(year^3)+(1|State)**	**44525.6408**
4	**0**	**year+I(year^2)+I(year^3)+(1|State)**	**306.5147**
	0.2006	year+I(year^2)+I(year^3)+(1|State)+month	306.7153
	2.1399	year+I(year^2)+(1|State)	308.6546
	4.0211	year+I(year^2)+(1|State)+month	310.5358
5	0	year+I(year^2)+I(year^3)+(1|State)+month	855.7763
	1.5440	**year+I(year^2)+I(year^3)+month**	**857.3203**

Table A11. Relationship between generalized linear mixed model covariates and northern long-eared bat (*Myotis septentrionalis*) in U.S. Fish and Wildlife Service Representation Unit (RPU) 1 based on site-night captures 1999 – 2019 based on generalized linear mixed models. Covariates and abbreviations include SE = standard error and year = year of capture.

	Estimate	SE	z value	Pr(>|z|)
(Intercept)	1.0398	0.0774	13.439	< 0.001
year	-0.2360	0.0657	-3.590	0.0003
I(year^2)	-0.2287	0.0586	-3.906	< 0.001

Table A12. Relationship between generalized linear mixed model covariates and northern long-eared bat (*Myotis septentrionalis*) site-night captures in U.S. Fish and Wildlife Service Representation Unit (RPU) 2 1999 – 2019. Covariates and abbreviations include SD = standard deviation, SE = standard error, state = state of capture, year = year of capture.

Groups Name		**Variance**	**SD**	
State (Intercept)		0.1919	0.438	
	Estimate	**SE**	**z value**	**Pr(>|z|)**
(Intercept)	1.2272	0.1063	11.546	< 0.001
year	-0.2873	0.0195	-14.704	< 0.001
I(year^2)	-0.1550	0.0084	-18.540	< 0.001
I(year^3)	-0.0324	0.0060	-5.386	< 0.001

Table A13. Relationship between generalized linear mixed model covariates and northern long-eared bat (*Myotis septentrionalis*) site-night captures in U.S. Fish and Wildlife Service Representation Unit (RPU) 4 1999 - 2019. Covariates and abbreviations include SD = standard deviation, SE = standard error, state = state of capture, and year = year of capture.

Groups Name		**Variance**	**SD**	
State (Intercept)		1.26	1.122	
	Estimate	**SE**	**z value**	**Pr(>|z|)**
(Intercept)	1.41140	0.4836	2.919	0.0035
year	-1.02972	0.3238	-3.180	0.0015
I(year^2)	0.02557	0.4298	0.059	0.9526
I(year^3)	0.40202	0.2012	1.998	0.0458

Table A14. Relationship between generalized linear mixed model covariates and northern long-eared bat (*Myotis septentrionalis*) site-night captures in U.S. Fish and Wildlife Service Representation Unit (RPU) 5 1999 – 2019. Covariates and abbreviations include month = month of capture, SE = standard error, and year = year of capture.

	Estimate	SE	z value	Pr(>|z|)
(Intercept)	0.7215	0.1161	6.217	< 0.001
year	-0.7757	0.1541	-5.033	< 0.001
I(year^2)	0.1871	0.0947	1.977	0.0481
I(year^3)	0.2690	0.0798	3.370	< 0.001
month	-0.2178	0.0661	-3.298	< 0.001

Table A15. Generalized linear mixed models with Akaike information criterion values < 5 for each U.S. Fish and Wildlife Service Representation Unit (RPU). Data were based on tricolored bat (*Perimyotis subflavus*; PESU) site-night captures 1999 – 2019 based on generalized linear mixed models. Covariates include month = month of capture, state = state of capture, and year = year of capture. Bolded models were identified as most parsimonious within the dataset.

RPU	∆AIC	Covariates	AIC
1	0	**year+I(year^2)+I(year^3)+(1|State)+month**	**10679.3752**
2	0	**year+I(year^2)+I(year^3)+(1|State)+month**	**6533.8932**
	4.9701	year+I(year^2)+(1|State)+month	6538.8634
3	0	year+I(year^2)+month	1744.6905
	0.1060	**year+I(year^2)**	**1744.7964**
	1.9151	year+I(year^2)+I(year^3)+month	1746.6056
	2.0000	year+I(year^2)+(1|State)+month	1746.6905
	2.0892	year+I(year^2)+I(year^3)	1746.7796
	2.1060	year+I(year^2)+(1|State)	1746.7964
	3.6290	year	1748.3194
	3.9151	year+I(year^2)+I(year^3)+(1|State)+month	1748.6056
	4.0892	year+I(year^2)+I(year^3)+(1|State)	1748.7796
	4.2737	year+month	1748.9642
	4.2819	year+(1|State)	1748.9723
	4.6201	year+(1|State)+month	1749.3106

Table A16. Relationship between generalized linear mixed model covariates and tricolored bat (*Perimyotis subflavus*) site-night captures from U.S. Fish and Wildlife Service Representation Unit (RPU) 1 1999 – 2019 based on generalized linear mixed models. Covariates and abbreviations include month = month of capture, year = year of capture, SD = standard deviation, SE = standard error, and state = state of capture.

Groups Name		**Variance**	**SD**	
State (Intercept)		0.1943	0.4408	
	Estimate	**SE**	**z value**	**Pr(>|z|)**
(Intercept)	1.0156	0.1286	7.899	< 0.001
year	-0.5466	0.0435	-12.568	< 0.001
I(year^2)	-0.0823	0.0194	-4.240	< 0.001
I(year^3)	0.1012	0.0176	5.751	< 0.001
month	0.192	0.0189	10.187	< 0.001

Table A17. Relationship between generalized linear mixed model covariates and tricolored bat (*Perimyotis subflavus*) site-night captures within U.S. Fish and Wildlife Service Representation Unit (RPU) 2 1999 – 2019. Covariates and abbreviations include month = month of capture, SD = standard deviation, SE = standard error, state = state of capture, and year = year of capture.

Groups Name		**Variance**	**SD**	
State (Intercept)		0.2518	0.5018	
	Estimate	**SE**	**z value**	**Pr(>|z|)**
(Intercept)	1.0881	0.2027	5.367	< 0.001
year	-0.4668	0.0550	-8.485	< 0.001
I(year^2)	-0.2406	0.0243	-9.892	< 0.001
I(year^3)	0.0531	0.0199	2.661	0.0078
month	0.2401	0.0257	9.342	< 0.001

Table A18. Relationship between generalized linear mixed model covariates and tricolored bat (*Perimyotis subflavus*) site-night captures within U.S. Fish and Wildlife Service Representation Unit (RPU) 3 1999 – 2019 based on generalized linear mixed models. Covariates and abbreviations include SE = standard error and year = year of capture.

	Estimate	**SE**	**z value**	**Pr(>|z|)**
(Intercept)	0.7598	0.0502	15.131	< 0.001
year	-0.2659	0.0548	-4.853	< 0.001
I(year^2)	-0.0786	0.0335	-2.345	0.019

Table A19. Generalized linear mixed models with Akaike information criterion (AIC) values < 5. Data were based on juvenile little brown bat (*Myotis lucifugus*; MYLU), northern long-eared bat (*Myotis septentrionalis*; MYSE), and tricolored bat (*Perimyotis subflavus*; PESU) site-night captures from the continental United States 1999 – 2019. Covariates include GRTS = NABat grid cell priority identification number, month = month of capture, year = year of capture, YSA = years since arrival of white-nose syndrome, state = state of capture, tempR = annual temperature range, tempM = annual temperature mean, and elev = mean elevation. Bolded models were identified as most parsimonious within the dataset.

	ΔAIC	Covariates	AIC
	0.0000	YSA+I(YSA^2)+I(YSA^3)+month+(1|State)+(1|GRTS)+tempM+elev	11041.3211
	0.5852	year+I(year^2)+month+(1|State)+(1|GRTS)+tempM+elev	11041.9063
	0.7174	YSA+I(YSA^2)+I(YSA^3)+month+(1|State)+(1|GRTS)+tempR+elev	11042.0385
	0.7321	YSA+month+(1|State)+(1|GRTS)+tempM+elev	11042.0532
	0.8386	year+I(year^2)+month+(1|State)+(1|GRTS)+elev	11042.1597
	0.9223	YSA+I(YSA^2)+I(YSA^3)+month+(1|State)+(1|GRTS)+elev	11042.2434
	1.0205	**YSA+month+(1|State)+(1|GRTS)+elev**	**11042.3416**
	1.2709	YSA+month+(1|State)+(1|GRTS)+tempR+elev	11042.5920
	2.0838	year+I(year^2)+month+(1|State)+(1|GRTS)+tempR+elev	11043.4049
	2.4279	year+I(year^2)+I(year^3)+month+(1|State)+(1|GRTS)+tempM+elev	11043.7490
MYLU	2.5049	YSA+I(YSA^2)+month+(1|State)+(1|GRTS)+tempM+elev	11043.8260
	2.6708	year+I(year^2)+I(year^3)+month+(1|State)+(1|GRTS)+elev	11043.9919
	2.7147	YSA+I(YSA^2)+month+(1|State)+(1|GRTS)+elev	11044.0358
	3.0351	YSA+I(YSA^2)+month+(1|State)+(1|GRTS)+tempR+elev	11044.3562
	3.0721	YSA+I(YSA^2)+I(YSA^3)+month+(1|State)+(1|GRTS)+tempM	11044.3932
	3.5387	year+month+(1|State)+(1|GRTS)+tempM+elev	11044.8598
	3.8528	year+month+(1|State)+(1|GRTS)+elev	11045.1740
	3.8976	year+I(year^2)+I(year^3)+month+(1|State)+(1|GRTS)+tempR+elev	11045.2187
	4.1053	year+I(year^2)+month+(1|State)+(1|GRTS)+tempM	11045.4264
	4.4953	YSA+month+(1|State)+(1|GRTS)+tempM	11045.8164
	4.6212	year+month+(1|State)+(1|GRTS)+tempR+elev	11045.9423
	0.0000	YSA+I(YSA^2)+month+(1|State)+(1|GRTS)+tempR+elev	11354.4283
	1.1951	**YSA+I(YSA^2)+month+(1|GRTS)+tempM**	**11355.6234**
MYSE	1.4236	YSA+I(YSA^2)+month+(1|GRTS)+tempR+elev	11355.8520
	1.6087	YSA+I(YSA^2)+month+(1|GRTS)+tempM+elev	11356.0370
	1.8094	YSA+I(YSA^2)+I(YSA^3)+month+(1|State)+(1|GRTS)+tempR+elev	11356.2377

	ΔAIC	Covariates	AIC
	2.3808	YSA+I(YSA^2)+month+(1|State)+(1|GRTS)+elev	11356.8091
	2.4815	YSA+I(YSA^2)+month+(1|State)+(1|GRTS)+tempM+elev	11356.9098
	2.9935	YSA+I(YSA^2)+month+(1|State)+(1|GRTS)+tempM	11357.4218
	3.0671	YSA+I(YSA^2)+I(YSA^3)+month+(1|GRTS)+tempM	11357.4954
	3.2500	YSA+I(YSA^2)+I(YSA^3)+month+(1|GRTS)+tempR+elev	11357.6784
	3.4017	YSA+I(YSA^2)+I(YSA^3)+month+(1|GRTS)+tempM+elev	11357.8300
	4.0259	YSA+I(YSA^2)+I(YSA^3)+month+(1|State)+(1|GRTS)+elev	11358.4542
	4.2424	YSA+I(YSA^2)+I(YSA^3)+month+(1|State)+(1|GRTS)+tempM+elev	11358.6707
	4.8638	YSA+I(YSA^2)+I(YSA^3)+month+(1|State)+(1|GRTS)+tempM	11359.2921
	0.0000	**YSA+month+(1|GRTS)+tempM**	**2806.8275**
	0.0567	YSA+month+(1|GRTS)+elev	2806.8842
	0.1838	YSA+month+(1|GRTS)+tempM+elev	2807.0113
	0.2642	YSA+I(YSA^2)+month+(1|GRTS)+elev	2807.0917
	0.6445	YSA+I(YSA^2)+month+(1|GRTS)+tempM+elev	2807.4720
	0.9371	YSA+I(YSA^2)+month+(1|GRTS)+tempM	2807.7646
	1.4183	YSA+month+(1|GRTS)+tempR+elev	2808.2458
	1.8190	YSA+I(YSA^2)+month+(1|GRTS)+tempR+elev	2808.6465
	2.0000	YSA+month+(1|State)+(1|GRTS)+tempM	2808.8275
	2.0567	YSA+month+(1|State)+(1|GRTS)+elev	2808.8842
	2.1838	YSA+month+(1|State)+(1|GRTS)+tempM+elev	2809.0113
PESU	2.2640	YSA+I(YSA^2)+I(YSA^3)+month+(1|GRTS)+elev	2809.0915
	2.2642	YSA+I(YSA^2)+month+(1|State)+(1|GRTS)+elev	2809.0917
	2.6288	YSA+I(YSA^2)+I(YSA^3)+month+(1|GRTS)+tempM+elev	2809.4563
	2.6445	YSA+I(YSA^2)+month+(1|State)+(1|GRTS)+tempM+elev	2809.4720
	2.9192	YSA+I(YSA^2)+I(YSA^3)+month+(1|GRTS)+tempM	2809.7467
	2.9371	YSA+I(YSA^2)+month+(1|State)+(1|GRTS)+tempM	2809.7646
	3.4183	YSA+month+(1|State)+(1|GRTS)+tempR+elev	2810.2458
	3.8119	YSA+I(YSA^2)+I(YSA^3)+month+(1|GRTS)+tempR+elev	2810.6394
	3.8190	YSA+I(YSA^2)+month+(1|State)+(1|GRTS)+tempR+elev	2810.6465
	4.1065	YSA+(1|GRTS)+month	2810.9340
	4.2640	YSA+I(YSA^2)+I(YSA^3)+month+(1|State)+(1|GRTS)+elev	2811.0915
	4.9192	YSA+I(YSA^2)+I(YSA^3)+month+(1|State)+(1|GRTS)+tempM	2811.7467

Table A20. Relationship between generalized linear mixed model covariates and juvenile little brown bat (*Myotis lucifugus*) site-night captures from the continental United States 1999 – 2019. Covariates and abbreviations include GRTS = NABat cell identification number, month = month of capture, SD = standard deviation, SE = standard error, state = state of capture, elev = mean elevation, and YSA = years since arrival of white-nose syndrome.

Groups Name		**Variance**	**SD**	
State (Intercept)		0.2416	0.4915	
GRTS (Intercept)		1.1347	1.0652	
	Estimate	**SE**	**z value**	**Pr(>|z|)**
(Intercept)	-1.1180	0.1433	-7.802	< 0.001
YSA	-0.0882	0.0409	-2.155	0.0312
month	1.1696	0.0545	21.468	< 0.001
elev	-0.2975	0.0676	-4.404	< 0.001

Table A21. Relationship between generalized linear mixed model covariates and juvenile northern long-eared bat (*Myotis septentrionalis*) site-night captures from the continental United States 1999 – 2019 based on generalized linear mixed models. Covariates and abbreviations include GRTS = NABat grid cell priority identification number, month = month of capture, YSA = years since arrival of white-nose syndrome, SD = standard deviation, SE = standard error, and tempM = annual temperature mean.

Groups Name		**Variance**	**SD**	
GRTS (Intercept)		0.6879	0.8294	
	Estimate	**SE**	**z value**	**Pr(>|z|)**
(Intercept)	-1.5866	0.06144	-25.822	< 0.001
YSA	0.0745	0.05921	1.258	0.2083
I(YSA^2)	-0.0834	0.03120	-2.674	0.0075
month	1.0996	0.04163	26.415	< 0.001
tempM	0.1419	0.03605	3.937	< 0.001
Zero-inflation model:				
	Estimate	**SE**	**z value**	**Pr(>|z|)**
(Intercept)	-19.29	1377.98	-0.014	0.989

Table A22. Relationship between generalized linear mixed model covariates and juvenile tricolored bat (*Perimyotis subflavus*) based on site-night captures from the continental United States 1999 – 2019 based on generalized linear mixed models. Covariates and abbreviations include GRTS = NABat grid cell priority identification number, month= month of capture, YSA = years since arrival of white-nose syndrome, SD = standard deviation, tempM = annual temperature mean, and SE = standard error.

Groups Name		**Variance**	**SD**	
GRTS (Intercept)		0.5262	0.7254	
	Estimate	**SE**	**z value**	**Pr(>|z|)**
(Intercept)	-1.6826	0.0835	-20.148	< 0.001
YSA	0.0043	0.0528	0.082	0.9348
month	1.1257	0.0693	16.235	< 0.001
TempM	0.1446	0.0582	2.486	0.0129
Zero-inflation model:				
	Estimate	**SE**	**z value**	**Pr(>|z|)**
(Intercept)	-19.72	2464.01	-0.008	0.994

Table A23. Generalized linear mixed models with Akaike information criterion (AIC) values < 5 for each RPU. Data were based on juvenile little brown bat (Myotis lucifugus) site-night captures from the continental United States 1999 – 2019. Covariates include month = month of capture, year = year of capture, YSA = years since arrival of white-nose syndrome, and state = state of capture. Bolded models were identified as most parsimonious within the dataset.

RPU	ΔAIC	Covariates	AIC
2	**0**	**YSA+I(YSA^2)+I(YSA^3)+(1|State)+DOY**	**13,301.6960**
	0	YSA+I(YSA^2)+(1|State)+DOY	265.7546
	0.7121	**YSA+I(YSA^2)+(1|State)**	**266.4667**
	1.4371	YSA+I(YSA^2)+I(YSA^3)+(1|State)+DOY	267.1917
	1.8839	YSA+(1|State)+DOY	267.6385
	1.9982	YSA+I(YSA^2)+I(YSA^3)+(1|State)	267.7528
	2.0448	YSA+(1|State)	267.7994
3	2.0943	year+(1|State)+month	267.8490
	2.2634	year+(1|State)	268.0180
	3.1958	year+I(year^2)+I(year^3)+(1|State)+month	268.9505
	3.3124	year+I(year^2)+I(year^3)+(1|State)	269.0670
	3.8560	year+I(year^2)+I(year^3)+month	269.6106
	3.9797	year+I(year^2)+(1|State)+month	269.7343
	4.2161	year+I(year^2)+(1|State)	269.9707
	0	**year+I(year^2)+(1|State)+month**	**345.9729**
	1.9986	year+I(year^2)+I(year^3)+(1|State)+month	347.9715
4	2.3467	year+I(year^2)+month	348.3196
	3.5853	year+(1|State)+month	349.5582
	4.1936	year+I(year^2)+I(year^3)+month	350.1665
	4.8043	YSA+I(YSA^2)+I(YSA^3)+DOY	350.7772
	0	**year+month**	**261.1665**
	1.2045	year+I(year^2)+month	262.3710
	1.3805	1	262.5470
	2.0000	year+(1|State)+month	263.1665
	2.0911	year	263.2576
5	2.2999	year+I(year^2)	263.4664
	2.9774	year+I(year^2)+I(year^3)+month	264.1440
	3.2045	year+I(year^2)+(1|State)+month	264.3710
	4.0911	year+(1|State)	265.2576
	4.2423	year+I(year^2)+I(year^3)	265.4089
	4.2999	year+I(year^2)+(1|State)	265.4664
	4.9774	year+I(year^2)+I(year^3)+(1|State)+month	266.1440

Table A24. Relationship between generalized linear mixed model covariates and juvenile little brown bats (*Myotis lucifugus*) site-night captures from the U.S. Fish and Wildlife Service Representation Unit (RPU) 2 of the continental United States 1999 – 2019. Covariates and abbreviations include DOY = day of year, YSA = years since arrival of white-nose syndrome, SD = standard deviation, state = state of capture and SE = standard error.

Groups Name		**Variance**	**SD**	
State (Intercept)		0.627	0.7919	
	Estimate	**SE**	**z value**	**Pr(>|z|)**
(Intercept)	-0.1847	0.1996	-0.93	0.355
YSA	0.4418	0.0779	5.67	< 0.001
I(YSA^2)	-0.3005	0.0612	-4.91	< 0.001
I(YSA^3)	0.0374	0.0090	4.14	< 0.001
DOY	1.3786	0.0432	31.91	< 0.001

Table A25. Relationship between generalized linear mixed model covariates and juvenile little brown bats (*Myotis lucifugus*) site-night captures from the U.S. Fish and Wildlife Service Representation Unit (RPU) 3 1999 – 2019. Covariates and abbreviations YSA = years since arrival of white-nose syndrome, SD = standard deviation, and SE = standard error.

Groups Name		**Variance**	**SD**	
State (Intercept)		2.043	1.429	
	Estimate	**SE**	**z value**	**Pr(>|z|)**
(Intercept)	0.6598	0.8893	0.742	0.458
YSA	1.2488	1.0549	1.184	0.236
I(YSA^2)	-0.5388	0.3882	-1.388	0.165

Table A26. Relationship between generalized linear mixed model covariates and juvenile little brown bats (*Myotis lucifugus*) site-night captures from U.S. Fish and Wildlife Service Representation Unit (RPU) 4 1999 – 2019. Covariates and abbreviations include month = month of capture, year = year of capture, SD = standard deviation, state = state of capture, and SE = standard error.

Groups Name		**Variance**	**SD**	
State (Intercept)		0.4898	0.6999	
	Estimate	**SE**	**z value**	**Pr(>|z|)**
(Intercept)	0.6250	0.5231	1.195	0.2322
year	-0.2814	0.2518	-1.117	0.2639
I(year^2)	-0.9971	0.4181	-2.385	0.0171
month	0.9906	0.2582	3.836	< 0.001

Table A27. Relationship between generalized linear mixed model covariates and juvenile little brown bats (*Myotis lucifugus*) site-night captures from the U.S. Fish and Wildlife Service Representation Unit (RPU) 5 1999 – 2019. Covariates and abbreviations month = month of capture, year = year of capture, and SE = standard error.

	Estimate	**SE**	**z value**	**Pr(>|z|)**
(Intercept)	-1.1464	0.2494	-4.598	< 0.001
year	0.2504	0.2137	1.172	0.2413
month	0.5225	0.2530	2.066	< 0.001

Table A28. Generalized linear mixed models with Akaike information criterion (AIC) values < 5 for each RPU (1-4). Data were based on juvenile northern long-eared bats (*Myotis septentrionalis*) site-night captures from the continental United States 1999 – 2019 based on generalized linear mixed models. Covariates include month = month of capture, year = year of capture, YSA = years since arrival of white-nose syndrome, and state = state of capture. Bolded models were identified as most parsimonious within the dataset.

RPU	ΔAIC	Covariates	AIC
1	**0**	**year+month**	**232.0446**
	0.140023	YSA+DOY	232.1846
	1.699316	YSA+I(YSA^2)+I(YSA^3)+DOY	233.7439
	1.774037	year+I(year^2)+month	233.8186
	2	year+(1|State)+month	234.0446
	2.020444	YSA+I(YSA^2)+DOY	234.065
	2.140023	YSA+(1|State)+DOY	234.1846
	2.219898	year+I(year^2)+I(year^3)+month	234.2644
	3.699436	YSA+I(YSA^2)+I(YSA^3)+(1|State)+DOY	235.744
	3.774037	year+I(year^2)+(1|State)+month	235.8186
	4.020444	YSA+I(YSA^2)+(1|State)+DOY	236.065
	4.219898	year+I(year^2)+I(year^3)+(1|State)+month	236.2644
2	0	**YSA+I(YSA^2)+(1|State)+DOY**	**15708.08**
	1.989065	YSA+I(YSA^2)+I(YSA^3)+(1|State)+DOY	15710.07
4	0	**year+I(year^2)+(1|State)+month**	**115.6852**
	0.873456	year+I(year^2)+I(year^3)+(1|State)+month	116.5587
5	**0**	**YSA+(1|State)+DOY**	**298.0367**
	0.310654	YSA+I(YSA^2)+(1|State)+DOY	298.3473
	1.723478	YSA+I(YSA^2)+I(YSA^3)+(1|State)+DOY	299.7602

Table A29. Relationship between generalized linear mixed model covariates and juvenile northern long-eared bats (*Myotis septentrionalis*) site-night captures from the U.S. Fish and Wildlife Service Representation Unit (RPU) 1 1999 – 2019. Covariates and abbreviations include month = month of capture, and year = year of capture, and SE = standard error.

	Estimate	**SE**	**z value**	**Pr(>|z|)**
(Intercept)	-1.355	0.2206	-6.143	< 0.001
year	-0.0821	0.2187	-0.376	0.7072
month	0.8858	0.2663	3.326	< 0.001

Table A30. Relationship between generalized linear mixed model covariates and juvenile northern long-eared bats (*Myotis septentrionalis*) site-night captures from U.S. Fish and Wildlife Service Representation Unit (RPU) 2 1999 – 2019. Covariates and abbreviations include DOY = day of year, YSA = years since arrival of white-nose syndrome, SD = standard deviation, state = state of capture and SE = standard error.

Groups Name		**Variance**	**SD**	
State (Intercept)		0.1967	0.4436	
	Estimate	**SE**	**z value**	**Pr(>|z|)**
(Intercept)	-1.3546	0.1364	-9.93	< 0.001
YSA	0.0932	0.0433	2.15	0.0312
I(YSA^2)	-0.1566	0.0238	-6.58	< 0.001
DOY	1.3425	0.035	38.39	< 0.001

Table A31. Relationship between generalized linear mixed model covariates and juvenile northern long-eared bats (*Myotis septentrionalis*) site-night captures from U.S. Fish and Wildlife Service Representation Unit (RPU) 4 1999 – 2019. Covariates and abbreviations include month = month of capture, SD = standard deviation, state = state of capture and SE = standard error.

Groups Name		**Variance**	**SD**	
State (Intercept)		0.7268	0.8526	
	Estimate	**SE**	**z value**	**Pr(>|z|)**
(Intercept)	-0.0943	0.4686	-0.201	0.8406
year	-1.66	0.6436	-2.579	0.0099
I(year^2)	-1.2878	0.3293	-3.911	< 0.001
month	0.9926	0.3497	2.838	0.0045

Table A32. Relationship between generalized linear mixed model covariates and juvenile northern long-eared bats (*Myotis septentrionalis*) site-night captures from the RPU 5 1999 – 2019. Covariates and abbreviations include DOY = day of year, YSA = years since arrival of white-nose syndrome, SD = standard deviation, and SE = standard error.

Groups Name		**Variance**	**SD**	
State (Intercept)		0.3779	0.6148	
	Estimate	**SE**	**z value**	**Pr(>|z|)**
(Intercept)	-1.7016	0.3596	-4.732	< 0.001
YSA	0.1728	0.1497	1.155	0.248
DOY	0.8637	0.1806	4.782	< 0.001

Table A33. Generalized linear mixed models with Akaike information criterion (AIC) values < 5 for each RPU (1-4). Data were based on juvenile tricolored bats (*Perimyotis subflavus*) site-night captures from the continental United States 1999 – 2019 based on generalized linear mixed models. Covariates include month = month of capture, year = year of capture, YSA = years since arrival of white-nose syndrome, and state = state of capture, RPU = U.S. Fish and Wildlife Service Representation Unit. Bolded models were identified as most parsimonious within the dataset.

RPU	ΔAIC	Covariates	AIC
1	0.0000	YSA+ I(YSA^2)+ I(YSA^3) + (1|State) + DOY	3456.4360
	0.3212	**YSA+ I(YSA^2) + (1|State) + DOY**	**3456.7572**
	4.7294	YSA + (1|State) + DOY	3461.1655
2	0.0000	YSA + I(YSA^2)+ DOY	1648.1069
	1.0536	**YSA+ DOY**	**1649.1605**
	1.5643	YSA + I(YSA^2) + I(YSA^3)+ DOY	1649.6712
	2.0000	YSA+ I(YSA^2) + (1|State) + DOY	1650.1069
	3.0536	YSA + (1|State) + DOY	1651.1605
	3.5643	YSA+ I(YSA^2)+ I(YSA^3) + (1|State) + DOY	1651.6712
3	**0.0000**	**YSA + (1|State) + DOY**	**473.0801**
	1.4619	YSA+ I(YSA^2) + (1|State) + DOY	474.5420
	2.4852	year + (1|State) + month	475.5653
	2.7681	YSA+ I(YSA^2)+ I(YSA^3) + (1|State) + DOY	475.8482
	2.8387	YSA + (1|State)	475.9188
	3.0267	year+ I(year^2) + (1|State) + month	476.1068
	3.8113	year + (1|State)	476.8914
	4.6142	year+ I(year^2)+ I(year^3) + (1|State) + month	477.6943
	4.7755	YSA+ I(YSA^2) + (1|State)	477.8556
	4.9114	year+ I(year^2) + (1|State)	477.9915

Table A34. Relationship between generalized linear mixed model covariates and juvenile tricolored bats (*Perimyotis subflavus*) site-night captures from U.S. Fish and Wildlife Service Representation Unit (RPU) 1 1999 – 2019. Covariates and abbreviations include DOY = day of year, YSA = years since arrival of white-nose syndrome, SD = standard deviation, and SE = standard error.

Groups Name		**Variance**	**SD**	
State (Intercept)		0.0333	0.1824	
	Estimate	**SE**	**z value**	**Pr(>|z|)**
(Intercept)	-1.5971	0.1177	-13.565	< 0.001
YSA	-0.3136	0.1039	-3.017	0.0026
I(YSA^2)	0.1361	0.0541	2.518	0.0118
DOY	1.3842	0.0637	21.718	< 0.001

Table A35. Relationship between generalized linear mixed model covariates and juvenile tricolored bats (*Perimyotis subflavus*) site-night captures from U.S. Fish and Wildlife Service Representation Unit (RPU) 2. Covariates and abbreviations DOY = day of year, YSA= year since the arrival of white-nose syndrome, SD = standard deviation, and SE = standard error.

	Estimate	**SE**	**z value**	**Pr(>|z|)**
(Intercept)	-1.6464	0.1060	-15.53	< 0.001
YSA	-0.3544	0.0852	-4.16	< 0.001
DOY	1.5320	0.0927	16.52	< 0.001

Table A36. Relationship between generalized linear mixed model covariates and juvenile tricolored bats (*Perimyotis subflavus*) site-night captures from U.S. Fish and Wildlife Service Representation Unit (RPU) 3 1999 – 2019. Covariates and abbreviations include DOY = day of year, YSA = years since arrival of white-nose syndrome, SD = standard deviation, and SE = standard error.

Groups Name		**Variance**	**SD**	
State (Intercept)		0.6141	0.7836	
	Estimate	**SE**	**z value**	**Pr(>|z|)**
(Intercept)	-0.8090	0.3442	-2.350	0.0188
YSA	-0.1829	0.1350	-1.355	0.1754
DOY	0.2833	0.1304	2.172	0.0298

Table A37. The *p*-values from Kruskal-Wallis tests and subsequent Wilcoxon rank sum tests based on year since arrival of white-nose syndrome categories for the forearm measurements of little brown bat (*Myotis lucifugus*; MYLU), northern long-eared bat (*Myotis septentrionalis*; MYSE), and tricolored bat (*Perimyotis subflavus*; PESU) captured within the continental United States 1999 – 2019.

Species	**Kruskal-Wallis**	**Wilcoxon**			
			Pre-arrival	**Invasion**	**Epidemic**
MYLU	< 0.001	Invasion	0.0015		
		Epidemic	< 0.001	0.1348	
		Established	< 0.001	< 0.001	0.1102
MYSE	0.0001	Invasion	1		
		Epidemic	0.0247	1	
		Established	1	1	0.9995
PESU	< 0.001	Invasion	< 0.001		
		Epidemic	< 0.001	0.0067	
		Established	0.0007	0.0131	1

Table A38. The *p*-values from Kruskal-Wallis tests and subsequent Wilcoxon rank sum tests based on year since arrival of white-nose syndrome categories based on body condition metrics ([body mass]/forearm) metrics of little brown bat (*Myotis lucifugus*) captured within the continental United States 1999 – 2019. Tests were run for data collected within each month (May – August).

Month	Kruskal-Wallis		Wilcoxon		
			Pre-arrival	**Invasion**	**Epidemic**
May	< 0.001	Invasion	0.0915		
		Epidemic	< 0.001	0.0769	
		Established	< 0.001	< 0.001	< 0.001
June	0.2325	Invasion	1		
		Epidemic	0.4266	0.6558	
		Established	1	1	1
July	< 0.001	Invasion	< 0.001		
		Epidemic	< 0.001	< 0.001	
		Established	0.0067	1	< 0.001
August	< 0.001	Invasion	0.3285		
		Epidemic	< 0.001	< 0.001	
		Established	0.0242	1	< 0.001

Table A39. The state-level *p*-values from Kruskal-Wallis tests and subsequent Wilcoxon rank sum tests based on year since arrival of white-nose syndrome categories based on body condition metrics ([body mass]/forearm) of little brown bat (*Myotis lucifugus*) captured within the continental United States 1999 – 2019. Tests were run for data collected at the state level within June.

State	Kruskal-Wallis		Wilcoxon		
			Pre-arrival	Invasion	Epidemic
New Jersey	0.1706	Invasion	0.5812		
		Epidemic	0.9752	1	
		Established	1	0.3333	1
Vermont	0.0054	Invasion	0.5591		
		Epidemic	0.0149	1	
		Established	1	0.2388	0.3962
West Virginia	< 0.001	Invasion	< 0.001		
		Epidemic	1	< 0.001	
		Established	1	0.0695	1
Wisconsin	0.3906	Invasion	0.5580		
		Epidemic	1	0.7156	

Table A40. The *p*-values from Kruskal-Wallis tests and subsequent Wilcoxon rank sum tests based on year since arrival of white-nose syndrome categories based on body condition metrics ([body mass]/forearm) of northern long-eared bat (*Myotis septentrionalis*) captured within the continental United States 1999 – 2019. Tests were run for data collected within each month (May – August).

Month	Kruskal-Wallis		Wilcoxon		
			Pre-arrival	Invasion	Epidemic
May	0.0037	Invasion	0.9337		
		Epidemic	1	1	
		Established	0.0061	0.0170	0.0356
June	< 0.001	Invasion	1		
		Epidemic	< 0.001	< 0.001	
		Established	< 0.001	< 0.001	1
July	0.0328	Invasion	1		
		Epidemic	0.0247	1	
		Established	1	1	0.9995
August	0.0162	Invasion	0.2654		
		Epidemic	1	1	
		Established	0.1218	0.0198	0.1157

Table A41. The West Virginia *p*-values from Kruskal-Wallis tests and subsequent Wilcoxon rank sum tests based on year since arrival of white-nose syndrome categories based on body condition metrics ([body mass]/forearm) of northern long-eared bat *(Myotis septentrionalis*) captured within the continental United States 1999 – 2019. Tests were run for data collected at the state level within June.

State	Kruskal-Wallis		Wilcoxon		
			Pre-arrival	Invasion	Epidemic
West Virginia	< 0.001	Invasion	1		
		Epidemic	< 0.001	1	
		Established	< 0.001	0.0602	0.1284

Table A42. The *p*-values from Kruskal-Wallis tests and subsequent Wilcoxon rank sum tests based on year since arrival of white-nose syndrome categories based on body condition metrics ([body mass]/forearm) of tricolored bat (*Perimyotis subflavus*) captured within the continental United States 1999 – 2019. Tests were run for data collected within each month (May – August) and all states with appropriate samples within the month of June.

Month	Kruskal-Wallis		Wilcoxon		
			Pre-arrival	Invasion	Epidemic
June	< 0.001	Invasion	< 0.001		
		Epidemic	< 0.001	0.0067	
		Established	0.0007	0.0131	1
July	< 0.001	Invasion	1		
		Epidemic	< 0.001	0.0038	
		Established	0.2482	1	< 0.001
August	0.3973	Invasion	0.7133		
		Epidemic	1	1	
		Established	1	0.9168	1

Table A43. The West Virginia *p*-values from Kruskal-Wallis tests and subsequent Wilcoxon rank sum tests based on year since arrival of white-nose syndrome categories based on body condition metrics ([body mass]/forearm) of tricolored bat (*Perimyotis subflavus*) captured within the continental United States 1999 – 2019. Tests were run for data collected at the state level within June.

State	Kruskal-Wallis		Wilcoxon		
			Pre-arrival	Invasion	Epidemic
West Virginia	< 0.001	Invasion	0.0146		
		Epidemic	0.0013	0.6779	
		Established	0.0045	1	1

Table 44. The *p*-values from Kruskal-Wallis tests and subsequent Wilcoxon rank sum tests based on year since arrival of white-nose syndrome categories based on mass of adult male little brown bat (*Myotis lucifugus*) captured within the continental United States 1999 – 2019. Tests were run for data collected within each month (May – August).

Month	Kruskal-Wallis		Wilcoxon		
			Pre-arrival	Invasion	Epidemic
June	< 0.001	Invasion	1		
		Epidemic	< 0.001	0.0009	
		Established	< 0.001	0.0036	1
July	< 0.001	Invasion	0.0012		
		Epidemic	0.0001	< 0.001	
		Established	0.0016	0.5107	< 0.001
August	< 0.001	Invasion	1		
		Epidemic	< 0.001	0.5163	
		Established	0.0012	0.0009	< 0.001

Table 45. The *p*-values from Kruskal-Wallis tests and subsequent Wilcoxon rank sum tests based on year since arrival of white-nose syndrome categories based on mass of adult male northern long-eared bat (*Myotis septentrionalis*) captured within the continental United States 1999 – 2019. Tests were run for data collected within each month (May – August).

Month	Kruskal-Wallis	Wilcoxon			
			Pre-arrival	Invasion	Epidemic
June	< 0.001	Invasion	0.0305		
		Epidemic	0.0004	1	
		Established	0.2564	1	1
July	0.0582	Invasion	0.2810		
		Epidemic	1	0.0791	
		Established	1	0.3408	1
August	0.0011	Invasion	1		
		Epidemic	1	1	
		Established	0.0011	0.0008	0.0052

Table 46. The *p*-values from Kruskal-Wallis tests and subsequent Wilcoxon rank sum tests based on year since arrival of white-nose syndrome categories based on body mass of tricolored bat (*Perimyotis subflavus*) captured within the continental United States 1999 – 2019.

Month	Kruskal-Wallis	Wilcoxon			
			Pre-arrival	Invasion	Epidemic
June	< 0.001	Invasion	0.0001		
		Epidemic	0.1036	0.0030	
		Established	0.0001	0.2478	0.0998
July	< 0.001	Invasion	0.4284		
		Epidemic	0.0005	0.0008	
		Established	1	0.3665	1
August	< 0.001	Invasion	1		
		Epidemic	0.0351	1	
		Established	0.2026	1	1

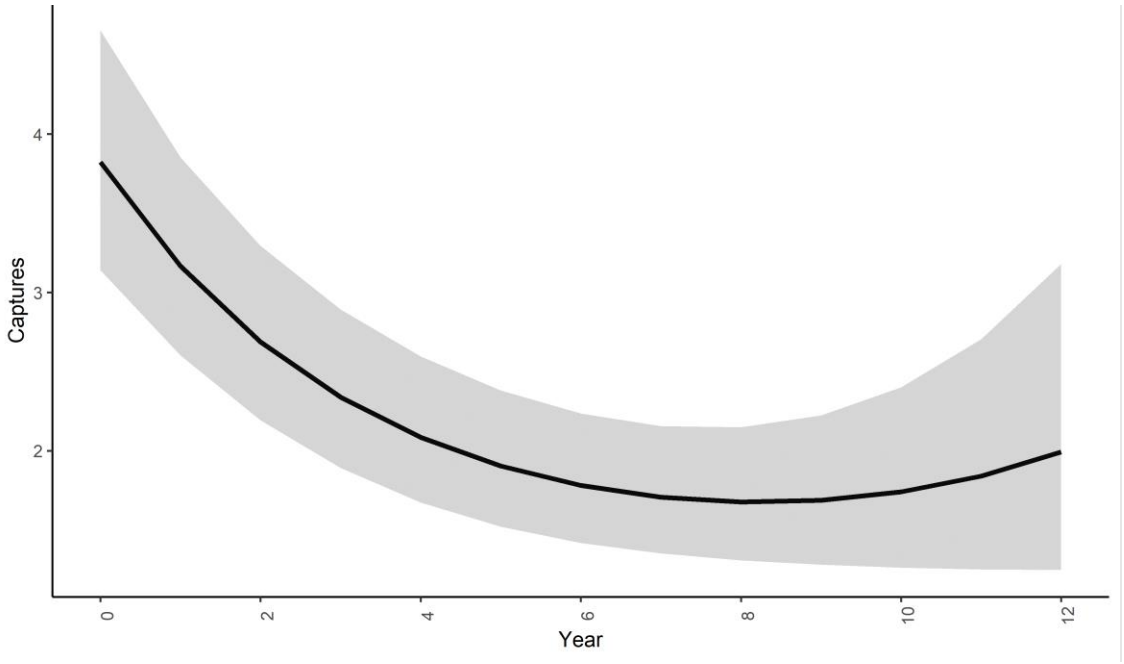

Figure A3. Model predicted relationship (and 95% confidence intervals) between year since arrival of white-nose syndrome and little brown bat (*Myotis lucifugus*) site-night captures from the continental United States 1999 – 2019 based on generalized linear mixed models.

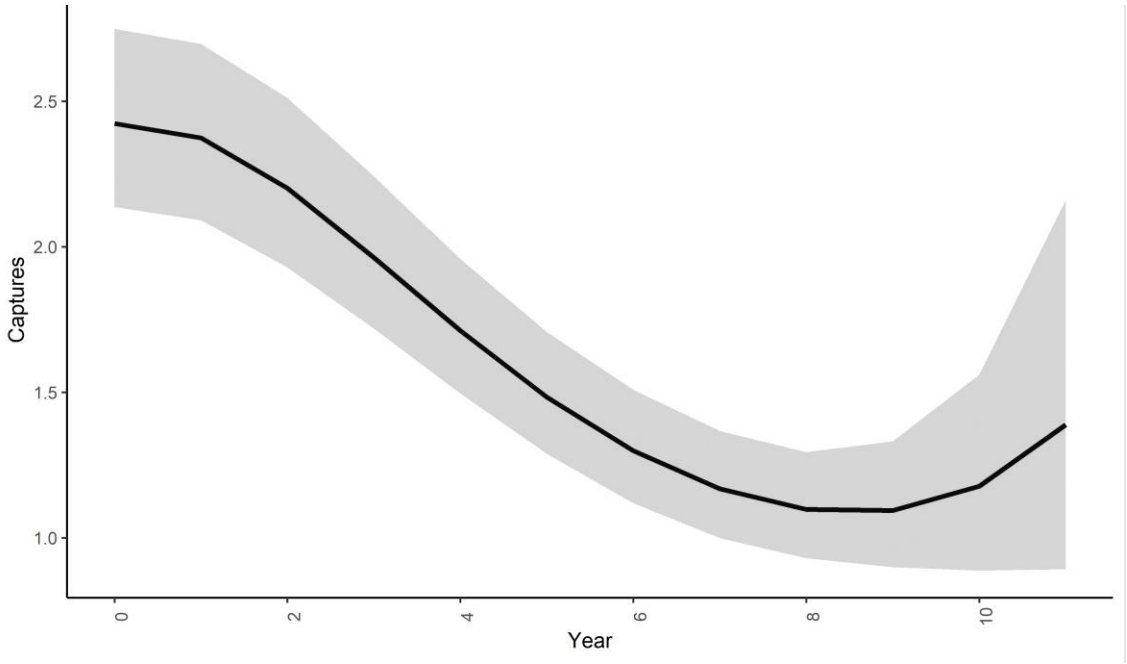

Figure A4. Model predicted relationship (and 95% confidence intervals) between year since arrival of white-nose syndrome and northern long-eared bat (*Myotis septentrionalis*) site-night captures from the continental United States 1999 – 2019 based on generalized linear mixed models.

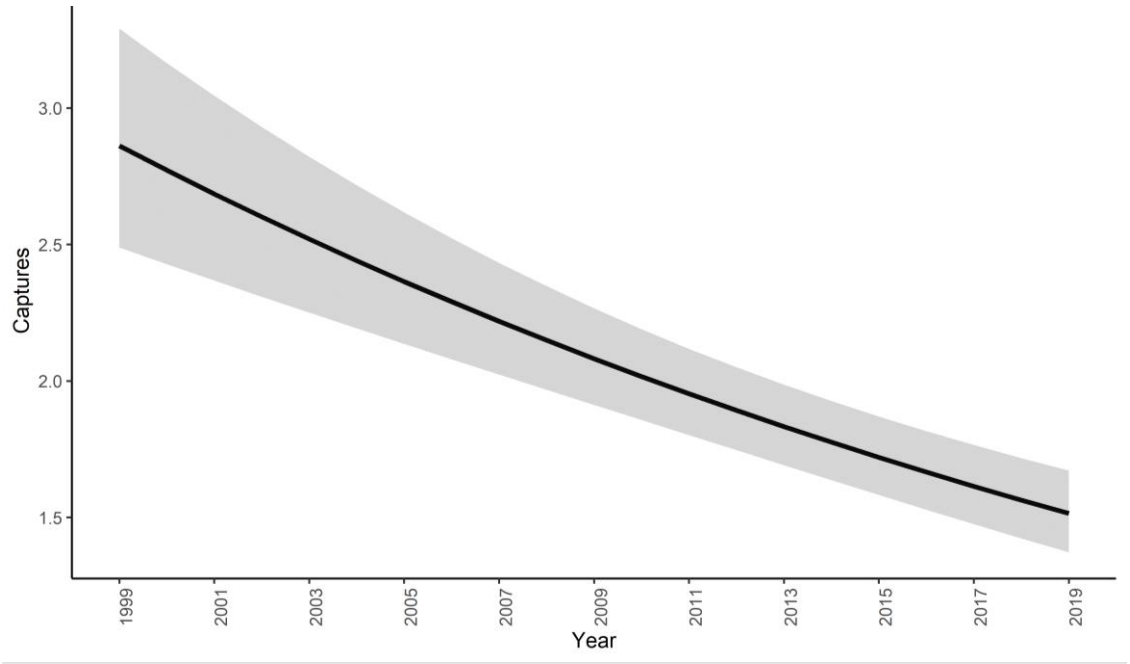

Figure A5. Model predicted relationship (and 95% confidence intervals) between year of capture and tricolored bat (*Perimyotis subflavus*) site-night captures from the continental United States 1999 – 2019 based on generalized linear mixed models.

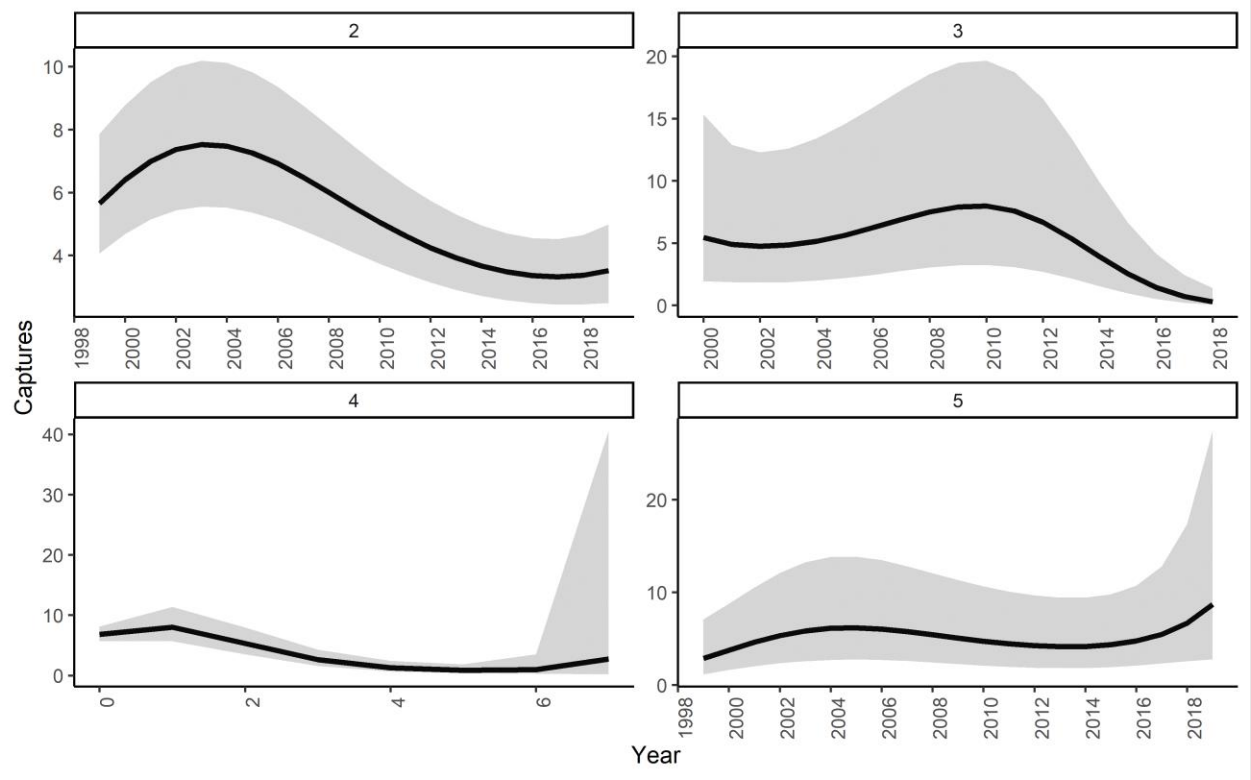

Figure A6. Model predicted relationship (and 95% confidence intervals) between year of capture (RPU 2, 3, and 5) and year since the arrival of white-nose syndrome (RPU 4) and little brown bat (Myotis lucifugus) based on site-night captures from the continental United States 1999 – 2019 based on generalized linear mixed models. U.S. Fish and Wildlife Service Representation Unit (RPU) as defined by the U.S. Fish and Wildlife Service.

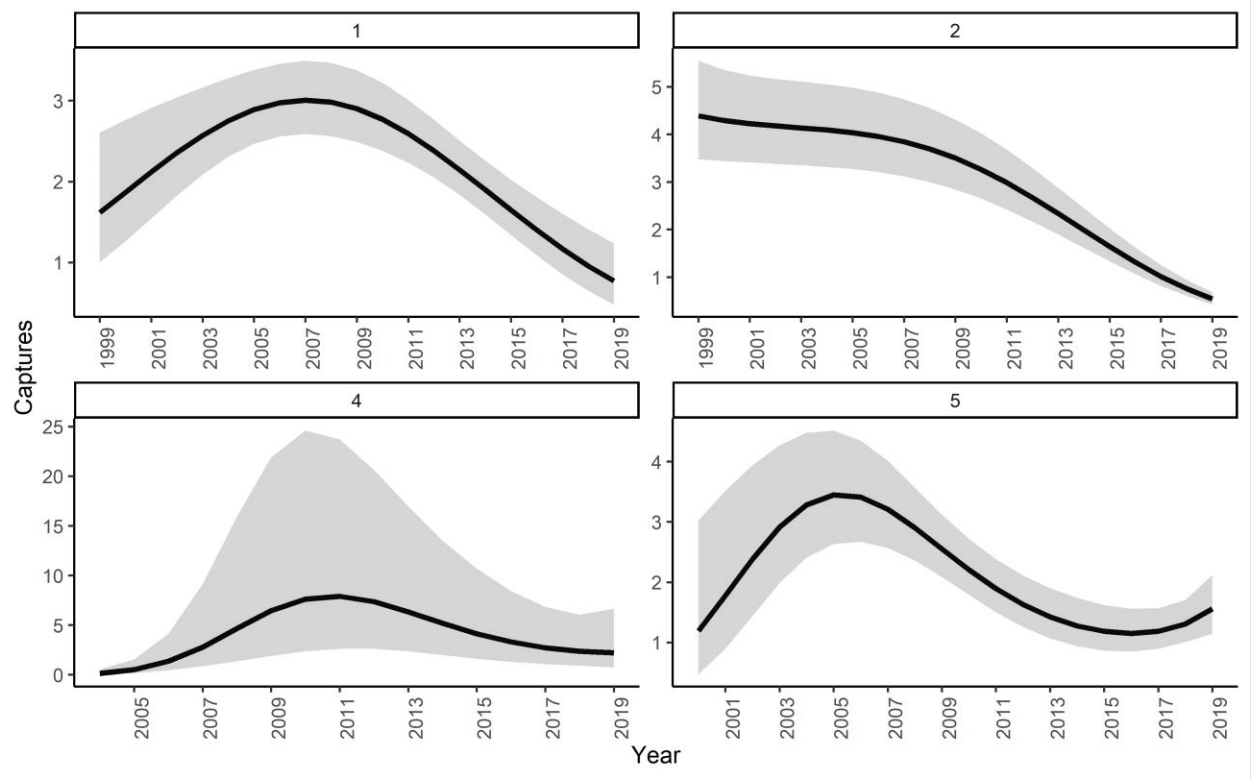

Figure A7. Model predicted relationship (and 95% confidence intervals) between year of capture and northern long-eared bats (*Myotis septentrionalis*) site-night captures by RPU (1, 2, 4, and 5) from the continental United States 1999 – 2019 based on generalized linear mixed models. Representation Unit (RPU) as defined by the U.S. Fish and Wildlife Service.

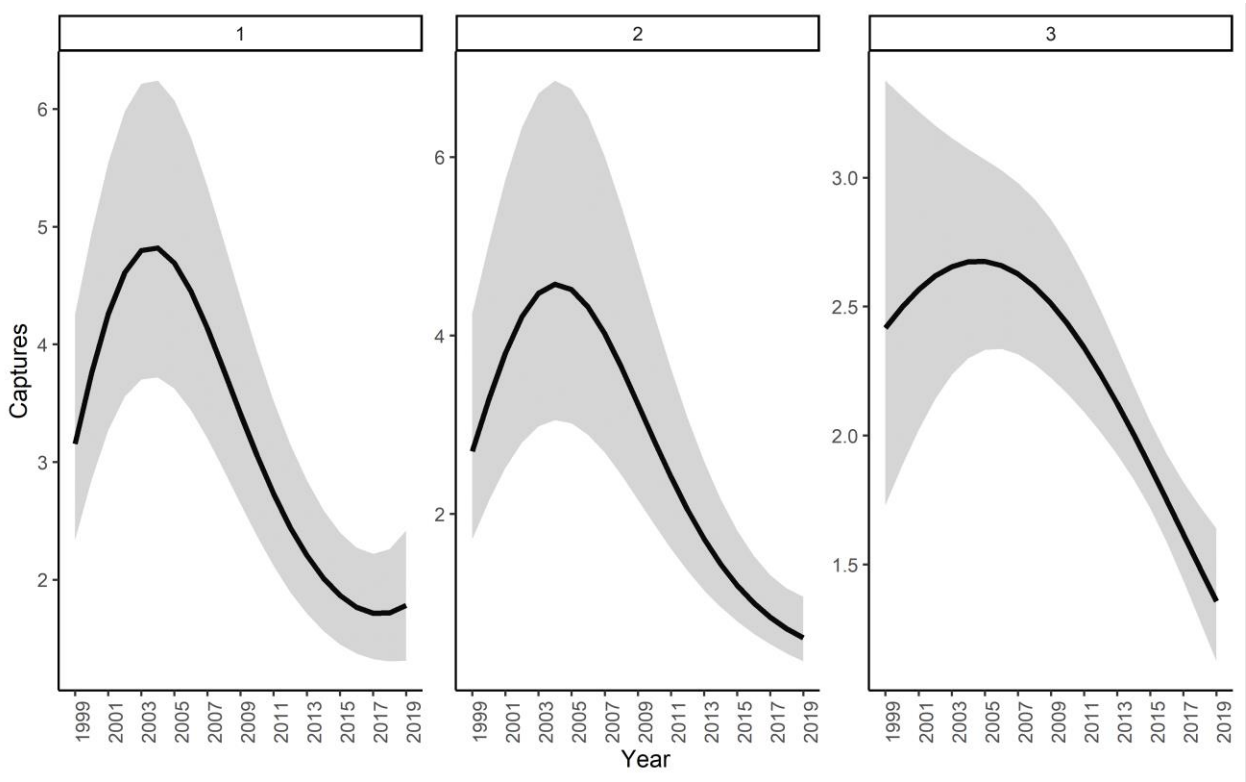

Figure A8. Model predicted relationship (and 95% confidence intervals) between year of capture (RPU 1 - 3) and tricolored bats (*Perimyotis subflavus*) site-night captures from the continental United States 1999 – 2019 based on generalized linear mixed models. Representation Unit (RPU) as defined by the U.S. Fish and Wildlife Service.

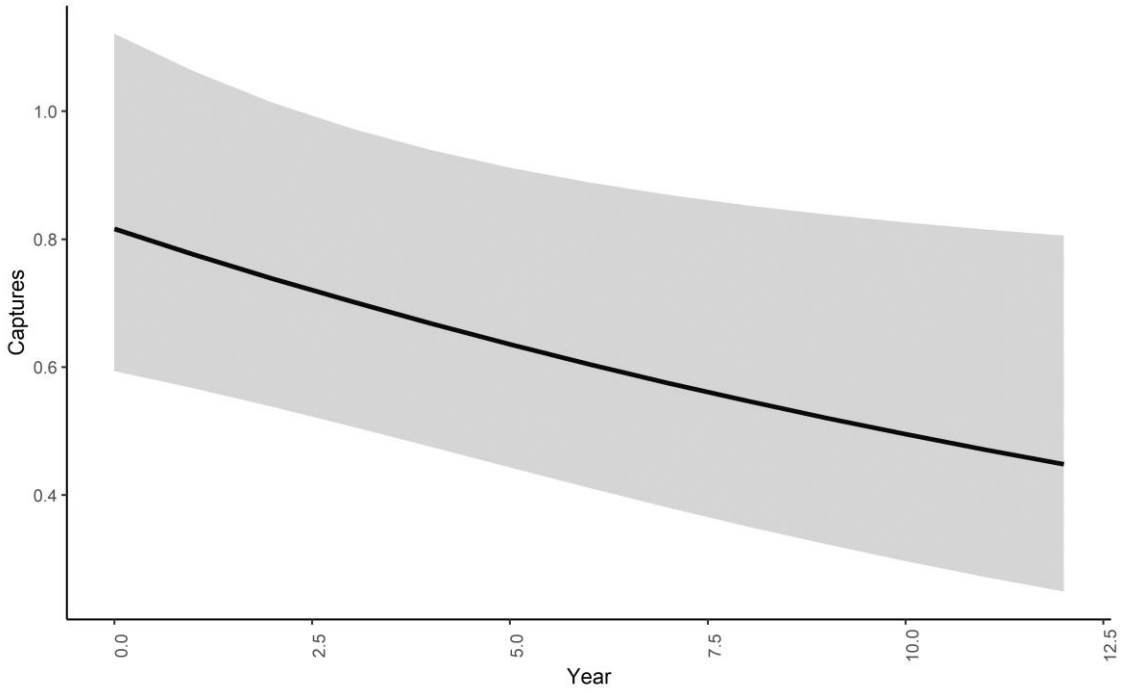

Figure A9. Model predicted relationship (and 95% confidence intervals) between year since the arrival of white-nose syndrome and juvenile little brown bats (*Myotis lucifugus*) site-night captures from the continental United States 1999 – 2019 based on generalized linear mixed models.

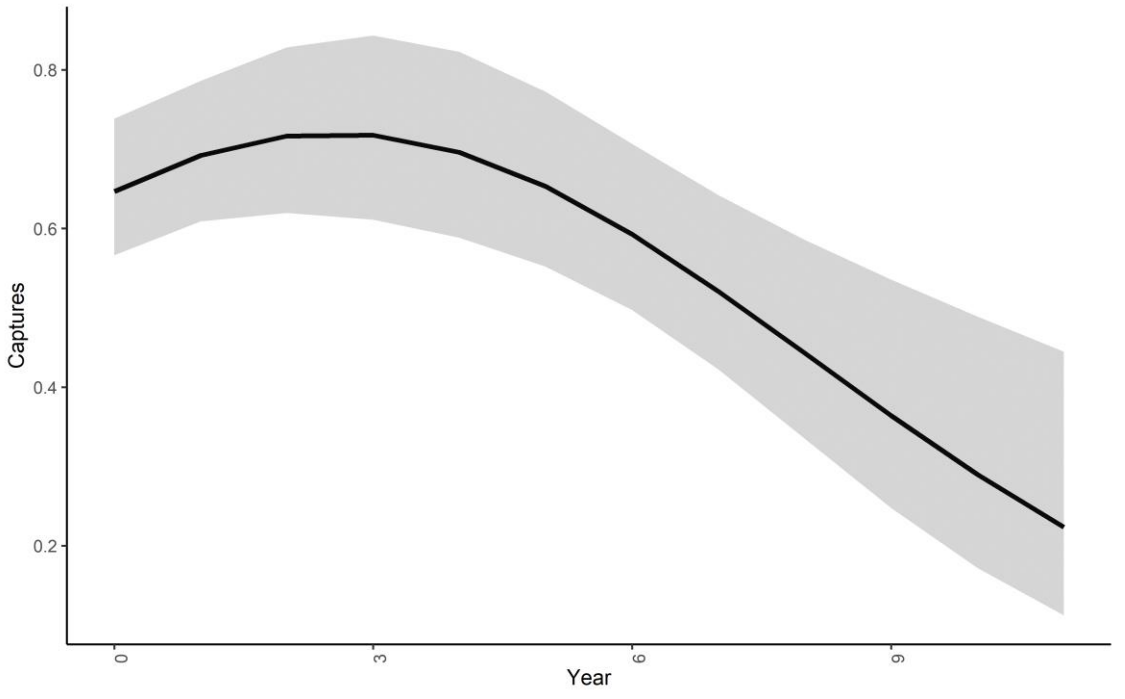

Figure A10. Model predicted relationship (and 95% confidence intervals) year since the arrival of white-nose syndrome and juvenile northern long-eared bats (*Myotis septentrionalis*) site-night captures from the continental United States 1999 – 2019.

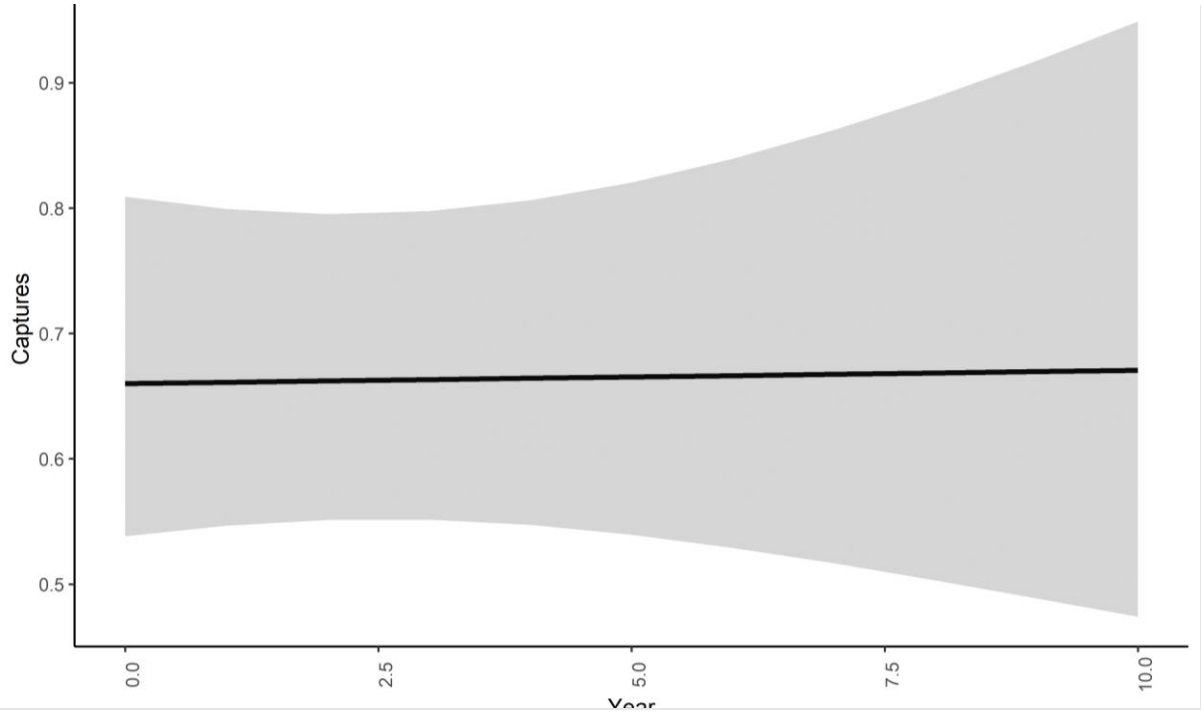

Figure A11. Model predicted relationship (and 95% confidence intervals) between year since the arrival of white-nose syndrome and juvenile tricolored bats (*Perimyotis subflavus*) site-night captures from the continental United States 1999 – 2019 based on generalized linear mixed models.

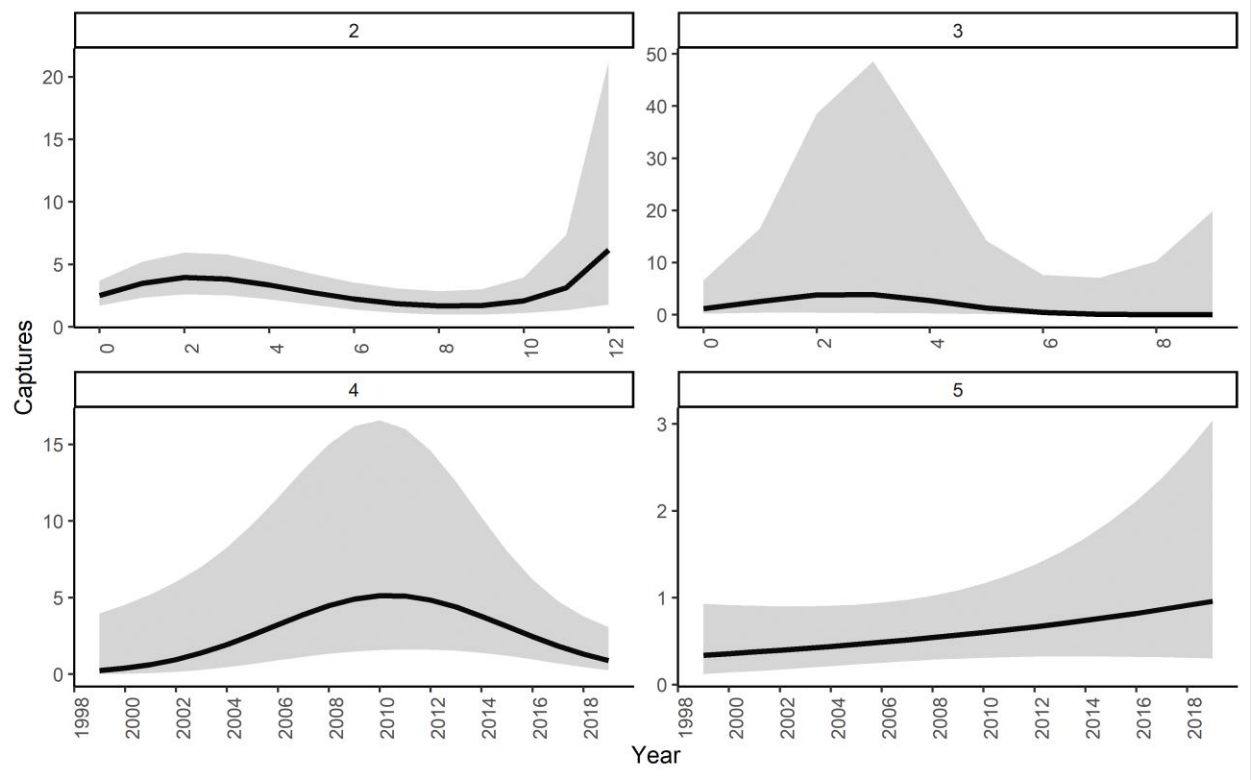

Figure A12. Model predicted relationship (and 95% confidence intervals) between year of capture (RPU 4 and 5) and year since the arrival of white-nose syndrome (RPU 2 and 3) and juvenile little brown bat (*Myotis lucifugus*) site-night captures from the continental United States 1999 – 2019 based on generalized linear mixed models. Representation Unit (RPU) as defined by the U.S. Fish and Wildlife Service.

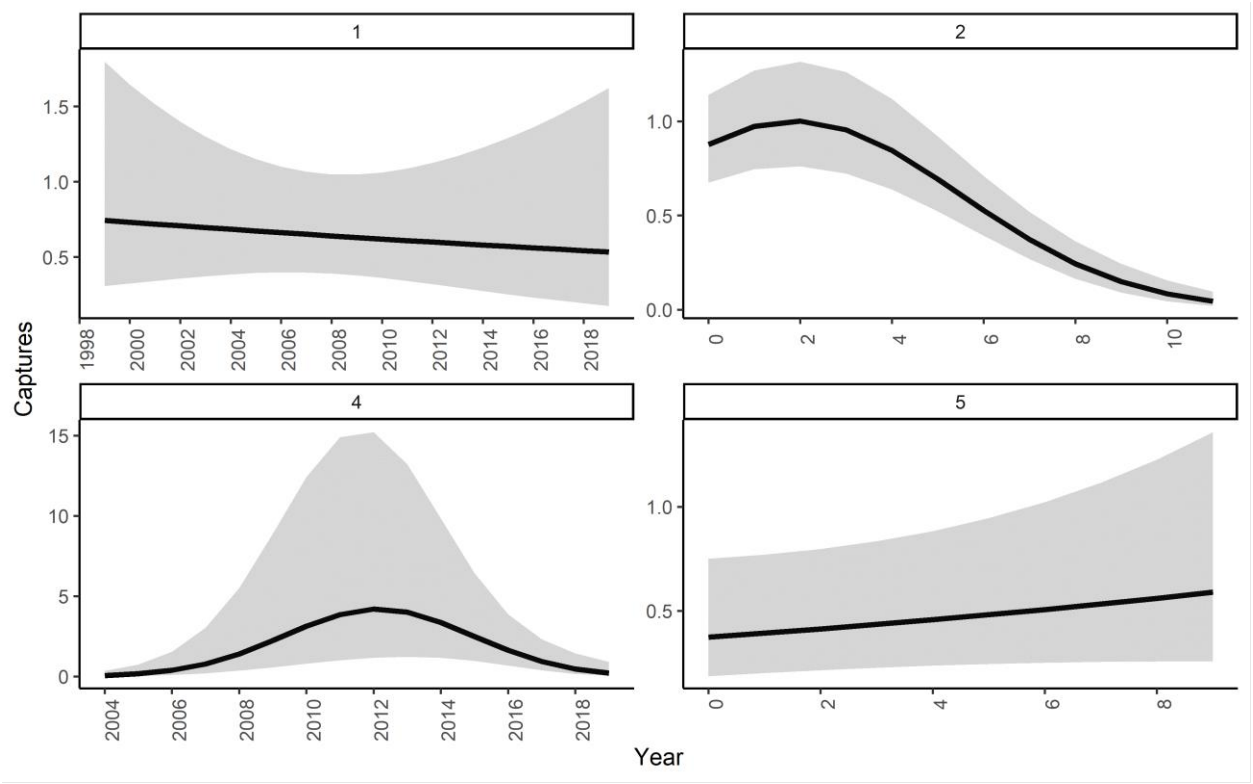

Figure A13. Model predicted relationship (and 95% confidence intervals) between year since the arrival of white-nose syndrome (RPU 2 and 5) or year of capture (RPU 1 and 4) and northern long-eared bats (*Myotis septentrionalis*) site-night captures from the continental United States 1999 – 2019. Representation Unit (RPU) as defined by the U.S. Fish and Wildlife Service.

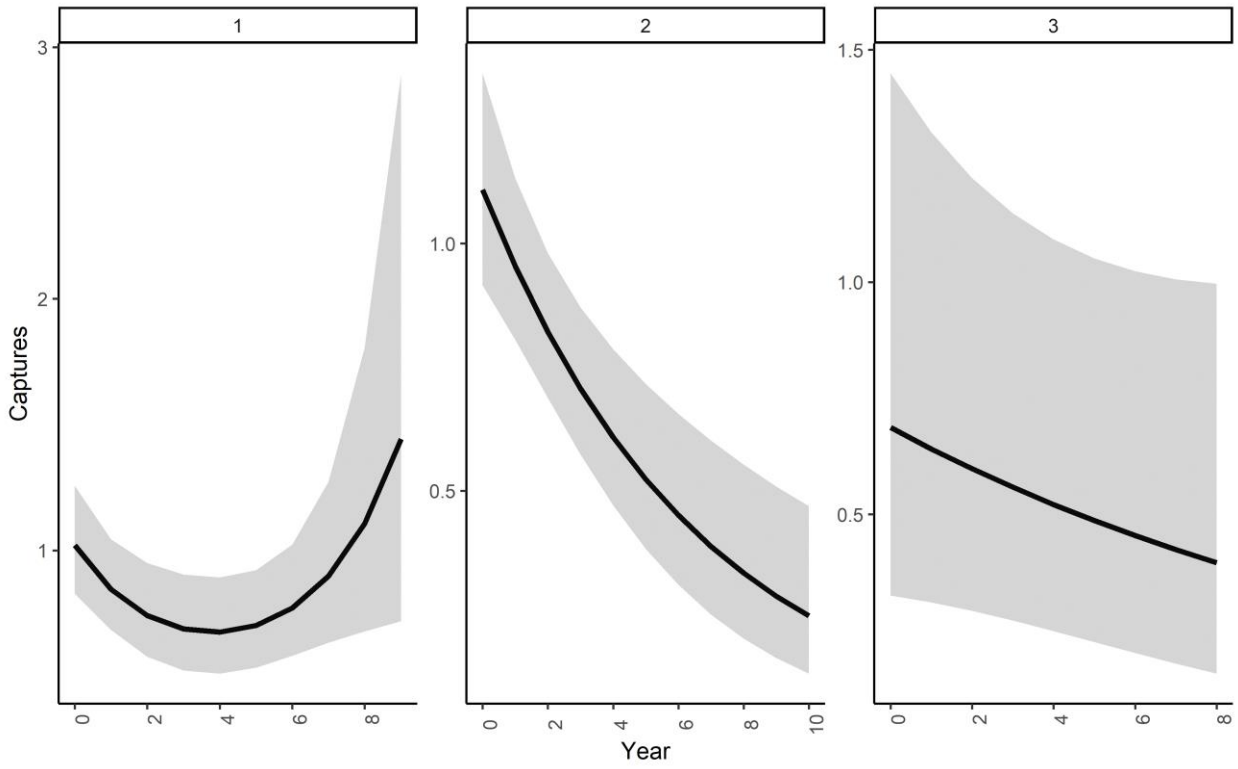

Figure A14. Model predicted relationship (and 95% confidence intervals) between year of capture (RPU 2) year since the arrival of white-nose syndrome (RPU 1 and 3) and juvenile tricolored bats (*Perimyotis subflavus*) site-night captures from the continental United States 1999 – 2019. Representation Unit (RPU) as defined by the U.S. Fish and Wildlife Service.

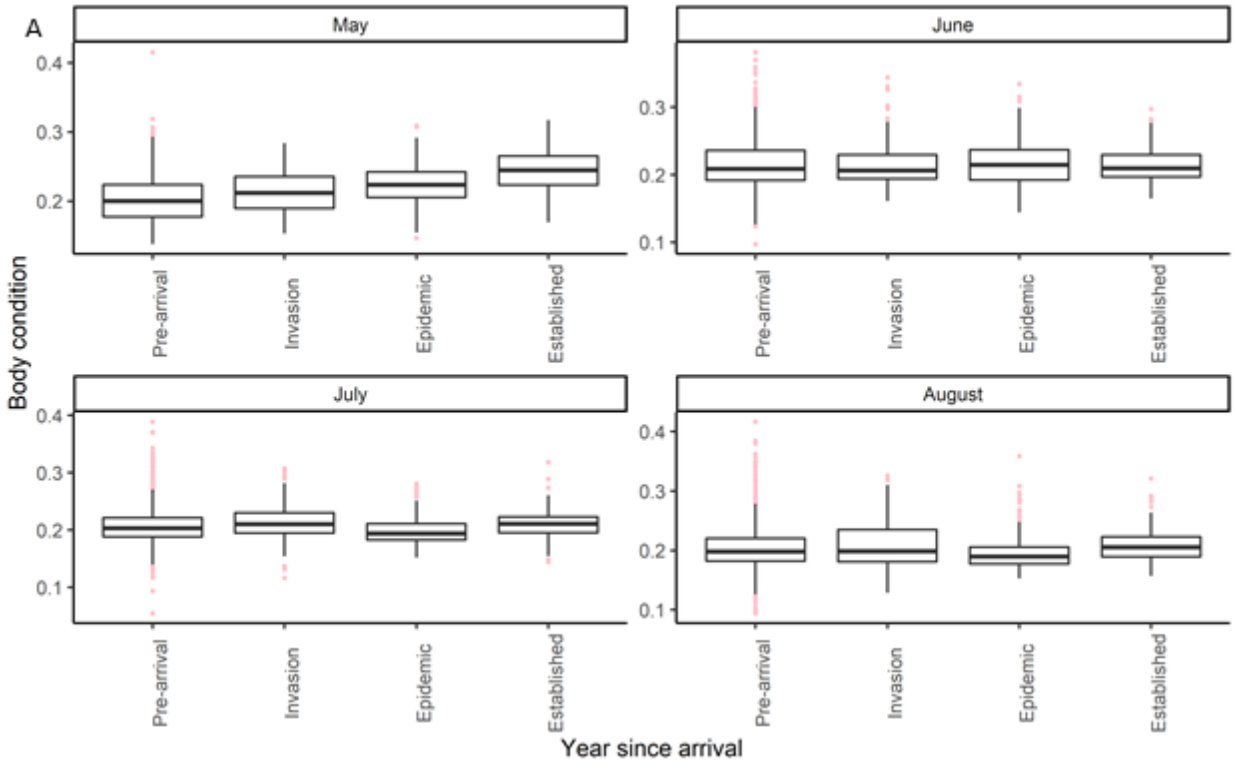
A
May
June
July
August
Body condition
Pre-arrival
Invasion
Epidemic
Established
Year since arrival

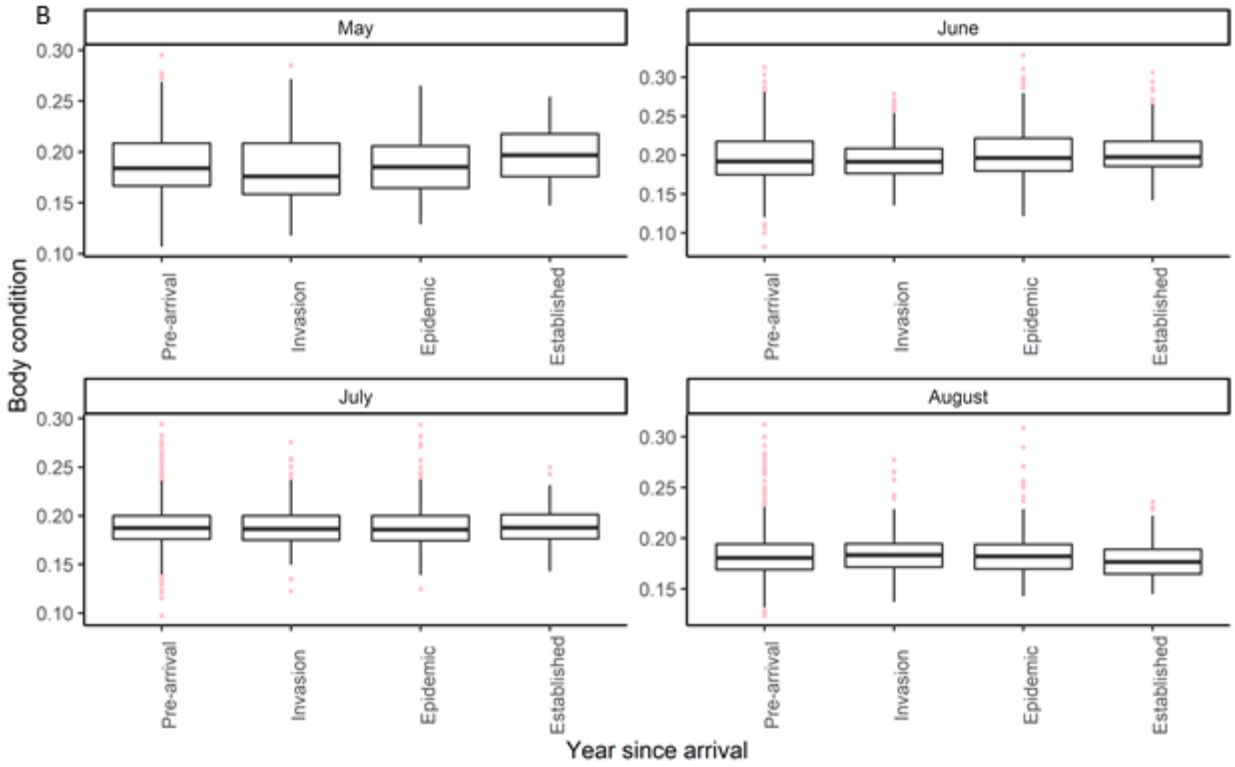
B
May
June
July
August
Body condition
Pre-arrival
Invasion
Epidemic
Established
Year since arrival

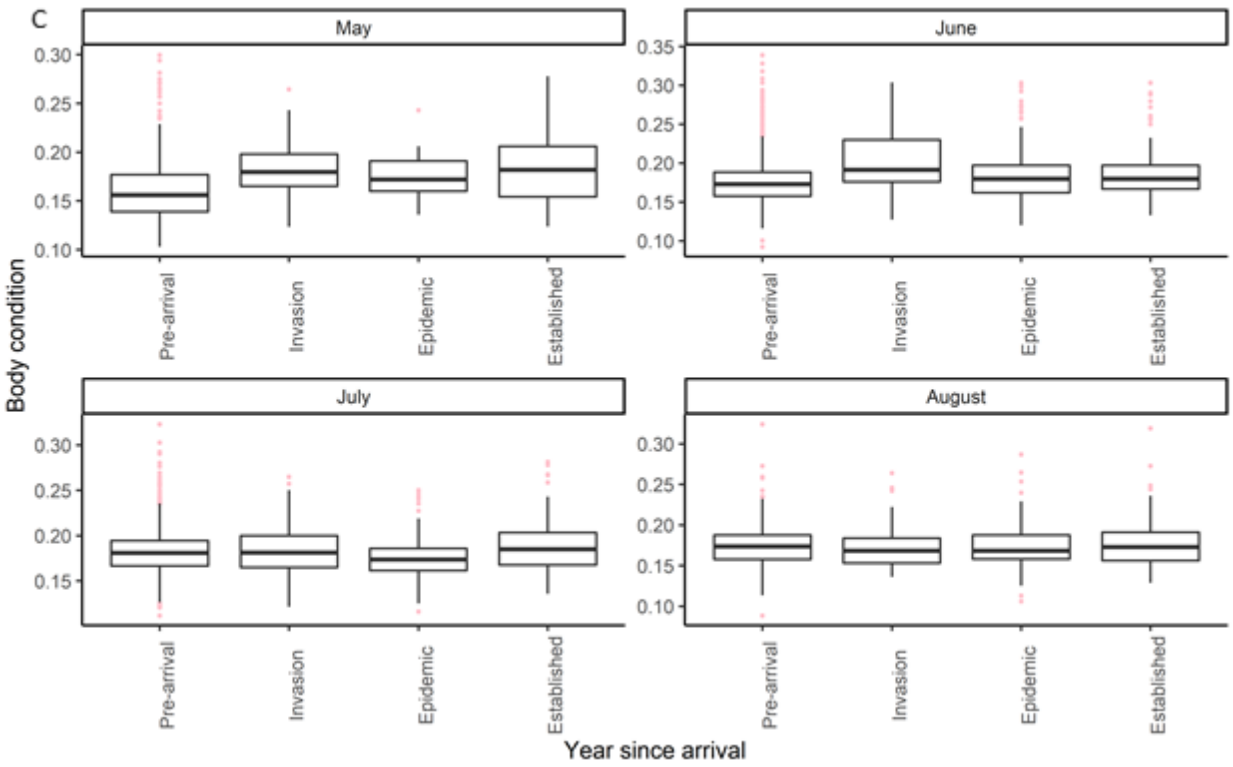

Figure A15. Boxplots displaying body condition metrics ([body mass]/forearm) of A) little brown bat (*Myotis lucifugus*), B) northern long-eared bat (*Myotis septentrionalis*), and C) tricolored bat (*Perimyotis subflavus*) captured within the continental United States 1999 – 2019. Box plots depict the minimum, first quartile, median, third quartile, and maximum, with outliers depicted as single points.

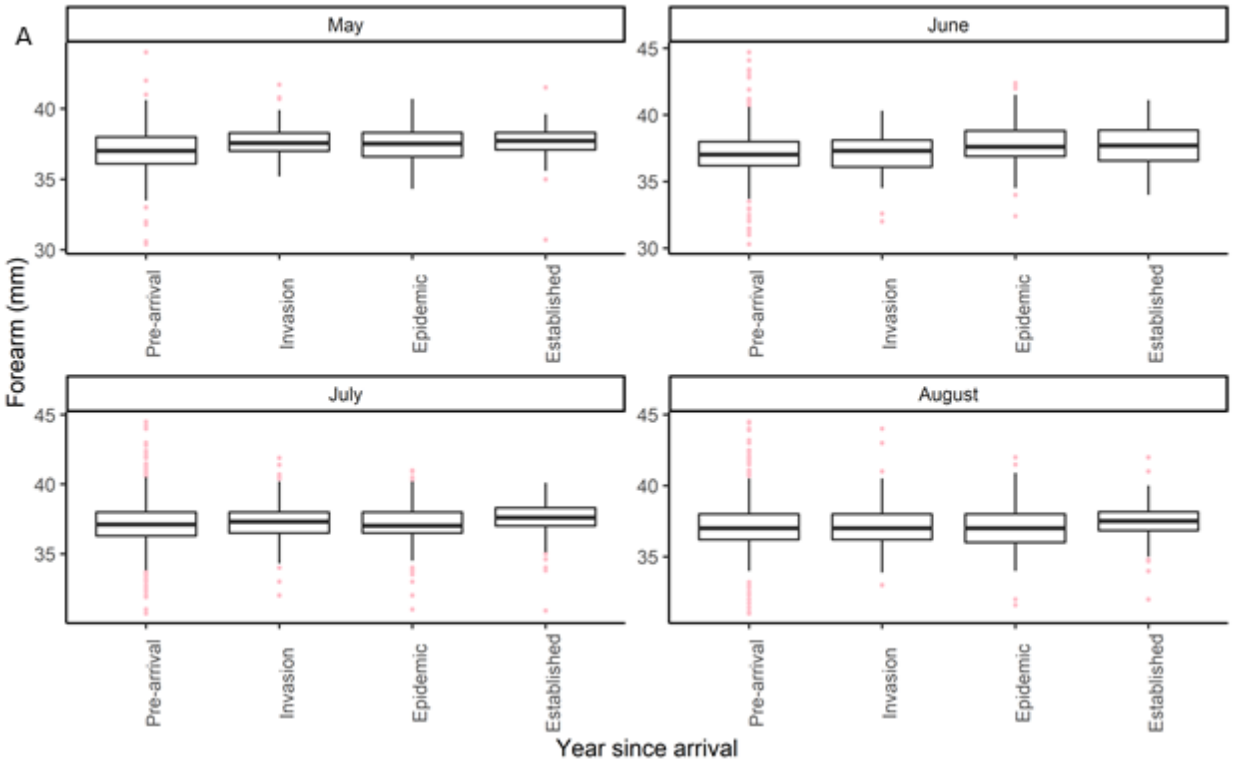
A
May
June
July
August
Forearm (mm)
Pre-arrival
Invasion
Epidemic
Established
Year since arrival

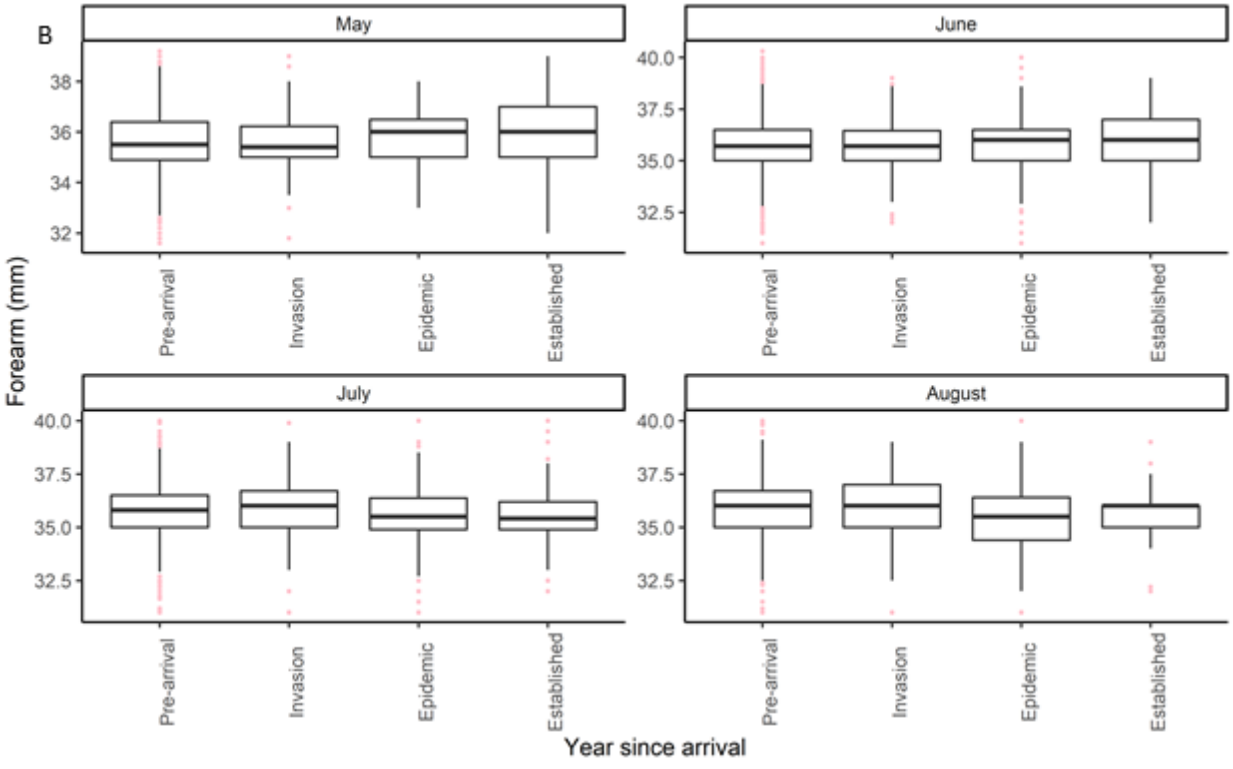
B
May
June
July
August
Forearm (mm)
Pre-arrival
Invasion
Epidemic
Established
Year since arrival

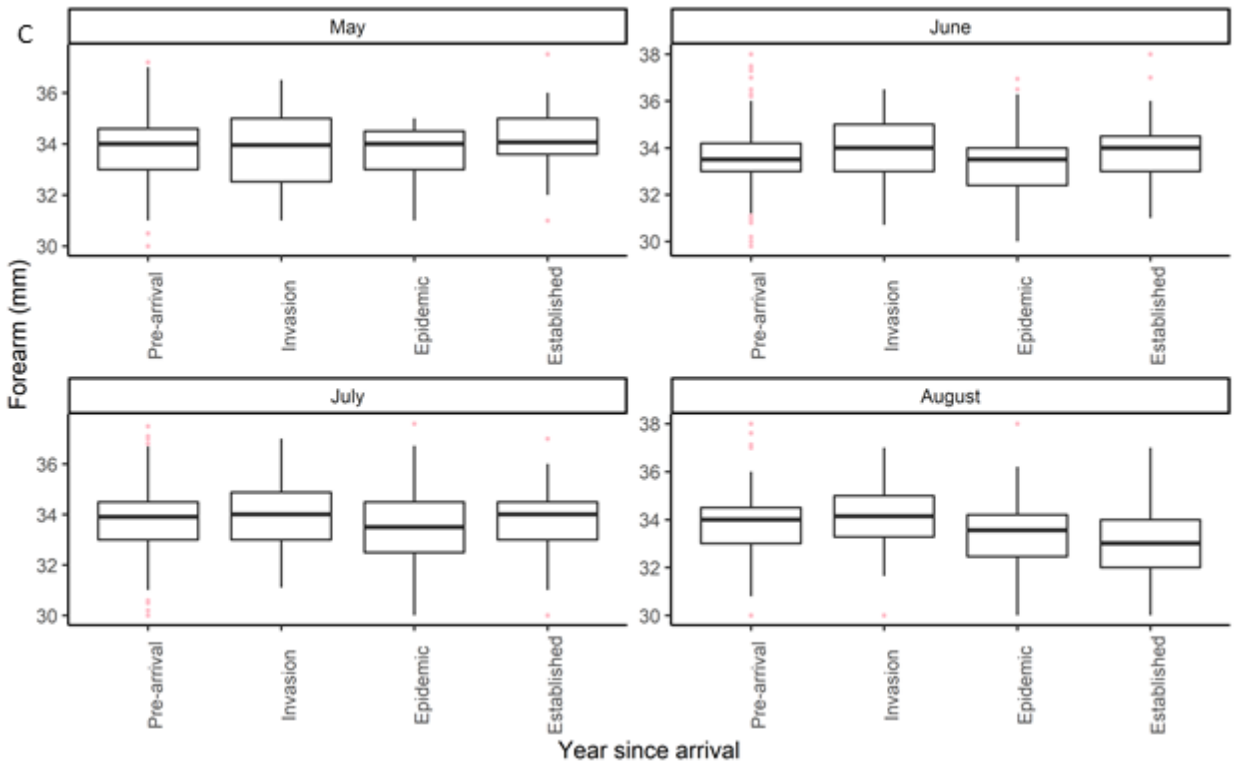

Figure A16. Boxplots displaying forearm measurements (mm = millimeter) for A) little brown bat (*Myotis lucifugus*), B) northern long-eared bat (*Myotis septentrionalis*), and C) tricolored bat (*Perimyotis subflavus*) captured within the continental United States 1999 – 2019. Box plots depict the minimum, first quartile, median, third quartile, and maximum, with outliers depicted as single points.

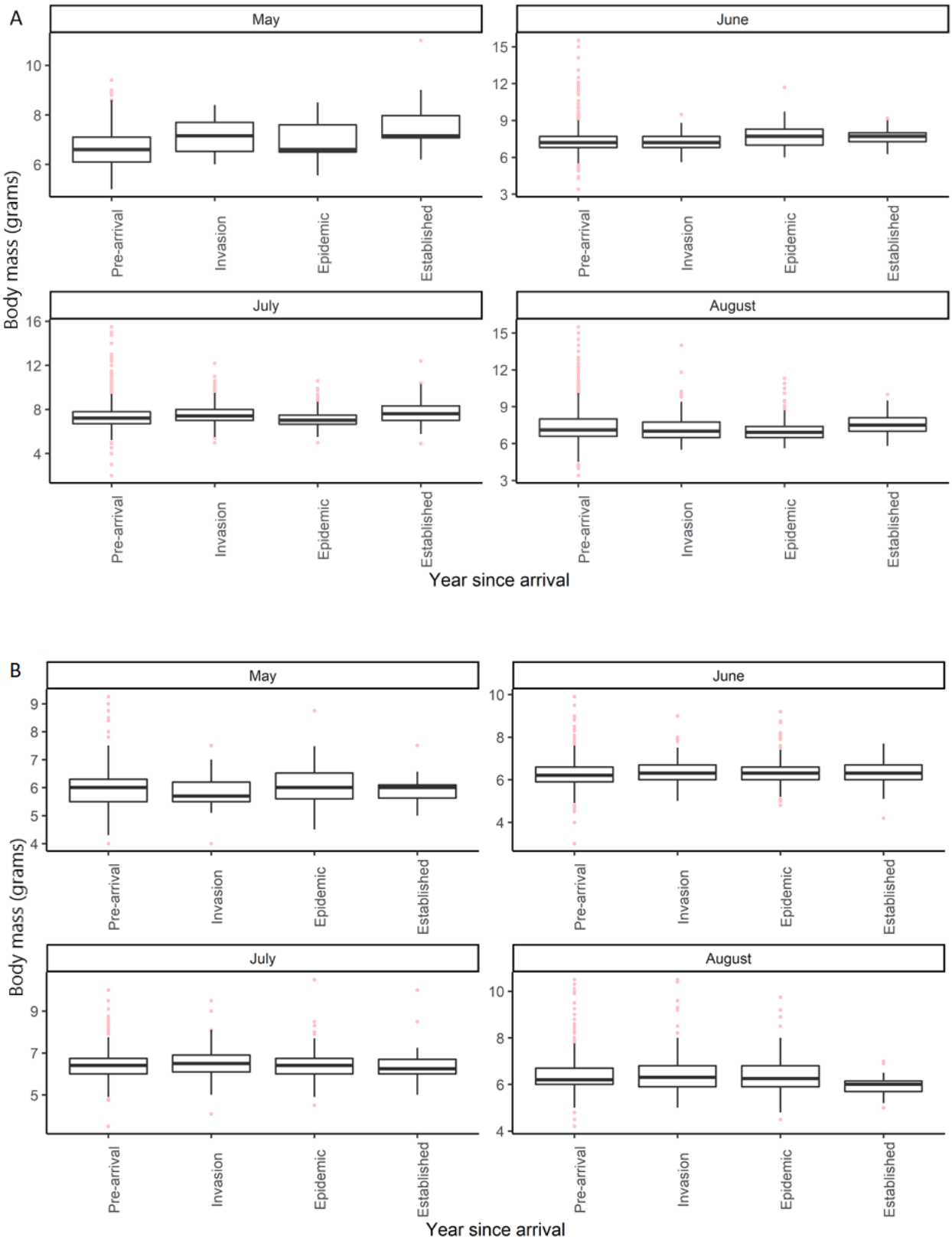
A
May
June
July
August
Body mass (grams)
Pre-arrival
Invasion
Epidemic
Established
Year since arrival
B
May
June
July
August
Body mass (grams)
Pre-arrival
Invasion
Epidemic
Established
Year since arrival

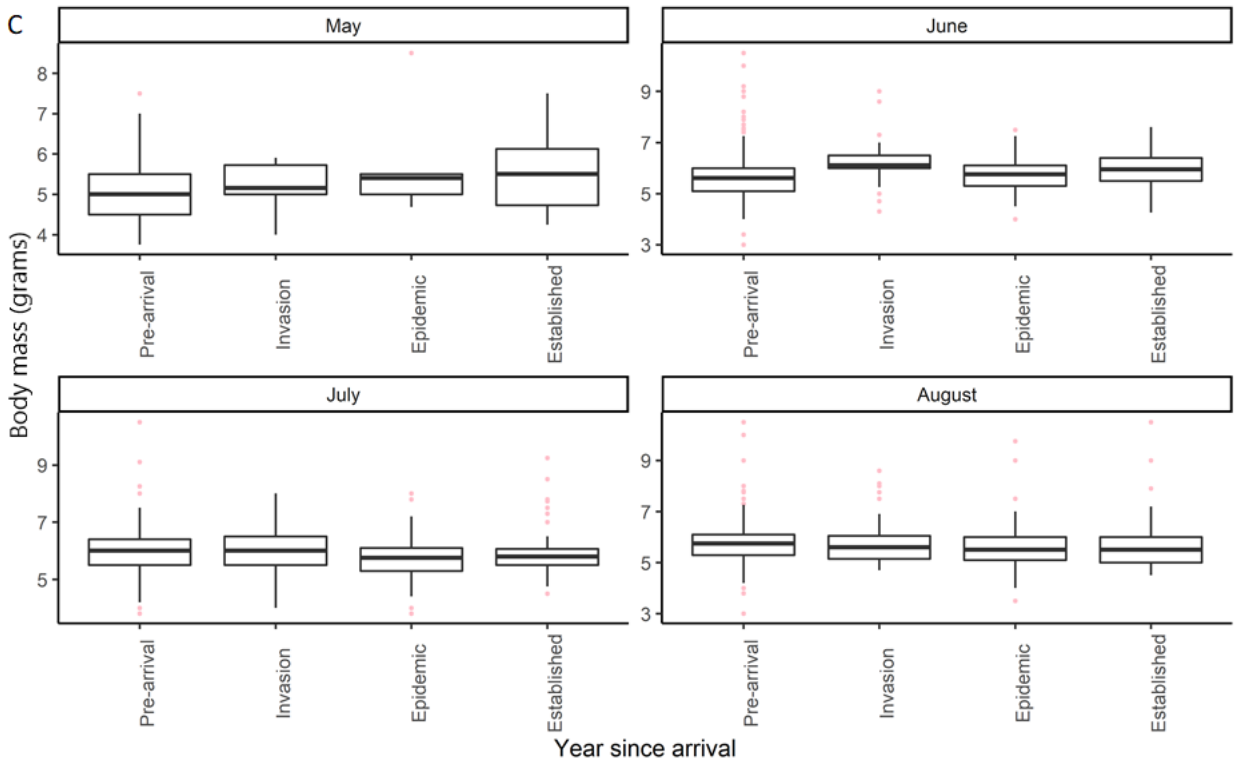

Figure A15. Mass measurements (grams) for adult male A) little brown bat (*Myotis lucifugus*), B) northern long-eared bat (*Myotis septentrionalis*), and C) tricolored bat (*Perimyotis subflavus*) captured within the continental United States 1999 – 2019. Box plots depict the minimum, first quartile, median, third quartile, and maximum, with outliers depicted as single points.

References Cited

Altringham, J. D. 2011. Bats: From Evolution to Conservation. Oxford University Press.

Cheng, T. L., A. Gerson, M. S. Moore, J. D. Reichard, J. DeSimone, C. K. R. Willis, W. F. Frick, and A. M. Kilpatrick. 2019. Higher fat stores contribute to persistence of little brown bat populations with white-nose syndrome. A. Tate, editor. Journal of Animal Ecology 88:591–600.

Deeley, S.M., and Ford, W.M., 2021, Pre- and post-White-nose Syndrome Bat Capture Models: U.S. Geological Survey data release, https://doi.org/10.5066/P9YDMOMH.

Deeley, Sabrina; Ford, William (2022), Capture data summary statistics reported as part of the Assessment of USFWS Capture Data for Little Brown, Northern Long-eared and Tricolored Bat Species Status Assessment, Dryad, Dataset, https://doi.org/10.5061/dryad.kwh70rz53

Florian, H. 2020. DHARMa: Residual Diagnostics for Hierarchical (Multi-Level / Mixed) Regression Models. https://CRAN.R-project.org/package=DHARMa.

Francl, K. E., W. M. Ford, D. W. Sparks, and V. Brack. 2012. Capture and reproductive trends in summer bat communities in West Virginia: Assessing the impact of white-nose syndrome. Journal of Fish and Wildlife Management 3:33–42.

Frick, W. F., D. S. Reynolds, and T. H. Kunz. 2010. Influence of climate and reproductive timing on demography of little brown myotis Myotis lucifugus. Journal of Animal Ecology 79:128–136.

Ingersoll, T. E., B. J. Sewall, and S. K. Amelon. 2013. Improved analysis of long-term monitoring data demonstrates marked regional declines of bat populations in the eastern United States. PLoS ONE 8:e65907.

Kruskal, W. H., and W. A. Wallis. 1952. Use of Ranks in One-Criterion Variance Analysis. Journal of the American Statistical Association 47:583–621. Taylor & Francis.

Kunz, T. H., J. A. Wrazen, and C. D. Burnett. 1998. Changes in body mass and fat reserves in pre-hibernating little brown bats (*Myotis lucifugus*). Ecoscience 5:8–17. Taylor & Francis.

Lacki, M. J., L. E. Dodd, R. S. Toomey, S. C. Thomas, Z. L. Couch, and B. S. Nichols. 2015. Temporal Changes in Body Mass and Body Condition of Cave-Hibernating Bats During Staging and Swarming. Journal of Fish and Wildlife Management 6:360–370.

Langwig, K. E., J. Voyles, M. Q. Wilber, W. F. Frick, K. A. Murray, B. M. Bolker, J. P. Collins, T. L. Cheng, M. C. Fisher, J. R. Hoyt, D. L. Lindner, H. I. McCallum, R. Puschendorf, E. B. Rosenblum, M. Toothman, C. K. Willis, C. J. Briggs, and A. M. Kilpatrick. 2015. Context-dependent conservation responses to emerging wildlife diseases. Frontiers in Ecology and the Environment 13:195–202.

Magnusson, A., H. Skaug, A. Nielsen, C. Berg, K. Kristensen, K. van Bentham, B. Bolker, N. Sadar, D. Luedecke, R. Lenth, J. O'Brien, and M. Brooks. 2020. Generalized Linear Mixed Models using Template Model Builder. https://github.com/glmmTMB/glmmTMB.

Pearce, R. D., T. J. O'Shea, and B. A. Wunder. 2008. Evaluation of morphological indices and total body electrical conductivity to assess body composition in big brown bats. Acta Chiropterologica 10:153–159.

Pebesma, E. 2018. Simple Features for R: Standardized Support for Spatial Vector Data. The R Journal 10:439–446.

Pettit, J. L., and J. M. O'Keefe. 2017. Impacts of white-nose syndrome observed during long-term monitoring of a midwestern bat community. Journal of Fish and Wildlife Management 8:69–78.

R Core Team. 2020. R: A language and environment for statistical computing. Vienna, Austria. http://www.R-project.org/.

Reeder, D. M., C. L. Frank, G. G. Turner, C. U. Meteyer, A. Kurta, E. R. Britzke, M. E. Vodzak, S. R. Darling, C. W. Stihler, A. C. Hicks, R. Jacob, L. E. Grieneisen, S. A. Brownlee, L. K. Muller, and D. S. Blehert. 2012. Frequent arousal from hibernation linked to severity of infection and mortality in bats with white-nose syndrome. PLoS ONE 7:e38920.

Reynolds, R. J., K. E. Powers, W. Orndorff, W. M. Ford, and C. S. Hobson. 2016. Changes in rates of capture and demographics of Myotis septentrionalis (northern long-eared bat) in Western Virginia before and after onset of white-nose syndrome. Northeastern Naturalist 23:195–204.

U.S. Fish and Wildlife Service. 2019. Where is it now? <https://www.whitenosesyndrome.org>. Accessed 3 Dec 2020.

U.S. Fish and Wildlife Service. 2020. Range-wide Indiana bat survey guidelines. https://www.fws.gov/midwest/endangered/mammals/inba/surveys/Pdf/FINAL%20Range-wide%20IBat%20Survey%20Guidelines%203.23.20.Pdf.

U.S. Geological Survey. 2020. U.S. Geological Survey North American Bat Monitoring Program. Database Version v5.3.11, NABat Request Number 10.

Wiens, A. and W.E. Thogmartin. 2021. In Support of the U.S. Fish and Wildlife Service 3-Bat Species Status Assessment: Gaussian Process Model Predictions for the Spread of White-Nose Syndrome across North America, https://doi:10.5066/P9RP7J4H.

Wilcoxon, F. 1945. Individual Comparisons by Ranking Methods. Biometrics Bulletin 1:80–83.

Chapter B. Summertime Analysis Statistical Report for Little Brown, Northern Long-eared and Tricolored Bat Species Status Assessment

By Christian Stratton[1], and Kathryn M. Irvine[2]

Introduction

We provide an overview of the false positive occupancy analysis for the summertime data provided to support the three bat species status assessment (SSA) for *Myotis lucifugus* (MYLU), *Myotis septentrionalis* (MYSE), and *Perimyotis subflavus* (PESU). The objectives outlined by the U.S. Fish and Wildlife Service's SSA team were to:

- estimate summertime distributions across the entire species range; and
- provide estimates of population annual rate of change in summertime occupancy λ within pre-defined spatial sub-regions within a species range.

We describe the available data types in the section 'Review of Available Datasets for Summertime Analysis' and the available modeling techniques based on the peer-reviewed literature in the section 'Statistical Methods Considered Overview.' We also provide a summary of the model fit to these data in the section 'Statistical Method Used for SSA Summertime Analysis' and results in the section 'Summertime Analysis Results.' Our intent is to provide the best available information to the USFWS given the time constraints of the work (dataset was considered finalized December 1, 2020 (NABat 2020)). One key feature of the analytic techniques that we considered was that they all included incorporating false positive detections. In our case, a false positive detection arises because the autoclassification software (e.g.,

[1] Montana State University, Deptartment of Mathematical Sciences, Bozeman MT 59717
[2] U.S. Geological Survey, N. Rocky Mountain Science Center, Bozeman MT 59717

Sonobat, Kaleidoscope) applied to bat echolocation call recording assigns the incorrect species. Failing to account for false positives in a statistical model can result in biased estimates for occupancy (Clement et al. 2014, Banner et al. 2018). Another consideration was the ambiguity regarding the sampling design used to select the NABat grid cells that have available data. The North American Bat Monitoring Program (NABat) sampling design is a spatially balanced master sample based on using the so called GRTS (Generalized Random Tessellation Stratified) design; however, data contributors may not have been using the NABat design to select sites for surveying bats. A "site" is a NABat cell (10 km x 10 km), which we consider as the analysis unit (e.g., grain size). Because the sampled grid cells could be the result of purposive or non-probability sampling, the available data may not be representative of the summertime distribution for these species and the estimated occupancy-environment relationships used to predict distributions could be biased (Irvine et al. 2018). Further, in some cases, the process leading to a manually vetted detection record for a species based on recording bat echolocation calls is also not clear. Since users of the NABat database were not required to include information on their vetting process, it is not possible to determine which automatically identified acoustic records were manually vetted. As a result, we cannot separate call files that were manually vetted to be 0 (i.e., represent a confirmed non-detection) from records that were not manually vetted at all (and should really be thought of as NA (not available) or missing values). Therefore, we cannot treat the manually vetted call files as detection/non-detection data and must instead treat them as detection only data. The structure of the dataset has implications for the modeling techniques that were available to us as discussed in the section 'Considerations of applicability of different false positive occupancy models for SSA analysis.'

Review of Available Datasets for Summertime Analysis

Response data types

For our analysis, we had five types of response data available: automatically identified stationary acoustic calls (section ‘Automatically identified stationary acoustic calls’), manually vetted stationary acoustic calls (section ‘Manually vetted acoustic calls’), automatically identified mobile acoustic calls (section ‘Automatically identified mobile acoustic calls’), manually vetted mobile acoustic calls (section ‘Manually vetted acoustic calls’), and capture records (section ‘Capture records’). Below, we describe each of these data sources in greater detail, combining the manually vetted calls (mobile and stationary) into a single category (section ‘Manually vetted acoustic calls’). Note that since our analysis was for the summertime distribution modeling portion of the SSA, we will only consider data collected between the morning of June 1 through the evening of Sept 1.

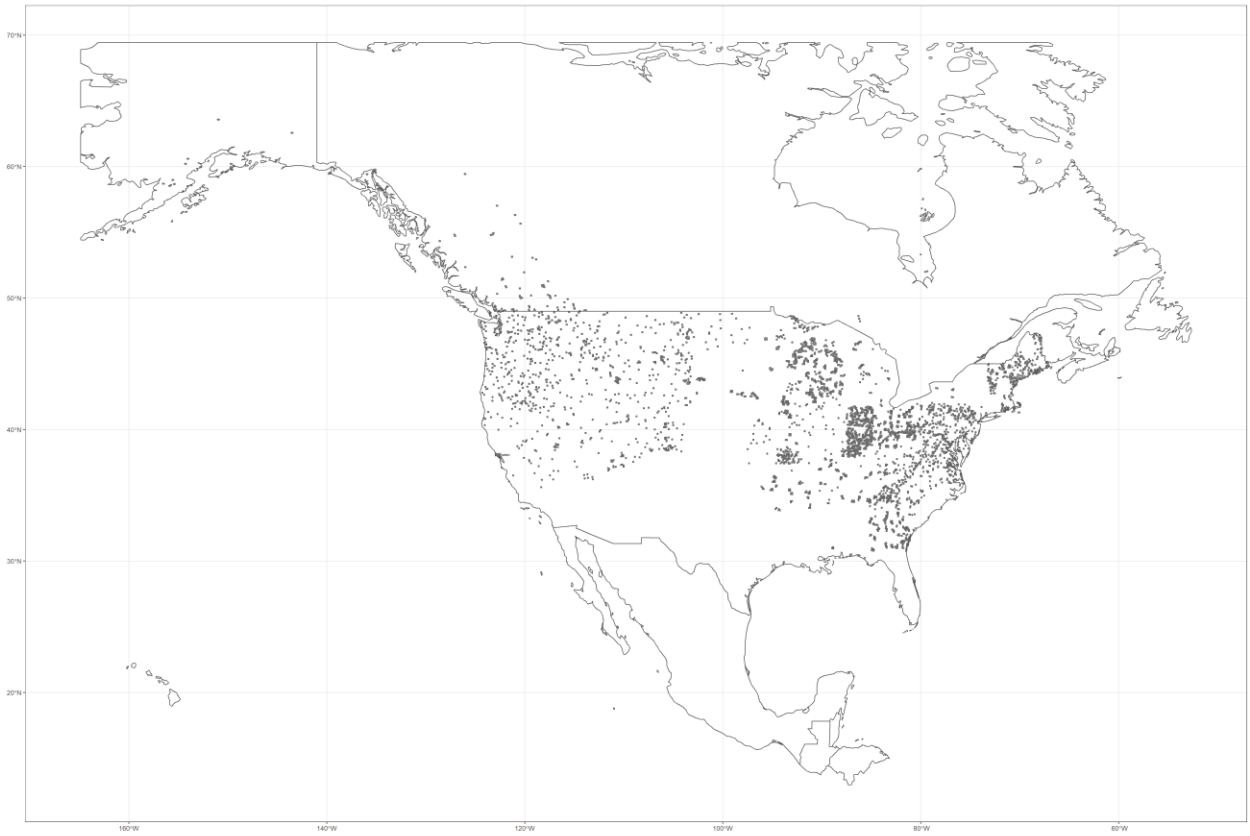

Figure B1. Map displaying the sampled North American Bat Monitoring Program (NABat) grid cells included in modeling of distributions of *Myotis lucifugus* (MYLU).

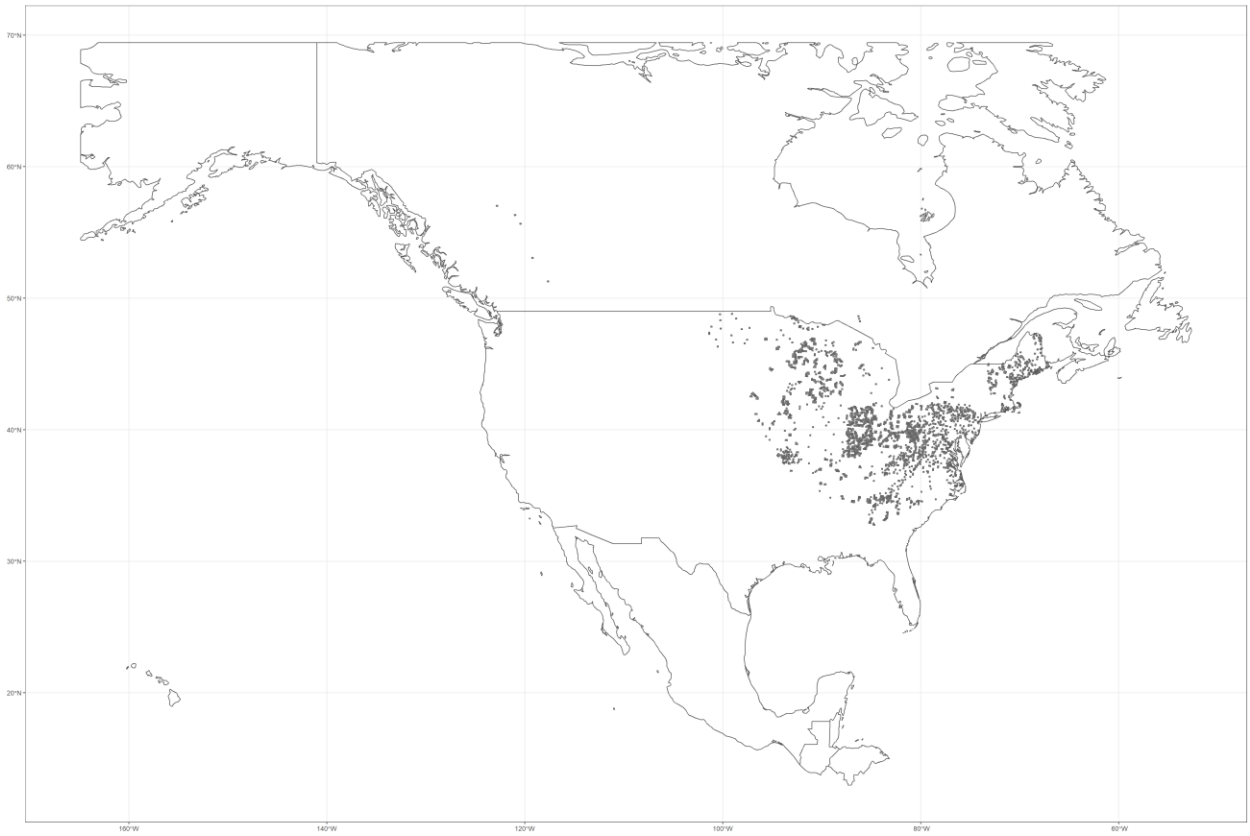

Figure B2. Map displaying the sampled North American Bat Monitoring Program (NABat) grid cells included in modeling of *Myotis septentrionalis* (MYSE) distributions.

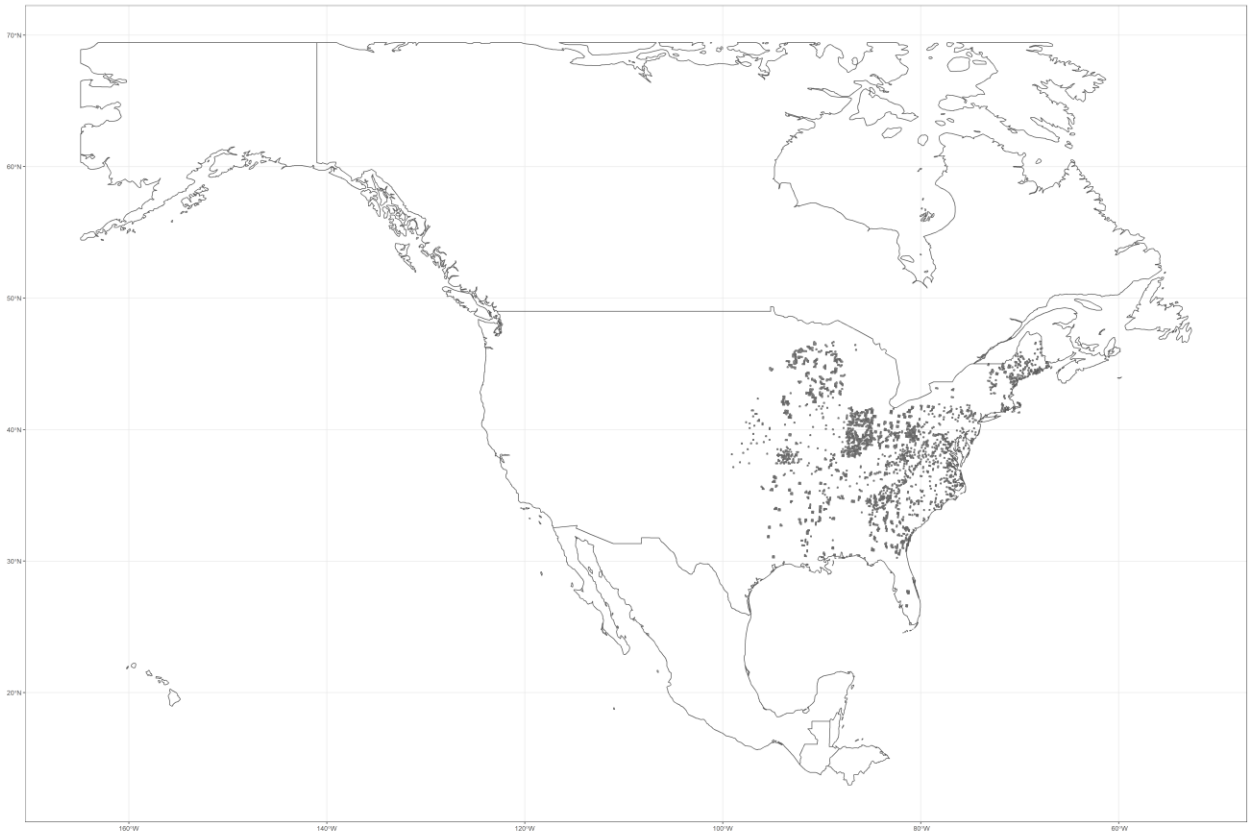

Figure B3. Map displaying the sampled North American Bat Monitoring Program (NABat) grid cells included in modeling of *Perimyotis subflavus* (PESU) distributions.

Automatically identified stationary acoustic calls

If data contributors were following NABat guidance, two to four stationary acoustic detectors were deployed within an NABat cell (10 km x 10 km) for one to four nights (Loeb et al. 2015). These stationary acoustic detector units then recorded calls from dusk until dawn. Finally, recorded calls were automatically classified using various classification software. The response is the number of calls that were automatically classified to one of the three target species (MYLU, MYSE, or PESU). Note that relying on the software only (so called autoIds) results in instances where no bats were detected (i.e., the 0 entries represent no detections for a detector-night). A zero could arise because that species does not occur in the grid cell or the species does occur and the detector failed to record at least one identifiable bat call for MYLU, MYSE, or PESU. The false zeros are examples of imperfect detection, which is a known consideration for bat surveys (Loeb et al. 2015).

Automatically identified mobile acoustic calls

If data contributors were following NABat guidance, mobile transects of length 25 to 48 km would be driven within an NABat cell (10 km x 10 km) (Loeb et al. 2015). The transect would be driven for multiple nights commencing 45 minutes after sunset. The acoustic detector units mounted on top of the vehicles would record bat calls. Finally, recorded calls would be automatically classified using various classification software. The response would be the same as the automatically identified stationary acoustic calls (section ‘Automatically identified stationary acoustic calls’); again, this dataset includes 0’s that were interpreted as no detections.

Capture records

To collect these data, field technicians physically captured bats and identified them. The observational unit for capture data was an individual bat. However, we aggregated up to the

night level for compatibility. The response in its raw form was simply a capture, though it could be number of bats captured if these data were aggregated to the night level. Note that these data represent presence only information - there is no information on when capture attempts were made, but no bats were captured. Furthermore, these records could be considered an unambiguous detection method.

Manually vetted acoustic calls

The manually vetted acoustic calls are our final source of data. Manual vetting refers to the process that a human reviewed a recorded call file and assigned a species identification. There are many ways people conduct manual vetting or hand review. Typically, only a subset of the high quality automatically identified acoustic calls (both stationary and mobile) are manually vetted. For the SSA dataset, a record of 0 based on the manual vetted data type could be the result of somebody confirming no call files were automatically identified to the species OR overturning all autoIDs recorded as MYLU, PESU or MYSE OR that no effort was put towards vetting calls for a given project. Consequently, these data also represent detection only information. Again, we assumed these to be an unambiguous detection method.

Summary of response types

Table B1 summarizes the types of summertime data we have available for the SSA.

Table B1. Summary of summertime data available for Species Status Assessment (SSA) analysis for little brown bat (*Myotis lucifugus*; MYLU), northern long-eared bat (*Myotis septentrionalis*; MYSE), and tricolored bat (*Perimyotis subflavus*; PESU). 'Source' refers to the five data types described. 'Obs. unit' refers to the finest resolution of the data, 'Temporal res.' refers to the finest temporal resolution available for each data type, 'Spatial res.' is the finest spatial resolution available for each data type, 'Type' denotes whether the data type was Detection/Non-detection information or Presence only information, and 'False positive status' refers to whether the data are considered ambiguous (subject to false positives) or unambiguous (no false positives).

Source	Obs. Unit	Temporal Res.	Spatial Res.	Type	False Positive Status
Auto ID stationary	Night	Night	NABat cell	Detection/Non-detection	Ambiguous
Manually ID stationary	Night	Night	NABat cell	Presence only	Unambiguous
Auto ID mobile	Night	Night	NABat cell	Detection/Non-detection	Ambiguous
Manually ID mobile	Night	Night	NABat cell	Presence only	Unambiguous
Capture	Individual bat	Night	NABat cell	Non-zero Count	Unambiguous

Data fusion and aggregation

To incorporate all five data sources into a coherent false positive occupancy modeling framework, we classify each response as one of: (0) non-detection, (1) ambiguous detection, or (2) unambiguous detection. This classification system was consistent with the false positive occupancy models developed by Miller et al. (2011), discussed in greater detail in the section 'Statistical Methods Considered Overview'. For the purpose of our analysis, a manual identification or capture record was considered an unambiguous detection and an automatically identified call was considered an ambiguous detection. Classifying each response in this manner is consistent with the recent literature applying false positive models from Miller et al. (2011) to

acoustic data (Balantic and Donovan 2019). One assumption of an occupancy modeling framework is that repeated visits to a site (or 10 x10 km cell in the context of our analysis) are temporally and spatially independent. Continuous periods of monitoring potentially violate the assumption of temporal independence, as we would expect sequential nights of monitoring to be similar due to runs in bat activity (see glossary) (Wright, Irvine, and Rodhouse 2016; Wright, Irvine, and Higgs 2019). To avoid the violation of temporal independence among revisits to a site, continuous periods of monitoring were aggregated to 7-day periods. The 7-day period started from the first visit to a grid cell *i*. For example, if the first visit occurred on a Tuesday, the next 6 nights would be included in the 7-day period if there were additional visits to that same grid cell *i*. If a site had visits greater than seven days apart, each was treated as an independent revisit. Regarding the spatial independence of revisits to a site, multiple assumptions were made (see below). These assumptions could not be assessed as event specific coordinates were not consistently made available from data contributors.

1. If multiple detectors were deployed simultaneously, they were assumed far enough apart from each other to maintain independence. We assume data contributors deployed their detectors following recommendations in the NABat plan.
2. If multiple detection methods occurred concurrently (i.e., mobile acoustic and stationary acoustic records occurred during the same span of time), they were assumed to be spatially independent.

Based on these assumptions, detection matrices were created for each species. The spatial scope of the observed data is described below (Table B2). We also provide a table of counts of the observed response categories across all visits to each site by species in Table B3; in Table B4,

we provide the relative proportion of each observed response category. The relative contribution of data types varied by species (Table B3 and Table B4).

Table B2. For little brown bat (*Myotis lucifugus*; MYLU), northern long-eared bat (*Myotis septentrionalis*; MYSE), and tricolored bat (*Perimyotis subflavus*; PESU) and year available 'n_sites_sampled' is the number of grid cells with bat data recorded, 'n_sites_range' is the number of available North American Bat Monitoring Program (NABat) grid cells within each species range, and 'prop_range_sampled' is the proportion of the species range sampled for a given year.

Species_code	year	n_sites_sampled	n_sites_range	prop_range_sampled
MYLU	2010	126	123505	0.001020
MYLU	2011	252	123505	0.002040
MYLU	2012	523	123505	0.004235
MYLU	2013	920	123505	0.007449
MYLU	2014	674	123505	0.005457
MYLU	2015	735	123505	0.005951
MYLU	2016	1026	123505	0.008307
MYLU	2017	1000	123505	0.008097
MYLU	2018	1042	123505	0.008437
MYLU	2019	856	123505	0.006931
MYSE	2010	128	51543	0.002483
MYSE	2011	185	51543	0.003589
MYSE	2012	417	51543	0.008090
MYSE	2013	807	51543	0.015657
MYSE	2014	518	51543	0.010050
MYSE	2015	557	51543	0.010807
MYSE	2016	636	51543	0.012339
MYSE	2017	576	51543	0.011175
MYSE	2018	543	51543	0.010535
MYSE	2019	505	51543	0.009798
PESU	2010	77	38479	0.002001
PESU	2011	208	38479	0.005406
PESU	2012	530	38479	0.013774
PESU	2013	898	38479	0.023337
PESU	2014	678	38479	0.017620
PESU	2015	630	38479	0.016373
PESU	2016	780	38479	0.020271
PESU	2017	726	38479	0.018867
PESU	2018	715	38479	0.018582
PESU	2019	689	38479	0.017906

Table B3. Counts of each response category across all visits to each site by bat species (little brown bat (*Myotis lucifugus*; MYLU), northern long-eared bat (*Myotis septentrionalis*; MYSE), and tricolored bat (*Perimyotis subflavus*; PESU) and year. '0' represents a non-detection, '1' represents an ambiguous detection (an automatically identified acoustic call), and '2' represents an unambiguous detection (a manually vetted acoustic call or capture record).

Species	Year	0	1	2
MYLU	2010	73	50	136
MYLU	2011	96	124	153
MYLU	2012	591	378	200
MYLU	2013	1290	672	572
MYLU	2014	763	784	447
MYLU	2015	944	1166	536
MYLU	2016	1387	1552	657
MYLU	2017	1410	1973	690
MYLU	2018	1422	1441	789
MYLU	2019	920	1491	518
MYSE	2010	102	10	143
MYSE	2011	120	23	119
MYSE	2012	738	35	104
MYSE	2013	1586	34	212
MYSE	2014	871	65	148
MYSE	2015	1156	222	148
MYSE	2016	1422	465	158
MYSE	2017	1606	741	203
MYSE	2018	1445	465	162
MYSE	2019	1210	436	74
PESU	2010	45	63	64
PESU	2011	39	206	98
PESU	2012	310	717	111
PESU	2013	1051	805	227
PESU	2014	617	490	214
PESU	2015	924	491	166
PESU	2016	1300	790	279
PESU	2017	1283	1155	280
PESU	2018	1088	948	192
PESU	2019	939	890	286

Table B4. Relative proportions of each response category across all visits to each site by bat species (little brown bat *(Myotis lucifugus*; MYLU), northern long-eared bat (*Myotis septentrionalis*; MYSE), and tricolored bat (*Perimyotis subflavus*; PESU)) and year. '0' represents a non-detection, '1' represents an ambiguous detection (an automatically identified acoustic call), and '2' represents an unambiguous detection (a manually vetted acoustic call or capture record).

Species	Year	0	1	2
MYLU	2010	0.28	0.19	0.53
MYLU	2011	0.26	0.33	0.41
MYLU	2012	0.51	0.32	0.17
MYLU	2013	0.51	0.27	0.23
MYLU	2014	0.38	0.39	0.22
MYLU	2015	0.36	0.44	0.20
MYLU	2016	0.39	0.43	0.18
MYLU	2017	0.35	0.48	0.17
MYLU	2018	0.39	0.39	0.22
MYLU	2019	0.31	0.51	0.18
MYSE	2010	0.40	0.04	0.56
MYSE	2011	0.46	0.09	0.45
MYSE	2012	0.84	0.04	0.12
MYSE	2013	0.87	0.02	0.12
MYSE	2014	0.80	0.06	0.14
MYSE	2015	0.76	0.15	0.10
MYSE	2016	0.70	0.23	0.08
MYSE	2017	0.63	0.29	0.08
MYSE	2018	0.70	0.22	0.08
MYSE	2019	0.70	0.25	0.04
PESU	2010	0.26	0.37	0.37
PESU	2011	0.11	0.60	0.29
PESU	2012	0.27	0.63	0.10
PESU	2013	0.50	0.39	0.11
PESU	2014	0.47	0.37	0.16
PESU	2015	0.58	0.31	0.10
PESU	2016	0.55	0.33	0.12
PESU	2017	0.47	0.42	0.10
PESU	2018	0.49	0.43	0.09
PESU	2019	0.44	0.42	0.14

Covariates

To fit a false positive occupancy model and produce model-based predictions for probability of occurrence at unsurveyed locations, we require spatially explicit covariates at both the occupancy and detection levels of the model. Covariates at the occupancy level of the model must be available at an annual resolution and for every NABat grid cell within the species range, while detection-level covariates must be available at a nightly resolution for surveyed locations. The shapefiles describing each species range were provided by the nabatr R package (Enns and Talbert 2021), curated by the USGS, and hosted on the USGS Github repository. Species ranges extended into Canada.

Site-level covariates

Site-level covariates were scraped from the NABat database, described in Table B5 below. Terrain ruggedness index was calculated relative to adjacent cells. That is, elevation was calculated at the centroid of each grid cell, and terrain ruggedness was calculated based on these values.

Table B5. Summary of grid cell level covariates included in false positive occupancy model for little brown bat (*Myotis lucifugus*; MYLU), northern long-eared bat (*Myotis septentrionalis*; MYSE), and tricolored bat (*Perimyotis subflavus*; PESU) and associated source of information.

Name	Source
Mean elevation	Digital elevation model (DEM) (30 sec arc)
Terrain ruggedness index	Derived from DEM
Annual mean precipitation	WorldClim 2.0 - Global bioclimatic variables
Annual mean temperature	WorldClim 2.0 - Global bioclimatic variables
Distance to nearest wind farm	OpenEI
Percent forest cover	MODIS (2010, 250m)
Percent water cover	MODIS (2010, 250m)

In appendices B-1 through B-4 we provide maps of the site-level covariates and comparisons of the distribution of each covariate in the cells that were sampled to the distribution of the covariates in the unsampled cells within a species range. These covariate space comparisons provide an indication of whether the sampled grid cells were representative or not of the environmental space across the range of a species. If there is a large misalignment, spatial predictions could be misleading (Irvine et al. 2018).

Detection-level covariates

Detection-level covariates were gathered from Daymet; this information was available at a daily resolution through Daymet (https://daymet.ornl.gov/). "Daymet provides long-term, continuous, gridded estimates of daily weather and climatology variables by interpolating and extrapolating ground-based observations through statistical modeling techniques" (https://daymet.ornl.gov/). Several fields available in the NABat metadata were excluded because there were too many records with 'NA'. For example, fields that would be useful to consider in future work are a measure of clutter, detection target, local habitat category, survey effort, and microphone type.

Table B6. Summary of night-level covariates summarized to a weekly period and included in false positive occupancy model for each bat species and associated source of information. Daymet (https://daymet.ornl.gov/).

Name	Source
Day length	Daymet
Precipitation	Daymet
Maximum air temperature	Daymet
Minimum air temperature	Daymet
Water vapor pressure	Daymet
Julian Date	Daymet

To be consistent with the temporal resolution of the response data used in modeling, we summarized daily Daymet covariates to a temporal resolution of a 7-day period in the following manner:

- *Day length*: the mean day length during the 7-day period
- *Precipitation*: an indicator was created describing whether precipitation occurred during the 7-day period, the indicator was 1 if at least 1mm of precipitation occurred within the 7-day period.
- *Maximum air temperature*: the maximum of daily maximum air temperatures within 7-day period
- *Minimum air temperature*: the minimum of daily minimum air temperatures within 7-day period
- *Water vapor pressure*: the average of daily water vapor pressures within 7-day period
- *Julian date*: the median of Julian dates within 7-day period

Statistical Methods Considered Overview

Given the quick turnaround required to inform the SSA, we restricted ourselves to considering only previously developed methods for false positive occupancy modeling appropriate for the available summertime bat data. Chambert, Miller, and Nichols (2015) provide a nice review of occupancy methods to handle false positives. They describe three methods in Table 1 of their paper. In the following sections, we describe each of these methods and how they relate to bat acoustic data. Several of these models have been applied to bat datasets (Clement et al. 2014, Banner et al. 2018) and recent work has improved on these original models to incorporate the fact that with acoustic bat data a false positive is related to the presence of another species (Wright et al. 2020).

Site versus observation level false positive

Before describing each of the three methods reviewed in Chambert, Miller, and Nichols (2015), we provide a bit of terminology distinction. In the context of two-level hierarchical occupancy designs, false positives can occur either 1) at the site level or 2) at the observation level.

A site-level false positive is defined as "the occurrence of a detection at an unoccupied site." Note that this type of false positive detection is conditional on the occupancy state of the site (i.e., you can only have a site-level false positive if the site is truly unoccupied). Conversely, an observation-level false positive is defined at the individual observation level and is not conditional on the occupancy state of the site. In the case of bat acoustic data, a particular call file can be assigned the incorrect species identification (ID), but the site or grid cell could still have that species present (observation-level false positive at a site that is truly occupied).

Site confirmation model

The site confirmation model was originally introduced by Miller et al. (2011) and relies on having unambiguous detection techniques available for a subset of sites/surveys. In this setting, the data consist of two types of detections: 1) ambiguous (the detection could be a true or false positive - such as auto ID acoustic records) and 2) unambiguous (a site can be ascertained as truly occupied - capture records, manually vetted calls). Unambiguous detections can arise in one of two ways: 1) multiple detection methods: from implementation of distinct detection methods at all or a subset of sites (i.e., capture records in addition to acoustic detections) and 2) multiple detection states: from multiple types of observations made during the same sampling period. The multiple detection methods approach was applied to bat acoustic and mist net data collected in Oregon and Washington by Clement et al. (2014). The site confirmation models assume that false positive detections can never be confirmed as such because they only arise from ambiguous detections. Consequently, unambiguous detections do not directly inform the detection process for the ambiguous data, but rather directly informs the occupancy probability. The statistical model notation for both the multiple detection methods and multiple detection states approaches is provided below.

Multiple detection methods model notation:

Let

- Z_i represent the latent occupancy state of site i
- ψ represent the occupancy probability
- *M1* denote the primary detection method (which generates ambiguous detections)
- *M2* denote the second method (which generates unambiguous detections)

- Assume l sites were visited T times using detection method *M1* and S times using method *M2*
- y_{it} denote the observation obtained with *M1* on the t^{th} visit to site i
- w_{is} denote the observation obtained with *M2* on the s^{th} visit to site i
- p_{11} represent the probability of detecting the species with *M1* if the site is occupied
- p_{10} represent the probability of detecting the species with *M1* if the site is unoccupied
- r_{11} represent the probability of detecting the species with *M2* if the site is occupied

$$Zi \sim Bernoulli(\psi)$$

$$y_{it}|z_i \sim Bernoulli(z_i p_{11} + (1 - z_i)p_{10})$$

$$w_{is}|z_i \sim Bernoulli(z_i r_{11})$$

Multiple detection states model notation:

Let

- Z_i represent the latent occupancy state of site i
- ψ represent the occupancy probability
- Assume each site was visited T times
- y_{it} represent the detection status of site i at visit t. Three types of observation can be made at each visit: no detection ($y = 0$), ambiguous detection ($y = 1$), unambiguous detection ($y = 2$).

- p_{11} represent the probability of detecting the target species if the site is occupied
- p_{10} represent the probability of detecting the target species if the site is unoccupied
- *b* represent the probability that a detection is classified as unambiguous given that the site is occupied

$$Z_i \sim Bernoulli(\psi)$$

$$y_{it}|z_i \sim Categorical(M)$$

where M_z=0 = [{1 − p_{10}}{ p_{10}}{0}] for observation states y = {0, 1, 2} when z_i = 0 and M_z=1 = [{1 − p_{11}}{(1 − b) × p_{11}}{b × p_{11}}] for observation states y = {0, 1, 2} when z_i = 1.

Calibration technique

This technique is only applicable if there is independent information about the primary detection method that directly informs the false positive rate (and even the true positive rate). Since that is not applicable in our case, we do not provide further details.

Observation confirmation [OC] model

The observation confirmation [OC] model relies on a posteriori confirmation of a subset of field detections (i.e., manually vetted call files to a specific bat species). The OC model was extended and applied to bat acoustic data by Banner et al. (2018) and then further improved for bat acoustic survey data in Wright et al. (2020). In the bat acoustic setting, observation (and site) level false positives can arise if a bat call is misidentified as belonging to the target species (or if wind or some other disturbance is classified as a bat call from that species). In some cases, these

calls can be manually vetted later to determine whether they were correctly identified. Important assumptions about the data collection process include:

1. confirmation of samples is focused on the observation (individual call) rather than the site level
2. several observations can be made during a visit to a site, and thus confirmed, within a replicate survey (or, that both true and false positives may be obtained from a given survey)
3. the assumption of an omnibus source of false positives that is independent from the occurrence and the detection of the focal species (Wright et al. (2020) developed a multiple species detection count false positive model that relaxes this assumption)

As a result, a true detection is defined as "signs from the focal species are present, found, and assigned to the focal species" and a false positive is defined as "signs from a non-focal species are present, found, and erroneously assigned to the focal species." The OC model assumes that 1) the occurrence of a false positive observation is independent of the occupancy status of the focal species and 2) the occurrences of true and false positives are independent events. The model notation is defined below.

We divide the available data into two groups: the confirmed and unconfirmed. Imagine T replicate surveys are conducted at R sites where observations are collected in the field but not confirmed. Let y_{it} denote the 0/1 response obtained from this subset. For the other subset, S surveys are conducted at J sites, where observations are both collected in the field and confirmed. Let v_{js} denote the response obtained from this subset. This response can take on one of four possible values: 0 (no observations were assigned to the focal species); 1 (all

observations found and assigned to the focal species were confirmed as belonging to a different species); 2 (all observations found and assigned to the focal species were confirmed as belonging to the focal species); and 3 (the observations assigned to the focal species were a mix of true and observation-level false positives). Let:

- s_1 denote the probability of obtaining at least one true positive
- s_0 denote the probability of obtaining at least one false positive
- Z_i represent the latent occupancy state of site i
- ψ represent the occupancy probability
- p_{11} represent the probability of detecting the target species if the site is occupied
- p_{10} represent the probability of detecting the target species if the site is unoccupied

then

$$Z_i \sim Bernoulli(\psi)$$

$$y_{it}|z_i \sim Bernoulli(z_i p_{11} + (1 - z_i)p_{10})$$

$$Z_j \sim Bernoulli(\psi)$$

$$v_{js}|z_j \sim Categorical(\Omega)$$

where Ω_z=0 = [{1 − s_0}{s_0}{0}{0}] for observation states {0, 1, 2, 3} when z_j = 0 and Ω_z=1 = [{(1 − s_1) × (1 − s_0)}{(1 − s_1) × s_0}{s_1 × (1 − s_0)}{s_1 × s_0}] for observation states {0, 1, 2, 3} when z_j = 1.

Considerations of applicability of different false positive occupancy models for SSA analysis

Chambert, Miller, and Nichols (2015) provide a great summary of when these methods are most useful, which we summarize here. The site confirmation method is most easily implemented and does not (typically) require expensive detection means. The observation confirmation method is well suited for acoustic records (or any detection method where the observations can be surveyed at a later date), though manual verification can be expensive necessitating a consideration of optimal allocation of effort (Banner et al. 2018). It is worth noting that data from the observation confirmation sampling design could be analyzed under the site confirmation framework. Chambert, Miller, and Nichols (2015) showed that when doing so, only a small amount of precision is lost, though it can introduce optimization issues. When available, the observation confirmation method is preferred and Banner et al. (2018) provided options for considering optimal survey designs to improve feasibility of this model for bat work. Of the false positive methods that could be applicable to bat acoustic data (multiple detection state site confirmation, multiple detection method site confirmation (Clement et al. 2014), observation confirmation (Banner et al. 2018), multiple species count detection model (Wright et al. 2020)), only the multiple detection states site confirmation model (MDSM) is an option for the summertime SSA data. We are limited to the MDSM model because of the structure of the unambiguous detection observations; namely, both unambiguous detection methods (capture data and manually vetted calls) are presence-only. As a result, we cannot estimate s_0 in the observation confirmation method or $r_{11}$from the multiple detection method site confirmation model as in previous work.

Statistical Method Used for SSA Summertime Analysis

Due to the statistical considerations outlined in the section 'Statistical Methods Considered Overview,' we chose the multiple detection state site confirmation model (MDSM) for the summertime statistical analysis. Each species was modeled independently. For details on the response aggregation strategy, see section 'Data fusion and aggregation.' To estimate the parameters in the model we used the surveyed NABat grid cells (denoted as *i*) within each year [2010 to 2019 see Table B2 for sample sizes available]. Each included grid cell *i* had one or more visits *j* within a given year. We accounted for the temporal correlation in occupancy state at a site between years explicitly in the mean structure of each model. We model the partially observed latent occupancy state (Z_i) and the observed response for grid cell *i* during visit *j* (y_{ij} conditional on Z_i) as follows

$$Z_i \sim Bernoulli(\psi_i)$$

$$y_{ij} | z_i \sim Categorical(M_{ij})$$

where $[M_{ij} | z_i = 0] = [\{1 - p_{10_j}\}\{p_{10_j}\}\{0\}]$ for observation states $y_{ij} = \{0, 1, 2\}$ when $z_i = 0$ and $[M_{ij} | z_i = 1] = [\{1 - p_{11_j}\}\{(1 - b_j) \times p_{11_j}\}\{b_j \times p_{11_j}\}$ for observation states $y_{ij} = \{0, 1, 2\}$ when $z_i = 1$. For this analysis, the probability the species occurring at site *i* (ψ_i) was modeled as a function of grid-cell specific covariates mean elevation, terrain ruggedness, annual mean precipitation, annual mean temperature, percent forest cover, percent water cover, distance to nearest wind farm, and the survey year using a logit link (see section 'Site-level covariates'). Each of the detection level parameters (p_{10}, p_{11}, b) were modeled by day length, daily precipitation, maximum air temperature, minimum air temperature, water vapor pressure and julian date using a logit link (see section 'Detection-level covariates'). All covariates were scaled

before fitting the model. Below, we discuss the assumptions of our modeling framework and assess the convergence of the fitted models. We provide for each species an estimate of the total change in occupancy from the year 2010 until 2019, λ_{tot}, and an estimate of the average annual rate of change, λ_{avg}, based on only the surveyed grid cells. The trend parameters λ_{tot} and λ_{avg} estimate net change, "[which] can be thought of as change in the mean or total response" (McDonald 2003, pg. 279). When these parameters are less than one, they indicate a decrease in average occupancy and greater than one suggests an increase in average occupancy. Following, Banner et al. (2018) λ_{tot} is an estimate of the total population change from 2010 to 2019 for each species:

$$\lambda_{tot} = \bar{\psi}_{2019} / \bar{\psi}_{2010},$$

where $\bar{\psi}_{\mathrm{t}} = \frac{1}{n} \sum_{i=1}^{n} \hat{\psi}_{i,t}$, which is the average estimated occupancy probability for the sampled grid cells *i* within a defined spatial extent within a species range. The average annual growth rate (λ_{avg}) is an estimate of the annual rate of change in occupancy based on surveyed grid cells *i* within a defined spatial extent within a species range:

$$\lambda_{avg} = \frac{1}{T-1} \sum_{t=2}^{T} \bar{\lambda}_{\mathrm{t}},$$

where $\bar{\lambda}_t = \frac{\bar{\psi}_t}{\bar{\psi}_{t-1}}$. These two metrics can differ substantially depending on the temporal trajectory in the average occupancy probabilities ($\bar{\psi}_t$). We provide summary figures for our model fits for MYLU, MYSE, and PESU in section 'Summertime Analysis Results' and additional estimates for each state within a species range were provided in the lambda.xls file to the USFWS SSA team.

Model assumption

When fitting the MDSM false positive occupancy model, the data must be consistent with two assumptions: (1) the occupancy state at each site is closed for the duration of each summer and (2) detections both within and between sites must be independent. We discuss each of these assumptions in greater detail next.

Closure

We assume that within each site (10 km x 10 km cell), the occupancy state does not change over the course of a summer. The species occurs within a grid cell throughout the entire summer period. The closure assumption is made at a species level, which means that particular individuals may move in and out of the grid cell throughout the summer. Also, the closure assumption does not require that a species roosts within a particular grid cell, just that the species uses a grid cell (MacKenzie et al. 2006). The actual behavior of how individuals are using a grid cell is unknown, they could be roosting or foraging.

Independence

We assume both that detection of the target species at one site does not affect detection of that species at another site and that detection of the target species during one visit to a site does not affect detection of that species during subsequent visits to that site. We assume there is no unexplained spatial or temporal correlation among observations both within and among sites. Any site-level temporal correlation in detections from year to year has been accounted for by year-specific intercept parameters in the occupancy-level of the model. The master sample design outlined within the NABat monitoring plan was constructed to ensure that sampled grid cells were far enough apart to be considered spatially independent (Loeb et al. 2015). However, as mentioned previously with the fusion of both stationary and mobile surveys and capture data,

the spatial independence assumptions are not necessarily satisfied because the mechanism for site or grid cell selection is unknown. To ensure that the data are consistent with the assumption of independent detections within a site, there must again be no unexplained sources of temporal or spatial correlation. Temporal correlation in detection within a site may arise from continuous periods of monitoring. To account for this potential source of temporal correlation, responses were aggregated up to a weekly level. Spatial correlation in detection within a site may arise from detection methods being deployed too close in proximity to each other. The NABat monitoring plan provides guidelines for how to deploy multiple detection methods simultaneously within the same site while still maintaining spatial independence in detections. However, point specific coordinates for detections were unavailable. Therefore, a direct assessment of the spatial independence assumption within a grid cell is not possible. As a result, we must assume the NABat plan was followed appropriately, and that if multiple detection methods were deployed within a cell concurrently (multiple stationary detection devices deployed simultaneously, stationary and mobile acoustic detectors deployed concurrently, etc.), they were deployed far enough apart to be spatially independent.

Model fitting and convergence

The proposed model was fit via Markov chain Monte Carlo (MCMC) using NIMBLE v0.9.1 in R (Valpine et al. 2017). Each model was fit using four independent chains and run for 10,000 iterations, with the first 5,000 being discarded as warmup iterations. Chambert, Miller, and Nichols (2015) note that the MDSM false positive occupancy model suffers from a lack of identifiability in model parameters, making it difficult to assess model convergence. Models were run multiple times from differing starting parameter values and carefully monitored for convergence. We used trace plots and Gelman-Rubin statistics for assessing convergence to the

posterior distribution. The Gelman-Rubin statistic is used to assess convergence of MCMC chains by comparing the within chain variance to the between chain variance; values close to one suggest convergence (Gelman and Rubin 1992). We used caterpillar plots summarizing the posterior distributions for all parameters from each model, available in Appendix B-1 (Figure B1.1, B1.2, and B1.3).

Summertime Analysis Results

We created a number of products that can be used to summarize our analysis. These products fall into one of two categories: (1) shapefiles describing the estimated occupancy probability with uncertainty for every NABat grid cell (surveyed and unsurveyed) within each species range and (2) an excel file describing the estimated change in occupancy (λ) with uncertainty for each geopolitical spatial subunit (e.g., a state) and USFWS defined regions of interest for each species (Irvine and Stratton 2021). Each of the metrics provided in the Excel file are described in greater detail in section 'Statistical Method Used for SSA Summertime Analysis' and in Banner et al. (2018). The shapefiles can be used to visualize estimated occupancy probabilities for geopolitical or Fish and Wildlife Service sub-regions of interest within a G.I.S. The shapefiles contain the covariates used for our analysis for further visualization by the USFWS SSA Team. We use the lambda.xls Excel file to create summary visualizations of average annual rate of change (λ_{avg}) and the total population change from 2010 to 2019 (λ_{tot}) for each species within the pre-defined USFWS service regions of interest (Figures B4, B7, and B10). We also show the average occupancy probability ($\bar{\psi}_t$) by USFWS regions of interest for each year and species (Figures B5, B8, and B11) and an estimate of annual rate of change ($\bar{\lambda}_t$) by USFWS regions of interest for each species (Figures B6, B9, B12).

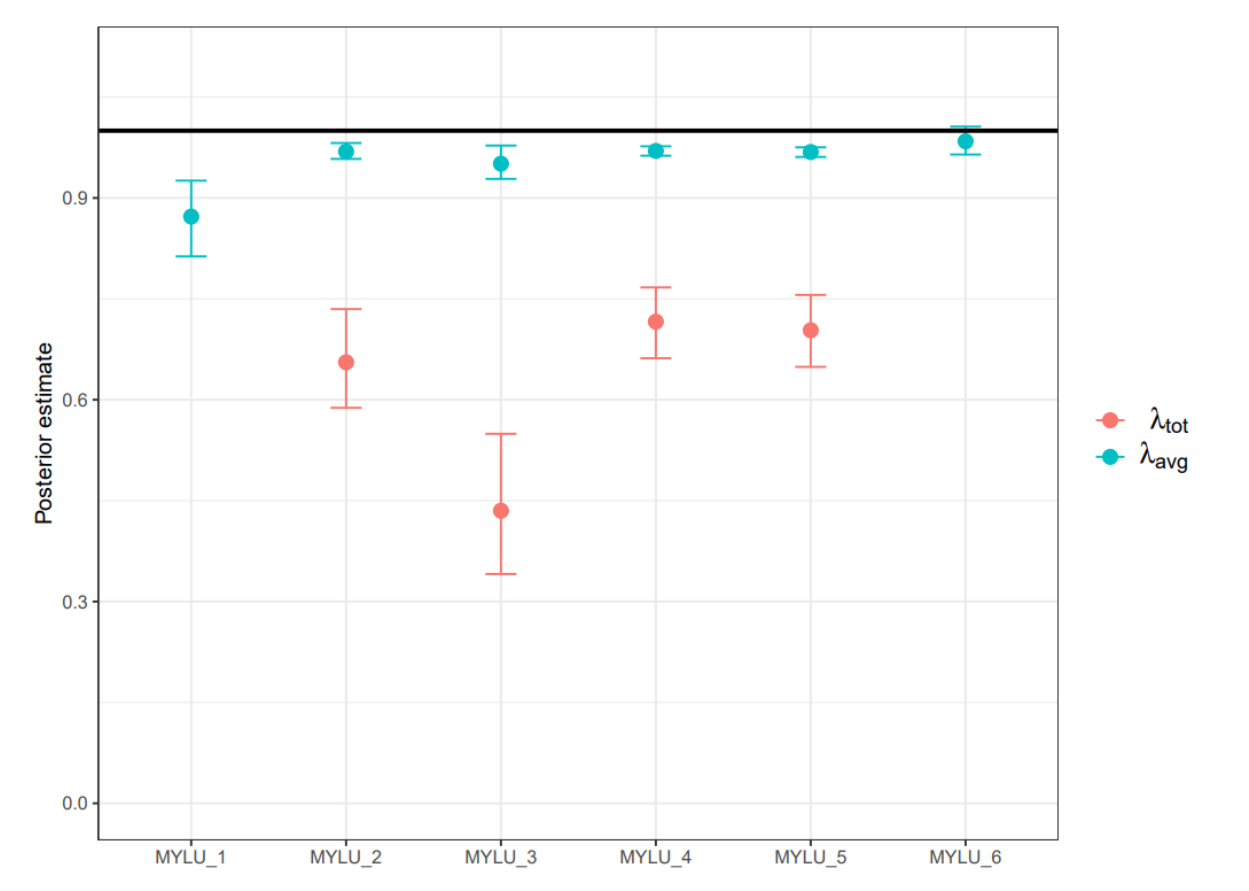

Figure B4. Estimates of the average annual rate of change (λavg) and total change (λtot) in occupancy from 2010 to 2019 based on sampled cells for little brown bats (*Myotis lucifugus*, MYLU) within Representation Units (RPU) as defined by the USFWS. Subarctic = MYLU_1, Eastern Hardwoods = MYLU_2, Mississippi Alluvial and Coastal Plains = MYLU_3, Great Plains = MYLU_4, Rocky Mountain = MYLU_5, and Pacific Coast and Alaskan = MYLU_6. The circle represents the posterior mean and the horizontal line segments represent the upper (97.5%) and lower (2.5%) posterior quantiles. Parameters less (greater) than one indicate a decrease (increase) in average occupancy. Sample sizes are reported in Table B2.

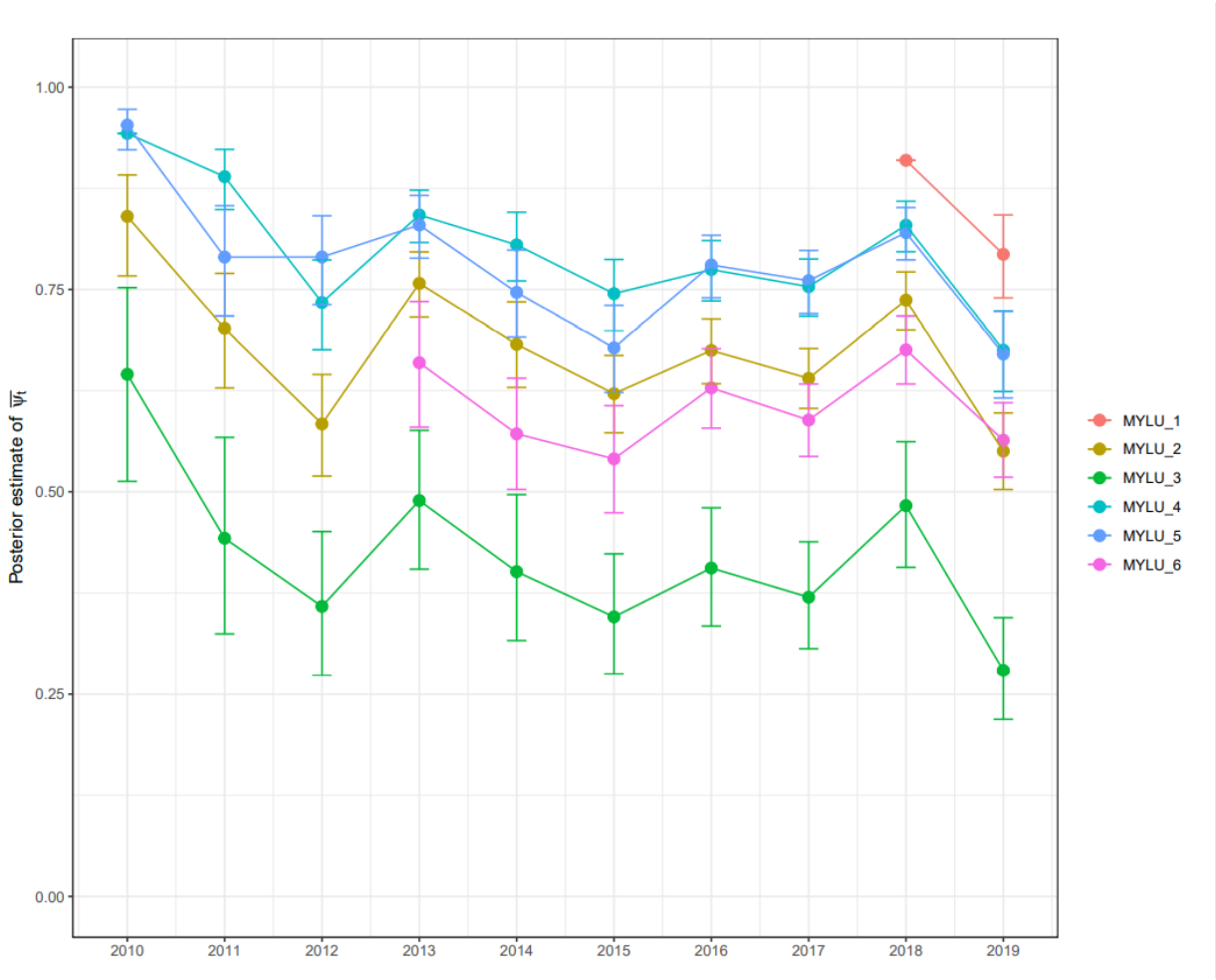

Figure B5. Estimates of the average occupancy probability ($\bar{\psi}_t$) based on sampled cells within each of the Representation Units (RPU) as defined by the USFWS (Subarctic = MYLU_1, Eastern Hardwoods = MYLU_2, Mississippi Alluvial and Coastal Plains = MYLU_3, Great Plains = MYLU_4, Rocky Mountain = MYLU_5, and Pacific Coast and Alaskan = MYLU_6) for little brown bats (*Myotis lucifugus*, MYLU) between 2010 and 2019.

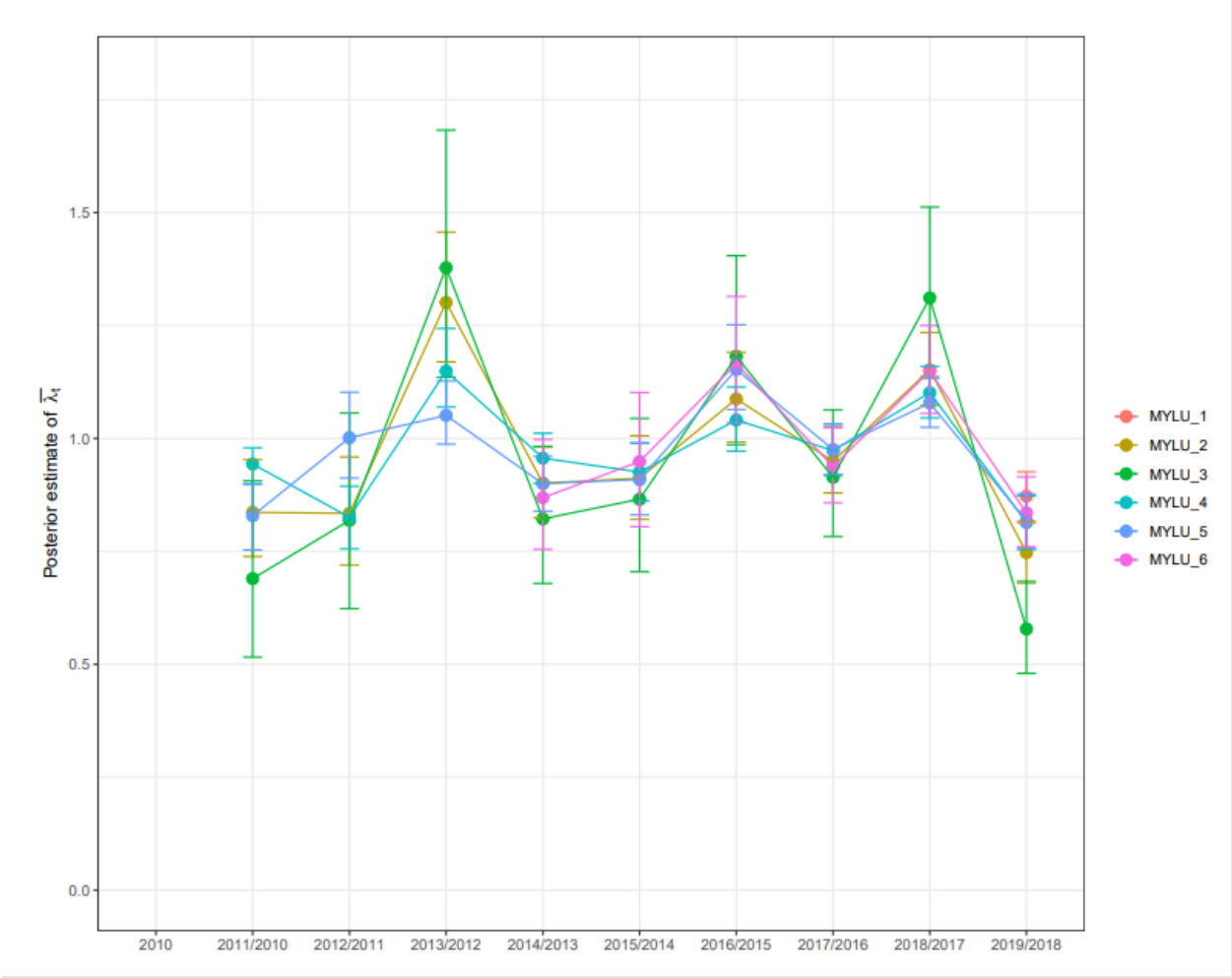

Figure B6. Estimates of the rate of change in occupancy ($\bar{\lambda}_t$) based on sampled cells within Representation Units (RPU) as defined by the USFWS (Subarctic = MYLU_1, Eastern Hardwoods = MYLU_2, Mississippi Alluvial and Coastal Plains = MYLU_3, Great Plains = MYLU_4, Rocky Mountain = MYLU_5, and Pacific Coast and Alaskan = MYLU_6) for little brown bats (*Myotis lucifugus*, MYLU) between 2010 and 2019. The rate of change in occupancy is the ratio between estimated average occupancy in a given year and the previous year. For example, "2013/2012" denotes the ratio of average occupancy between 2013 and 2012. A value greater than (less than) 1 implies the average occupancy in year 2013 was higher (lower) than year 2012.

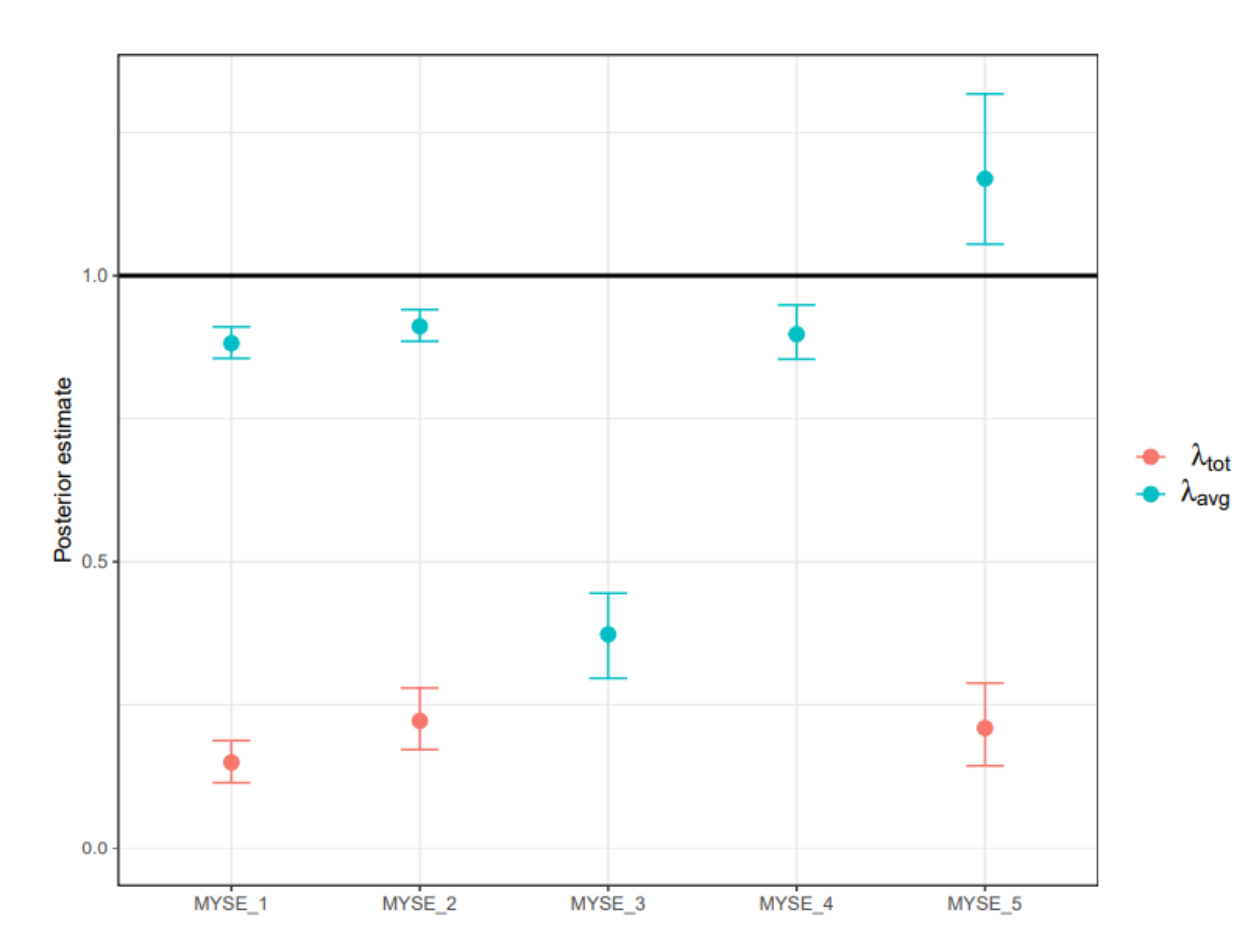

Figure B7. Estimates of the average annual rate of change (λ_{avg}) and total change (λ_{tot}) in occupancy based on sampled cells for northern long-eared bats (*Myotis septentrionalis*, MYSE) for each of the Representation Units (RPU) as defined by the USFWS (Mississippi Alluvial Plan = MYSE_1, Eastern Hardwoods = MYSE_2, Subarctic = MYSE_3, Great Plains = MYSE_4, and Coastal = MYSE_5). The circle represents the posterior mean and the horizontal line segments represent the upper (97.5%) and lower (2.5%) posterior quantiles. Parameters less (greater) than one indicate a decrease (increase) in average occupancy.

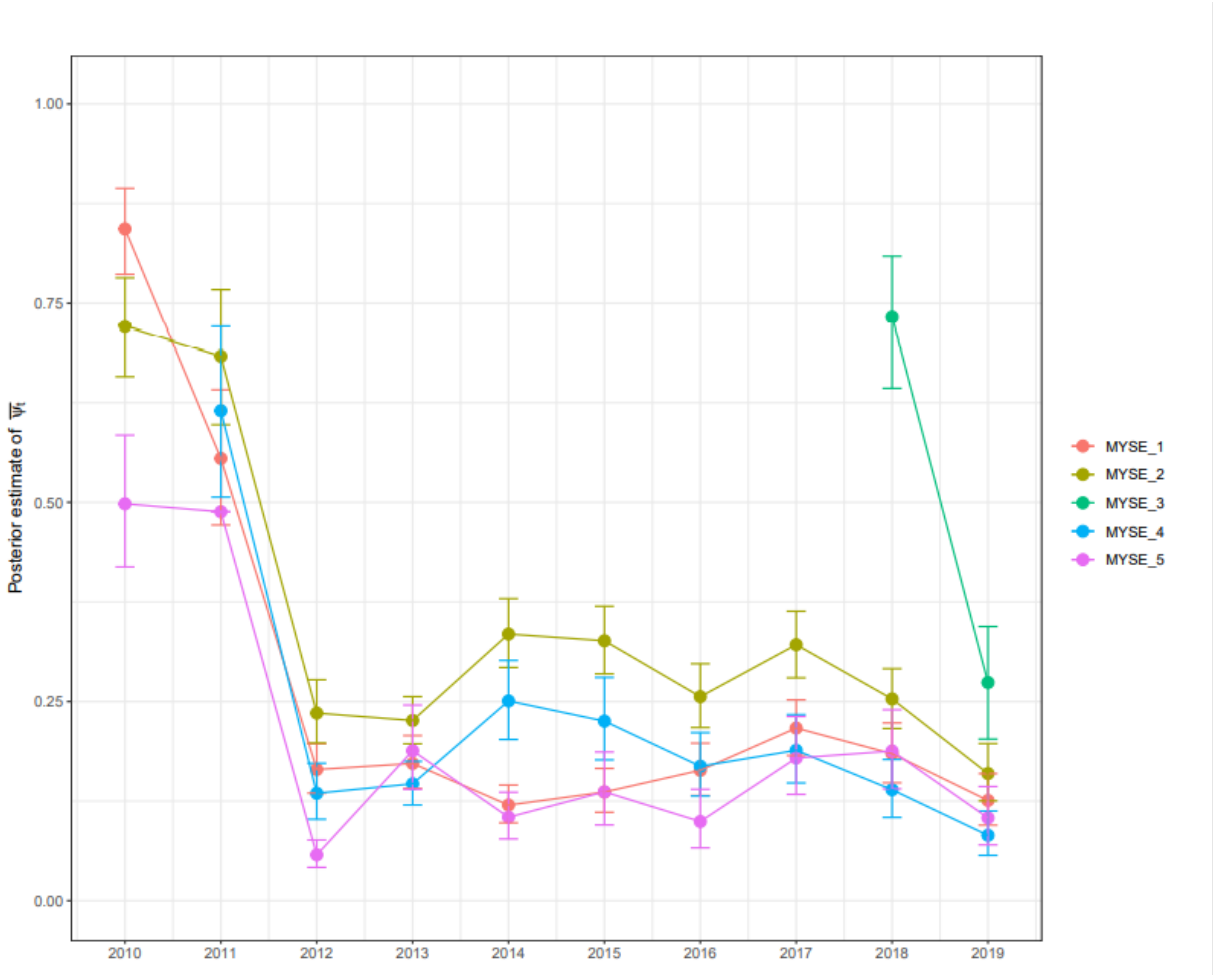

Figure B8. Estimates of the average occupancy probability ($\bar{\psi}_t$) based on sampled cells within each of five for each of the Representation Units (RPU) as defined by the USFWS (Mississippi Alluvial Plan = MYSE_1, Eastern Hardwoods = MYSE_2, Subarctic = MYSE_3, Great Plains = MYSE_4, and Coastal = MYSE_5) for northern long-eared bats (*Myotis septentrionalis,* MYSE) between 2010 and 2019. The circle represents the posterior mean and the horizontal line segments represent the upper (97.5%) and lower (2.5%) posterior quantiles.

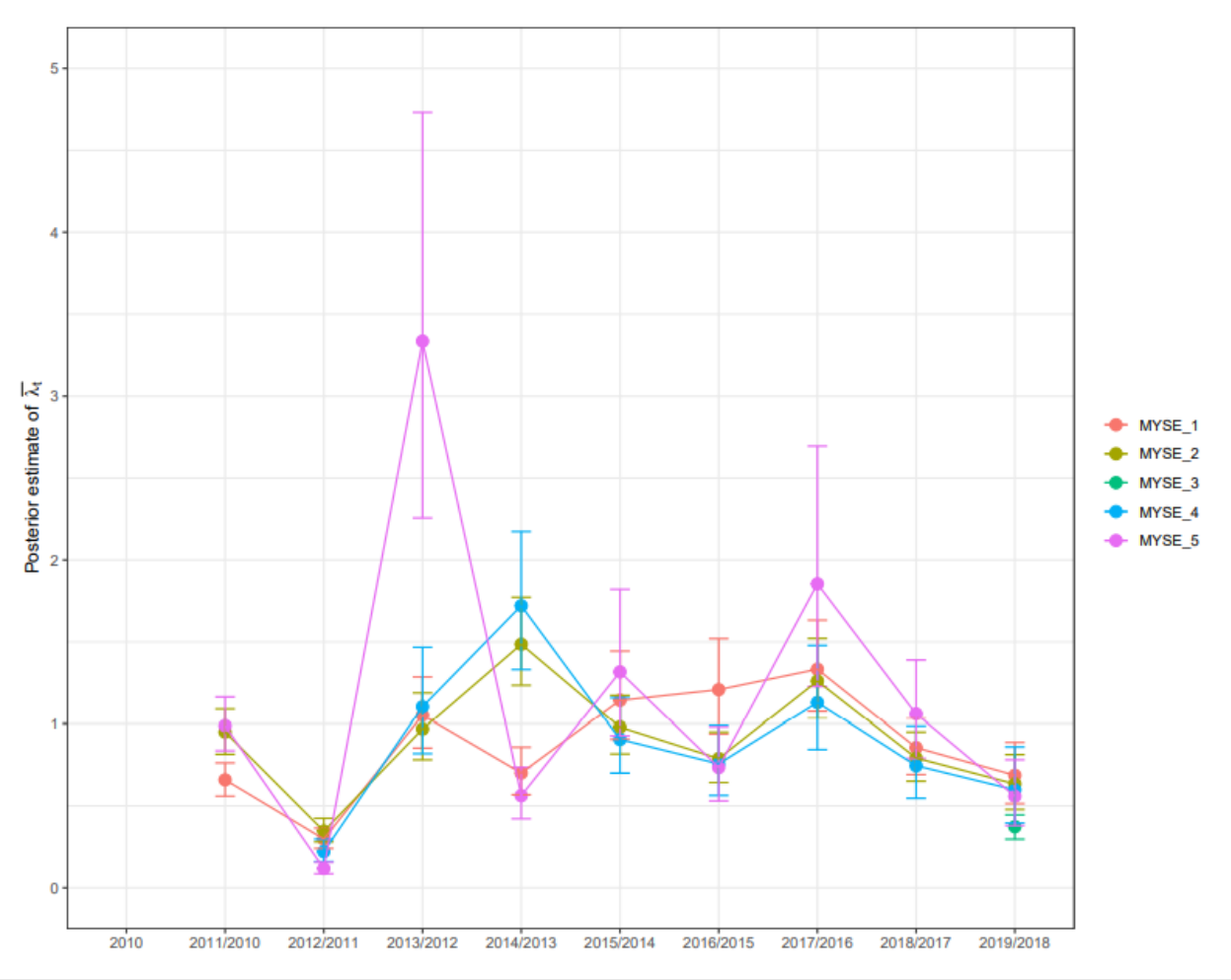

Figure B9. Estimates of the rate of change in occupancy ($\bar{\lambda}_t$) based on sampled cells within each of the Representation Units (RPU) as defined by the USFWS (Mississippi Alluvial Plan = MYSE_1, Eastern Hardwoods = MYSE_2, Subarctic = MYSE_3, Great Plains = MYSE_4, and Coastal = MYSE_5) for northern long-eared bats (*Myotis septentrionalis,* MYSE) between 2010 and 2019. The rate of change in occupancy is the ratio between estimated average occupancy in a given year and the previous year. For example, "2013/2012" denotes the ratio of average occupancy between 2013 and 2012.

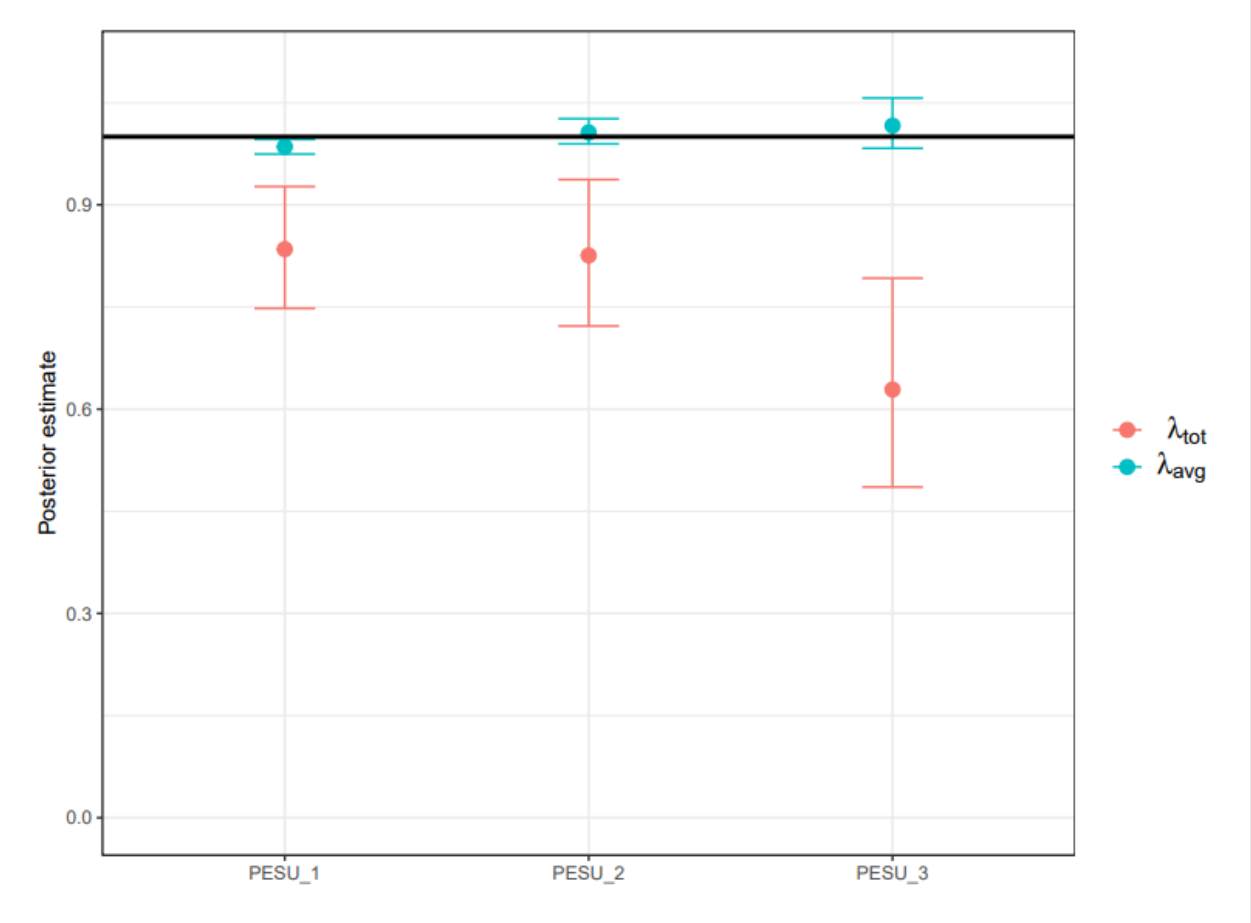

Figure B10. Estimates of the average annual rate of change (λ_{avg}) and total change (λ_{tot}) in occupancy based on sampled cells within each Representation Units (RPU) as defined by the USFWS (North = PESU_1, East = PESU_2, and South = PESU_3) for tricolored bats (*Perimyotis subflavus,* PESU). The circle represents the posterior mean and the horizontal line segments represent the upper (97.5%) and lower (2.5%) posterior quantiles.

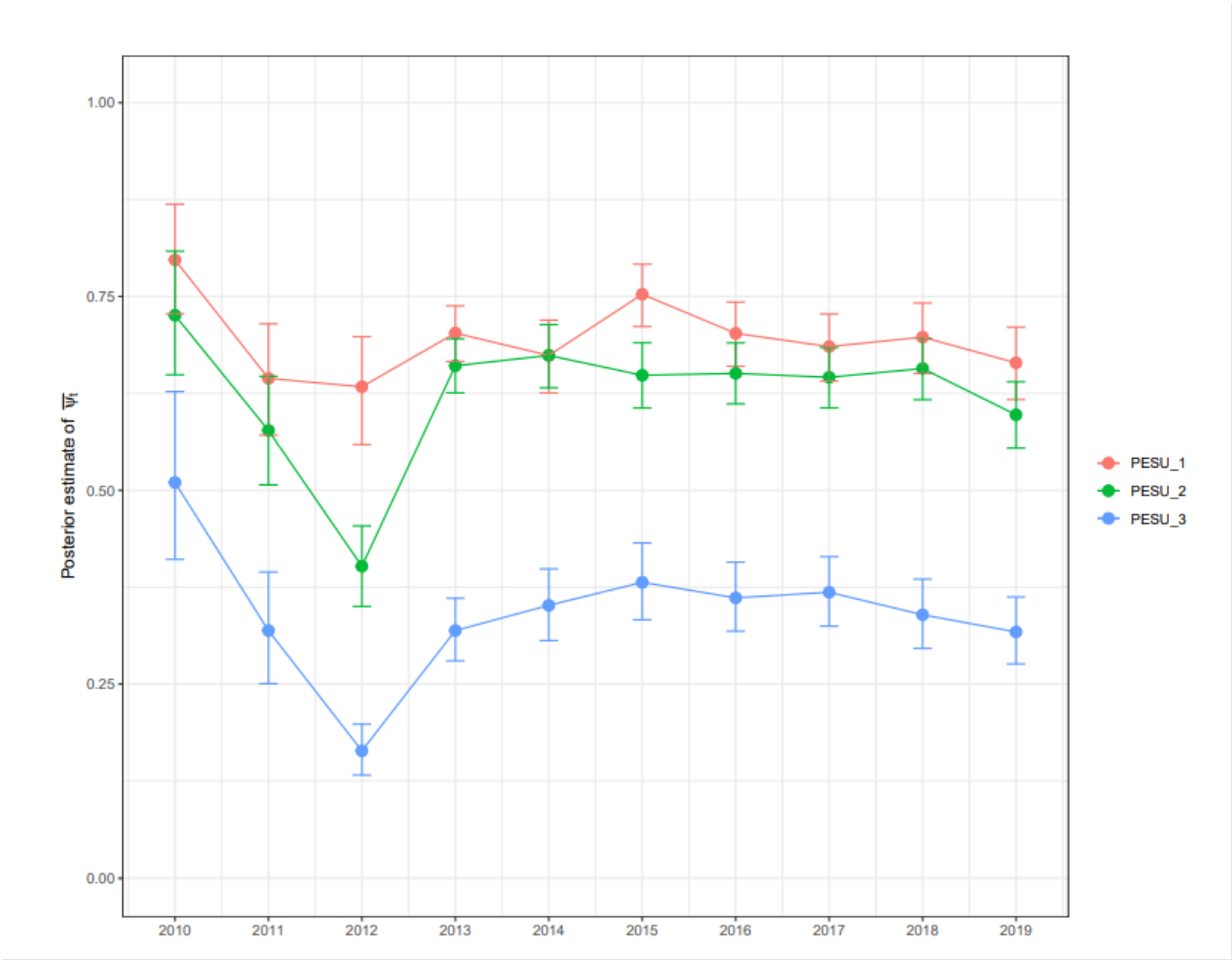

Figure B11. Estimates of the average occupancy probability ($\bar{\psi}_t$) across sampled cells within each of the Representation Units (RPU) as defined by the USFWS (North = PESU_1, East = PESU_2, and South = PESU_3) for tricolored bats (*Perimyotis subflavus,* PESU) between 2010 and 2019. The circle represents the posterior mean and the horizontal line segments represent the upper (97.5%) and lower (2.5%) posterior quantiles.

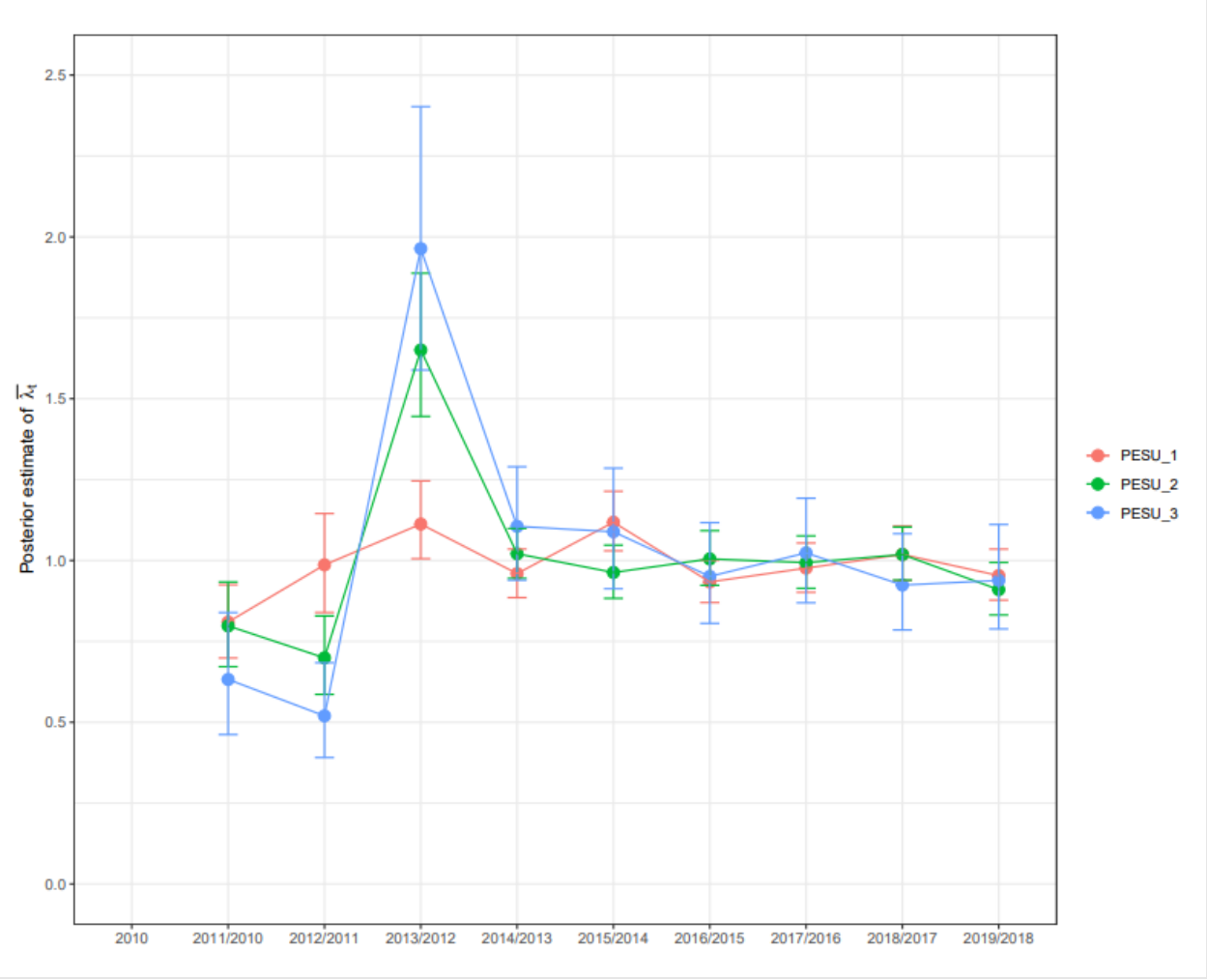

Figure B12. Estimates of the rate of change in occupancy ($\bar{\lambda}_t$) based on sampled cells within each of the Representation Units (RPU) as defined by the USFWS (North = PESU_1, East = PESU_2, and South = PESU_3) for tricolored bats (*Perimyotis subflavus,* PESU) between 2010 and 2019. The rate of change in occupancy is the ratio between estimated average occupancy in a given year and the previous year. For example, "2013/2012" denotes the ratio of average occupancy between 2013 and 2012.

Acknowledgments

C. Stratton's participation was made possible by USGS Ecosystems Mission Area Pre-listing funding for Little Brown Bats and USGS NABat-WNS Cyclical funds awarded to the Northern Rocky Mountain Science Center. K.M. Irvine's participation was funded by USGS NABat-WNS Cyclical funds awarded to the Northern Rocky Mountain Science Center.

References Cited

Balantic, C., and T. Donovan. 2019. Dynamic Wildlife Occupancy Models Using Automated Acoustic Monitoring Data. Ecological Applications 0 (0): 1–14.

Banner, K. M., K. M. Irvine, T. J. Rodhouse, W. J. Wright, R. M. Rodriguez, and A. R. Litt. 2018. Improving Geographically Extensive Acoustic Survey Designs for Modeling Species Occurrence with Imperfect Detection and Misidentification. Ecology and Evolution 8 (12): 6144–56. https://doi.org/10.1002/ece3.4162.

Chambert, T., D. A. W. Miller, and J. D. Nichols. 2015. Modeling False Positive Detections in Species Occurrence Data Under Different Study Designs. Ecology 96 (2): 332–39. https://doi.org/10.1890/14-1507.1.

Clement, M. J., T. J. Rodhouse, P. C. Ormsbee, J. M. Szewczak, and J. D. Nichols. 2014. Accounting for False-Positive Acoustic Detections of Bats Using Occupancy Models. Journal of Applied Ecology 51 (5): 1460–7. https://doi.org/10.1111/1365-2664.12303.

Enns, K.D. and Talbert, C.B., 2021, North American Bat Monitoring Program: R Data Connection Package, Version 1.0.0: U.S. Geological Survey software release, https://doi.org/10.5066/P9LSLF93

Gelman, A., and D. B. Rubin. 1992. Inference from Iterative Simulation Using Multiple Sequences. Statistical Science 7 (4): 457–511.

Irvine, K. M., T. J. Rodhouse, W. J. Wright, and T. R. Olsen. 2018. Occupancy Modeling Species-Environment Relationships with Non-Ignorable Survey Designs. Ecological Applications 8 (12): 6144–56. https://doi.org/10.1002/eap.1754.

Irvine, K.M. and C. Stratton. 2021. Rangewide summertime model predictions for three bat species (*Myotis lucifigus, Myotis septentrionalis*, and *Perimyotis subflavus*) from acoustic and mist net data 2010 to 2019: US Geological Survey data release, https://doi.org/10.5066/P9XZ8D6N.

Loeb, S. C., T. J. Rodhouse, L. E. Ellison, C. L. Lausen, J. D. Reichard, K. M. Irvine, T. E. Ingersoll, et al. 2015. A plan for the North American Bat Monitoring Program (NABat). U.S. Department of Agriculture Forest Service, Southern Research Station, Asheville, NC.

MacKenzie, D. I., J. D. Nichols, J. A. Royle, K. H. Pollock, L. L. Bailey, and J. E. Hines. 2006. Occupancy Estimation and Modeling: Inferring Patterns and Dynamics of Species Occurrence. Burlington, MA: Elsevier: Academic Press.

McDonald, T. L. 2003. Review of Environmental Monitoring Methods: Survey Designs. Environmental Monitoring and Assessment 85: 277–92.

Miller, D. A., J. D. Nichols, B. T. McClintock, E. H. Campbell Grant, L. L. Bailey, and L. A. Weir. 2011. Improving Occupancy Estimation When Two Types of Observational Error Occur: Non-Detection and Species Misidentification. Ecology 92 (7): 1422–8.

North American Bat Monitoring Program (NABat). Database v5.3.11 (Provisional Release): U.S. Geological Survey. Accessed 2020-12-01. NABat Request Number 10. https://doi.org/10.5066/P9UXA6CF

Valpine, P. de, D. Turek, C. J. Paciorek, C. Anderson-Bergman, D. Temple Lang, and R. Bodik. 2017. Programming with models: writing statistical algorithms for general model structures with NIMBLE. Journal of Computational and Graphical Statistics 26: 403–12.

Wright, W. J., K. M. Irvine, E. S. Almberg, and A. R. Litt. 2020. Modelling Misclassification in Multi-Species Acoustic Data When Estimating Occupancy and Relative Activity. Methods in Ecology and Evolution 11 (1): 71–81. https://doi.org/10.1111/2041-210X.13315.

Wright, W. J., K. M. Irvine, and M. D. Higgs. 2019. Identifying Occupancy Model Inadequacies: Can Residuals Separately Assess Detection and Presence? Ecology 100 (6): e02703. https://doi.org/10.1002/ecy.2703.

Wright, W. J., K. M. Irvine, and T. J. Rodhouse. 2016. A Goodness-of-Fit Test for Occupancy Models with Correlated Within-Season Visits. Ecology & Evolution 6 (15): 5404–15. https: //doi.org/10.1002/ece3.2292.

Appendix B-1. Mean Elevation

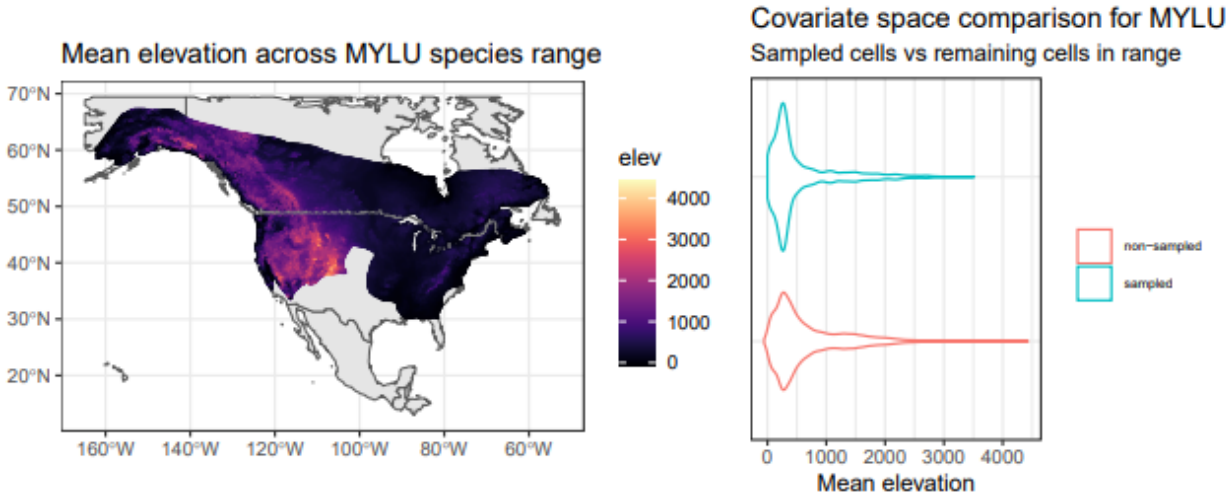

Figure B1.1. Mean elevation across *Myotis lucifugus* (MYLU) species range.

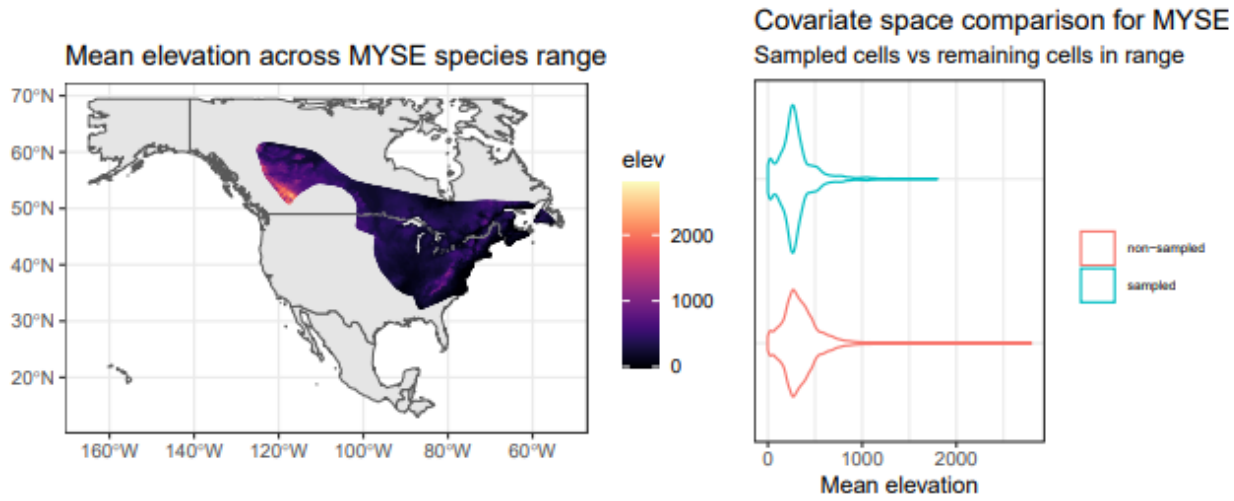

Figure B1.2. Mean elevation across *Myotis septentrionalis* (MYSE) species range.

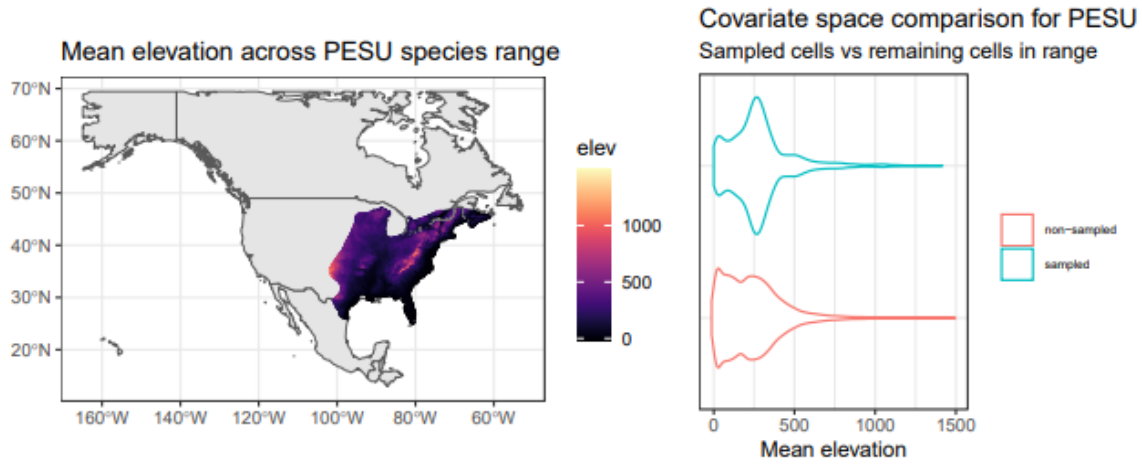

Figure B1.3 Mean elevation across *Perimyotis subflavus* (PESU) species range.

Appendix B-2. Terrain Ruggedness Index

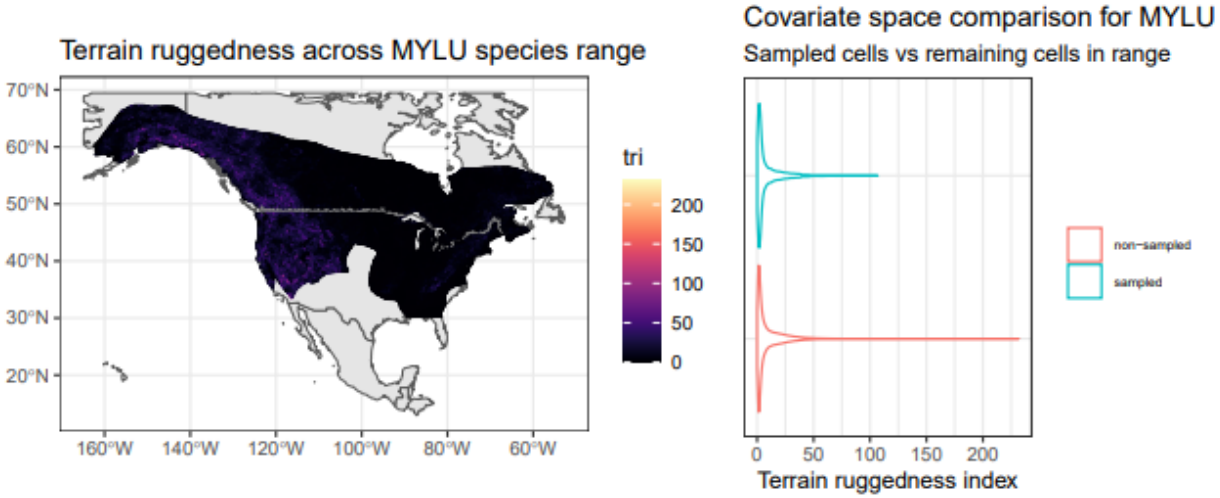

Figure B2.1. Terrain Ruggedness across *Myotis lucifugus* (MYLU) species range.

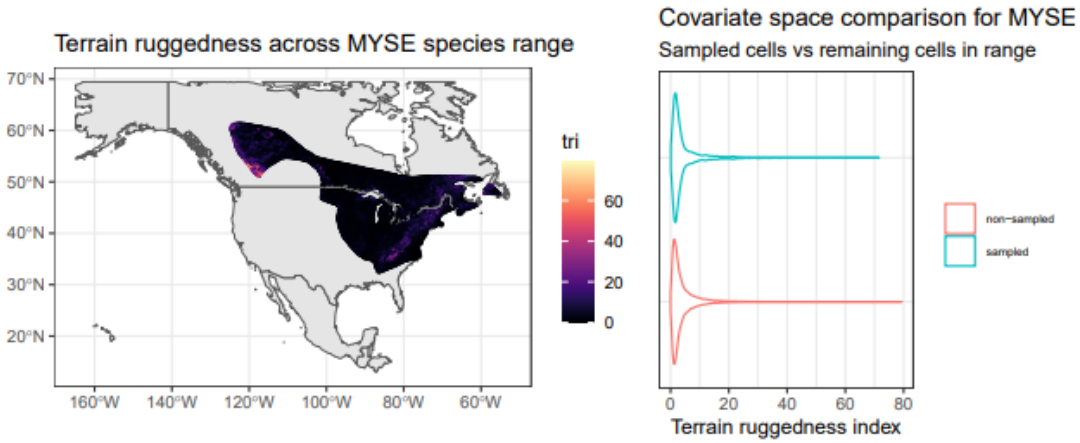

Figure B2.2. Terrain ruggedness across *Myotis septentrionalis* (MYSE) species range.

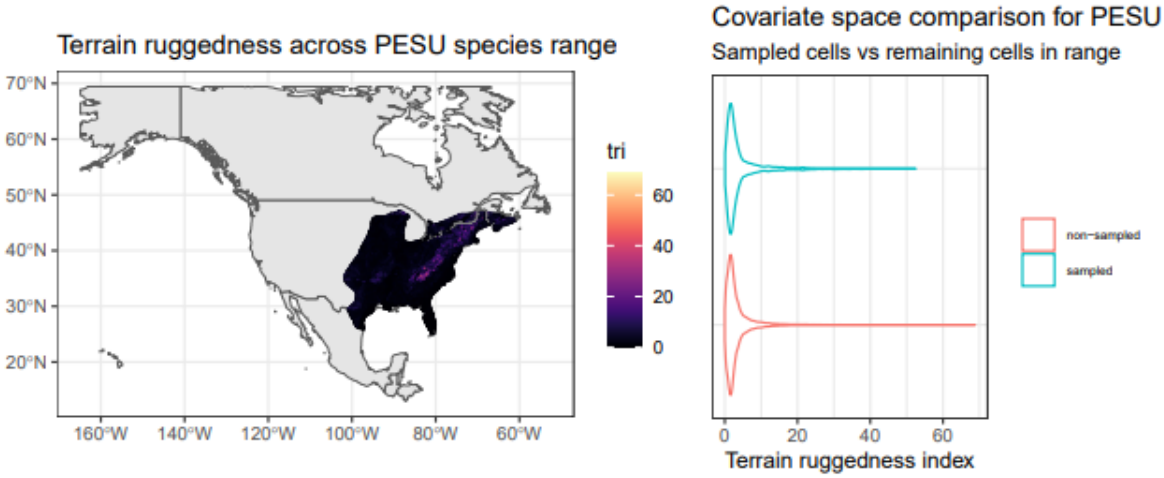

Figure B2.3. Terrain ruggedness across *Perimyotis subflavus* (PESU) species range.

Appendix B-3. Mean Annual Precipitation

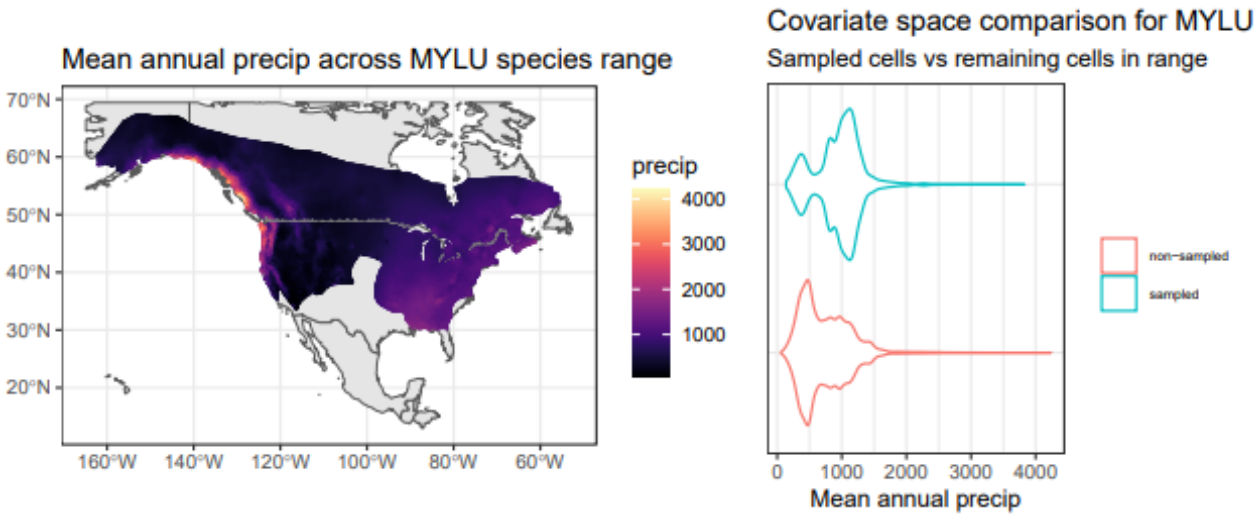

Figure B3.1. Mean annual precipitation across *Myotis lucifugus* (MYLU) species range.

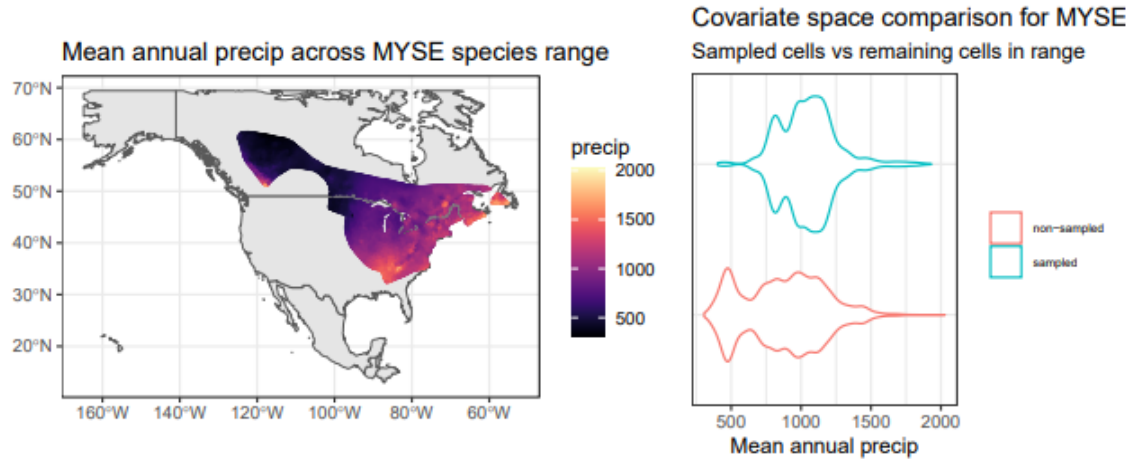

Figure B3.2. Mean annual precipitation across *Myotis septentrionalis* (MYSE) species range.

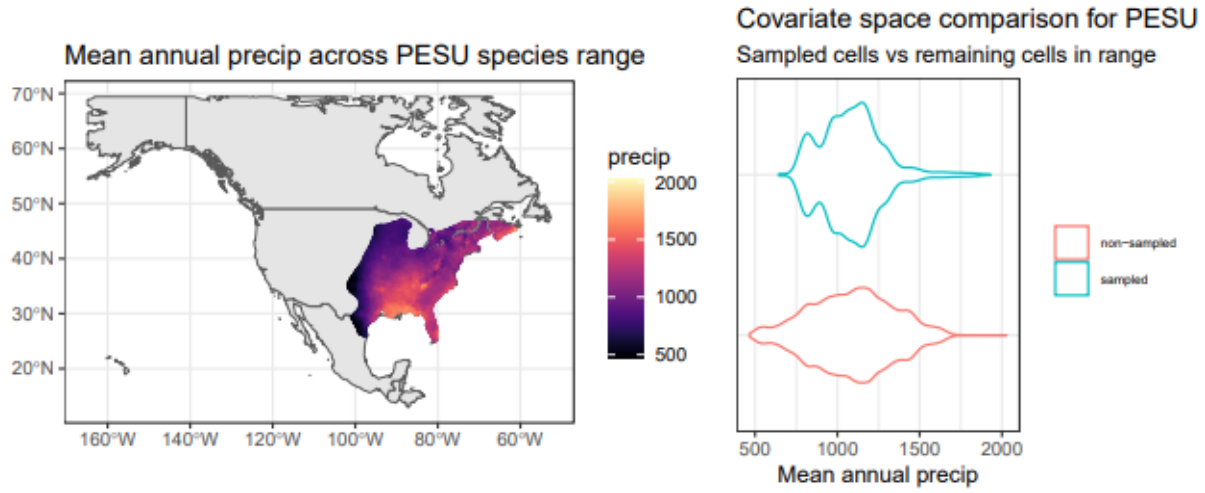

Figure B3.3. Mean annual precipitation across *Perimyotis subflavus* (PESU) species range.

Appendix B-4. Mean Annual Temperature

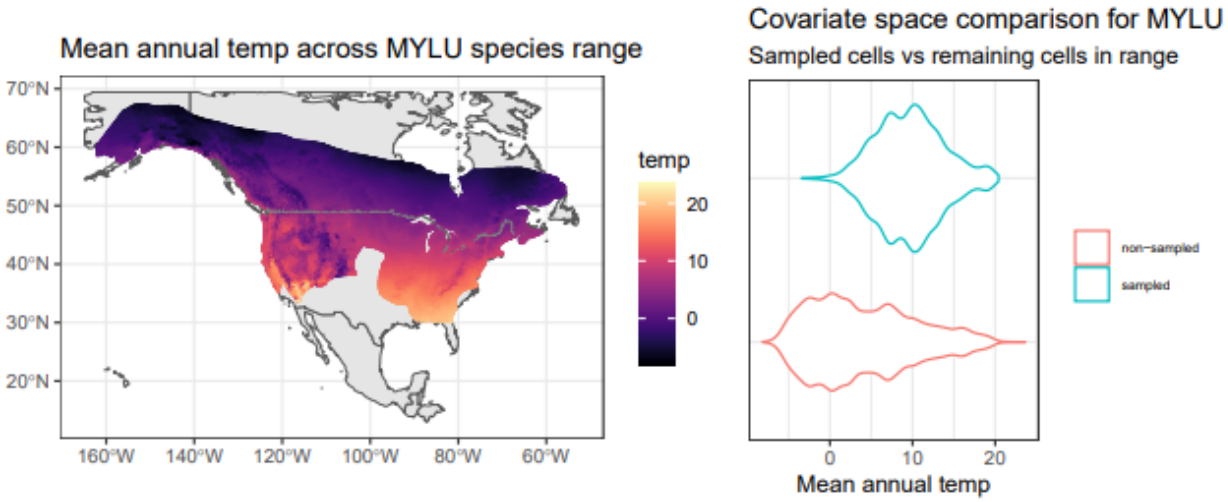

Figure B4.1. Mean Annual temperature across *Myotis lucifugus* (MYLU) species range.

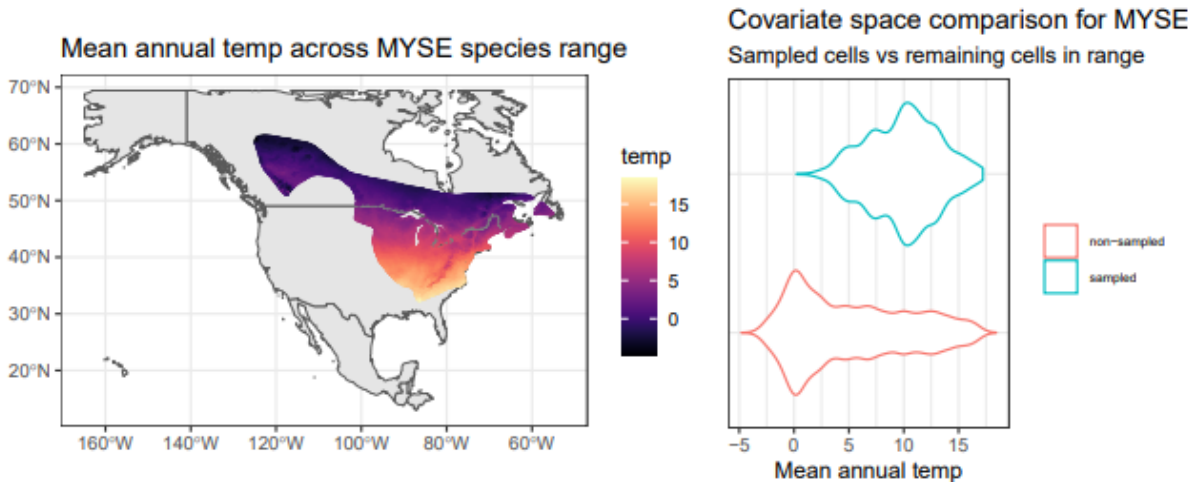

Figure B4.2. Mean annual temperature across *Myotis septentrionalis* (MYSE) species range.

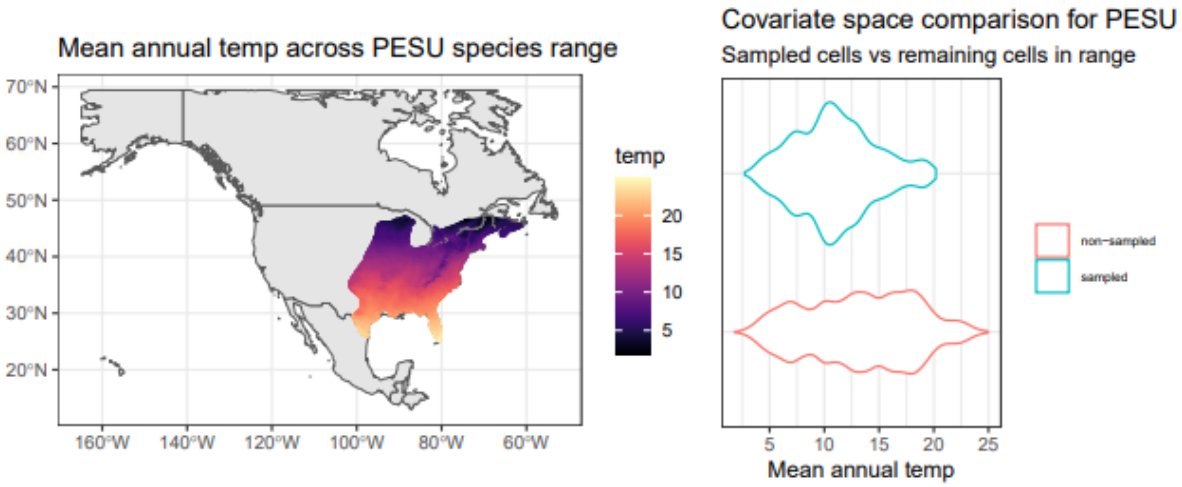

Figure B4.3. Mean annual temperature across *Perimyotis subflavus* (PESU) species range.

Percent Forest Cover

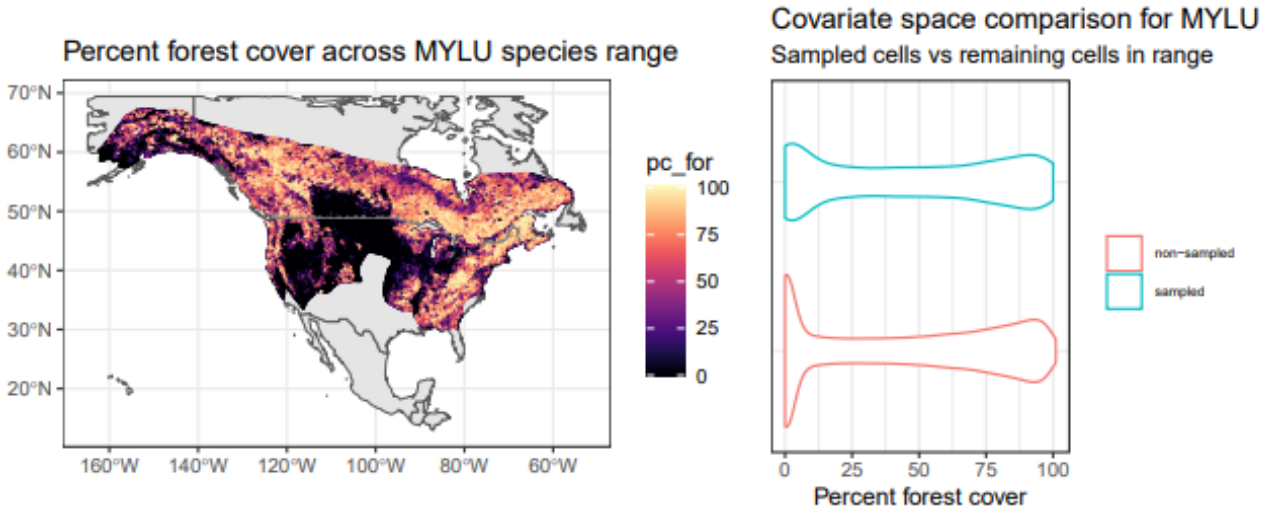

Figure B4.4. Percent forest cover across *Myotis lucifugus* (MYLU) species range.

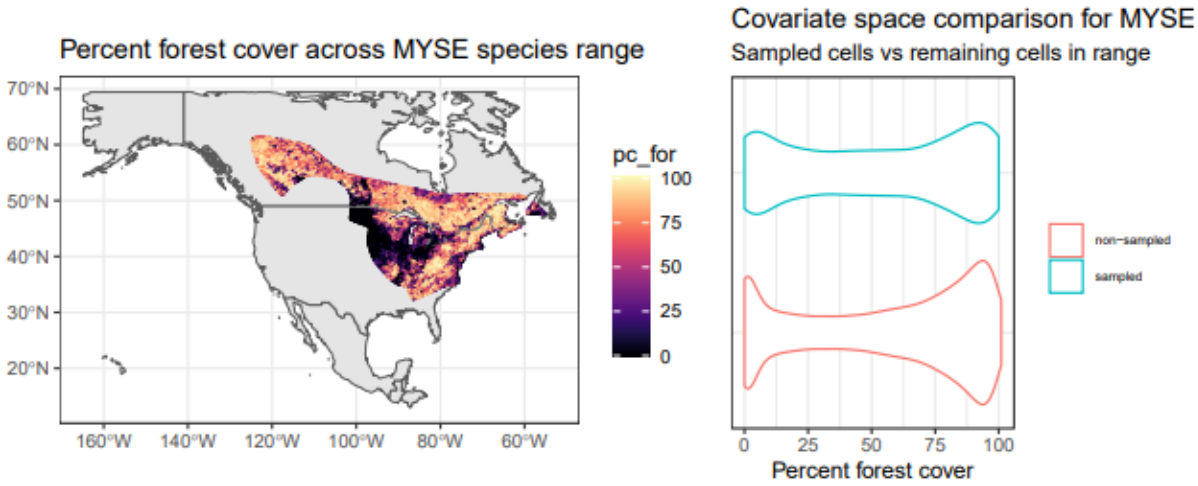

Figure B4.5. Percent forest cover across *Myotis septentrionalis* (MYSE) species range.

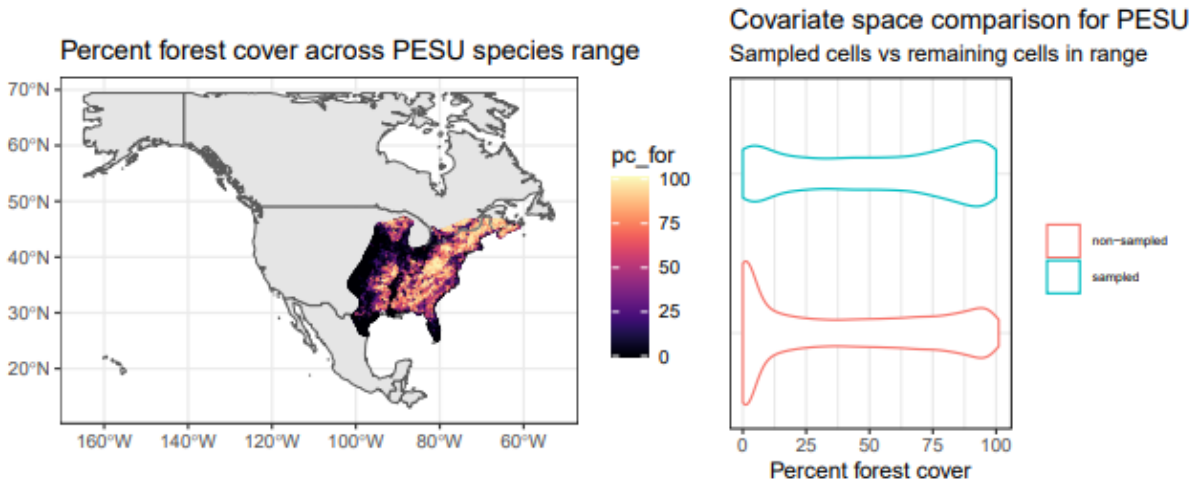

Figure B4.6. Percent forest cover across *Perimyotis subflavus* (PESU) species range.

Percent Water Cover

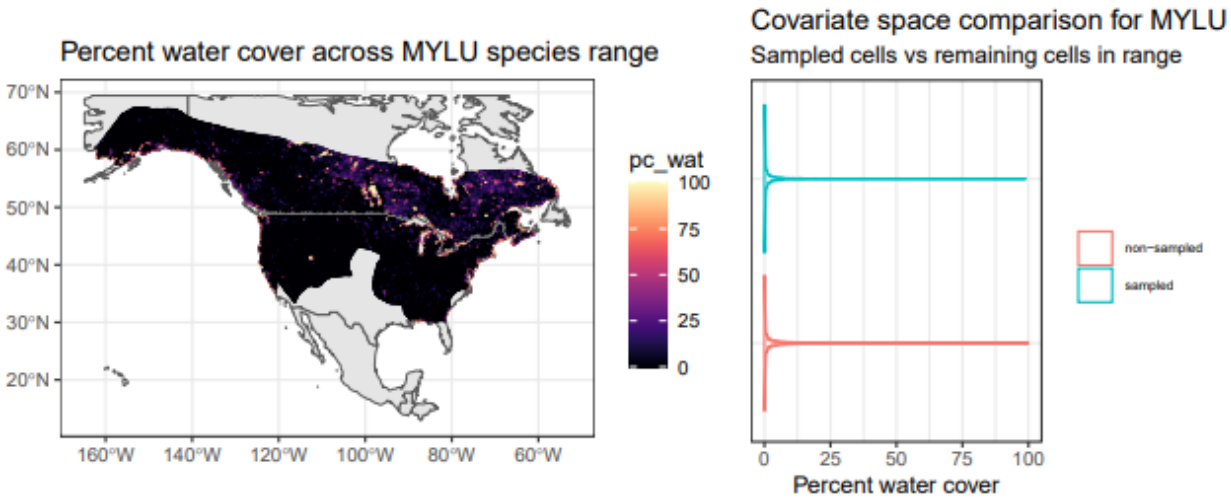

Figure B4.7. Percent water cover across *Myotis lucifugus* (MYLU) species range.

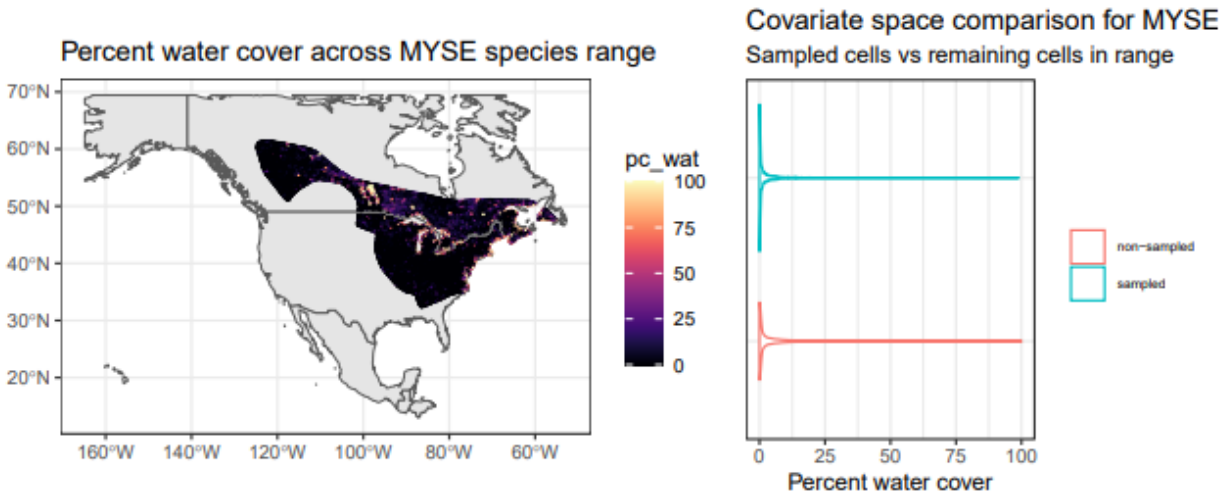

Figure B4.8. Percent water cover across *Myotis septentrionalis* (MYSE) species range.

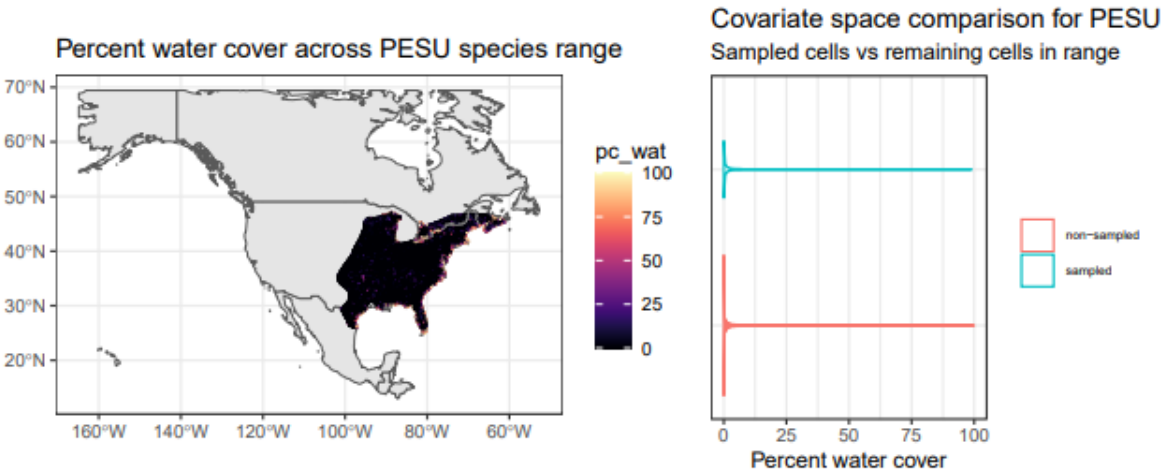

Figure B4.9. Percent water cover across *Perimyotis subflavus* (PESU) species range.

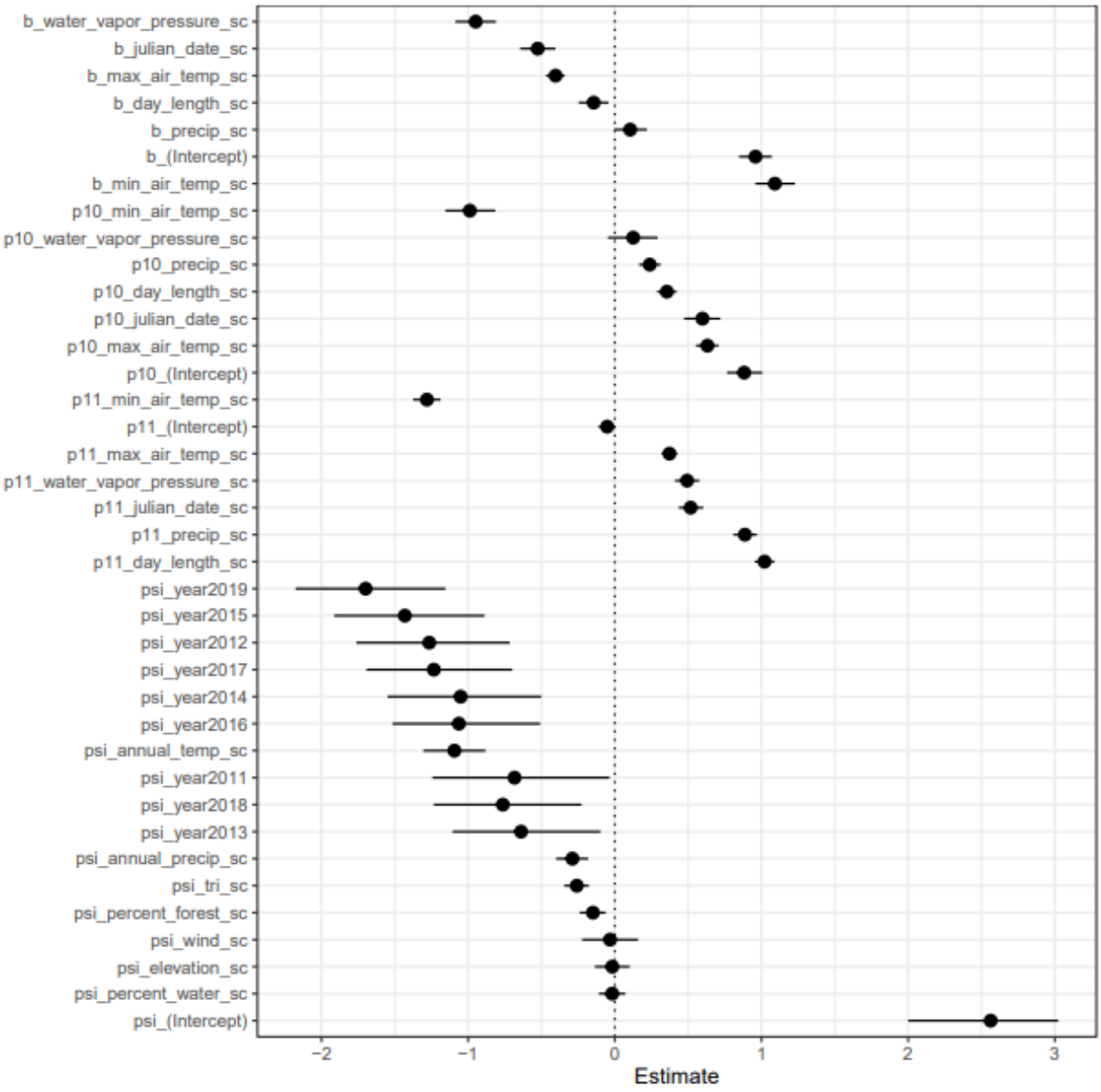

Figure B4.10. Posterior mean estimates (with accompanying 95% credibility intervals) for all model parameters from the *Myotis lucifugus* (MYLU) model. Detection-level parameters denoted by a 'b_' or 'p10_' or 'p11_'. The occupancy level parameters were denoted by 'psi_.'

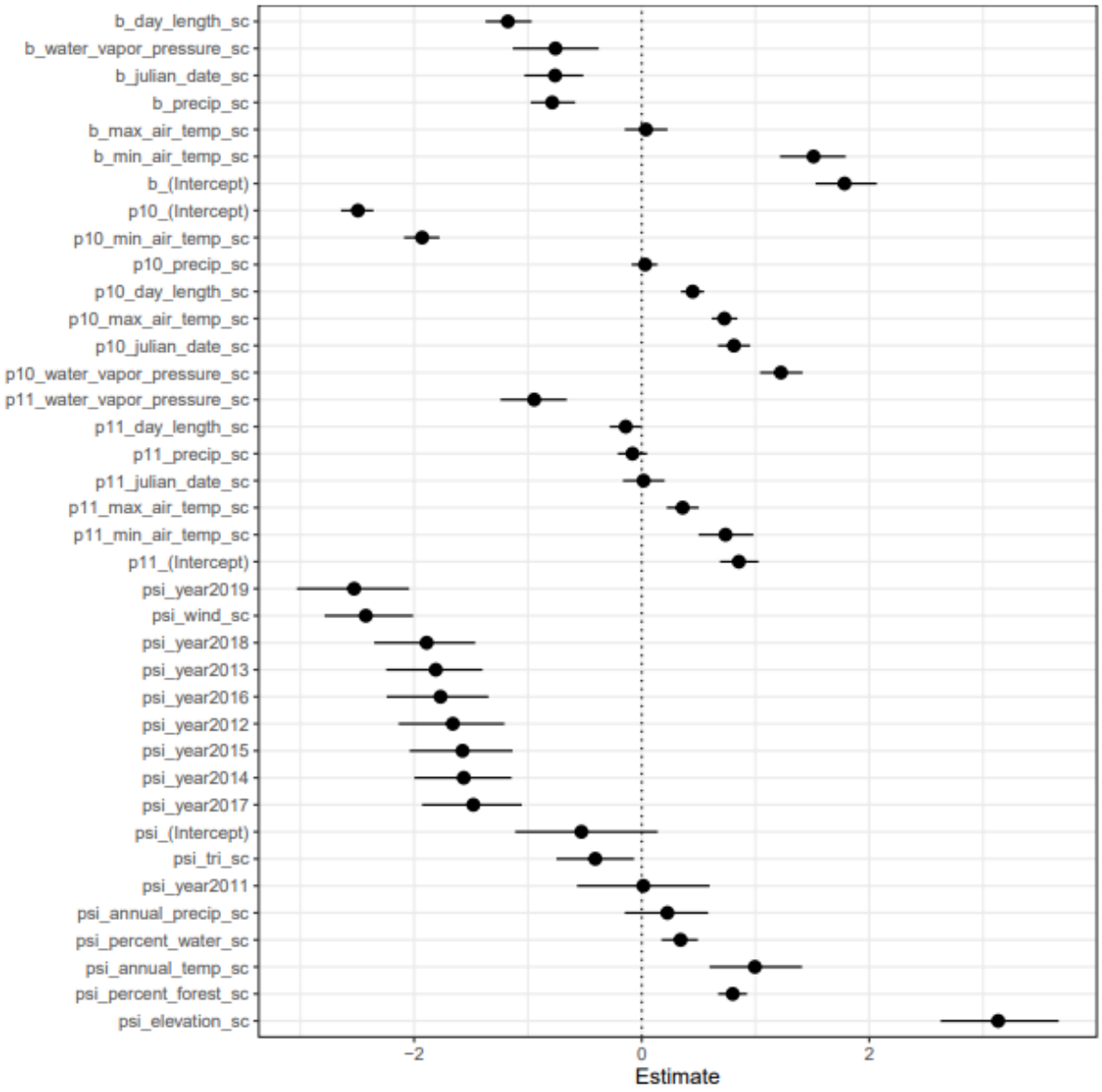

Figure B4.11. Posterior mean estimates (with accompanying 95% credibility intervals) for all model parameters from the *Myotis septentrionalis* (MYSE) model. Detection-level parameters denoted by a 'b_' or 'p10_' or 'p11_'. The occupancy level parameters were denoted by 'psi_.'

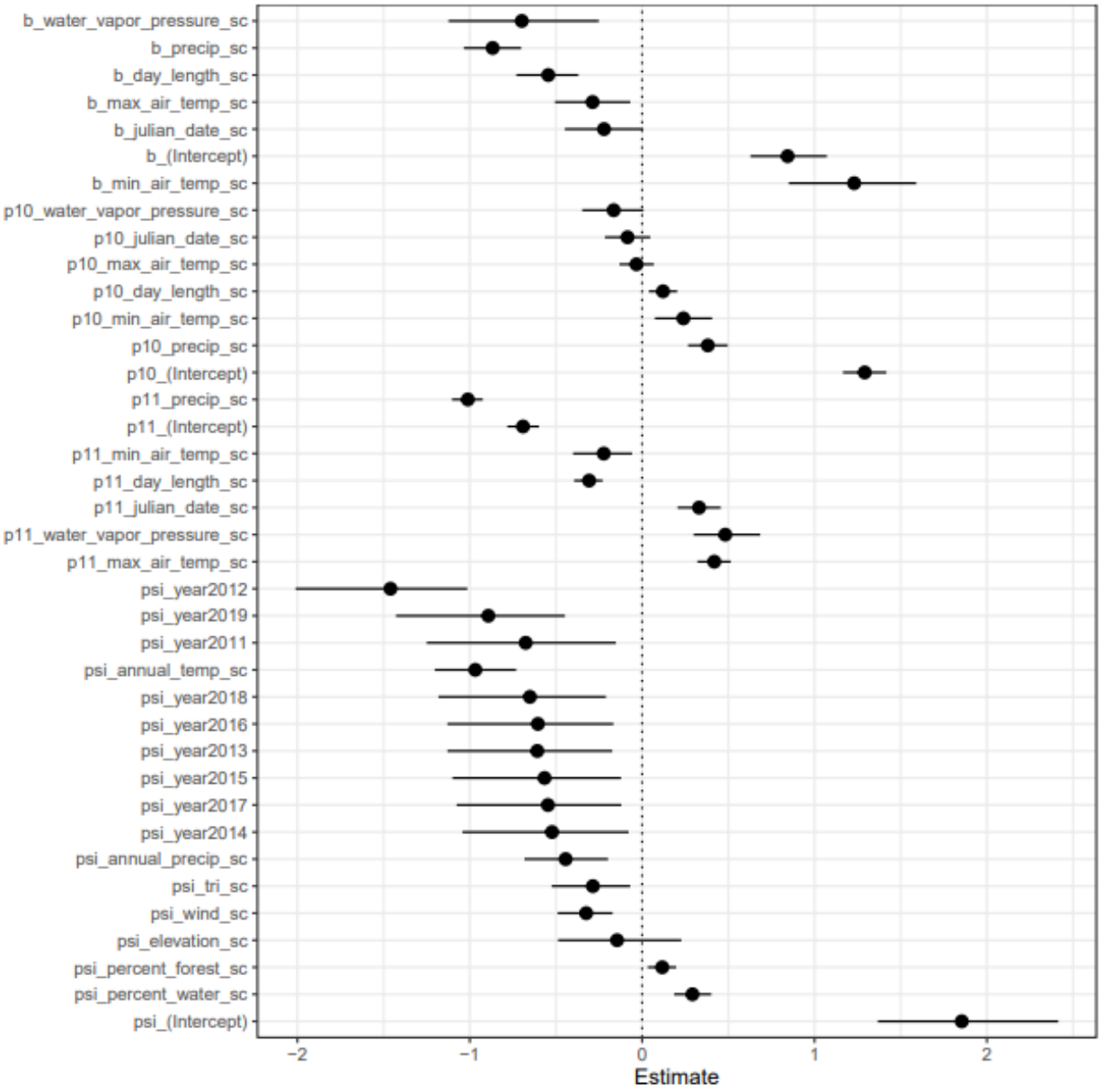

Figure B4.12. Posterior mean estimates (with accompanying 95% credibility intervals) for all model parameters from the *Perimyotis subflavus* (PESU) model. Detection-level parameters denoted by a 'b_' or 'p10_' or 'p11_'. The occupancy level parameters were denoted by 'psi_.'

Chapter C. Summer Mobile Acoustic Transect Analysis for Little Brown, Northern Long-eared and Tricolored Bat Species Status Assessment

By Michael Whitby[1], Brad J. Udell[2], Ashton M. Wiens[3], Tina Cheng[1], Winifred F. Frick[1,4], Brian E. Reichert[2], and Jonathan D. Reichard[5]

Introduction

We assisted in the Species Status Assessment for *Myotis lucifugus (MYLU)*, *Myotis septentrionalis (MYSE)*, and *Perimyotis subflavus (PESU)*, conducting analyses to estimate changes in bat echolocation activity recorded during mobile transect surveys. Bat activity recorded during mobile acoustic transects provide an index of abundance and can be used to determine changes in populations over time (Roche et al. 2011, Jones et al. 2013). Mobile acoustic transects in Europe have revealed that a ~3% annual decline of common bat species is detectable within 5-8 years given modest sampling effort (Roche et al. 2011, Jones et al. 2013). For species rarely detected (~ 1.8 passes per transect), it may take 10-15 years to detect a 2.5% annual decline by mobile transect surveys (Jones et al. 2013). A recent study using a subset of mobile transect monitoring data provided to the SSA found substantial declines in relative abundance for both *Myotis lucifugus* and *Perimyotis subflavus* (Evans et al. 2021). Therefore, we expect that mobile transect surveys should be able to detect large changes in populations for *Myotis lucifugus*, *Myotis septentrionalis*, and *Perimyotis*

[1] Bat Conservation International
[2] U.S. Geological Survey, Fort Collins Science Center, Fort Collins, CO 80526
[3] U.S. Geological Survey, Upper Midwest Environmental Sciences Center, La Crosse, WI 54603
[4] University of California, Santa Cruz, CA 95064
[5] U.S. Fish and Wildlife Service, Ecological Services, Hadley, Massahusettes, 01035, USA

subflavus over the past decade related to the main stressor on North American hibernating bat populations, the emergence of white-nose syndrome (WNS).

Our objectives were to determine changes in bat populations using mobile acoustic transects at four different spatial scales relevant to inform the Species Status Assessment, including: (1) restricted to where mobile acoustic transects were conducted; (2) predicted range-wide but bounded by the spatial extent of sampling; (3) predicted within Representation Units defined by the U.S. Fish and Wildlife Service (USFWS), and (4) predicted for each state.

To determine the changes in bat populations, we first modeled bat activity as counts of echolocation call sequences recorded along mobile acoustic transects. We used three categories of variables to model the count of call sequences along a transect:

1. Stressors to populations — We examined the influence of WNS and wind energy development over time.
2. Spatial variation in activity — We used latitude, longitude, and habitat covariates to account for changes in activity across landscapes.
3. Sampling variation — We accounted for day of year, sampled transect length, detector type, and ID software used.

We then predicted the number of call sequences at each spatial scale and year. Finally, we derived the rate of change in population from the change in the predicted number of call sequences.

Methods

Data Acquisition and Curation

We acquired data from the North American Bat Monitoring Program (NABat) database supplemented with data contributed from West Virginia and New York. These two states have mobile acoustic sampling programs that began in 2009 but their mobile acoustic data have not been contributed to the NABat Program database. R code referred to below is thoroughly documented and available in a data release (Whitby et al. 2021).

Mobile Acoustic Data from NABat Database

We obtained data stored in the NABat database (NABat 2020).

Data were curated using the file *`SSAmobile_01_formatNABatData.Rmd`*. Steps included:

1. Set missing detectors and software to an 'unknown' category.
2. Removed data if transect length was not provided or estimable (due to missing geocoordinates of calls recorded along a transect).
3. Removed data with multiple entries in the NABat database (multiple grid cell/date combinations) by:
    A. Retained one instance of GRTS ID (see glossary) with same number of auto-ID records but different batch_id and/or vetted echolocation calls.
    B. Added call sequence count and transect length of GRTS ID with multiple location names.
    C. Added call sequence count and transect length of GRTS ID with multiple transect lengths recorded.

D. Used the max call sequence count when multiple counts but same transect length is listed.

Of the 10,799 transect runs that passed initial data filtering, 64.2% had lengths documented by the contributor. We assigned transect lengths to an additional 4.9% of runs based on data previously provided for a location (0.5% were based on data from the same year; 4.4% were based on data from other years). We estimated transect length for the remining 30.9% of runs. We estimated transect length using a linear mixed model with form:

Eq.1 Model to estimate transect length:

$$Transect_{Length_{syr}} \sim \mu + \alpha_s + \beta_1(\max\_estimated\_length_{syr}) + \beta_2(avg\_estimated\_length_{syr}) + e_{syr}$$

Where:

- $Transect\_Length_{syr}$ represent the transect length as documented by the data contributor for the r^{th} survey of y^{th} year at the s^{th} site.
- μ represent overall mean.
- α_s represent the site level difference from overall mean (μ) for each site *s*.
- β_1 ($max\_estimated\_length_{syr}$) represent the association between the actual transect length and the max estimated length on the r^{th} survey of y^{th} year at the s^{th} site.

- B_2 (avg_estimated_length$_{syr}$) represent the association between the actual transect length and the average estimated length on the r^{th} survey of y^{th} year at the s^{th} site.

We used 6,897 runs at 1,077 unique grid cells to model actual transect length based on estimated length. The model performed well with a conditional $R^2 = 0.994$ (predicting length given each site level random effect) and marginal $R^2 = 0.692$ (predicting length using the mean site level effect across all sites).

Mobile Acoustic Data from West Virginia

Biologists in West Virginia began conducting mobile acoustic transects in 2009 and have continued to conduct almost all transects with a consistent methodology since that time. Data from West Virginia have not been uploaded to the NABat database and were provided under a data-sharing agreement between the West Virginia Division of Natural Resources and Bat Conservation International[1].

Data from West Virginia were curated using the R code in *SSAmobile_02_formatWVdata.R* utilizing custom functions located in *SSAmobile_f_formatWVdata.R*.

Data curation included:

1. Reconciling errors in Transect ID:
    A. Remove run number from end of name.
    B. Fix typos and remove extraneous information (e.g., date) in names.

[1] Data are not publicly available or have limited availability owing to restrictions stemming from sensitivity concerns from West Virginia Division of Natural Resources. Contact West Virginia Division of Natural Resources for more information.

C. Match transect names with <2 letter difference.

2. Merge date and length information with call sequence information.
3. Check documented transect date and file date stamp; remove any transect with >1-week discrepancy in dates.
4. Infer length information to transects with missing data:
   A. If a run length was not provided, use the average of all runs (regardless of year) for that route.
5. Remove runs with zero length.
6. Add location coordinate information:
   A. Exact location of transects (e.g., start point) was not provided.
   B. County of transect was provided.
   C. We assigned a point based on the county most commonly listed for a route.
   D. The grid cell of the county centroid was used for analysis.

Mobile Acoustic Data from New York

Biologists in New York state began conducting a statewide mobile transect program in 2009 and have continued that program every year with consistent methodology. Data from the New York Department of Environmental Conservation (NYDEC) were provided to Bat Conservation International through the United States Fish and Wildlife Service. Supplementary information on length of transects was provided directly to Bat Conservation International by the NYDEC.

Data curation included:

1. Fixing route name mismatches.

2. Assigning the mean length of all transects (19.4 miles) for transects without length information.

Final Data Curation

Data from the NABat database, West Virginia, and New York were joined with stressor and habitat covariates (year of *Pd* arrival, wind energy risk index, habitat composition) with `SSAmobile_04_combineData.R`. A dataset for each species was created by filtering for grid cells within a species range (as defined by the USFWS). The following data were removed from final analyses:

- Data from Canada due to our inability to calculate a comparable wind energy index (see below).
- Data collected from September through April as these months fall outside the summer maternity season.
- Data where no observations of a species were recorded on any run at a site (i.e., all zeros) were removed to prevent zero inflation.
- Sites with only one run were removed due to the lack of information they provide for trend analysis. Sites with multiple runs within a single year were retained for analysis because these data provide information on the effect of day of year and sampling variability.

Data from 6,887 runs at 698 unique grid cells passed data curation for *Myotis lucifugus* (Figure C1; Table C1). Individual grid cells were sampled for an average of 4.3 calendar years (range 1–11).

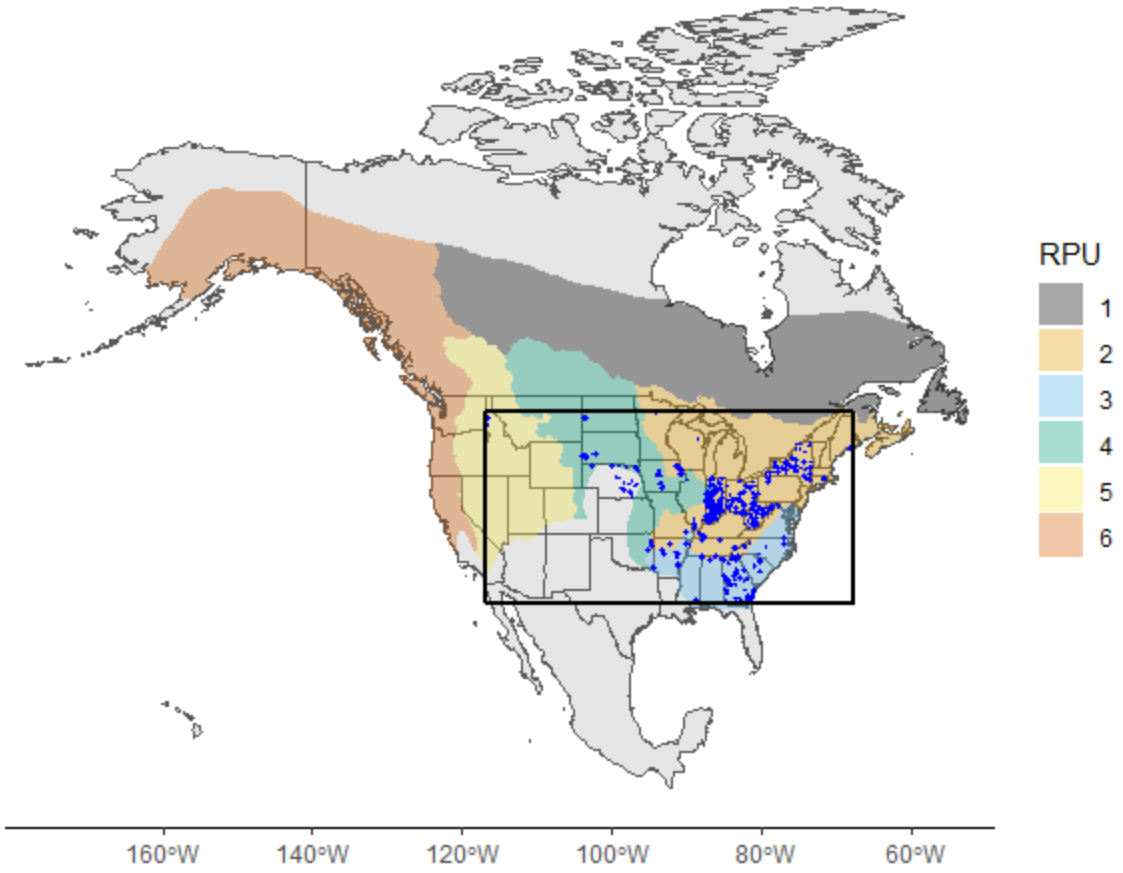

Figure C1. Sampling sites that recorded *Myotis lucifugus* calls at least once from 2009-2020 (blue points). The bounding box used for predictions (black box) is overlaid the Representation Units (RPU) as defined by the U.S. Fish and Wildlife Service (color shading).

Table C1. Sampling effort for sites that recorded *Myotis lucifugus* from 2009-2020.

Year	Sites	Runs	States
2009	98	164	3
2010	131	328	6
2011	203	435	8
2012	391	1066	14
2013	438	1276	16
2014	320	694	20
2015	250	498	18
2016	317	639	20
2017	297	582	19
2018	267	555	21
2019	259	533	21
2020	50	117	5

Data from 1,944 runs at 121 unique grid cells passed data curation for *Myotis septentrionalis* (Figure C2; Table C2). Individual grid cells were sampled for an average of 6.7 calendar years (range 1–11).

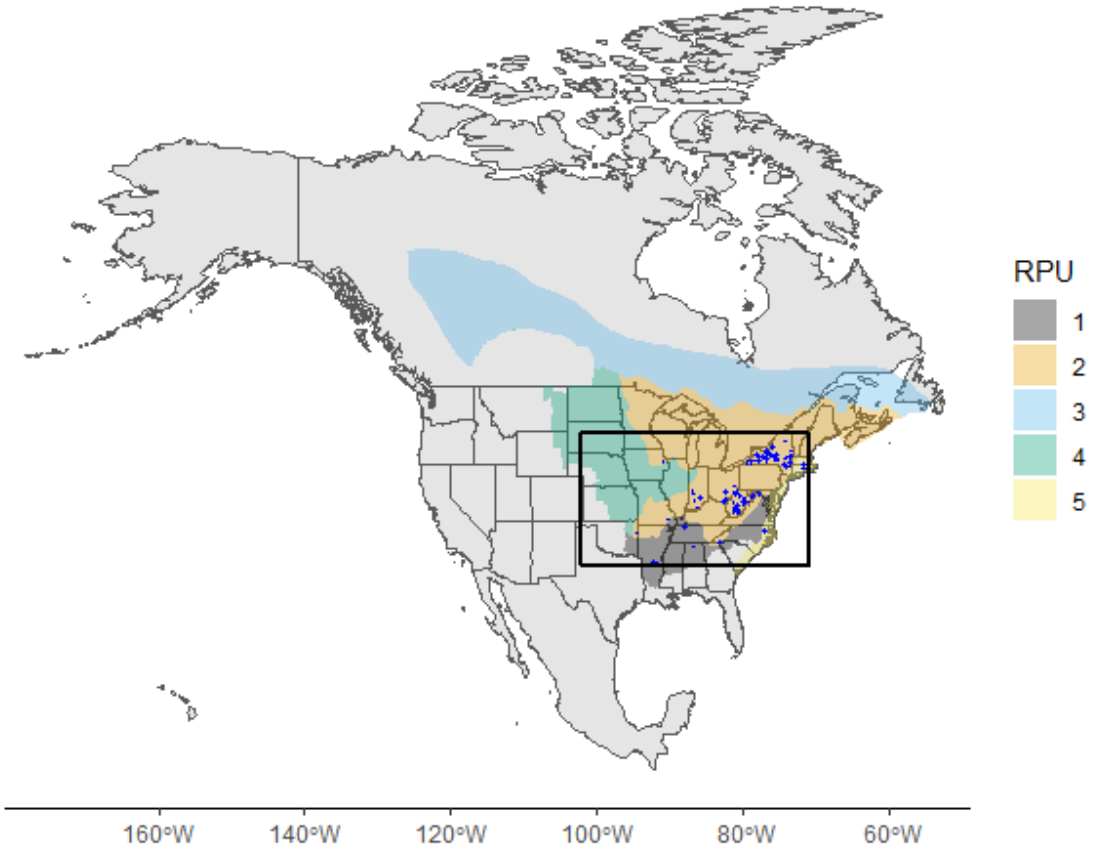

Figure C2. Sampling sites that recorded *Myotis septentrionalis* calls at least once from 2009-2020 (blue points). The bounding box used for predictions (black box) is overlaid the Representation Units (RPU) defined by the U.S. Fish and Wildlife Service (color shading).

Table C2. Sampling effort for sites that recorded *Myotis septentrionalis* from 2009-2020.

Year	Sites	Runs	States
2009	62	112	2
2010	73	197	3
2011	74	192	6
2012	91	254	13
2013	88	250	13
2014	73	175	15
2015	65	150	13
2016	66	139	15
2017	68	154	10
2018	75	160	14
2019	64	140	15
2020	6	21	3

Data from 8,843 runs at 958 unique grid cells passed data curation for *Perimyotis subflavus* (Figure C3; Table C3). Individual grid cells were sampled for an average of 4.2 calendar years (range 1–11).

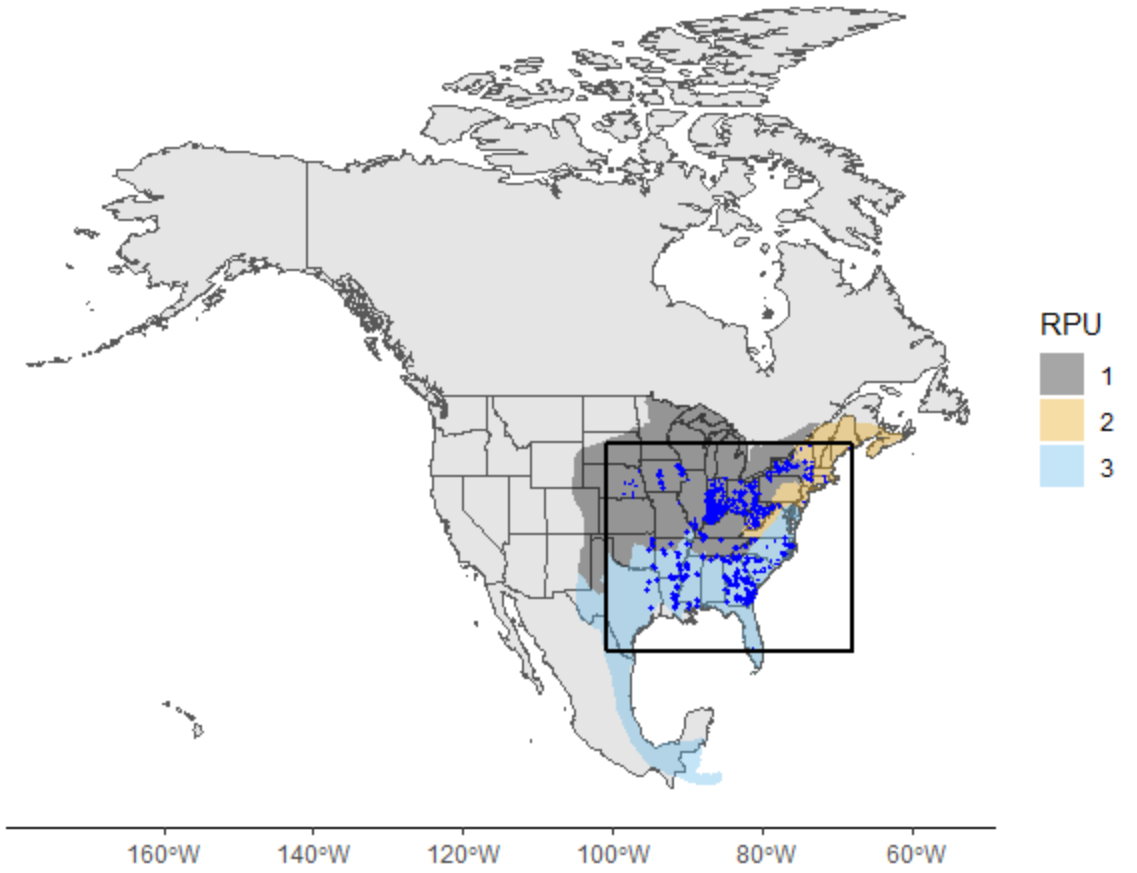

Figure C3. Sampling sites that recorded *Perimyotis subflavus* calls at least once from 2009-2020 (blue points). The bounding box used for predictions (black box) is overlaid the Representation Units (RPU) defined by the U.S. Fish and Wildlife Service (color shading).

Table C3. Sampling effort for sites that recorded *Perimyotis subflavus* from 2009-2020.

Year	Sites	Runs	States
2009	87	145	3
2010	132	338	6
2011	224	501	8
2012	526	1388	16
2013	580	1648	17
2014	464	962	19
2015	348	666	17
2016	430	841	20
2017	380	720	18
2018	378	744	23
2019	375	760	22
2020	57	130	6

Covariates

Populations Stressors

Years since detection of *Pseudogymnoascus destructans* (*Pd*)

To determine whether bat activity of *Myotis lucifugus*, *Myotis septentrionalis*, and *Perimyotis subflavus* changed in relation to the spread of WNS, we use a covariate to represent the number of years since detection of *Pd*. Since mobile transects are not conducted at hibernacula where the arrival of *Pd* is documented using standard survey techniques of swab sampling and qPCR detection (Muller et al. 2013) or visual signs of disease (Janicki et al. 2015), we estimated the year of *Pd* arrival across the landscape. Estimated year of *Pd* arrival is used to approximate when WNS might show impacts on summer populations (Dzal et al. 2011). We used estimates of *Pd* arrival for each grid cell from a Gaussian process model trained on 596 known years of detection from standard *Pd*/WNS surveillance surveys conducted at hibernacula (Wiens et al. 2021). The model predicts year of arrival (YOA) of *Pd* in calendar years (e.g., 2014). We convert YOA to a scaled covariate of years since detection (YSD) of *Pd* for each site and year a mobile transect was conducted by subtracting the year of arrival rounded to the nearest integer from the

calendar year. Negative values of YSD indicate years before *Pd* is estimated to have arrived. A YSD of zero indicates the year *Pd* is estimated to have arrived.

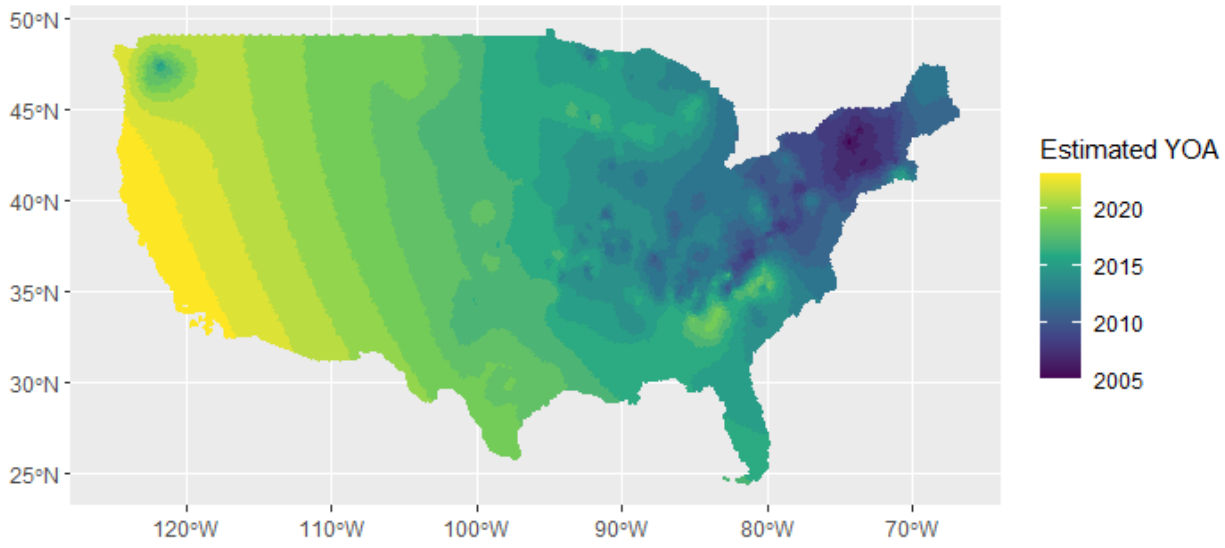

Figure C4. Estimated year of arrival (YOA) of *Pseudogymnoascus destructans* (*Pd*) as predicted with a Gaussian process model (Wiens et al. 2021)

Risk Index from Wind Energy Development

Another major potential stressor on bat populations is mortality from collisions with wind energy turbines (O'Shea et al. 2016, Kunz et al. 2007). To determine whether bat activity of *Myotis lucifugus*, *Myotis septentrionalis*, and *Perimyotis subflavus* changed in relation to increases in installed wind energy turbines in the United States, we calculated a covariate to measure the relative mortality risk from collision with wind energy turbines for each grid cell. The metric uses installed wind energy capacity in megawatts each year and mean dispersal distances estimated for each species from empirical banding records. Details of the wind energy risk index can be found in Appendix C-1.

Spatial Variation

Latitude and Longitude

The latitude and longitude of the center of each grid cell was used to account for geographic variation in activity associated with large scale geographic patterns (e.g., ecoregions, mountain ranges, etc.) that are not captured in other covariates.

Habitat Composition

We extracted habitat composition of land cover types in each grid cell from the NABat Database. Land cover composition was derived from the land cover classification scheme of the Canada Centre for Remote Sensing (CCRS 2013). This dataset determines land cover classes at a resolution of 250 m from the MODIS satellite from 2010 images. We extracted a single value for each grid cell. We were not able to account for changes in habitat composition since the land cover dataset is not updated annually. We used the following habitat classes:

- Forest cover (any class with 'forest' in the name)
- Wetland
- Water
- Urban Area

We extracted habitat covariate data using *`covar_queries_loop.Rmd`*.

Sampling Variation

Day of Year

Bat activity is known to change over the course of the summer maternity season. In these three species, adults migrate into an area during the late spring and form stable maternity colonies in the early summer. Young of the year become volant in mid-late July, normally within

1 week of each other. This is quickly followed by fall migration out of an area in early to mid-August. Therefore, changing the sampling day between years could influence the number of call sequences recorded.

Transect Length

Changes in transect length could influence the number of call sequences recorded. We used transect length as a predictor variable rather than using an offset term because an offset requires known length for each transect and approximately 30% of transects lengths were estimated (see above).

Bat Detector Type

To account for any variation in recording call sequences due to changes in use of bat detector (and microphone) type, we included detector type as a random effect.

ID Software

ID software can change the absolute number of call sequences detected and was included as a random effect.

Data Analysis

Data were analyzed using three R markdown files with embedded script (Whitby et al. 2021): *SSAmobile_06?_buildModels_SPPC* (where ? is a-c and SPPC=the four-letter species code), *SSAmobile_07b_predictions*, and *SSAmobile_08_Results*. These rMarkdown files used functions found in the R script *SSAmobile_f_analysisFunctions* file to conduct much of the analysis.

We used generalized linear mixed models (GLMMs) of the negative binomial family (quadratic parameterization; Hardin & Hilbe 2007) with a log link to describe the effects of

predictors on the number of calls recorded along transect runs. Models were fit using R package glmmTMB (Brooks et al. 2017, Magnusson et al. 2020) in Microsoft R Open version 4.0.2 (Microsoft and R Core Team 2020). R code referred to here is thoroughly documented in the data release Whitby et al. (2021).

The general form of the model was:

Eq. 2 General model form for estimating changes in bat call sequences with mobile transects:

$$
\begin{aligned}
Call\ Sequences_{syr} \sim\ & \mu \\
& + \ (\beta_1 + v_s)(bs_3^1(YSD\ Pds)) + \beta_2(Wind\ Energy\ Risk\ Index_{sy}) \\
& + \beta_3(ns_{best1-9}^3(Latitudes)) + \beta_4(ns_{best1-9}^3(Longitudes)) \\
& + \beta_5(\%\ Forests) + \beta_6(\%\ Wetlands) + \beta_7(\%\ Urbans) + \beta_8(\%\ Waters) \\
& + \beta_9(ns_{best1-3}^3(Day\ of\ Yearsyr)) + \beta_{10}(log(LengthSampledsyr)) \\
& + \alpha Detectord + \alpha Softwarei \\
& + \alpha Routes + \alpha Yearsy \\
& + esyr
\end{aligned}
$$

Where:

- *Call Sequences*$_{syr}$ represents the number of recording files identified to species of interest on the r^{th} survey of y^{th} year at the s^{th} site.
- μ represents the overall mean number of call sequences.
- $\boldsymbol{bs_3^1}$ (YSD *Pd*$_s$) represents the first-degree basis spline with 3 degrees of freedom of the number of years since detection of *Pd* for site *s.* We attempted to allow the effect (i.e., slope) to vary by site (indicated by $+v_s$). However, models for *Myotis lucifugus* and *Myotis septentrionalis* did not converge with this term included and it was removed for these two species.
- *Wind Energy Risk Index*$_{sy}$ represents Wind Energy Index at grid cell *s* for year *y*.

- $\boldsymbol{ns^{3}_{best1-9}}(\text{Latitude}_{s})$ represents the best-fitting natural cubic with 1 to 9 degrees of freedom of the latitude of site *s* (note: the number of parameters/effects/betas estimated will equal the number of degrees of freedom chosen). Using AIC, we determined that 5, 5, and 9 degrees of freedom best explained latitudinal variation for *Myotis lucifugus*, *Myotis septentrionalis*, and *Perimyotis subflavus* respectively.
- $\boldsymbol{ns^{3}_{best1-9}}(\text{Longitude}_{s})$ represents the best-fitting natural cubic with 1 to 9 degrees of freedom of the longitude of site *s* (note: the number of parameters/effects/betas estimated will equal the number of degrees of freedom chosen). Using AIC, we determined that 7, 3, and 5 degrees of freedom best explained longitudinal variation for *Myotis lucifugus*, *Myotis septentrionalis*, and *Perimyotis subflavus* respectively.
- % $\text{Forest}_{\boldsymbol{s}}$ represents the percent forest cover in grid cell *s*.
- % $\text{Wetland}_{\mathbf{s}}$ represents the percent wetland habitat in grid cell *s*.
- % $\text{Urban}_{\mathbf{s}}$ represents the percent urban area in grid cell *s*.
- % $\text{Water}_{\mathbf{s}}$ represents the percent of grid cell *s* covered in water.
- $\boldsymbol{ns^{3}_{best1-3}}(\text{Day of Year}_{syr})$ represents the best-fitting natural cubic spline (with up to 3 degrees of freedom) of day of year the r^{th} survey of the y^{th} year at the s^{th} site was conducted. Using AIC, we determined that 3 degrees of freedom was the best fitting model for all three species.
- $\log(\text{Length Sampled}_{\mathbf{syr}})$ represents the log of the length of the r^{th} survey of y^{th} year at the s^{th} site.

- $\alpha_{Detector_d}$ represents the random effect of detector d; mean difference from overall mean (μ) for detector type *d.*
- $\alpha_{Software_i}$ represents the random effect of software I; mean difference from overall mean (μ) for Auto Identification type *i.*
- α_{Route_s} represents the random effect of site s; mean difference from overall mean (μ) for site *s.*
- α_{Year_y} represent the random effect of year y; mean difference from overall mean (μ) for year *y.*
- e_{syr} represents the residual unaccounted-for error.

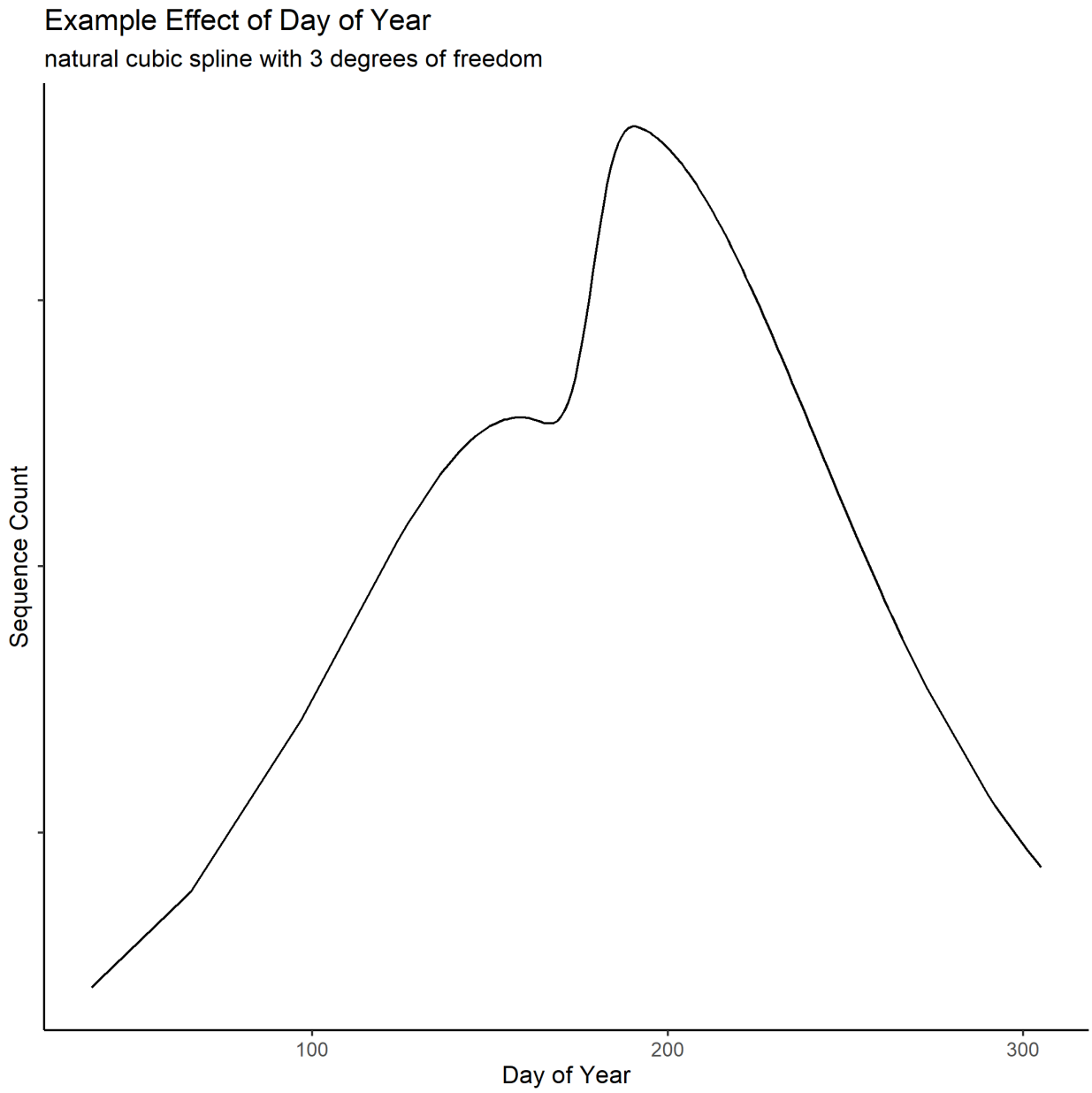

Figure C5. Example of a cubic natural spline with three degrees of freedom fitted to bat activity (sequence count) by day of year.

Splines were used for years since detection of *Pd* as well as latitude, longitude, and day of year to allow for non-linear responses. For example, bat activity does not correlate linearly with day of year. Bat activity increases in the spring as bats emerge from hibernacula and move across the landscape to summer habitats. Amount of activity is generally static when

populations are stable and non-migratory during gestation, parturition, and lactation (day ~150-~175). Local population sizes can nearly double around day 175 when young of the year become volant, which may influence bat activity. As bats leave summer habitats to return to hibernacula, a steady decrease in activity may occur. An example is shown in Figure C5.

In addition to using splines, fixed predictor variables were scaled by their mean and standard deviation in the data set. This results in each predictor having a mean of 0 and SD of 1. This was necessary to put all variables on a common scale and to achieve model convergence. Caution must be taken when interpreting values as they are representative of the covariate effect given the number of standard deviations from the mean rather that a direct relationship with the unscaled predictor.

Model performance was evaluated using the performance (Lüdecke et al. 2021) and DHARMa (Hartig 2021) packages. Specifically, we examined the models for multicollinearity, heteroscedasticity, homogeneity, uniformity, dispersion, and outliers.

Calculating Rate of Change (λ)

Counts of call sequences for each species were predicted using a bootstrapping procedure to predict responses 100 times. We conducted bootstrapping with the bootMer function of R package lme4 (Bates et al. 2015). Predictions were made using spatially and temporally explicit values of stressor covariates (e.g., habitat and wind energy risk index) at the grid cell level and constant sampling covariates, including the mean of detector and software random effects. Predictions were conditional on year random effects and for day 211 (~July 29th) every year. Transect length was held constant at 25 miles (40.2 km). Counts of call sequences of each species for each site were predicted from 2009-

2020. Range-wide predictions were constrained to a bounding box within the minimum and maximum latitude and longitude of sampled sites (Figure C1 – Figure C3).

For each area of interest (e.g., sampled sites, state, or Representation Unit), the sum of activity predicted in cells within that area was used to calculate lambda (λ) within that region using Equation 3. Cumulative lambda was taken as the change from year 1 to the current year (i.e., the denominator in Eq 3 remained constant at year 1).

Eq. 3 Calculation of lambda for the area (a) of interest. y=year:

$$\frac{\sum PredictedSequences_{ya}}{\sum PredictedSequences_{(y-1)a}}$$

The predicted median count of call sequences and lambda for each simulation and data subset (observation sites, range wide, Representation Unit, state) are plotted with boxplots that show the median, upper quantile (75th percentile), lower quantile (25th percentile), min, max, and outliers of the 100 simulations.

Results

Models for all three species fit well (Table C4). We detected heteroskedasticity in the residuals of models for *Myotis lucifugus* and *Perimyotis subflavus*, indicating that additional predictors might be needed to explain variation in the call sequences recorded along transects.

The full modeling effort process and results are available through a USGS data release (Whitby et al. 2021).

Table C4. Final model diagnostics for the general model (see Data Analysis section) for the three bat species.

	Myotis lucifugus	*Myotis septentrionalis*	*Perimyotis subflavus*
Heteroskedasticity	Yes	No	Yes
Spatial autocorrelation	No	No	No
Conditional R2	63.9%	47.5 %	69.2 %
Marginal R2	34.9%	27.8 %	50.7 %

Variable Importance

The scaling of variables allows the coefficient estimates of each predictor to be compared as a rough measure of variable importance. Larger absolute values indicate a greater variable importance. While this relationship roughly holds true for splines (natural and basis) the interpretation of spline coefficients is extremely difficult. Similar to interpretation of interactions of fixed effects, each spline basis can only be interpreted in conjunction with the other spline basis (e.g., a spline of 3 degrees of freedom must be interpreted using all 3 basis). This interpretation is complicated by the many (up to 9) bases used in our analysis and that each basis is non-linear (i.e., each basis is its own cubic (natural spline) or tent function (basis spline)). The sign of the spline coefficient is not indicative of a negative or positive relationship with the response. However, the absolute value is still a measure of variable importance with respect to the response.

Years since *Pd* detection (YSD) and the wind energy risk index were important variables for predicting number of call sequences for each species (Figure C6). Generally, latitude and longitude were also important predictors of the number of call sequences recorded, although there was high variability in some of the coefficient estimates. Habitat variables were slightly

informative in most instances (did not overlap zero). Day of Year was also an important predictor of activity for all species.

A

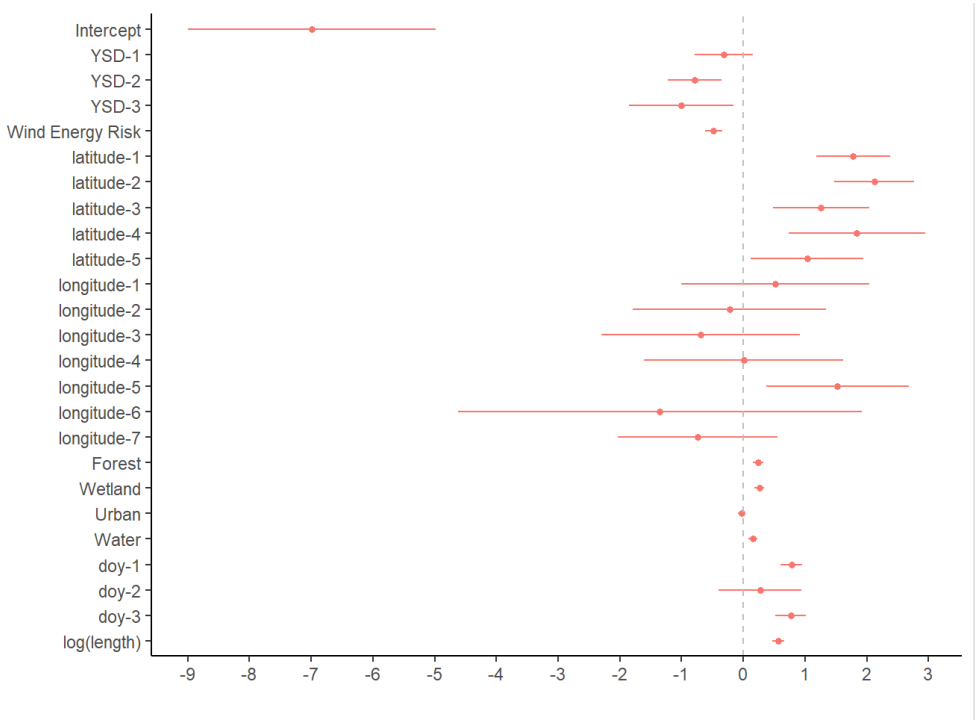
Intercept
YSD-1
YSD-2
YSD-3
Wind Energy Risk
latitude-1
latitude-2
latitude-3
latitude-4
latitude-5
longitude-1
longitude-2
longitude-3
longitude-4
longitude-5
longitude-6
longitude-7
Forest
Wetland
Urban
Water
doy-1
doy-2
doy-3
log(length)
-9 -8 -7 -6 -5 -4 -3 -2 -1 0 1 2 3

B

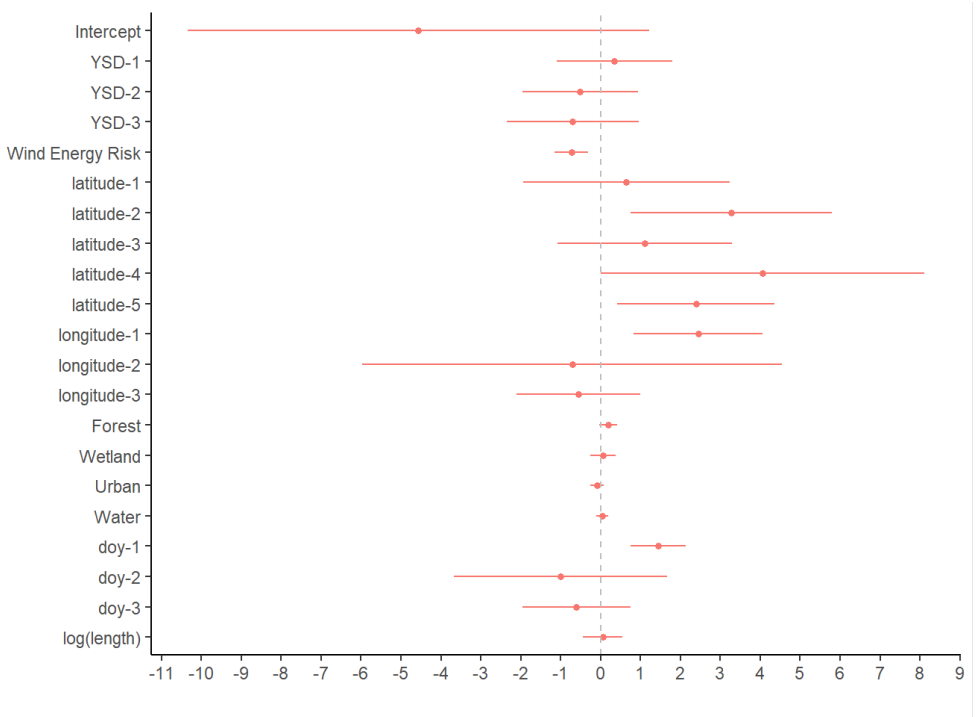
Intercept
YSD-1
YSD-2
YSD-3
Wind Energy Risk
latitude-1
latitude-2
latitude-3
latitude-4
latitude-5
longitude-1
longitude-2
longitude-3
Forest
Wetland
Urban
Water
doy-1
doy-2
doy-3
log(length)
-11 -10 -9 -8 -7 -6 -5 -4 -3 -2 -1 0 1 2 3 4 5 6 7 8 9

C

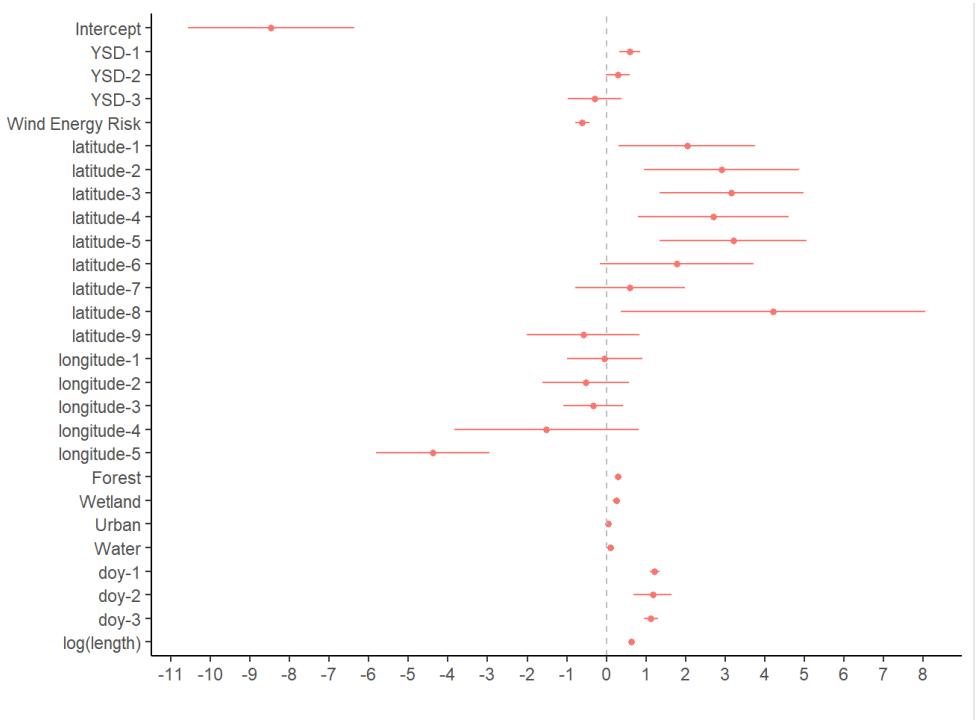

Figure C6. Parameter estimates and 95% confidence intervals for (A) *Myotis lucifugus*, (B) *Myotis septentrionalis*, and (C) *Perimyotis subflavus* along mobile acoustic transects. See the section 'Variable Importance' above for details of interpretation. YSD is year since *Pseudogymnoascus destructans (Pd)* detection; DOY is day of year; length is length of transect.

Response to *Pd* Year of Arrival

The count of call sequences of *Myotis lucifugus, Myotis septentrionalis, Perimyotis subflavus* along mobile transects all declined steeply within 2-4 years of the predicted arrival of *Pd* (Figure C7). Four years after the arrival of *Pd*, declines for *Myotis lucifugus* and *Myotis septentrionalis* appear shallower as the predicted number of calls sequences per transect approach zero. For *Perimyotis subflavus*, which has higher call sequences per transect (note differences in scale of y-axes), call sequences continue to decline each year.

A

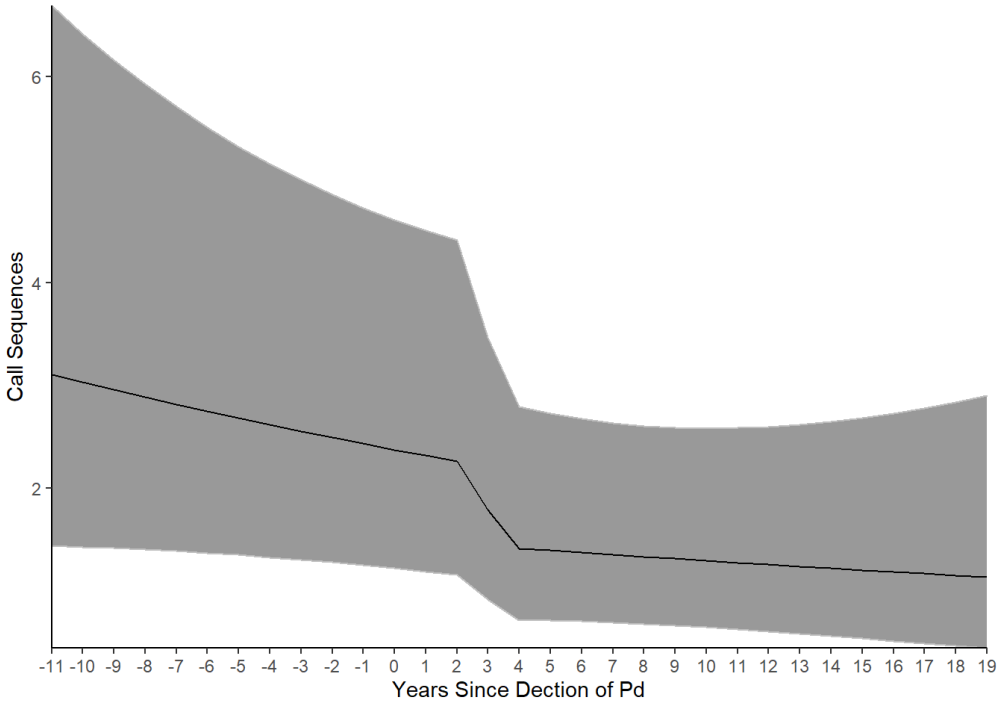
Call Sequences
6
4
2
-11 -10 -9 -8 -7 -6 -5 -4 -3 -2 -1 0 1 2 3 4 5 6 7 8 9 10 11 12 13 14 15 16 17 18 19
Years Since Dection of Pd

B

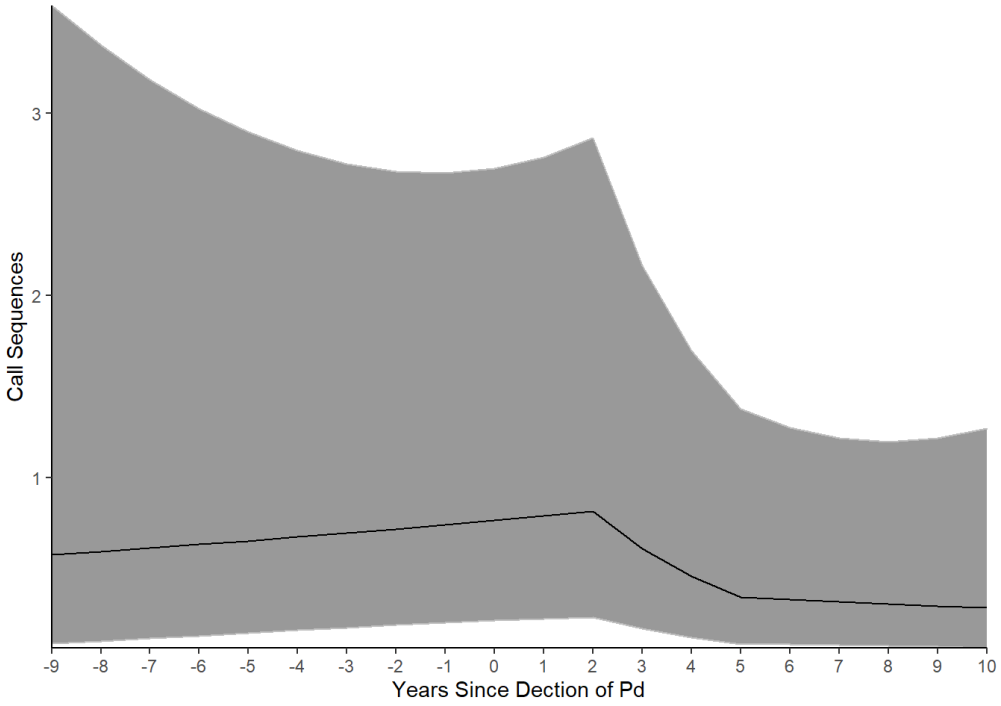
Call Sequences
3
2
1
-9 -8 -7 -6 -5 -4 -3 -2 -1 0 1 2 3 4 5 6 7 8 9 10
Years Since Dection of Pd

C

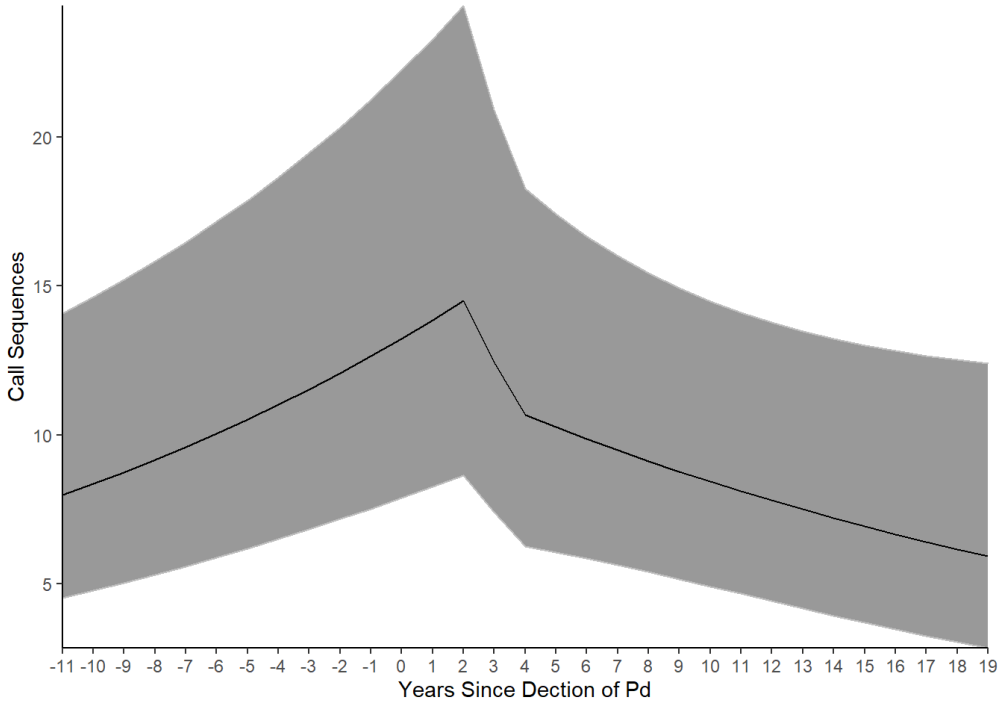

Figure C7. Relationship between years since detection of *Pseudogymnoascus destructans (Pd)* and activity of (A) *Myotis lucifugus*, (B) *Myotis septentrionalis*, and (C) *Perimyotis subflavus* along mobile acoustic transects. Plots are generated with all covariates, except year since *Pd* detection (*Pd* YSD), held at their mean.

Response to Wind Energy Risk Index

All species exhibited a decline in counts of call sequences as the wind energy risk index increased (Figure C8).

A

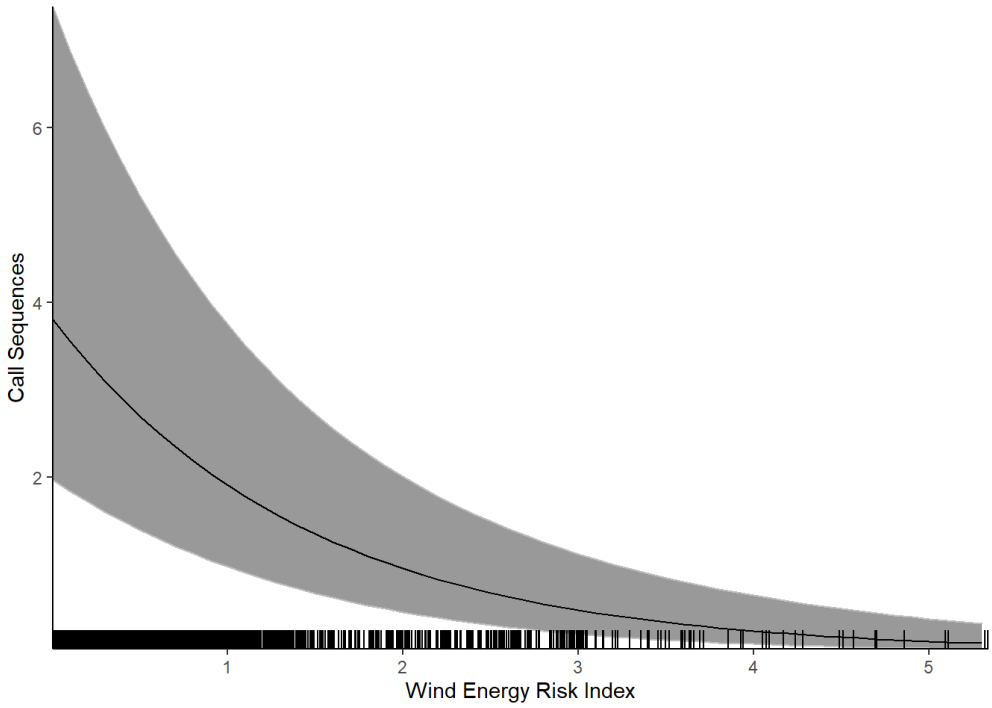
Call Sequences
6
4
2
1
2
3
4
5
Wind Energy Risk Index

B

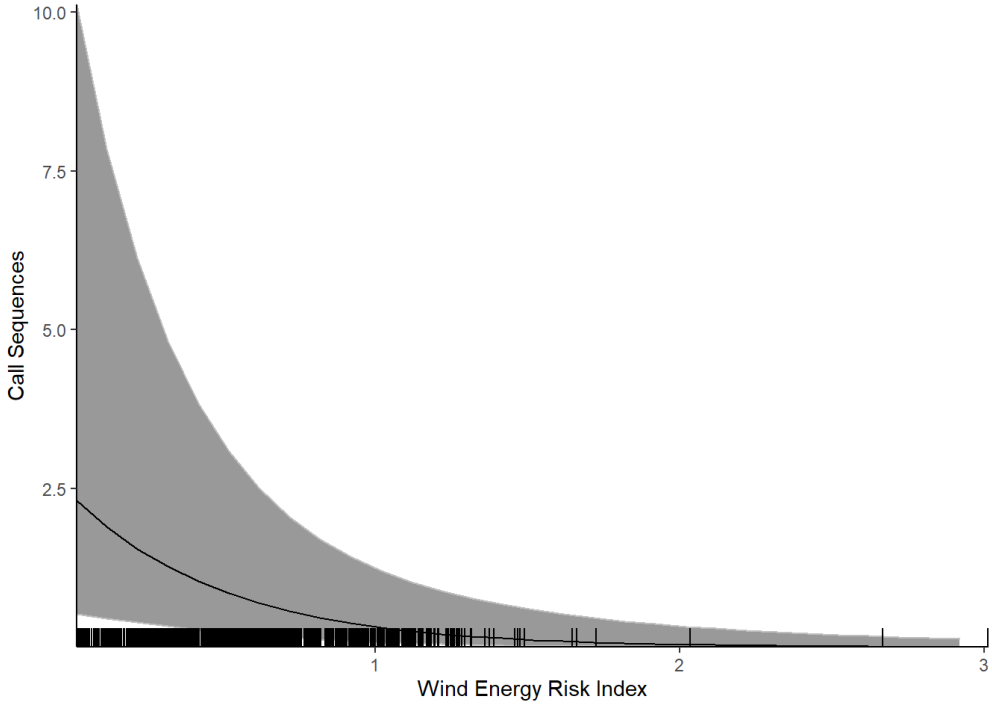
Call Sequences
10.0
7.5
5.0
2.5
1
2
3
Wind Energy Risk Index

C

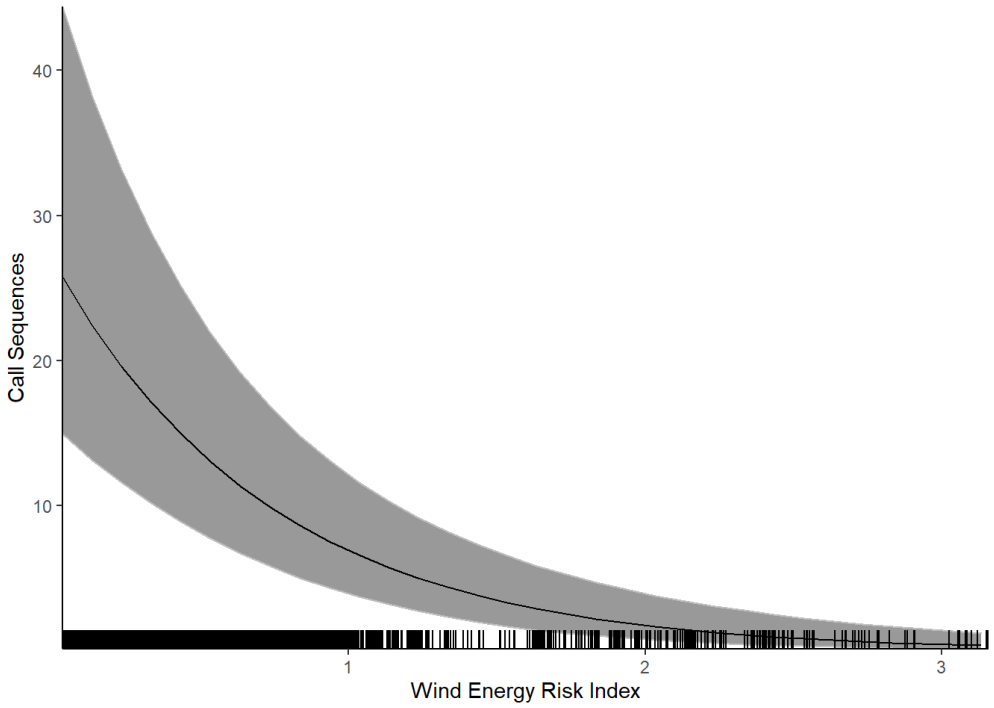

Figure C8. Relationship between Wind Energy Risk Index and activity of (A) *Myotis lucifugus*, (B) *Myotis septentrionalis*, and (C) *Perimyotis subflavus* along mobile acoustic transects. Inner tick marks represent values of original data used to build the model.

Rate of Change (λ) at Sampled Sites

The count of call sequences of *Myotis lucifugus* at sites with observations was projected to decline from a median of 2.64 call sequences per transect in 2009 to 0.96 in 2020. The median predicted total decline from 2009-2020 in *Myotis lucifugus* at sites that were sampled is 62% (Figure C9; Table C5).

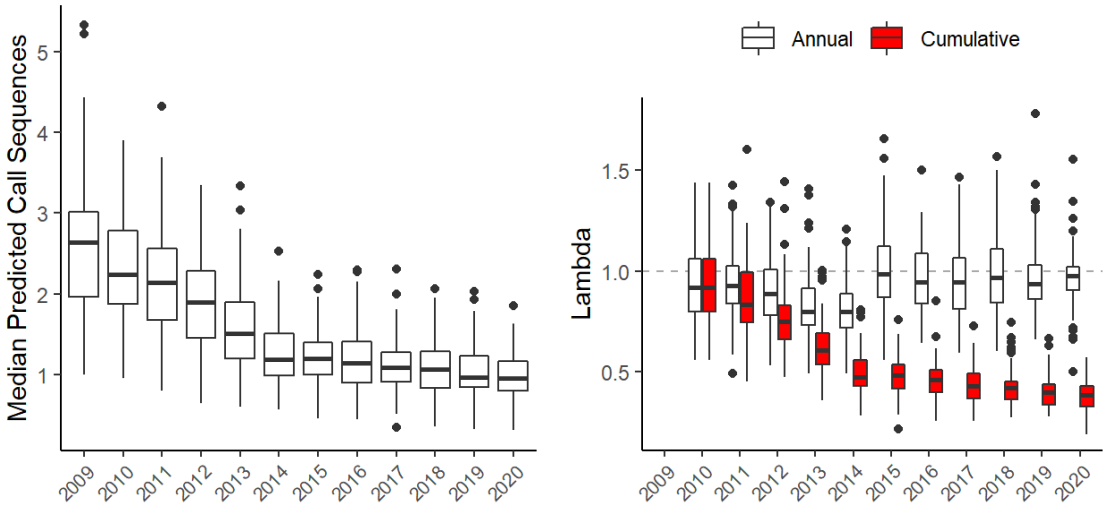

Figure C9. Distribution of median predicted call sequences (left panel) and annual and cumulative rate of change (lambda) (right panel) over 100 simulations at all sites where *Myotis lucifugus* were recorded at least once. Cumulative lambda values are relative to 2009. Boxplots represent the first (25th percentile), second (median), and third (75th percentile) quartiles. Whiskers extend to the minimum and maximum values that are not outliers (points; over 1.5 times interquartile range from nearest quartile).

Table C5. Median activity, annual rate of change, and cumulative rate of change from 100 simulations at all sites where *Myotis lucifugus* were recorded.

Year	Median Total Call Sequences	Median Annual Lambda	Median Cumulative Lambda
2009	2.64	—	—
2010	2.24	0.92	0.92
2011	2.14	0.93	0.83
2012	1.90	0.89	0.75
2013	1.51	0.80	0.60
2014	1.19	0.80	0.47
2015	1.20	0.99	0.48
2016	1.14	0.94	0.46
2017	1.09	0.95	0.43
2018	1.07	0.97	0.42
2019	0.97	0.94	0.40
2020	0.96	0.97	0.38

The count of call sequences of *Myotis septentrionalis* at sites with observations was projected to decline from a median of 0.53 call sequences per transect in 2009 to 0.09 call sequences in 2020. The median predicted total decline from 2009-2020 in *Myotis septentrionalis* at sites that were sampled is 83% (Figure C10; Table C6).

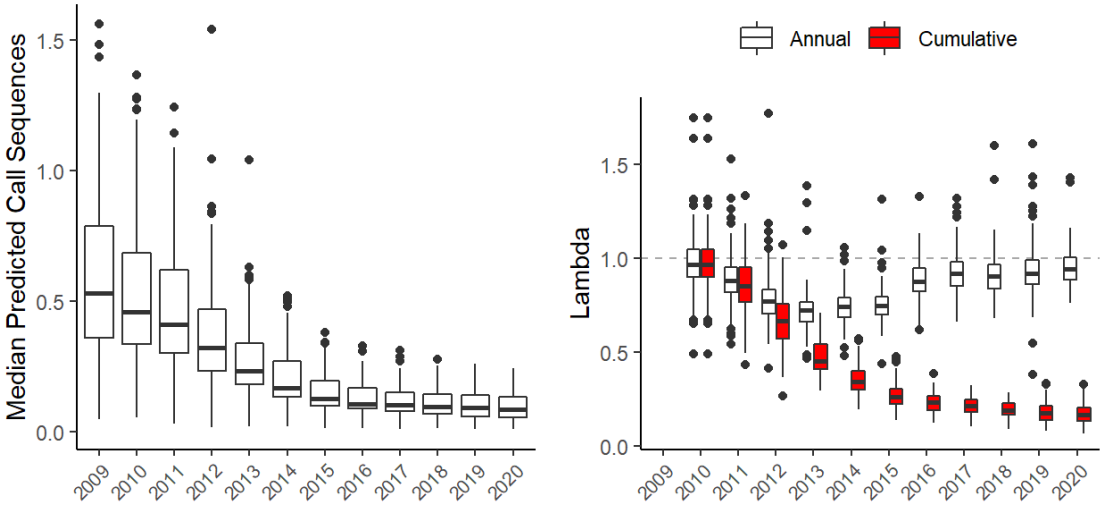

Figure C10. Distribution of median predicted call sequences (left panel) and annual and cumulative rate of change (lambda) (right panel) over 100 simulations at all sites that recorded *Myotis septentrionalis* at least once units. Cumulative lambda values are relative to 2009 activity. Boxplots represent the first (25th percentile), second (median), and third (75th percentile) quartiles. Whiskers extend to the minimum and maximum values that are not outliers (points; over 1.5 times interquartile range from nearest quartile).

Table C6. Median activity, annual rate of change, and cumulative rate of change from 100 simulations at all sites that recorded *Myotis septentrionalis* at least once.

Year	Median Total Call Sequences	Median Annual Lambda	Median Cumulative Lambda
2009	0.53		
2010	0.46	0.97	0.97
2011	0.41	0.88	0.85
2012	0.32	0.77	0.67
2013	0.23	0.72	0.45
2014	0.17	0.74	0.34
2015	0.13	0.75	0.26
2016	0.11	0.87	0.23
2017	0.10	0.92	0.21
2018	0.10	0.90	0.19
2019	0.09	0.92	0.18
2020	0.09	0.94	0.17

The count of call sequences of *Perimyotis subflavus* at sites with observations was projected to decline from a median of 12.17 call sequences per transect in 2009 to 4.44 call sequences in 2020. The median predicted total decline from 2009-2020 in *Perimyotis subflavus* at sites that were sampled is 50% (Figure C11; Table C7).

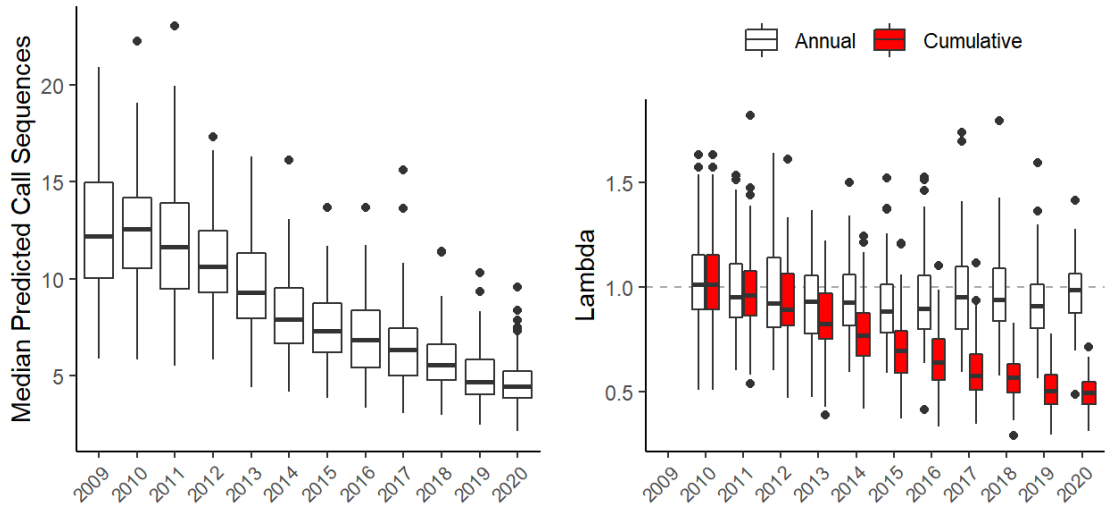

Figure C11. Distribution of median predicted call sequences (left panel) and annual and cumulative rate of change (lambda) (right panel) over 100 simulations at all sites that recorded *Perimyotis subflavus* at least once units. Cumulative lambda values are relative to 2009 activity. Boxplots represent the first (25th percentile), second (median), and third (75th percentile) quartiles. Whiskers extend to the minimum and maximum values that are not outliers (points; over 1.5 times interquartile range from nearest quartile).

Table C7. Median activity, annual rate of change (lambda), and cumulative rate of change from 100 simulations at all sites that recorded *Perimyotis subflavus* at least once.

Year	Median Total Call Sequences	Median Annual Lambda	Median Cumulative Lambda
2009	12.17		
2010	12.55	1.01	1.01
2011	11.66	0.96	0.96
2012	10.64	0.93	0.89
2013	9.30	0.93	0.83
2014	7.90	0.93	0.77
2015	7.29	0.89	0.70
2016	6.85	0.90	0.64
2017	6.36	0.96	0.58
2018	5.57	0.94	0.57
2019	4.68	0.91	0.50
2020	4.44	0.99	0.50

Rate of Change (λ) across the Species Range in the United States

We calculated predicted counts in call sequences across the species range within the minimum and maximum latitude and longitude sampled for each species (represented by black bounding box in Figure C1, Figure C2, and Figure C3).

Call sequences of *Myotis lucifugus* were projected to have declined from a median call rate of 1.59 sequences/25 mile transect to 0.69 sequences per transect, a total decline of 53% across most of the species range in the United States (Figure C12; Table C8).

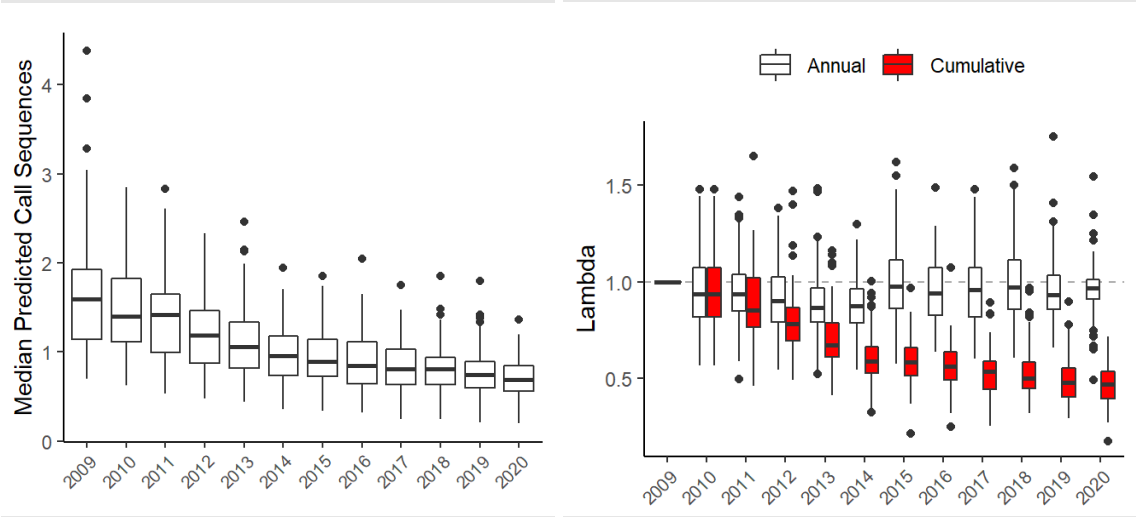

Figure C12. Distribution of median predicted call sequences (left panel) and annual and cumulative rate of change (lambda) (right panel) across the *Myotis lucifugus* range (Figure C1) over 100 simulations. Cumulative lambda values are relative to 2009 activity. Boxplots represent the first (25th percentile), second (median), and third (75th percentile) quartiles. Whiskers extend to the minimum and maximum values that are not outliers (points; over 1.5 times interquartile range from nearest quartile).

Table C8. Median activity, annual rate of change, and cumulative rate of change of *Myotis lucifugus* across 100 simulations at across the species range (Figure C1).

Year	Median Activity	Annual Lambda	Cumulative Lambda
2009	1.59	—	—
2010	1.40	0.94	0.94
2011	1.42	0.94	0.85
2012	1.19	0.90	0.78
2013	1.06	0.86	0.67
2014	0.96	0.88	0.59
2015	0.89	0.98	0.58
2016	0.85	0.94	0.56
2017	0.81	0.96	0.54
2018	0.81	0.97	0.50
2019	0.75	0.93	0.48
2020	0.69	0.97	0.47

Call sequences of *Myotis septentrionalis* were predicted to decline from a median of 0.11 calls per transect in 2009 to 0.02 calls per transect in 2020, a decline of 79% across most of the species range in the United States (Figure C13; Table C9).

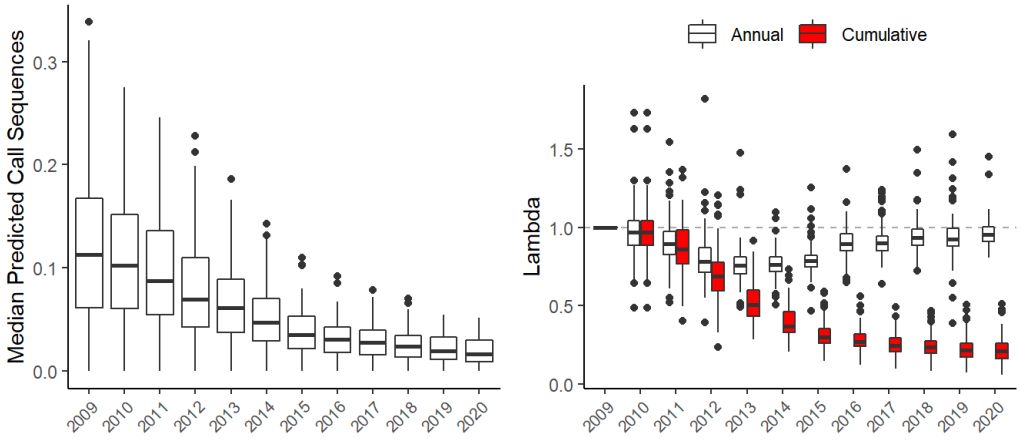

Figure C13. Distribution of median predicted call sequences (left panel) and annual and cumulative lambda (right panel) across the range of *Myotis septentrionalis* (Figure C2) over 100 simulations. Cumulative lambda values are relative to 2009 activity. Boxplots represent the first (25th percentile), second (median), and third (75th percentile) quartiles. Whiskers extend to the minimum and maximum values that are not outliers (points; over 1.5 times interquartile range from nearest quartile).

Table C9. Median activity, median annual rate of change, and median cumulative rate of change of *Myotis septentrionalis* across 100 simulations at across the species range (Figure C2).

Year	Median Activity	Annual Lambda	Cumulative Lambda
2009	0.11		
2010	0.10	0.97	0.97
2011	0.09	0.89	0.86
2012	0.07	0.78	0.69
2013	0.06	0.76	0.51
2014	0.05	0.76	0.37
2015	0.04	0.79	0.30
2016	0.03	0.89	0.27
2017	0.03	0.90	0.25
2018	0.02	0.93	0.23
2019	0.02	0.93	0.22
2020	0.02	0.95	0.21

Call sequences of *Perimyotis subflavus* were projected to have declined from a high of 6.31 in 2009 to 1.26 in 2020, a total decline of 53% across most of the species range in the United States (Table C10; Figure C14).

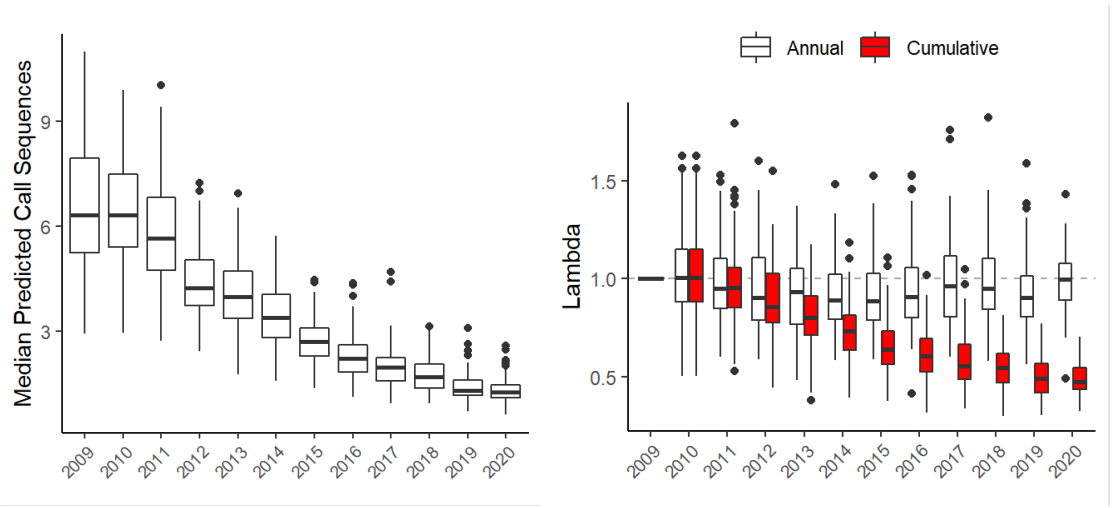

Figure C14. Distribution of median predicted call sequences (left panel) and annual and cumulative lambda (right panel) across the range of *Perimyotis subflavus* (Figure C3) over 100 simulations. Cumulative lambda values are relative to 2009 activity. Boxplots represent the first (25th percentile), second (median), and third (75th percentile) quartiles. Whiskers extend to the minimum and maximum values that are not outliers (points; over 1.5 times interquartile range from nearest quartile).

Table C10. Median activity, annual rate of change, and cumulative rate of change of *Perimyotis subflavus* across 100 simulations at across the species range (Figure C3).

Year	Median Activity	Annual Lambda	Cumulative Lambda
2009	6.31		
2010	6.32	1.01	1.01
2011	5.66	0.95	0.95
2012	4.22	0.90	0.86
2013	3.98	0.94	0.80
2014	3.39	0.89	0.73
2015	2.70	0.89	0.64
2016	2.22	0.91	0.61
2017	1.96	0.96	0.56
2018	1.68	0.95	0.54
2019	1.29	0.91	0.49
2020	1.26	1.00	0.47

Rate of Change (λ) in Representation Units

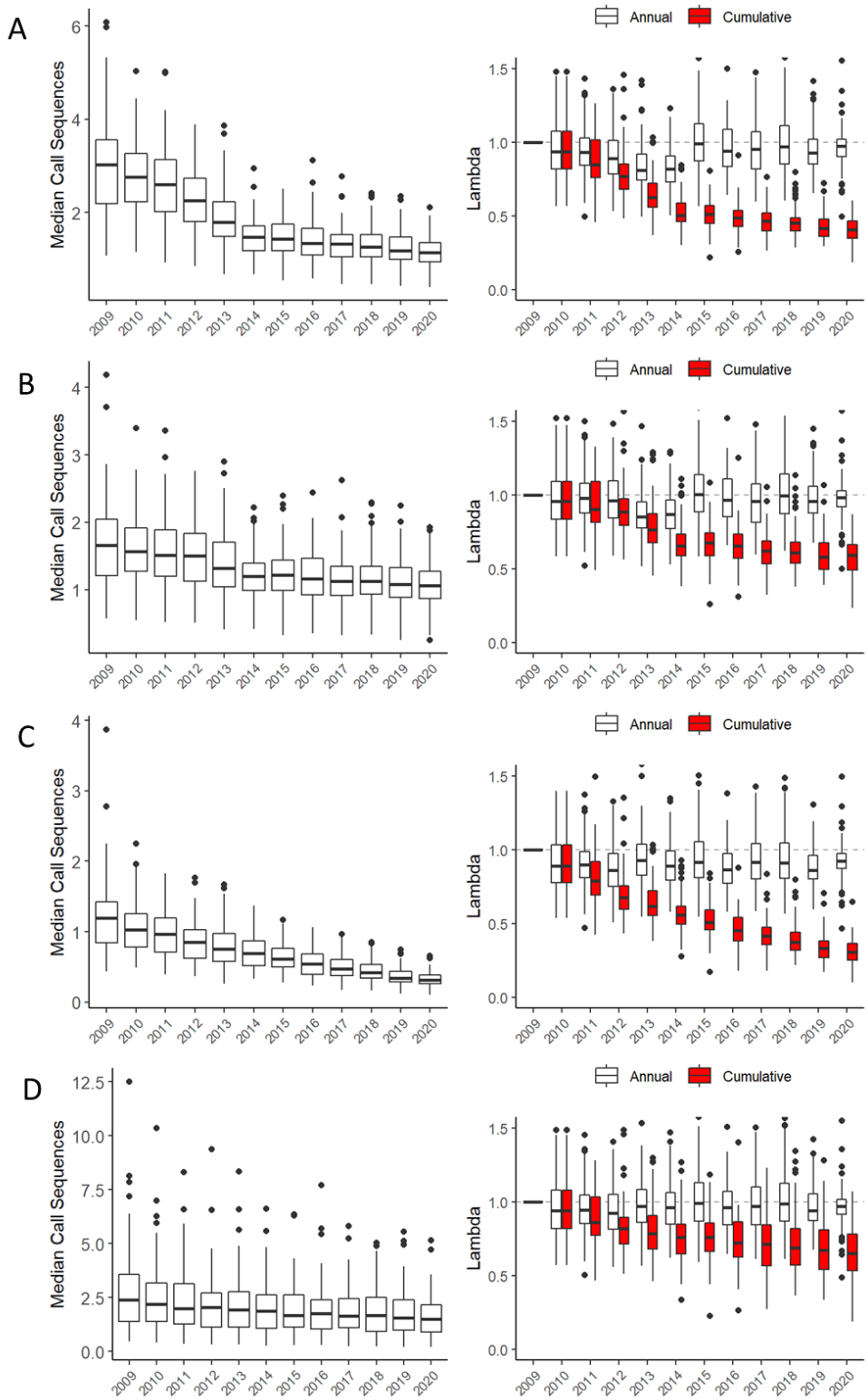

Figure C15. Distribution of median predicted call sequences (left panels) and annual and cumulative rate of change (lambda) (right panels) at all sites in *Myotis lucifugus* Representation Units (RPUs) over 100 simulations (A = RPU 2, B = RPU 3, C = RPU 4, D = RPU 5). Cumulative lambda values are relative to 2009 activity. Boxplots represent the first (25th percentile), second (median), and third (75th percentile) quartiles. Whiskers extend to the minimum and maximum values that are not outliers (points; over 1.5 times interquartile range from nearest quartile). Representation Units1 and 6 are not shown because no sampling for *Myotis lucifugus* occurred in those Representation Units (see Figure C1).

Table C11. Annual and cumulative changes in activity for each Representation Unit (RPU) where sampling occurred for *Myotis lucifugus* from 2009-2020.

RPU	Statistic	2009	2010	2011	2012	2013	2014	2015	2016	2017	2018	2019	2020
2	Annual Lambda	NA	0.93	0.93	0.89	0.81	0.82	0.99	0.94	0.95	0.97	0.93	0.97
2	Cumulative Lambda	1.00	0.93	0.85	0.77	0.63	0.50	0.51	0.49	0.46	0.45	0.42	0.41
2	Median Activity	3.02	2.76	2.60	2.25	1.79	1.47	1.43	1.34	1.32	1.26	1.18	1.13
3	Annual Lambda	NA	0.96	0.98	0.96	0.85	0.87	1.00	0.97	0.96	1.00	0.96	0.98
3	Cumulative Lambda	1.00	0.96	0.90	0.89	0.76	0.65	0.68	0.65	0.62	0.61	0.58	0.59
3	Median Activity	1.66	1.56	1.51	1.50	1.32	1.20	1.22	1.16	1.13	1.13	1.08	1.06
4	Annual Lambda	NA	0.89	0.90	0.86	0.93	0.89	0.92	0.86	0.91	0.91	0.86	0.92
4	Cumulative Lambda	1.00	0.89	0.79	0.67	0.62	0.56	0.51	0.45	0.41	0.37	0.33	0.30
4	Median Activity	1.20	1.03	0.96	0.85	0.76	0.70	0.62	0.54	0.47	0.42	0.35	0.31
5	Annual Lambda	NA	0.94	0.94	0.92	0.97	0.96	0.99	0.96	0.97	0.98	0.94	0.97
5	Cumulative Lambda	1.00	0.94	0.86	0.82	0.78	0.76	0.76	0.72	0.71	0.69	0.67	0.65
5	Median Activity	2.39	2.20	1.98	2.03	1.93	1.87	1.68	1.76	1.64	1.66	1.56	1.49

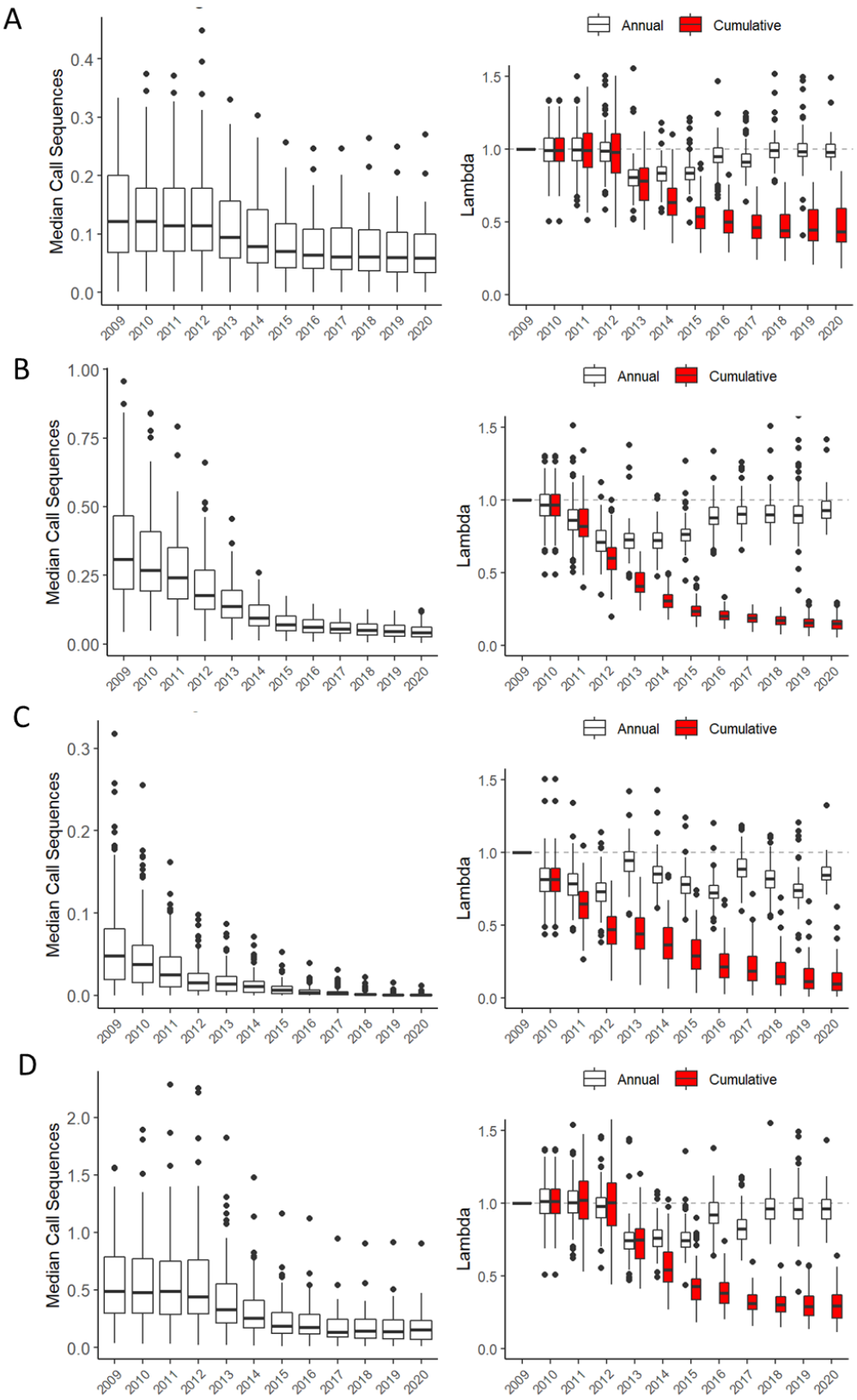
A
B
C
D
Median Call Sequences
Lambda
Annual
Cumulative
2009
2010
2011
2012
2013
2014
2015
2016
2017
2018
2019
2020

Figure C16. Distribution of median predicted call sequences (left panels) and annual and cumulative rate of change (lambda) (right panels) at all sites in *Myotis septentrionalis* Representation Units (RPUs) over 100 simulations (A = RPU 1, B = RPU 2, C = RPU 4, D = RPU 5). Cumulative lambda values are relative to 2009 activity. Boxplots represent the first (25th percentile), second (median), and third (75th percentile) quartiles. Whiskers extend to the minimum and maximum values that are not outliers (points; over 1.5 times interquartile range from nearest quartile). Representation Unit 3 is not shown because no sampling for *Myotis septentrionalis* occurred in that Representation Unit (see Figure C2).

Table C12. Annual and cumulative changes in activity for each Representation Unit (RPU) where sampling of *Myotis septentrionalis* occurred from 2009-2020.

RPU	Statistic	2009	2010	2011	2012	2013	2014	2015	2016	2017	2018	2019	2020
1	Annual Lambda	NA	0.99	1.00	0.99	0.80	0.83	0.83	0.95	0.91	0.99	0.98	0.98
1	Cumulative Lambda	1.00	0.99	0.99	0.98	0.78	0.63	0.54	0.50	0.46	0.44	0.44	0.43
1	Median Activity	0.12	0.12	0.11	0.11	0.09	0.08	0.07	0.06	0.06	0.06	0.06	0.06
2	Annual Lambda	NA	0.96	0.86	0.71	0.72	0.72	0.76	0.88	0.90	0.90	0.89	0.93
2	Cumulative Lambda	1.00	0.96	0.82	0.60	0.41	0.30	0.23	0.20	0.19	0.17	0.15	0.15
2	Median Activity	0.31	0.27	0.24	0.18	0.14	0.09	0.07	0.06	0.05	0.05	0.05	0.04
4	Annual Lambda	NA	0.81	0.79	0.73	0.95	0.85	0.78	0.72	0.89	0.82	0.74	0.84
4	Cumulative Lambda	1.00	0.81	0.65	0.47	0.44	0.37	0.29	0.21	0.19	0.15	0.11	0.09
4	Median Activity	0.05	0.04	0.03	0.02	0.01	0.01	0.01	0.00	0.00	0.00	0.00	0.00
5	Annual Lambda	NA	1.01	1.00	0.98	0.74	0.76	0.74	0.92	0.82	0.96	0.96	0.96
5	Cumulative Lambda	1.00	1.01	1.02	1.00	0.75	0.54	0.43	0.38	0.31	0.30	0.29	0.29
5	Median Activity	0.49	0.48	0.49	0.44	0.33	0.25	0.19	0.18	0.14	0.14	0.14	0.15

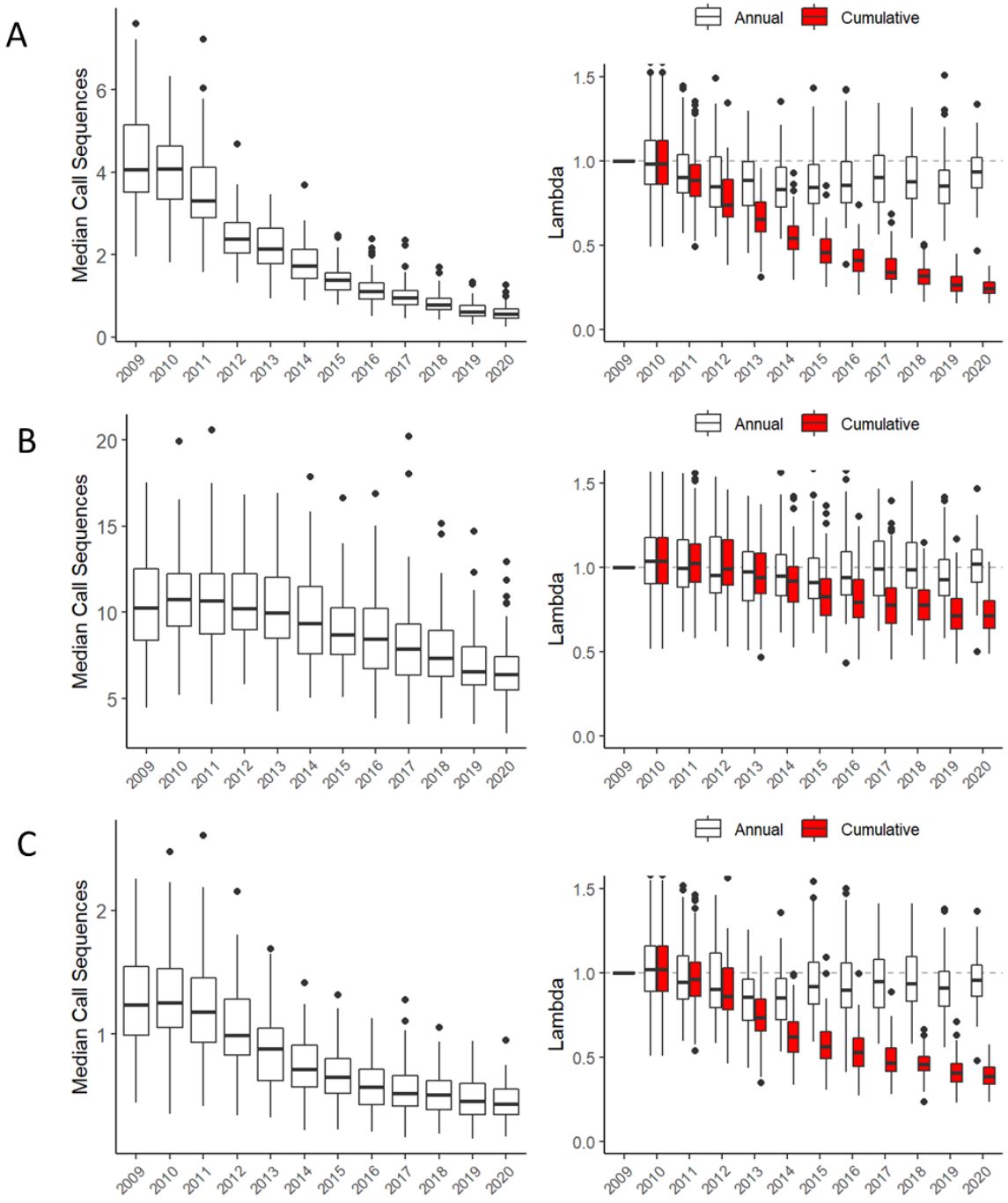

Figure C17. Distribution of median predicted call sequences (left panels) and annual and cumulative rate of change (lambda) (right panels) at all sites in *Perimyotis subflavus* Representation Units (RPU) over 100 simulations (A = RPU 1, B = RPU 2, C = RPU 3). Cumulative lambda values are relative to 2009 activity. Boxplots represent the first (25th percentile), second (median), and third (75th percentile) quartiles.

Whiskers extend to the minimum and maximum values that are not outliers (points; over 1.5 times interquartile range from nearest quartile).

Table C13. Annual and cumulative changes in activity for each Representation Unit (RPU) of *Perimyotis subflavus* from 2009-2020. NA indicates data were not available.

RPU	Statistic	2009	2010	2011	2012	2013	2014	2015	2016	2017	2018	2019	2020
1	Annual	NA	0.98	0.90	0.85	0.88	0.83	0.84	0.85	0.90	0.88	0.85	0.94
1	Cumulative	1.00	0.98	0.89	0.74	0.65	0.54	0.45	0.41	0.34	0.32	0.26	0.24
1	Median Activity	4.07	4.09	3.31	2.38	2.15	1.73	1.39	1.12	0.96	0.78	0.61	0.56
2	Annual	NA	1.04	0.99	0.95	0.97	0.95	0.91	0.94	0.99	0.98	0.93	1.02
2	Cumulative	1.00	1.04	1.02	0.99	0.94	0.92	0.83	0.79	0.77	0.78	0.71	0.71
2	Median Activity	10.29	10.75	10.66	10.21	9.99	9.37	8.69	8.46	7.88	7.36	6.58	6.39
3	Annual	NA	1.02	0.95	0.90	0.86	0.85	0.92	0.90	0.95	0.94	0.91	0.96
3	Cumulative	1.00	1.02	0.96	0.86	0.73	0.62	0.56	0.53	0.47	0.46	0.41	0.38
3	Median Activity	1.24	1.26	1.18	0.99	0.88	0.71	0.65	0.57	0.52	0.51	0.45	0.44

Rate of Change (λ) in States

In individual states, Myotis lucifugus declined between 9% and 77% from 2009 to 2020. The average state level decline was 44% (Table C14).

Table C14. Annual and cumulative changes in activity projected for US states for *Myotis lucifugus* from 2009-2020. NA indicates data were not available.

State	Statistic	2009	2010	2011	2012	2013	2014	2015	2016	2017	2018	2019	2020
Alabama	Annual Lambda	NA	0.96	0.98	0.97	0.95	0.96	1.00	0.97	0.97	0.99	0.95	0.98
Alabama	Cumulative Lambda	1.00	0.96	0.92	0.91	0.88	0.84	0.85	0.81	0.80	0.80	0.76	0.75
Alabama	Median Activity	1.77	1.66	1.64	1.57	1.43	1.40	1.41	1.39	1.29	1.32	1.26	1.21
Arkansas	Annual Lambda	NA	0.96	0.97	0.95	0.88	0.88	0.97	0.94	0.96	0.97	0.93	0.98
Arkansas	Cumulative Lambda	1.00	0.96	0.90	0.87	0.76	0.67	0.66	0.62	0.59	0.57	0.54	0.54
Arkansas	Median Activity	1.50	1.41	1.36	1.33	1.11	0.94	0.89	0.86	0.80	0.79	0.72	0.71
Connecticut	Annual Lambda	NA	0.96	0.96	0.91	0.78	0.79	1.01	0.93	0.97	0.99	0.95	0.99
Connecticut	Cumulative Lambda	1.00	0.96	0.89	0.83	0.65	0.51	0.53	0.49	0.47	0.47	0.45	0.45
Connecticut	Median Activity	3.90	3.82	3.70	3.37	2.56	2.08	2.02	1.92	1.92	1.90	1.71	1.79
Delaware	Annual Lambda	NA	0.96	0.97	0.93	0.79	0.79	1.02	0.97	0.96	1.00	0.96	0.99
Delaware	Cumulative Lambda	1.00	0.96	0.90	0.86	0.68	0.53	0.55	0.53	0.51	0.51	0.50	0.49
Delaware	Median Activity	5.84	5.65	5.55	5.14	3.84	2.98	3.04	3.01	2.85	2.98	2.83	2.80
District of Columbia	Annual Lambda	NA	0.95	0.95	0.91	0.78	0.78	1.01	0.96	0.96	1.00	0.96	0.99
District of Columbia	Cumulative Lambda	1.00	0.95	0.88	0.82	0.65	0.50	0.52	0.49	0.47	0.47	0.46	0.46
District of Columbia	Median Activity	3.37	3.40	2.83	2.89	2.06	1.67	1.81	1.62	1.58	1.62	1.56	1.53
Florida	Annual Lambda	NA	0.96	0.98	0.98	0.97	0.97	1.00	0.97	0.97	0.99	0.95	0.98

State	Statistic	2009	2010	2011	2012	2013	2014	2015	2016	2017	2018	2019	2020
Florida	Cumulative Lambda	1.00	0.96	0.92	0.91	0.90	0.87	0.88	0.84	0.84	0.83	0.79	0.77
Florida	Median Activity	1.11	1.08	1.01	1.04	0.96	0.94	0.96	0.93	0.88	0.94	0.91	0.88
Georgia	Annual Lambda	NA	0.96	0.98	0.97	0.91	0.92	1.00	0.98	0.98	0.99	0.95	0.98
Georgia	Cumulative Lambda	1.00	0.96	0.92	0.91	0.84	0.77	0.78	0.75	0.74	0.74	0.71	0.70
Georgia	Median Activity	0.93	0.93	0.87	0.84	0.79	0.71	0.73	0.70	0.69	0.70	0.66	0.66
Idaho	Annual Lambda	NA	0.92	0.92	0.89	0.97	0.95	1.00	0.97	0.97	0.99	0.94	0.98
Idaho	Cumulative Lambda	1.00	0.92	0.83	0.75	0.72	0.70	0.70	0.67	0.66	0.65	0.63	0.61
Idaho	Median Activity	2.31	2.17	2.00	1.79	1.77	1.68	1.54	1.61	1.53	1.51	1.53	1.43
Illinois	Annual Lambda	NA	0.85	0.85	0.84	0.78	0.77	0.96	0.94	0.90	0.89	0.87	0.94
Illinois	Cumulative Lambda	1.00	0.85	0.73	0.60	0.48	0.36	0.35	0.34	0.30	0.26	0.23	0.21
Illinois	Median Activity	2.46	1.95	1.66	1.30	1.01	0.79	0.73	0.70	0.56	0.48	0.39	0.36
Indiana	Annual Lambda	NA	0.86	0.89	0.83	0.78	0.76	0.96	0.94	0.91	0.92	0.92	0.95
Indiana	Cumulative Lambda	1.00	0.86	0.76	0.62	0.50	0.37	0.36	0.34	0.31	0.28	0.26	0.25
Indiana	Median Activity	2.49	2.03	1.88	1.40	1.05	0.79	0.76	0.75	0.63	0.59	0.52	0.49
Iowa	Annual Lambda	NA	0.88	0.78	0.76	0.85	0.78	0.89	0.81	0.84	0.75	0.69	0.84
Iowa	Cumulative Lambda	1.00	0.88	0.69	0.52	0.44	0.34	0.31	0.26	0.20	0.15	0.11	0.09
Iowa	Median Activity	0.83	0.73	0.56	0.41	0.35	0.27	0.24	0.19	0.15	0.10	0.07	0.05
Kansas	Annual Lambda	NA	0.91	0.89	0.70	0.93	0.88	0.77	0.76	0.83	0.84	0.84	0.87
Kansas	Cumulative Lambda	1.00	0.91	0.80	0.56	0.52	0.46	0.35	0.28	0.22	0.19	0.16	0.13
Kansas	Median Activity	1.47	1.28	1.25	0.79	0.75	0.65	0.49	0.40	0.31	0.26	0.22	0.20
Kentucky	Annual Lambda	NA	0.94	0.96	0.94	0.79	0.78	1.00	0.97	0.96	0.98	0.95	0.98
Kentucky	Cumulative Lambda	1.00	0.94	0.88	0.84	0.66	0.52	0.53	0.51	0.49	0.48	0.47	0.46

State	Statistic	2009	2010	2011	2012	2013	2014	2015	2016	2017	2018	2019	2020
Kentucky	Median Activity	2.60	2.36	2.46	2.15	1.66	1.31	1.33	1.28	1.18	1.28	1.14	1.14
Louisiana	Annual Lambda	NA	0.96	0.98	0.96	0.97	0.96	0.98	0.95	0.96	0.99	0.93	0.97
Louisiana	Cumulative Lambda	1.00	0.96	0.91	0.89	0.88	0.85	0.85	0.80	0.79	0.77	0.72	0.70
Louisiana	Median Activity	1.30	1.19	1.18	1.15	1.09	1.03	1.07	0.99	0.94	0.96	0.88	0.86
Maine	Annual Lambda	NA	0.92	0.91	0.89	0.79	0.79	0.93	0.83	0.97	1.00	0.96	0.99
Maine	Cumulative Lambda	1.00	0.92	0.82	0.74	0.59	0.46	0.44	0.37	0.36	0.35	0.34	0.35
Maine	Median Activity	1.35	1.26	1.14	0.99	0.79	0.64	0.59	0.49	0.45	0.46	0.45	0.45
Maryland	Annual Lambda	NA	0.95	0.96	0.92	0.78	0.79	1.02	0.96	0.95	1.00	0.96	0.99
Maryland	Cumulative Lambda	1.00	0.95	0.89	0.84	0.66	0.51	0.54	0.50	0.48	0.48	0.47	0.47
Maryland	Median Activity	6.66	6.10	5.94	5.43	4.09	3.15	3.34	3.15	2.99	3.15	2.93	2.92
Massachusetts	Annual Lambda	NA	0.95	0.95	0.90	0.80	0.81	1.00	0.92	0.97	0.98	0.95	0.99
Massachusetts	Cumulative Lambda	1.00	0.95	0.88	0.82	0.66	0.53	0.54	0.50	0.48	0.48	0.46	0.45
Massachusetts	Median Activity	3.28	3.28	2.86	2.69	2.05	1.66	1.61	1.52	1.46	1.48	1.39	1.37
Michigan	Annual Lambda	NA	0.94	0.93	0.89	0.80	0.80	1.00	0.96	0.95	0.98	0.92	0.97
Michigan	Cumulative Lambda	1.00	0.94	0.85	0.77	0.62	0.49	0.50	0.48	0.46	0.44	0.40	0.40
Michigan	Median Activity	4.70	4.34	4.03	3.47	2.88	2.27	2.21	2.01	1.94	1.87	1.74	1.66
Minnesota	Annual Lambda	NA	0.91	0.93	0.94	0.97	0.94	0.96	0.92	0.95	0.96	0.88	0.95
Minnesota	Cumulative Lambda	1.00	0.91	0.83	0.80	0.76	0.74	0.70	0.65	0.62	0.59	0.53	0.51
Minnesota	Median Activity	1.17	0.99	0.88	0.83	0.80	0.75	0.72	0.62	0.59	0.56	0.45	0.41
Mississippi	Annual Lambda	NA	0.96	0.98	0.97	0.92	0.92	1.00	0.97	0.98	0.99	0.95	0.98
Mississippi	Cumulative Lambda	1.00	0.96	0.91	0.90	0.85	0.78	0.79	0.75	0.74	0.74	0.70	0.70
Mississippi	Median Activity	1.62	1.55	1.53	1.47	1.30	1.18	1.22	1.17	1.13	1.13	1.08	1.05

State	Statistic	2009	2010	2011	2012	2013	2014	2015	2016	2017	2018	2019	2020
Missouri	Annual Lambda	NA	0.93	0.92	0.90	0.83	0.83	0.95	0.91	0.92	0.93	0.89	0.94
Missouri	Cumulative Lambda	1.00	0.93	0.83	0.77	0.63	0.52	0.51	0.46	0.43	0.39	0.35	0.33
Missouri	Median Activity	2.48	2.21	2.12	1.79	1.51	1.29	1.18	1.07	0.96	0.92	0.79	0.75
Nebraska	Annual Lambda	NA	0.91	0.89	0.85	0.95	0.89	0.88	0.84	0.92	0.88	0.86	0.88
Nebraska	Cumulative Lambda	1.00	0.91	0.80	0.68	0.64	0.59	0.52	0.45	0.40	0.35	0.30	0.26
Nebraska	Median Activity	1.39	1.21	1.11	0.97	0.85	0.80	0.72	0.63	0.57	0.50	0.44	0.38
New Hampshire	Annual Lambda	NA	0.94	0.91	0.83	0.79	0.79	0.98	0.90	0.96	0.99	0.94	0.99
New Hampshire	Cumulative Lambda	1.00	0.94	0.84	0.70	0.56	0.43	0.44	0.40	0.38	0.37	0.36	0.36
New Hampshire	Median Activity	2.40	2.31	2.04	1.73	1.28	1.06	0.98	0.88	0.85	0.90	0.80	0.81
New Jersey	Annual Lambda	NA	0.96	0.97	0.92	0.78	0.79	1.02	0.96	0.97	1.00	0.95	0.99
New Jersey	Cumulative Lambda	1.00	0.96	0.90	0.86	0.67	0.53	0.55	0.52	0.51	0.51	0.49	0.49
New Jersey	Median Activity	6.07	5.60	5.50	4.89	3.68	2.99	3.07	2.90	2.89	3.02	2.79	2.73
New York	Annual Lambda	NA	0.96	0.94	0.87	0.77	0.78	1.01	0.95	0.97	0.97	0.94	0.99
New York	Cumulative Lambda	1.00	0.96	0.87	0.78	0.60	0.47	0.49	0.46	0.44	0.43	0.41	0.41
New York	Median Activity	3.69	3.73	3.38	2.91	2.25	1.75	1.75	1.63	1.67	1.63	1.47	1.43
North Carolina	Annual Lambda	NA	0.96	0.98	0.97	0.82	0.84	1.01	0.97	0.93	1.00	0.96	0.99
North Carolina	Cumulative Lambda	1.00	0.96	0.91	0.90	0.74	0.62	0.64	0.63	0.57	0.57	0.54	0.55
North Carolina	Median Activity	2.59	2.45	2.37	2.38	1.88	1.68	1.66	1.59	1.52	1.52	1.50	1.46
North Dakota	Annual Lambda	NA	0.89	0.97	0.91	0.97	0.92	0.92	0.82	0.93	0.96	0.82	0.96
North Dakota	Cumulative Lambda	1.00	0.89	0.83	0.78	0.75	0.69	0.64	0.54	0.49	0.46	0.38	0.36
North Dakota	Median Activity	0.88	0.74	0.72	0.69	0.65	0.59	0.54	0.46	0.42	0.39	0.32	0.31
Ohio	Annual Lambda	NA	0.93	0.93	0.86	0.77	0.76	1.00	0.95	0.93	0.97	0.94	0.96

State	Statistic	2009	2010	2011	2012	2013	2014	2015	2016	2017	2018	2019	2020
Ohio	Cumulative Lambda	1.00	0.93	0.84	0.73	0.58	0.43	0.44	0.42	0.39	0.37	0.36	0.34
Ohio	Median Activity	2.30	1.94	1.88	1.77	1.27	0.96	0.97	0.92	0.87	0.83	0.78	0.74
Oklahoma	Annual Lambda	NA	0.91	0.89	0.73	0.96	0.85	0.77	0.75	0.84	0.90	0.87	0.95
Oklahoma	Cumulative Lambda	1.00	0.91	0.80	0.57	0.54	0.47	0.36	0.29	0.23	0.21	0.18	0.16
Oklahoma	Median Activity	0.64	0.59	0.51	0.31	0.30	0.23	0.15	0.10	0.07	0.06	0.05	0.05
Oregon	Annual Lambda	NA	0.92	0.88	0.86	0.97	0.92	1.00	0.97	0.96	0.99	0.93	0.98
Oregon	Cumulative Lambda	1.00	0.92	0.80	0.68	0.65	0.61	0.61	0.59	0.57	0.56	0.53	0.53
Oregon	Median Activity	1.81	1.71	1.59	1.31	1.24	1.18	1.15	1.15	1.09	1.09	1.02	1.03
Pennsylvania	Annual Lambda	NA	0.95	0.93	0.85	0.77	0.78	1.01	0.95	0.97	0.98	0.94	0.99
Pennsylvania	Cumulative Lambda	1.00	0.95	0.86	0.74	0.58	0.44	0.46	0.44	0.42	0.42	0.39	0.39
Pennsylvania	Median Activity	4.97	4.82	4.50	3.83	2.77	2.15	2.25	2.04	2.10	1.97	1.88	1.78
Rhode Island	Annual Lambda	NA	0.96	0.96	0.91	0.78	0.79	1.01	0.91	0.97	0.98	0.95	0.99
Rhode Island	Cumulative Lambda	1.00	0.96	0.89	0.84	0.66	0.52	0.54	0.48	0.47	0.47	0.45	0.45
Rhode Island	Median Activity	3.69	3.80	3.66	3.23	2.45	1.98	2.00	1.80	1.82	1.78	1.67	1.65
South Carolina	Annual Lambda	NA	0.96	0.98	0.97	0.84	0.86	1.01	0.97	0.98	1.00	0.96	0.98
South Carolina	Cumulative Lambda	1.00	0.96	0.91	0.91	0.77	0.66	0.67	0.66	0.64	0.64	0.61	0.62
South Carolina	Median Activity	1.51	1.43	1.41	1.42	1.18	1.05	1.07	1.05	1.02	1.04	0.99	0.97
South Dakota	Annual Lambda	NA	0.88	0.94	0.92	0.97	0.93	0.92	0.86	0.94	0.94	0.83	0.93
South Dakota	Cumulative Lambda	1.00	0.88	0.81	0.75	0.72	0.68	0.63	0.55	0.52	0.48	0.41	0.37
South Dakota	Median Activity	1.04	0.88	0.84	0.81	0.77	0.70	0.64	0.54	0.50	0.48	0.40	0.37
Tennessee	Annual Lambda	NA	0.96	0.98	0.96	0.79	0.79	1.01	0.97	0.97	0.99	0.96	0.99
Tennessee	Cumulative Lambda	1.00	0.96	0.90	0.89	0.71	0.57	0.58	0.56	0.55	0.55	0.53	0.52

State	Statistic	2009	2010	2011	2012	2013	2014	2015	2016	2017	2018	2019	2020
Tennessee	Median Activity	1.99	1.86	1.85	1.77	1.35	1.08	1.09	1.09	1.03	1.05	0.99	0.99
Texas	Annual Lambda	NA	0.93	0.95	0.86	0.96	0.88	0.85	0.87	0.90	0.92	0.88	0.95
Texas	Cumulative Lambda	1.00	0.93	0.86	0.75	0.71	0.64	0.54	0.48	0.42	0.39	0.34	0.33
Texas	Median Activity	0.18	0.18	0.16	0.13	0.12	0.09	0.06	0.04	0.03	0.02	0.02	0.01
Vermont	Annual Lambda	NA	0.94	0.91	0.79	0.78	0.79	0.99	0.90	0.96	0.99	0.95	0.99
Vermont	Cumulative Lambda	1.00	0.94	0.84	0.66	0.53	0.42	0.42	0.39	0.37	0.36	0.35	0.35
Vermont	Median Activity	2.70	2.60	2.44	1.82	1.38	1.13	1.06	0.96	0.94	0.97	0.89	0.90
Virginia	Annual Lambda	NA	0.94	0.96	0.94	0.79	0.79	1.01	0.96	0.93	1.00	0.96	0.99
Virginia	Cumulative Lambda	1.00	0.94	0.88	0.85	0.67	0.52	0.55	0.52	0.48	0.49	0.48	0.47
Virginia	Median Activity	4.85	4.53	4.41	3.99	3.11	2.48	2.54	2.37	2.28	2.35	2.27	2.18
West Virginia	Annual Lambda	NA	0.91	0.92	0.90	0.78	0.78	1.01	0.94	0.96	0.99	0.95	0.97
West Virginia	Cumulative Lambda	1.00	0.91	0.82	0.75	0.59	0.46	0.47	0.44	0.43	0.43	0.41	0.40
West Virginia	Median Activity	4.55	4.24	3.91	3.40	2.67	2.10	2.15	2.02	1.93	2.03	1.89	1.76
Wisconsin	Annual Lambda	NA	0.92	0.90	0.90	0.93	0.92	0.97	0.95	0.94	0.95	0.90	0.95
Wisconsin	Cumulative Lambda	1.00	0.92	0.81	0.74	0.69	0.64	0.62	0.59	0.57	0.53	0.48	0.46
Wisconsin	Median Activity	3.09	2.85	2.51	2.34	2.27	2.01	2.04	1.97	1.72	1.67	1.47	1.40

Median counts of call sequences of *Myotis septentrionalis* were predicted to decline in all but three states (Alabama, Louisiana, and Georgia). Declines in the other 33 States ranged from 31% to 100% with a mean of an 91% decline in these states from 2009-2020 (Table C15).

Table C15. Annual and Cumulative changes in activity for each U.S. state for *Myotis septentrionalis* mobile acoustic transects. NA indicates data were not available.

State	Statistic	2009	2010	2011	2012	2013	2014	2015	2016	2017	2018	2019	2020
Alabama	Annual Lambda	NA	1.02	1.03	1.04	0.93	0.96	0.97	1.00	1.02	1.02	1.02	1.02
Alabama	Cumulative Lambda	1.00	1.02	1.05	1.09	1.01	0.95	0.95	0.92	0.99	0.99	1.00	1.03
Alabama	Median Activity	0.08	0.09	0.09	0.09	0.08	0.08	0.08	0.08	0.08	0.09	0.09	0.10
Arkansas	Annual Lambda	NA	1.00	0.99	0.95	0.83	0.85	0.80	0.90	0.93	0.96	0.94	0.98
Arkansas	Cumulative Lambda	1.00	1.00	1.00	0.96	0.79	0.65	0.54	0.47	0.45	0.44	0.40	0.38
Arkansas	Median Activity	0.07	0.08	0.07	0.07	0.06	0.05	0.04	0.04	0.03	0.03	0.03	0.03
Colorado	Annual Lambda	NA	0.91	0.77	0.56	0.92	0.75	0.65	0.83	0.87	0.70	0.82	0.70
Colorado	Cumulative Lambda	1.00	0.91	0.70	0.39	0.35	0.27	0.17	0.14	0.13	0.09	0.07	0.05
Colorado	Median Activity	0.03	0.03	0.02	0.01	0.01	0.01	0.00	0.00	0.00	0.00	0.00	0.00
Connecticut	Annual Lambda	NA	1.00	0.94	0.83	0.74	0.76	0.73	0.83	0.93	0.92	0.92	0.96
Connecticut	Cumulative Lambda	1.00	1.00	0.95	0.81	0.58	0.44	0.32	0.27	0.25	0.24	0.22	0.21
Connecticut	Median Activity	0.47	0.47	0.45	0.37	0.27	0.19	0.14	0.13	0.12	0.11	0.11	0.10
Delaware	Annual Lambda	NA	1.00	0.98	0.91	0.74	0.76	0.74	0.91	0.91	0.96	0.95	0.96
Delaware	Cumulative Lambda	1.00	1.00	0.99	0.92	0.67	0.50	0.37	0.35	0.31	0.31	0.29	0.28
Delaware	Median Activity	0.36	0.35	0.34	0.31	0.23	0.16	0.12	0.11	0.10	0.10	0.10	0.10
District of Columbia	Annual Lambda	NA	0.98	0.93	0.84	0.74	0.75	0.74	0.88	0.90	0.96	0.95	0.95
District of Columbia	Cumulative Lambda	1.00	0.98	0.91	0.78	0.57	0.42	0.31	0.28	0.25	0.25	0.23	0.23
District of Columbia	Median Activity	0.01	0.01	0.01	0.01	0.01	0.01	0.00	0.00	0.00	0.00	0.00	0.00
Georgia	Annual Lambda	NA	1.02	1.03	1.04	0.94	0.97	0.99	1.00	1.02	1.03	1.03	1.02
Georgia	Cumulative Lambda	1.00	1.02	1.05	1.09	1.03	1.00	0.99	0.98	1.05	1.04	1.07	1.10
Georgia	Median Activity	0.12	0.12	0.12	0.13	0.12	0.12	0.11	0.12	0.12	0.13	0.14	0.14
Illinois	Annual Lambda	NA	0.74	0.71	0.68	0.74	0.72	0.66	0.86	0.78	0.76	0.81	0.88

State	Statistic	2009	2010	2011	2012	2013	2014	2015	2016	2017	2018	2019	2020
Illinois	Cumulative Lambda	1.00	0.74	0.53	0.37	0.27	0.19	0.13	0.11	0.09	0.07	0.06	0.05
Illinois	Median Activity	0.05	0.03	0.02	0.01	0.01	0.01	0.00	0.00	0.00	0.00	0.00	0.00
Indiana	Annual Lambda	NA	0.75	0.77	0.58	0.73	0.64	0.64	0.85	0.77	0.79	0.86	0.86
Indiana	Cumulative Lambda	1.00	0.75	0.57	0.33	0.24	0.16	0.10	0.09	0.07	0.05	0.05	0.04
Indiana	Median Activity	0.11	0.07	0.06	0.04	0.03	0.02	0.01	0.01	0.01	0.00	0.00	0.00
Iowa	Annual Lambda	NA	0.81	0.55	0.50	0.77	0.63	0.63	0.66	0.61	0.44	0.44	0.66
Iowa	Cumulative Lambda	1.00	0.81	0.45	0.23	0.17	0.11	0.07	0.05	0.03	0.01	0.01	0.00
Iowa	Median Activity	0.02	0.01	0.01	0.00	0.00	0.00	0.00	0.00	0.00	0.00	0.00	0.00
Kansas	Annual Lambda	NA	0.88	0.78	0.43	0.93	0.83	0.54	0.60	0.68	0.66	0.70	0.71
Kansas	Cumulative Lambda	1.00	0.88	0.70	0.31	0.28	0.23	0.13	0.08	0.05	0.04	0.03	0.02
Kansas	Median Activity	0.02	0.02	0.02	0.01	0.00	0.00	0.00	0.00	0.00	0.00	0.00	0.00
Kentucky	Annual Lambda	NA	0.96	0.98	0.94	0.74	0.74	0.73	0.92	0.92	0.93	0.94	0.93
Kentucky	Cumulative Lambda	1.00	0.96	0.93	0.89	0.65	0.47	0.35	0.33	0.29	0.28	0.26	0.25
Kentucky	Median Activity	0.20	0.18	0.18	0.16	0.12	0.08	0.06	0.06	0.06	0.05	0.05	0.05
Louisiana	Annual Lambda	NA	1.01	1.02	0.99	1.02	1.02	0.98	0.96	1.00	1.00	0.99	1.01
Louisiana	Cumulative Lambda	1.00	1.01	1.04	1.02	1.03	1.05	1.03	0.98	1.01	1.00	0.98	0.98
Louisiana	Median Activity	0.03	0.03	0.03	0.04	0.03	0.04	0.04	0.04	0.04	0.04	0.04	0.04
Maryland	Annual Lambda	NA	0.98	0.94	0.85	0.74	0.75	0.74	0.89	0.89	0.96	0.95	0.95
Maryland	Cumulative Lambda	1.00	0.98	0.92	0.81	0.57	0.44	0.32	0.29	0.25	0.25	0.24	0.23
Maryland	Median Activity	0.52	0.48	0.45	0.37	0.26	0.20	0.15	0.13	0.12	0.12	0.11	0.11
Massachusetts	Annual Lambda	NA	1.00	0.90	0.74	0.74	0.76	0.72	0.82	0.91	0.91	0.90	0.96
Massachusetts	Cumulative Lambda	1.00	1.00	0.89	0.69	0.48	0.38	0.28	0.23	0.21	0.19	0.17	0.17
Massachusetts	Median Activity	0.34	0.31	0.30	0.23	0.16	0.12	0.08	0.07	0.06	0.06	0.05	0.05
Michigan	Annual Lambda	NA	0.95	0.79	0.57	0.68	0.61	0.84	0.89	0.78	0.92	0.79	0.88
Michigan	Cumulative Lambda	1.00	0.95	0.74	0.43	0.28	0.17	0.14	0.12	0.10	0.09	0.07	0.06
Michigan	Median Activity	0.50	0.45	0.32	0.15	0.10	0.05	0.04	0.03	0.02	0.02	0.01	0.01

State	Statistic	2009	2010	2011	2012	2013	2014	2015	2016	2017	2018	2019	2020
Minnesota	Annual Lambda	NA	0.70	0.61	0.72	1.01	0.90	0.73	0.70	0.84	0.69	0.55	0.74
Minnesota	Cumulative Lambda	1.00	0.70	0.43	0.32	0.31	0.28	0.21	0.14	0.12	0.09	0.05	0.03
Minnesota	Median Activity	0.02	0.01	0.01	0.00	0.00	0.00	0.00	0.00	0.00	0.00	0.00	0.00
Mississippi	Annual Lambda	NA	1.02	1.03	1.03	0.85	0.87	0.88	0.98	0.98	0.99	0.99	1.00
Mississippi	Cumulative Lambda	1.00	1.02	1.05	1.08	0.91	0.77	0.69	0.67	0.67	0.67	0.67	0.68
Mississippi	Median Activity	0.06	0.07	0.06	0.07	0.05	0.05	0.04	0.04	0.04	0.03	0.03	0.03
Missouri	Annual Lambda	NA	0.93	0.89	0.85	0.80	0.80	0.74	0.84	0.86	0.86	0.86	0.91
Missouri	Cumulative Lambda	1.00	0.93	0.81	0.72	0.55	0.43	0.33	0.27	0.23	0.21	0.19	0.17
Missouri	Median Activity	0.09	0.08	0.06	0.05	0.04	0.03	0.02	0.02	0.01	0.01	0.01	0.01
Nebraska	Annual Lambda	NA	0.89	0.80	0.69	0.97	0.80	0.77	0.70	0.88	0.76	0.80	0.79
Nebraska	Cumulative Lambda	1.00	0.89	0.72	0.50	0.49	0.39	0.30	0.21	0.19	0.15	0.12	0.09
Nebraska	Median Activity	0.10	0.09	0.07	0.05	0.05	0.04	0.03	0.02	0.01	0.01	0.01	0.01
New Hampshire	Annual Lambda	NA	0.95	0.82	0.59	0.74	0.76	0.69	0.74	0.91	0.93	0.90	0.96
New Hampshire	Cumulative Lambda	1.00	0.95	0.79	0.48	0.34	0.26	0.18	0.13	0.12	0.11	0.10	0.10
New Hampshire	Median Activity	0.37	0.34	0.29	0.16	0.12	0.09	0.06	0.05	0.04	0.04	0.04	0.04
New Jersey	Annual Lambda	NA	1.01	0.97	0.85	0.74	0.76	0.74	0.90	0.94	0.95	0.94	0.96
New Jersey	Cumulative Lambda	1.00	1.01	0.98	0.85	0.61	0.46	0.35	0.32	0.29	0.28	0.26	0.26
New Jersey	Median Activity	0.42	0.44	0.41	0.36	0.25	0.21	0.16	0.13	0.12	0.12	0.11	0.11
New York	Annual Lambda	NA	1.01	0.89	0.72	0.70	0.74	0.74	0.86	0.93	0.85	0.90	0.96
New York	Cumulative Lambda	1.00	1.01	0.89	0.65	0.44	0.33	0.25	0.22	0.20	0.17	0.15	0.15
New York	Median Activity	0.75	0.74	0.66	0.45	0.31	0.21	0.17	0.14	0.15	0.12	0.11	0.11
North Carolina	Annual Lambda	NA	1.01	1.01	1.02	0.79	0.82	0.83	0.96	0.87	0.99	0.99	0.98
North Carolina	Cumulative Lambda	1.00	1.01	1.03	1.05	0.83	0.64	0.54	0.52	0.45	0.45	0.45	0.44
North Carolina	Median Activity	0.54	0.57	0.56	0.58	0.45	0.37	0.30	0.28	0.25	0.25	0.24	0.24
Ohio	Annual Lambda	NA	0.95	0.87	0.70	0.71	0.67	0.72	0.87	0.84	0.87	0.89	0.89

State	Statistic	2009	2010	2011	2012	2013	2014	2015	2016	2017	2018	2019	2020
Ohio	Cumulative Lambda	1.00	0.95	0.81	0.58	0.39	0.27	0.20	0.17	0.15	0.13	0.12	0.11
Ohio	Median Activity	0.51	0.46	0.40	0.27	0.19	0.12	0.09	0.08	0.07	0.06	0.05	0.04
Oklahoma	Annual Lambda	NA	0.92	0.82	0.56	1.00	0.85	0.64	0.65	0.77	0.86	0.82	0.97
Oklahoma	Cumulative Lambda	1.00	0.92	0.73	0.42	0.41	0.35	0.21	0.14	0.11	0.09	0.08	0.07
Oklahoma	Median Activity	0.02	0.01	0.01	0.00	0.00	0.00	0.00	0.00	0.00	0.00	0.00	0.00
Pennsylvania	Annual Lambda	NA	0.98	0.88	0.67	0.71	0.72	0.74	0.88	0.93	0.90	0.88	0.95
Pennsylvania	Cumulative Lambda	1.00	0.98	0.86	0.60	0.40	0.29	0.22	0.20	0.18	0.17	0.15	0.14
Pennsylvania	Median Activity	1.31	1.22	1.08	0.71	0.49	0.35	0.27	0.23	0.22	0.20	0.19	0.19
Rhode Island	Annual Lambda	NA	1.00	0.96	0.85	0.74	0.76	0.73	0.77	0.94	0.91	0.93	0.96
Rhode Island	Cumulative Lambda	1.00	1.00	0.96	0.84	0.60	0.46	0.33	0.27	0.24	0.23	0.21	0.21
Rhode Island	Median Activity	0.26	0.27	0.25	0.22	0.15	0.13	0.09	0.07	0.07	0.06	0.06	0.06
South Carolina	Annual Lambda	NA	1.01	1.03	1.04	0.85	0.87	0.89	0.98	0.97	1.01	1.00	1.00
South Carolina	Cumulative Lambda	1.00	1.01	1.05	1.09	0.91	0.76	0.68	0.67	0.67	0.68	0.68	0.69
South Carolina	Median Activity	0.26	0.27	0.27	0.28	0.23	0.21	0.17	0.16	0.16	0.16	0.15	0.16
South Dakota	Annual Lambda	NA	0.79	0.88	0.89	1.01	0.93	0.85	0.75	0.95	0.88	0.73	0.88
South Dakota	Cumulative Lambda	1.00	0.79	0.70	0.63	0.62	0.60	0.51	0.37	0.37	0.33	0.25	0.21
South Dakota	Median Activity	0.13	0.10	0.08	0.07	0.07	0.07	0.05	0.04	0.04	0.03	0.02	0.01
Tennessee	Annual Lambda	NA	1.00	1.01	1.01	0.75	0.76	0.75	0.94	0.95	0.96	0.95	0.95
Tennessee	Cumulative Lambda	1.00	1.00	1.02	1.02	0.77	0.56	0.44	0.40	0.38	0.37	0.36	0.34
Tennessee	Median Activity	0.19	0.19	0.19	0.19	0.14	0.11	0.07	0.07	0.08	0.08	0.07	0.07
Texas	Annual Lambda	NA	0.93	0.90	0.67	0.99	0.82	0.76	0.78	0.90	0.93	0.88	0.98
Texas	Cumulative Lambda	1.00	0.93	0.82	0.56	0.55	0.46	0.36	0.27	0.24	0.23	0.21	0.20
Texas	Median Activity	0.00	0.00	0.00	0.00	0.00	0.00	0.00	0.00	0.00	0.00	0.00	0.00
Vermont	Annual Lambda	NA	0.96	0.82	0.52	0.74	0.76	0.70	0.75	0.91	0.92	0.91	0.96
Vermont	Cumulative Lambda	1.00	0.96	0.80	0.44	0.30	0.24	0.17	0.13	0.12	0.11	0.10	0.10
Vermont	Median Activity	0.59	0.56	0.43	0.23	0.16	0.13	0.09	0.07	0.06	0.06	0.06	0.06

State	Statistic	2009	2010	2011	2012	2013	2014	2015	2016	2017	2018	2019	2020
Virginia	Annual Lambda	NA	0.96	0.96	0.96	0.74	0.75	0.74	0.91	0.84	0.96	0.96	0.94
Virginia	Cumulative Lambda	1.00	0.96	0.92	0.90	0.65	0.49	0.37	0.34	0.28	0.27	0.26	0.25
Virginia	Median Activity	0.75	0.70	0.67	0.63	0.46	0.35	0.26	0.23	0.21	0.20	0.20	0.19
West Virginia	Annual Lambda	NA	0.88	0.86	0.83	0.74	0.73	0.73	0.86	0.92	0.95	0.95	0.90
West Virginia	Cumulative Lambda	1.00	0.88	0.76	0.65	0.45	0.34	0.25	0.22	0.20	0.19	0.18	0.17
West Virginia	Median Activity	0.51	0.42	0.38	0.32	0.23	0.17	0.12	0.10	0.10	0.09	0.09	0.08
Wisconsin	Annual Lambda	NA	0.89	0.76	0.75	0.96	0.93	0.93	0.94	0.92	0.89	0.85	0.92
Wisconsin	Cumulative Lambda	1.00	0.89	0.68	0.52	0.49	0.46	0.41	0.39	0.37	0.33	0.28	0.26
Wisconsin	Median Activity	0.11	0.09	0.06	0.05	0.05	0.05	0.04	0.04	0.03	0.02	0.02	0.02

Perimyotis subflavus call sequences declined from 2009-2020 in all but 2 states (Georgia and Alabama). Declines ranged from 6% to 93% with an average decline of 35% Table C16.

Table C16. Annual and Cumulative changes in activity for each U.S. state for *Perimyotis subflavus* mobile acoustic transects. NA indicates data were not available.

State	Statistic	2009	2010	2011	2012	2013	2014	2015	2016	2017	2018	2019	2020
Alabama	Annual Lambda	NA	1.05	1.01	1.01	1.04	1.02	0.98	0.99	1.04	1.03	0.97	1.05
Alabama	Cumulative Lambda	1.00	1.05	1.05	1.08	1.09	1.14	1.11	1.11	1.16	1.21	1.15	1.19
Alabama	Median Activity	12.76	13.58	13.56	14.19	13.83	14.20	14.08	14.98	14.80	15.05	14.71	15.13
Arkansas	Annual Lambda	NA	1.01	0.95	0.88	0.92	0.86	0.82	0.84	0.90	0.89	0.84	0.96
Arkansas	Cumulative Lambda	1.00	1.01	0.96	0.83	0.76	0.67	0.55	0.48	0.40	0.39	0.31	0.30
Arkansas	Median Activity	18.34	18.70	18.00	16.36	14.99	13.22	10.80	9.57	8.13	7.09	5.84	5.33
Connecticut	Annual Lambda	NA	1.05	0.95	0.88	0.86	0.86	0.91	0.86	0.97	0.94	0.91	0.98
Connecticut	Cumulative Lambda	1.00	1.05	0.99	0.86	0.73	0.63	0.56	0.50	0.46	0.44	0.40	0.38

State	Statistic	2009	2010	2011	2012	2013	2014	2015	2016	2017	2018	2019	2020
Connecticut	Median Activity	1.06	1.07	0.96	0.87	0.77	0.62	0.57	0.48	0.47	0.45	0.40	0.39
Delaware	Annual Lambda	NA	1.05	0.97	0.92	0.86	0.86	0.93	0.91	0.95	0.95	0.92	0.97
Delaware	Cumulative Lambda	1.00	1.05	1.01	0.93	0.78	0.67	0.62	0.58	0.52	0.51	0.46	0.44
Delaware	Median Activity	6.36	6.82	6.32	6.01	4.96	4.36	3.86	3.62	3.38	3.22	2.88	2.77
District of Columbia	Annual Lambda	NA	1.04	0.95	0.90	0.86	0.85	0.93	0.90	0.94	0.94	0.91	0.97
District of Columbia	Cumulative Lambda	1.00	1.04	0.98	0.88	0.74	0.63	0.58	0.54	0.48	0.47	0.42	0.40
District of Columbia	Median Activity	13.90	13.43	12.30	12.09	9.57	8.46	7.67	7.16	6.70	6.13	5.55	5.50
Florida	Annual Lambda	NA	1.07	1.03	1.04	0.94	0.93	0.96	0.97	1.04	1.01	0.96	1.03
Florida	Cumulative Lambda	1.00	1.07	1.09	1.15	1.05	0.99	0.95	0.95	0.95	0.98	0.90	0.93
Florida	Median Activity	8.28	8.97	8.87	9.58	8.44	7.23	6.90	6.98	6.54	6.49	5.98	5.74
Georgia	Annual Lambda	NA	1.06	1.02	1.03	0.97	0.96	0.97	0.98	1.04	1.02	0.97	1.03
Georgia	Cumulative Lambda	1.00	1.06	1.07	1.11	1.06	1.04	1.01	1.03	1.04	1.06	1.03	1.06
Georgia	Median Activity	9.18	10.01	9.78	10.18	10.27	10.32	10.34	10.37	10.97	10.90	10.69	11.14
Illinois	Annual Lambda	NA	0.93	0.85	0.82	0.86	0.82	0.83	0.84	0.84	0.79	0.77	0.89
Illinois	Cumulative Lambda	1.00	0.93	0.78	0.64	0.54	0.43	0.36	0.32	0.25	0.21	0.16	0.14
Illinois	Median Activity	5.51	4.97	4.04	2.93	2.48	1.93	1.57	1.30	1.05	0.78	0.55	0.47
Indiana	Annual Lambda	NA	0.94	0.88	0.83	0.86	0.83	0.85	0.86	0.85	0.83	0.82	0.90
Indiana	Cumulative Lambda	1.00	0.94	0.82	0.66	0.57	0.46	0.39	0.35	0.28	0.25	0.20	0.17
Indiana	Median Activity	5.45	4.96	4.20	3.20	2.66	2.05	1.71	1.51	1.33	1.09	0.82	0.73
Iowa	Annual Lambda	NA	0.90	0.76	0.72	0.91	0.79	0.78	0.73	0.80	0.68	0.61	0.80
Iowa	Cumulative Lambda	1.00	0.90	0.68	0.49	0.43	0.35	0.27	0.21	0.16	0.12	0.07	0.06
Iowa	Median Activity	1.73	1.53	1.20	0.81	0.75	0.62	0.47	0.35	0.28	0.19	0.12	0.09

State	Statistic	2009	2010	2011	2012	2013	2014	2015	2016	2017	2018	2019	2020
Kansas	Annual Lambda	NA	0.95	0.84	0.61	1.02	0.85	0.67	0.66	0.76	0.75	0.75	0.88
Kansas	Cumulative Lambda	1.00	0.95	0.80	0.49	0.49	0.42	0.27	0.20	0.14	0.11	0.09	0.07
Kansas	Median Activity	5.56	5.32	4.49	2.58	2.60	2.17	1.33	0.93	0.72	0.53	0.39	0.34
Kentucky	Annual Lambda	NA	1.00	0.94	0.90	0.86	0.84	0.89	0.90	0.92	0.90	0.88	0.94
Kentucky	Cumulative Lambda	1.00	1.00	0.93	0.84	0.72	0.59	0.52	0.49	0.42	0.40	0.35	0.31
Kentucky	Median Activity	19.82	19.36	18.30	16.60	14.60	10.95	10.05	9.12	8.58	7.58	6.27	5.87
Louisiana	Annual Lambda	NA	1.03	1.01	0.95	1.06	1.02	0.90	0.94	1.00	0.99	0.90	1.03
Louisiana	Cumulative Lambda	1.00	1.03	1.03	0.99	1.02	1.06	0.96	0.93	0.91	0.92	0.81	0.83
Louisiana	Median Activity	17.99	18.82	18.65	17.80	18.87	18.69	16.96	16.47	15.20	15.31	13.50	13.79
Maine	Annual Lambda	NA	1.01	0.91	0.86	0.86	0.87	0.85	0.76	0.98	0.95	0.92	0.98
Maine	Cumulative Lambda	1.00	1.01	0.92	0.78	0.67	0.57	0.48	0.38	0.35	0.35	0.31	0.30
Maine	Median Activity	0.21	0.20	0.18	0.16	0.14	0.12	0.10	0.08	0.07	0.07	0.06	0.06
Maryland	Annual Lambda	NA	1.04	0.95	0.90	0.86	0.86	0.93	0.90	0.94	0.95	0.91	0.97
Maryland	Cumulative Lambda	1.00	1.04	0.98	0.89	0.75	0.64	0.58	0.55	0.49	0.47	0.43	0.41
Maryland	Median Activity	9.78	9.82	9.37	8.32	6.90	5.89	5.40	4.91	4.51	4.28	3.77	3.79
Massachusetts	Annual Lambda	NA	1.04	0.94	0.87	0.86	0.87	0.90	0.84	0.98	0.95	0.92	0.99
Massachusetts	Cumulative Lambda	1.00	1.04	0.98	0.84	0.72	0.63	0.55	0.49	0.45	0.44	0.40	0.39
Massachusetts	Median Activity	0.57	0.62	0.57	0.51	0.43	0.34	0.34	0.27	0.27	0.26	0.23	0.23
Michigan	Annual Lambda	NA	0.97	0.86	0.78	0.85	0.79	0.90	0.89	0.88	0.88	0.81	0.91
Michigan	Cumulative Lambda	1.00	0.97	0.83	0.64	0.53	0.41	0.38	0.35	0.29	0.27	0.22	0.20
Michigan	Median Activity	2.72	2.72	2.30	1.77	1.49	1.20	1.18	1.02	0.89	0.75	0.60	0.53
Minnesota	Annual Lambda	NA	0.88	0.79	0.82	1.04	0.92	0.83	0.80	0.91	0.80	0.66	0.87

State	Statistic	2009	2010	2011	2012	2013	2014	2015	2016	2017	2018	2019	2020
Minnesota	Cumulative Lambda	1.00	0.88	0.69	0.56	0.56	0.52	0.44	0.37	0.32	0.27	0.17	0.15
Minnesota	Median Activity	0.85	0.79	0.59	0.49	0.48	0.44	0.39	0.30	0.27	0.21	0.15	0.12
Mississippi	Annual Lambda	NA	1.05	1.00	0.98	0.99	0.98	0.93	0.95	1.01	0.99	0.93	1.03
Mississippi	Cumulative Lambda	1.00	1.05	1.04	1.03	1.00	1.00	0.92	0.90	0.89	0.89	0.82	0.84
Mississippi	Median Activity	17.92	19.19	19.01	19.69	18.85	18.07	16.87	17.68	16.31	16.36	14.96	14.99
Missouri	Annual Lambda	NA	0.97	0.88	0.83	0.89	0.83	0.80	0.80	0.85	0.81	0.78	0.90
Missouri	Cumulative Lambda	1.00	0.97	0.86	0.70	0.62	0.51	0.41	0.35	0.27	0.24	0.18	0.17
Missouri	Median Activity	18.35	17.63	15.57	12.58	11.28	9.07	7.06	5.78	4.62	3.67	2.79	2.47
Nebraska	Annual Lambda	NA	0.93	0.83	0.73	1.03	0.87	0.76	0.72	0.86	0.76	0.72	0.85
Nebraska	Cumulative Lambda	1.00	0.93	0.77	0.57	0.57	0.50	0.38	0.30	0.23	0.19	0.13	0.11
Nebraska	Median Activity	1.68	1.59	1.31	1.00	1.01	0.91	0.68	0.51	0.43	0.32	0.23	0.20
New Hampshire	Annual Lambda	NA	1.03	0.91	0.83	0.86	0.87	0.88	0.80	0.97	0.94	0.91	0.98
New Hampshire	Cumulative Lambda	1.00	1.03	0.93	0.76	0.65	0.55	0.48	0.40	0.36	0.36	0.32	0.31
New Hampshire	Median Activity	0.44	0.46	0.40	0.33	0.29	0.25	0.22	0.18	0.16	0.16	0.14	0.14
New Jersey	Annual Lambda	NA	1.05	0.96	0.90	0.86	0.86	0.93	0.90	0.96	0.95	0.91	0.97
New Jersey	Cumulative Lambda	1.00	1.05	1.01	0.91	0.77	0.66	0.61	0.56	0.51	0.50	0.45	0.43
New Jersey	Median Activity	2.91	3.14	2.90	2.68	2.17	1.86	1.75	1.57	1.46	1.45	1.26	1.21
New York	Annual Lambda	NA	1.04	0.92	0.84	0.84	0.85	0.92	0.87	0.96	0.91	0.89	0.97
New York	Cumulative Lambda	1.00	1.04	0.96	0.79	0.66	0.55	0.49	0.46	0.41	0.39	0.34	0.32
New York	Median Activity	1.41	1.47	1.36	1.07	0.91	0.77	0.72	0.63	0.59	0.54	0.46	0.46
North Carolina	Annual Lambda	NA	1.05	0.99	0.99	0.90	0.89	0.95	0.95	0.96	0.99	0.95	1.00
North Carolina	Cumulative Lambda	1.00	1.05	1.03	1.04	0.92	0.84	0.79	0.78	0.72	0.73	0.67	0.68

State	Statistic	2009	2010	2011	2012	2013	2014	2015	2016	2017	2018	2019	2020
North Carolina	Median Activity	13.04	13.52	13.17	13.73	12.37	11.45	10.64	10.72	9.99	9.48	8.67	8.65
Ohio	Annual Lambda	NA	0.99	0.91	0.84	0.85	0.82	0.90	0.88	0.90	0.89	0.87	0.92
Ohio	Cumulative Lambda	1.00	0.99	0.89	0.73	0.62	0.50	0.45	0.41	0.34	0.33	0.27	0.25
Ohio	Median Activity	4.70	4.82	4.22	3.42	2.85	2.21	2.06	1.81	1.65	1.40	1.21	1.12
Oklahoma	Annual Lambda	NA	0.97	0.88	0.65	1.04	0.84	0.66	0.67	0.77	0.81	0.77	0.95
Oklahoma	Cumulative Lambda	1.00	0.97	0.85	0.55	0.55	0.48	0.31	0.22	0.16	0.14	0.11	0.10
Oklahoma	Median Activity	5.35	5.11	4.31	2.53	2.55	1.99	1.19	0.72	0.51	0.36	0.28	0.25
Pennsylvania	Annual Lambda	NA	1.03	0.92	0.84	0.84	0.84	0.92	0.89	0.95	0.92	0.89	0.96
Pennsylvania	Cumulative Lambda	1.00	1.03	0.94	0.77	0.64	0.53	0.48	0.44	0.39	0.38	0.33	0.31
Pennsylvania	Median Activity	3.65	3.73	3.33	2.84	2.35	1.94	1.74	1.64	1.44	1.37	1.13	1.06
Rhode Island	Annual Lambda	NA	1.05	0.95	0.89	0.86	0.87	0.91	0.85	0.98	0.94	0.91	0.98
Rhode Island	Cumulative Lambda	1.00	1.05	0.99	0.89	0.75	0.65	0.58	0.51	0.47	0.46	0.42	0.40
Rhode Island	Median Activity	0.72	0.78	0.71	0.65	0.53	0.45	0.42	0.35	0.33	0.33	0.29	0.29
South Carolina	Annual Lambda	NA	1.06	1.01	1.02	0.91	0.90	0.95	0.96	1.01	0.99	0.96	1.01
South Carolina	Cumulative Lambda	1.00	1.06	1.06	1.10	0.99	0.90	0.85	0.85	0.82	0.83	0.78	0.78
South Carolina	Median Activity	10.93	11.64	11.17	12.07	10.65	10.21	9.84	10.14	9.87	9.29	9.30	9.43
South Dakota	Annual Lambda	NA	0.88	0.86	0.85	1.05	0.92	0.83	0.77	0.93	0.84	0.69	0.88
South Dakota	Cumulative Lambda	1.00	0.88	0.76	0.64	0.65	0.60	0.50	0.41	0.36	0.31	0.21	0.19
South Dakota	Median Activity	1.05	0.92	0.78	0.64	0.66	0.60	0.51	0.41	0.37	0.30	0.21	0.18
Tennessee	Annual Lambda	NA	1.03	0.97	0.95	0.87	0.85	0.89	0.90	0.94	0.92	0.89	0.95
Tennessee	Cumulative Lambda	1.00	1.03	0.99	0.95	0.80	0.68	0.61	0.57	0.51	0.48	0.43	0.40
Tennessee	Median Activity	22.68	23.02	21.70	20.95	17.83	15.03	13.69	12.86	11.74	10.53	9.11	8.86

State	Statistic	2009	2010	2011	2012	2013	2014	2015	2016	2017	2018	2019	2020
Texas	Annual Lambda	NA	0.96	0.98	0.83	1.04	0.95	0.75	0.81	0.88	0.86	0.75	0.97
Texas	Cumulative Lambda	1.00	0.96	0.93	0.75	0.78	0.74	0.55	0.47	0.39	0.36	0.26	0.25
Texas	Median Activity	2.03	2.03	1.83	1.38	1.35	1.23	0.75	0.54	0.43	0.31	0.18	0.16
Vermont	Annual Lambda	NA	1.03	0.91	0.80	0.86	0.86	0.88	0.81	0.97	0.93	0.91	0.98
Vermont	Cumulative Lambda	1.00	1.03	0.93	0.73	0.62	0.53	0.46	0.40	0.36	0.35	0.31	0.30
Vermont	Median Activity	0.53	0.56	0.47	0.37	0.33	0.28	0.24	0.21	0.19	0.18	0.16	0.16
Virginia	Annual Lambda	NA	1.03	0.96	0.94	0.86	0.86	0.93	0.91	0.93	0.95	0.92	0.96
Virginia	Cumulative Lambda	1.00	1.03	0.99	0.94	0.79	0.67	0.62	0.58	0.52	0.50	0.46	0.43
Virginia	Median Activity	17.54	17.80	16.69	16.22	13.78	11.30	10.38	10.28	9.20	8.44	7.60	7.43
West Virginia	Annual Lambda	NA	1.00	0.93	0.89	0.85	0.84	0.91	0.89	0.93	0.93	0.90	0.94
West Virginia	Cumulative Lambda	1.00	1.00	0.92	0.82	0.70	0.59	0.52	0.49	0.43	0.42	0.37	0.34
West Virginia	Median Activity	18.68	19.43	16.79	15.81	12.99	10.55	9.76	8.76	8.38	7.69	6.63	6.19
Wisconsin	Annual Lambda	NA	0.93	0.81	0.81	0.98	0.93	0.90	0.90	0.92	0.86	0.79	0.94
Wisconsin	Cumulative Lambda	1.00	0.93	0.76	0.61	0.60	0.55	0.49	0.47	0.41	0.37	0.29	0.27
Wisconsin	Median Activity	1.93	1.83	1.43	1.21	1.13	1.13	1.00	0.91	0.81	0.68	0.54	0.49

References Cited

Bates, D., M. Maechler, B. Bolker, S. Walker. 2015. Fitting Linear Mixed-Effects Models Using lme4. Journal of Statistical Software 67: 1-48. doi:10.18637/jss.v067.i01.

Brooks, M. E., K. Kristensen, K. J. van Benthem, A. Magnusson, C. W. Berg, A. Nielsen, H, J. Skaug, M. Maechler, and B. M. Bolker. 2017. glmmTMB Balances Speed and Flexibility Among Packages for Zero-Inflated Generalized Linear Mixed Modeling. The R Journal 9: 378400. https://doi.org/gf4kbz.

Canada Centre for Remote Sensing (CCRS). 2013. 2010 Land Cover of North America at 250 meters. http://www.cec.org/north-american-environmental-atlas/.

Dzal, Y., L. P. McGuire, N. Veselka, and M. B. Fenton. 2011. Going, going, gone: the impact of white-nose syndrome on the summer activity of the little brown bat (Myotis lucifugus). Biology letters 7: 392-394.

Evans, K. O., A. D. Smith, and D. Robinson. 2021. Statistical power of mobile acoustic monitoring to detect population change in southeastern U.S. bat species, a case study. Ecological Indicators 125: 107524.

Hardin, J. W., and J. M. Hilbe. 2007. Generalized linear models and extensions. Stata Press.

Hartig, F. 2021. DHARMa: Residual diagnostics for hierarchical)multi-level/mixed) regression models. R package version 0.4.4. https://CRAN.R-project.org/package=DHARMa

Janicki, A. F., W. F. Frick, A. M. Kilpatrick, K. L. Parise, J. T. Foster, and G. F. McCracken. 2015. Efficacy of visual surveys for white-nose syndrome at bat hibernacula. PLoS One 10:p.e0133390.

Jones, K. E., J. A. Russ, A. T. Bashta, Z. Bilhari, C. Catto, I. Csősz, A. Gorbachev, P. Győrfi, A. Hughes, I. Ivashkiv, N. Koryagina, A. Kurali, S. Langton, A. Collen, G. Margiean, I. Pandourski, S. Parsons, I. Prokofev, A. Szodoray-Paradi, F. Szodoray-Paradi, E. Tilova, C. L. Walters, A. Weatherill, and O. Zavarzin. 2013. Indicator Bats Program: A System for the Global Acoustic Monitoring of Bats. In Biodiversity Monitoring and Conservation (eds B. Collen, N. Pettorelli, J. E. M. Baillie and S. M. Durant). https://doi.org/10.1002/9781118490747.ch10.

Kunz, T. H., E. B. Arnett, W. P. Erickson, A. R. Hoar, G. D. Johnson, R. P. Larkin, M. Dale Strickland, R. W. Thresher, and M. D. Tuttle. 2007. Ecological impacts of wind energy development on bats: questions, research needs, and hypotheses. Frontiers in Ecology and the Environment 5: 315-324.

Lüdecke, D., M.S. Ben-Shachar, I. Patil, P. Waggoner, and D. Makowski 2021 performance: An R Package for Assessment, Comparison and Testing of Statistical Models. Journal of Open Source Software, 6(60), 3139. https://doi.org/10.21105/joss.03139

Magnusson, A., H. Skaug, A. Nielsen, C. Berg, K. Kristensen, M. Maechler, K. van Bentham, B. Bolker, and M. Brooks. 2020. glmmTMB: Generalized Linear Mixed Models Using Template Model Builder. https://github.com/glmmTMB/glmmTMB.

Microsoft, and R Core Team. 2020. Microsoft r Open. Redmond, Washington: Microsoft. https://mran.microsoft.com/.

Muller, L. K., J. M. Lorch, D. L. Lindner, M. O'Connor, A. Gargas, and D.S. Blehert. 2013. Bat white-nose syndrome: a real-time TaqMan polymerase chain reaction test targeting the intergenic spacer region of Geomyces destructans. Mycologia 105: 253-259.

North American Bat Monitoring Program (NABat). Database v5.3.11 (Provisional Release): U.S. Geological Survey. Accessed 2020-11-18. NABat Request Number 11. https://doi.org/10.5066/P9UXA6CF

O'Shea, T. J., P. M. Cryan, D. T. Hayman, R. K. Plowright, and D. G. Streicker. 2016. Multiple mortality events in bats: a global review. Mammal review 46: 175-190.

Roche, N., S. Langton, T. Aughney, J. M. Russ, F. Marnell, D. Lynn, and C. Catto. 2011. A car-based monitoring method reveals new information on bat populations and distributions in Ireland. Animal Conservation 14:642–651.

Talbert, C., and B. Reichert. 2018. North American Grid-Based Sampling Frame: Continental United States at a 5x5km resolution: U.S. Geological Survey data release, https://doi.org/10.5066/P9M00P17.

Whitby, M., B. Udell, A. Wiens, T. Cheng, W. Frick, B.E. Reichert, and J. Reichard. 2021. In Support of the USFWS 3-Species Status Assessment: Summer Mobile Acoustic Transect Analysis. U.S. Geological Survey data release. https://doi.org/10.5066/P9W9OZU0.

Wiens, A. and W.E. Thogmartin. 2021. In Support of the U.S. Fish and Wildlife Service 3-Bat Species Status Assessment: Gaussian Process Model Predictions for the Spread of White-Nose Syndrome across North America, https://doi:10.5066/P9RP7J4H.

Appendix C-1. Wind energy influence covariate

By Brad J. Udell[1], Bethany R. Straw[1], Brian E. Reichert[1], and Jennifer Szymanski[2]

A ‘wind energy influence’ covariate was calculated for each North American Bat Monitoring Program (NABat) grid cell, year, and species, based on the deployment of wind energy facilities on the landscape each year (locations and rated capacity in megawatts), species specific mean dispersal distances, and the spatial context of each grid cell. The purpose of this metric was to quantify the potential relative risk of a bat dispersing from each grid cell and encountering a wind energy facility. Unlike distance to nearest wind farm, this metric also accounts for the relevant biological scale of movement for each species (the average migration distance), the intensity of wind energy deployment at wind farms (here the rated megawatt capacity), and contributions of risk from multiple wind farms rather than only the nearest (Udell et al. 2021).

Dispersal kernels are functions that model the probability of animal dispersal between locations given distance. For example, the exponential dispersal kernel is common (Moilanen and Hanski 2001) which has a single parameter, the inverse mean dispersal distance. Dispersal kernels are thus functions that rescale distance by the biological scale of effect.

[1] U.S. Geological Survey, Fort Collins Science Center, Fort Collins, Colorado, 80526, USA
[2] Division of Endangered Species, U.S. Fish and Wildlife Service, USGS - Upper Mississippi River Science Center, La Crosse, WI 54603, USA

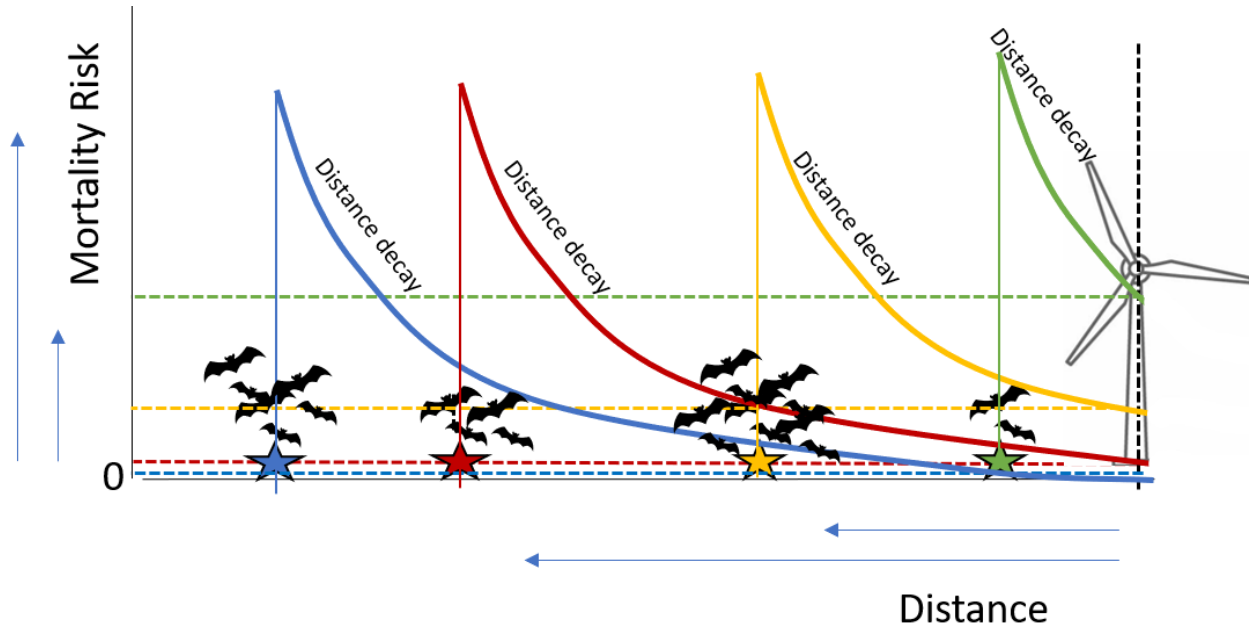

Figure C1.1. Using exponential dispersal kernels to model the relative probability of bats dispersing to a wind facility given the distance from the origin. The per individual probability of dispersal is $\exp(-\alpha d_{ij})$, where α is the inverse dispersal distance and d_{ij} is the distance to the wind facility. All else being equal, the mortality risk of bats dispersing from a location is based on the distance between the origin and the wind facility.

The capacity of wind energy facilities (in megawatts) is commonly used as an offset (take/megawatt) for collision risk (Kunz et al. 2007) because it is linked with the density and size of turbines at a wind facility, and thus the potential area of encounter with bats. Assuming that the rated capacity of a wind facility is a proxy for collision risk, the next section details how a wind energy deployment landscape (locations and capacities) was combined with spatial weighting based on distance and species dispersal distances to calculate the relative risk metric for each grid cell, species, and year.

Methods

A detailed description of methods, summarized below, and resulting data layers are documented in Udell et al (2021). The total rated capacity (megawatts) in each grid cell was determined for each year based on the U.S. Wind Turbine Database (Hoen et al. 2018). Thus, wind energy facilities from Canada and Mexico were not included. Total capacity megawatts from each grid cell with wind energy were spatially allocated (smoothed) across all the continental United States (CONUS) grid cells according to a spatial weighting scheme.

An exponential distance decay function (Equation 1) was used to model the relative probability of movement p_{ij} between locations given distance between them d_{ij} and the inverse of the average dispersal distance $\alpha = \frac{1}{\text{mean dispersal distance}}$ of each species (Table C1.1).

Eq.1: Unscaled distance weight calculation for wind index

$$p_{ij} = exp\ (-\alpha * d_{ij})$$

These values (p_{ij}) were treated as the unscaled distance weights, and under this relationship, self-contributions (where distance = 0) yield an unscaled proximity weight of 1 $(\exp(0) = 1)$. Then, these weights were rescaled to sum to one for each cell with wind energy (equation 2), so that the total megawatts on the landscape were the same before and after spatial smoothing.

Eq.1: Function for scaling distance weights

$$w_{ij} = \frac{p_{ij}}{\sum_i p_{ij}}$$

The pairwise megawatt influences (MWI_{ij}) between each focal grid cell with wind i and all grid cells j were calculated by multiplying the megawatts in the focal cell (MW_i) by the proximity weights (w_{ij}).

Eq. 2: Pairwise megawatts influence between grid cells

$$MWI_{ij} = w_{ij} * MW_i$$

Then the pairwise contributions of megawatt influence to each cell were summed up across all wind locations.

Eq. 3: Total wind influence per grid cell

$$MWI_j = \sum_i MWI_{ij}$$

The average migration distance of each species was determined from the banding records and recoveries in the NABat U.S. Historic Bat Banding database. Banding records from the U.S. Bat Banding Program collected between 1921 and 1995 were filtered to identify recapture events. The capture locations were attributed to the centroid of the NABat grid cell and distance between them was calculated using the *distm* function of the geosphere package, which accounts for the curvature of the earth (Hijmans 2019) in program R.

Table C1.1. Distance traveled in meters between captures of bat species determined from the North American Bat Monitoring Program (NABat) banding database.

Species	Mean	Median	SD	n
Myotis lucifugus	130.9	77	2 37.5	1065
Myotis septentrionalis	125.2	61	1 47.7	11
Perimyotis subflavus	259.8	46	3 82.2	31

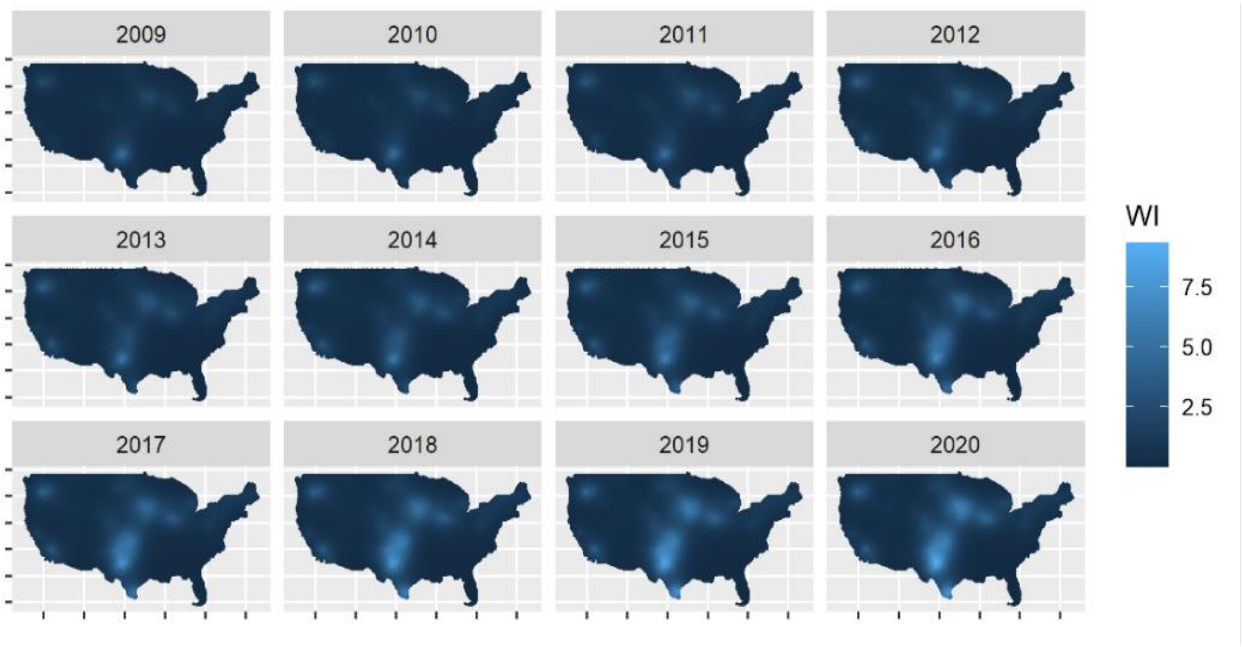

Figure C1.2. Wind energy influence index (WI) for *Myotis lucifugus*, from 2009 to 2020.

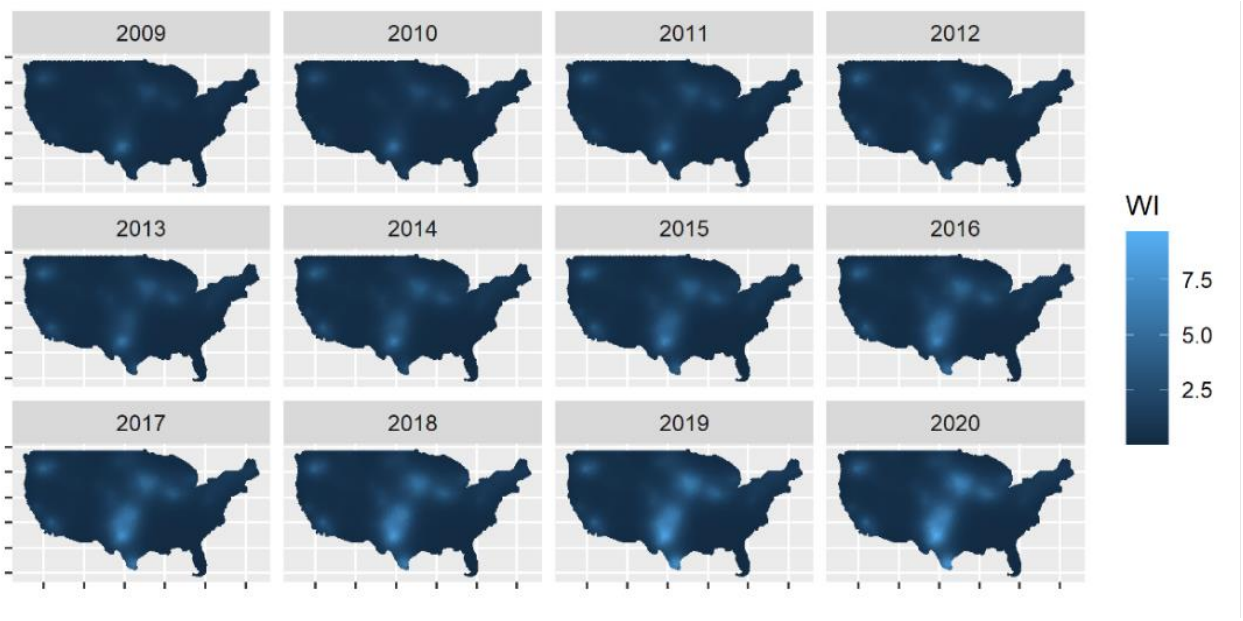

Figure C1.3. Wind energy influence index for *Myotis septentrionalis*, from 2009 to 2020.

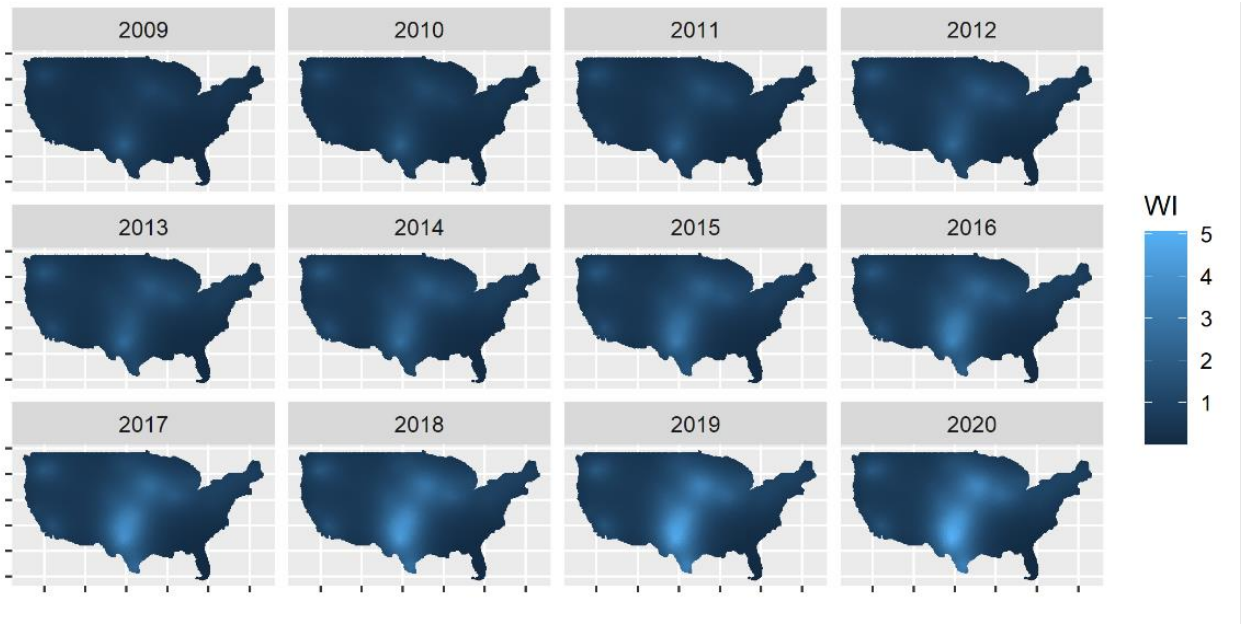

Figure C1.4. Wind energy influence index for *Perimyotis subflavus*, from 2009 to 2020.

References Cited

Hijman R.J. 2019. geosphere: Spherical Trigonometry. R package version 1.5-14. https://CRAN.R-project.org/package=geosphere

Hoen, B.D., Diffendorfer, J.E., Rand, J.T., Kramer, L.A., Garrity, C.P., and Hunt, H.E., 2018, United States Wind Turbine Database (v3.2, (October 10, 2020): U.S. Geological Survey, American Clean Power Association, and Lawrence Berkeley National Laboratory data release, https://doi.org/10.5066/F7TX3DN0.

Kunz, T.H., E.B. Arnett, B. M. Cooper, W. P. Erickson, R. P. Larkin, T. Mabee, M. L. Morrison, D. M. Strickland, and J. M. Szewczak. 2007. Assessing impacts of wind-energy development on nocturnally active birds and bats: a guidance document. The Journal of Wildlife Management 71(8): 2449-2486.

Moilanen, A., I. Hanski. 2001. On the Use of Connectivity Measures in Spatial Ecology. Oikos Vol. 95, No. 1, pp. 147-151.

Udell, B.J., Straw, B.R., Reichert, B.E., and J. Szymanski. 2021. In Support of the U.S. Fish and Wildlife Service 3-Bat Species Status Assessment: Wind Energy Influence: U.S. Geological Survey data release, https://doi.org/10.5066/P9V5H833.

Glossary

bat activity Echolocation call sequences detected and identified during acoustic surveys.

call sequence Sequence of echolocation pulses detected in a single acoustic recording file and identified to species.

grid cell 10km x 10km grid cell within the grid-based sampling frame of the NABat Master Sample for the continental United States (Talbert and Reichert 2018).

GRTS ID Identifier of the NABat grid cell where a mobile acoustic transect survey was conducted.

lambda (λ) In our analysis of mobile acoustic transects, we use lambda (λ) to refer to the change in call sequences recorded during surveys from one time period to another.

run Run refers to a single sampling occasion of a transect. In our analysis, run was defined as a single date in a grid cell (aggregating all records within each grid cell), which could combine multiple transects, or transect segments, if those transects occurred within the same grid cell. Thus, grid cells are the spatial sampling unit used for the analysis, and we accounted for differences in sampling effort by including the length of each transect/segment that occurred in the grid cell as a covariate.

years since detection of *Pd* (YSD) We use a model (described above) to predict the year of arrival of *Pd* in calendar years (e.g., 2014). We convert the year of arrival (YOA) to a scaled covariate of years since detection (YSD) of *Pd* for each sampled grid cell and year. Negative values of YSD indicate years before *Pd* is estimated to have arrived. Zero indicates the year *Pd* is estimated to have arrived.

MW Megawatt

Representation Units (RPU) Geographic units of interest for each species, defined by the United States Fish and Wildlife Service.

Chapter D. Winter Colony Count Analysis for Little Brown, Northern Long-eared and Tricolored Bat Species Status Assessment

By Tina Cheng[1], Brian E. Reichert[2], Wayne E. Thogmartin[3], Brad J. Udell[2], Ashton M. Wiens[3], Michael Whitby[1], Winifred F. Frick[1,4], Jonathan D. Reichard[5], and Jennifer Szymanski[6]

Introduction

To assist with the current species status assessment for *Myotis septentrionalis*, *Myotis lucifugus*, and *Perimyotis subflavus*, we assessed population trends from count surveys of wintering colonies at hibernacula for these three bat species.

Our objective was to provide annual estimates of the population growth rate (lambda) considering impacts caused by white-nose syndrome (WNS) and variation occurring among sites and years. Estimates of lambda were made available to be used in the Bat Tool and combined with other variables to gain further inference of population trends.

Methods

Winter colony counts were downloaded from the North American Bat Monitoring Program database (NABat 2021). In using these data, we made the following assumptions: (1) each count represents an accurate estimate of number of bats present at a site at the time of survey; (2) site surveys are comparable among years and differences in counts among years are

[1] Bat Conservation International
[2] U.S. Geological Survey, Fort Collins Science Center, Fort Collins, CO 80526
[3] U.S. Geological Survey, Upper Midwest Environmental Sciences Center, La Crosse, WI 54603
[4] University of California, Santa Cruz, CA 95064
[5] U.S. Fish and Wildlife Service, Ecological Services, Hadley, Massahusettes, 01035, USA
[6] Division of Endangered Species, U.S. Fish and Wildlife Service, USGS - Upper Mississippi River Science Center, La Crosse, WI 54603, USA

due to changes in number of bats present at a site rather than differences in survey methods or effort; (3) species were identified correctly; (4) changes in counts following detection of the pathogenic fungus *Pseudogymnoascus destructans* (*Pd*) to a site are due to stochastic yearly variation or the effects of WNS.

In addition to these assumptions, we also curated the data to remove inaccuracies and to aggregate surveys to the best representative count in a winter year for a species at a site. For data curation, we made the following assumptions: (1) winter surveys of hibernating bat colonies occur from the beginning of November to the end of March; (2) count surveys are unique to a NABat 10 km^2 to the site, species, and date sampled; (3) if multiple count surveys exist within the same day at the same site for the same species, these represent different sectional counts within the site and counts are summed to produce a single count for that day; (4) if multiple count surveys exist within a month or winter year, the best representative count is the highest count.

Following data curation, we further trimmed the data in preparation for this specific analysis. Below, we outline in detail our steps for data curation and preparation.

Data Curation

1. We removed “blanks” in the data:
    A. cases where species was not noted
    B. cases where count of live bats (count_alive) is not noted
2. Truncate to just winter surveys (winter defined as Nov - Mar)
3. Clean-up site_name errors
4. Remove species that were never counted at a site

5. Trim to unique counts
6. Sum multiple counts occurring within a day
7. Multiple counts within a month: take the maximum count
8. Multiple counts within a year: take the maximum count
9. Add spatial layers (admin1, admin2, region) and YOA (see glossary)

Prepare data for analyses

Following data curation, we performed the following steps to further prepare the data for analyses:

1. Filter counts for just SSA species (*Myotis septentrionalis*, *Myotis lucifugus*, *Perimyotis subflavus*)
2. Remove counts before 1990

We removed counts collected prior to 1990 because surveys were uncommon and because historical counts may be unreliable and uncomparable to current surveys.

3. Remove sites that do not have an assigned year of *Pd* arrival (YOA)

To include the effect of WNS in our analyses, we only retained sites where *Pd* has been detected at a site.

4. Only include sites with at least one pre and post count

To control for heterogeneity occurring at the site-level, we only included sites in the analyses where a count survey had been conducted at least once prior to and at least once following *Pd* arrival at the site.

5. Remove sites whose maximum count prior to *Pd* detection was fewer than 10 bats

Sites with fewer than 10 bats exhibited a high amount of variability and it is unclear to what extant this variability is driven by imperfect sampling versus changes in true local abundance. Counts less than 10 produced biologically unrealistic estimates of the population growth rate (>2).

Analyses: Estimating counts

We explored various ways to capture the variability in counts through linear mixed effects models using the lmer function in R. We fit log-linear models with the response variable in the model as ln(count+1). We used covariates as fixed and random effects that represent specific hypotheses about sources of variation in winter counts for all three species. We fit models separately for each species but used the same set of covariates and model selection criteria for each species. We modeled year as a fixed effect (year as a continuous linear variable) and the effect of WNS as a categorical variable with two states (pre-WNS, WNS). We also included an interaction term allowing the effect of year to vary by WNS state. We used random effects to allow for yearly and site-level variation as both random effects on intercepts and nested by site or year (see below).

The continuous variable of year represents the year-to-year log-linear population trend. We represent the effect of WNS as an instantaneous change (in population modeling terms) in the year of *Pd* arrival (main effect of the WNS term with two states: pre-WNS and WNS), and also as a change in lambda after year of *Pd* arrival (the interaction between the continuous year term and the binary term for WNS state).

The random effect grouped by site accounts for site-to-site variation in counts (sites have different mean relative abundances and/or different trends but they all follow a common

distribution). The random effect grouped by year accounts for year-to-year variation that is not attributable to WNS status at a site. We compared a set of models representing variation through random effects that occur through the intercept via (1|site) or through the slope(s) representing population change via (year|site).

We compared the following models using the Akaike information criteria (AIC).

$$log(count) \sim year + wns + (1|site)$$

$$log(count) \sim year + wns + wns * year + (1|site)$$

$$log(count) \sim year + wns + (1|year)$$

$$log(count) \sim year + wns + (1|site) + (1|year)$$

$$log(count) \sim year + wns + (1|site) + (year|site) + (1|year)$$

$$log(count) \sim year + wns + wns * year + (1|site) + (1|year)$$

$$log(count) \sim year + wns + wns * year + (1|site) + (year|site) + (1|year)$$

We used function lmer in R package *lme4* and compared models using an information-theoretic framework using the AIC (Burnham and Anderson 2002). We found the following model to be best-supported by AIC and used this model to estimate counts:

Eq.1: $log(count) \sim year + wns + wns * year + (1|site) + (1|year)$

We used a parametric bootstrap with 1,000 iterations to generate a distribution of predicted counts for a species at a site in a winter year. From bootstrapped values, we calculated the median estimates of the predicted count with 95% confidence intervals at various spatial levels - at the individual site, the state, the USFWS defined region, and across all the data (range-wide) for each species. We also calculated the median estimates of the predicted count with 95%

confidence intervals at the same spatial scales but aggregated at year since *Pd* detection (YSD) rather than year.

Calculating Lambda

We calculated lambda (λ) as the proportional change in the (back-transformed) predicted count in a given year or year since *Pd* detection relative to the prior year:

$$\lambda = \frac{count_t}{count_{t-1}}$$

We calculated median estimates of lambda with 95% confidence intervals for each species in a year or year since *Pd* detection at the site, state, region, and across all the data (range-wide).

Weighted lambda

When aggregating lambda across a spatial region to obtain the region-wide population growth rate, taking the mean across all hibernacula assumes equal contributions from each regardless of their winter colony sizes (i.e., counts). To account for differences in hibernacula counts when aggregating across spatial regions, we calculated a weighted lambda based on the proportional predicted count of each hibernaculum to the regional total. We obtained a weighted average for lambda at state, regional, and range-wide spatial scales as follows:

First, we calculated the total predicted count for a species at a given spatial scale for each year or year since *Pd* detection (*j*):

$$tot.count_j = \sum count_j$$

We then calculated the count proportion for each site (*i*) in a year or year since *Pd* detection (*j*) as the proportion of that count divided by the total count:

$$count.prop_{i,j} = count_{i,j}/tot.count_j$$

We then calculated a weighted lambda by multiplying lambda by the count proportion at that site (*i*) in a given year or year since *Pd* detection (*j*) and summing across sites to produce a weighted lambda for each year or year since *Pd* detection:

$$\lambda.wtd_j = \sum(\lambda_{i,j} * count.prop_{i,j})$$

Lambda by disease stage

We also summarized lambda by disease stage in order to quantify the WNS impact, or severity of decline, relative to pre-arrival counts. We identified five stages of disease progression:

- pre-arrival: YSD < 0
- invasion: YSD 1-2
- epidemic: YSD 2-4
- established: YSD 5-7
- endemic: YSD 7+

In general, disease stages correspond with expected progression of WNS (Frick et al. 2017). In pre-arrival, *Pd* has not yet been detected at the site. During the invasion stage, *Pd* is invading sites and some proportion of the bats are exposed to the fungus and may be exhibiting WNS symptoms and mortality. During the epidemic stage, a majority of the hibernating bats are infected with *Pd*, individuals are exhibiting WNS symptoms, and colonies are experiencing higher levels of mortality. By the established stage, *Pd* is prevalent on hibernating bats and on hibernacula substrates, but mass mortality may have already occurred and

individuals persisting at the site may represent survivors. Finally, the endemic stage is an extension of the established stage and represents sites with long-term *Pd* establishment and greater than 7 years of *Pd*/WNS occurring at a site.

To calculate lambda by disease stage, we first summarized pre-arrival counts for each site so that these could be used as a reference point of change for counts conducted in WNS disease stages. To obtain a representative pre-arrival count by site, we took the median value of predicted counts across all pre-arrival years for a species at a site and for each bootstrap run. (Note: variability in counts among pre-arrival years was not propagated.) In order to weigh each lambda by the proportion count at each site, we calculated the count proportion of each pre-arrival predicted count by species, spatial scale, and bootstrap run. We then joined the median predicted pre-arrival count by species, by site, and by bootstrap run. We calculated the weighted lambda for each species (*s*), ysd (*i*), spatial scale (*j*), bootstrap run (*k*), and site (*z*):

$$\lambda_{s,i,j,k,z} = (count_{s,i,j,k,z}/count.prearrival_{s,j,k,z}) * (count.prearrival_{s,j,k,z}/total.count.prearrival_{s,j,k})$$

We obtained a single weighted lambda by species (*s*), ysd (*i*), spatial scale (*j*), and bootstrap run (*k*) by summarizing across sites:

$$\lambda.wtd_{s,i,j,k} = \sum \lambda_{s,i,j,k,z}$$

Finally, we calculated a proportion change in count (λ - 1) representing the amount of decline relative to the pre-arrival count. We report median predicted values with 95% confidence intervals (CI) on weighted lambda, summarized to the species, spatial scale, and disease stage.

Results

Results and model predictions from the analyses describe herein are available through a USGS data release (Cheng et al. 2021) and summarized below.

Sample size

Number of winter surveys by year included in the analyses (after data filtering) varied by year, with the most amount of sampling occurring in the years following the first case of WNS in North America (after 2006) (Figure D1). Number of winter surveys peak around 2010/2011 for all three species and then declined again (Figure D1). Data filtering most notably reduced the number of surveys for *Myotis septentrionalis* and *Perimyotis subflavus* given that many wintering colonies for these species had fewer than 10 bats prior to *Pd* detection at the site.

Predicted median counts

Predicted median counts indicate that populations were most likely stable prior to *Pd* arrival and declined coincident with *Pd* detection at the site for all three species (Figure D2). Declines in colony counts are most evident in reference to year since *Pd* detection (YSD), but are still evident when summarized by actual year, even though years contain a mixture of sites where *Pd* has and has not yet arrived across the range of sampled sites.

Weighted lambda

Trends in weighted lambda for all three species also indicate that populations declined coincident with the arrival of *Pd* (Figure D3). For *Myotis lucifugus*, there is a spike in weighted lambda in the year *Pd* is first detected (YSD=0), where the median predicted value and upper 95% confidence interval exceeds a biologically plausible value of 2 (if only accounting for birth

and death in the population) (Figure D3). We also found wide 95% confidence intervals indicating high levels of uncertainty in the first year of *Pd* detection (YSD = 0) for *Myotis septentrionalis* (Figure D3). For both *Myotis septentrionalis* and *Perimyotis subflavus*, sharp declines in colony counts are evident coincident with the arrival of *Pd* (Figure D3).

Percent change in counts relative to pre-arrival

Our results indicate severe (95-99%) decline for all three species by the endemic stage of WNS disease progression (YSD > 7) (Table D2; Figure D4). During *Pd* invasion, declines were moderate (36-51%) but increased with each additional stage of WNS progression (Table D2; Figure D4). Uncertainty around declines was also greatest during the invasion stage and decreased with WNS progression (Table D2; Figure D4).

Conclusions

Prior to WNS, hibernating bat colonies were likely stable for all three species (*Myotis septentrionalis*, *Perimyotis subflavus* and *Myotis lucifugus*) albeit with a large amount of uncertainty around those estimates (for all three species, 95% confidence limits for weighted lambda overlap 1.0 in all years prior to the detection of *Pd*). Colonies declined with the onset of *Pd*/WNS for all three species with winter counts showing >95% decline on average by the endemic stage of WNS progression.

Declining colony trends with the onset of *Pd*/WNS were most notable for *Myotis septentrionalis* and *Perimyotis subflavus*. Declines were also evident in *Myotis lucifugus*, but the population growth rate was more variable over the years than the other two species. In particular, in the year of *Pd* detection (YSD = 0), estimates of the population growth rate and the upper 95% confidence interval increased dramatically for *Myotis lucifugus* while they declined for *Myotis*

septentrionalis and *Perimyotis subflavus*. Multiple sources of variation may account for these inflated rates of population growth including sampling error, immigration, or movement of bats to more visible areas of the hibernacula. Future efforts should focus on accounting for these additional sources of variability in annual counts. Uneven representation of sites in the latter years of WNS may also have biased count estimates, such as in years 11 and 12 following *Pd* detection, where only a handful of sites represent these late years of *Pd* persistence in *Myotis lucifugus.* Continued sampling from a broad selection of sites would help inform long-term population trends for colonies persisting with WNS.

We report results from a statistical model rather than inferring from data summaries for several reasons. First, we used statistical modeling to explore various hypotheses in count patterns. For example, within a statistical framework, we are able to build models and compare them using AIC to ask if models that included WNS as a predictor variable explained count trends better than models that did not take WNS into account. Within this comparative framework, we found that WNS was an important driver in count variation and trends over time. Secondly, we used statistical modeling to account for site-to-site variation, year-to-year variation, and survey effort, thereby allowing us to evaluate the main effects of count over time and the impacts of WNS on counts. While plotting raw data can provide initial insights in count trends over time, they force the observer to visually estimate patterns, which can be subject to individual bias. In contrast, statistical methods allow us to objectively quantify relationships between variables while also quantifying the amount of statistical uncertainty around those results. For these reasons, we used a statistical modeling framework for this assessment.

Table D1. Number of count surveys/sites for three bat species by year after filtering data for analyses (and prior to data filtering for analyses).

Year	*Myotis lucifugus*	*Myotis septentrionalis*	*Perimyotis subflavus*
1990	41 (50)	2 (13)	39 (53)
1991	35 (44)	5 (18)	40 (56)
1992	29 (33)	7 (19)	25 (39)
1993	38 (39)	4 (18)	39 (42)
1994	27 (29)	5 (17)	22 (30)
1995	31 (43)	4 (19)	38 (46)
1996	38 (48)	5 (30)	35 (51)
1997	36 (43)	7 (26)	35 (47)
1998	37 (48)	4 (27)	35 (50)
1999	48 (60)	11 (38)	45 (61)
2000	54 (61)	12 (44)	51 (68)
2001	62 (84)	16 (50)	71 (111)
2002	45 (58)	10 (43)	57 (88)
2003	59 (80)	17 (49)	68 (96)
2004	61 (81)	13 (58)	64 (96)
2005	70 (97)	17 (65)	75 (117)
2006	49 (74)	7 (49)	57 (103)
2007	72 (89)	32 (68)	92 (116)
2008	62 (82)	10 (37)	64 (102)
2009	107 (143)	34 (87)	112 (161)
2010	95 (140)	34 (83)	106 (185)
2011	119 (175)	32 (96)	153 (225)
2012	124 (191)	34 (111)	170 (319)
2013	152 (249)	27 (139)	205 (360)
2014	119 (205)	24 (118)	201 (393)
2015	117 (203)	23 (117)	226 (452)
2016	87 (143)	13 (76)	157 (395)
2017	70 (142)	9 (41)	128 (403)
2018	57 (88)	4 (20)	112 (457)
2019	45 (84)	4 (16)	88 (362)
2020	59 (79)	1 (6)	78 (244)

Table D2. Median percent change in counts (with 95% CI) by disease stage in three bat species relative to pre-arrival (of *Pseudogymnoascus destructans*) median predicted counts.

Species	Invasion	Epidemic	Established	Endemic
Myotis lucifugus	22% (-48,18)	-64% (-78,-33)	-84% (-90,-76)	-96% (-100,-90)
Myotis septentrionalis	-37% (-54,-10)	-56% (-70,-37)	-73% (-85,-59)	-94% (-100,-78)
Perimyotis subflavus	-50% (-57,-42)	-63% (-71,-55)	-80% (-88,-71)	-99% (-100,-90)

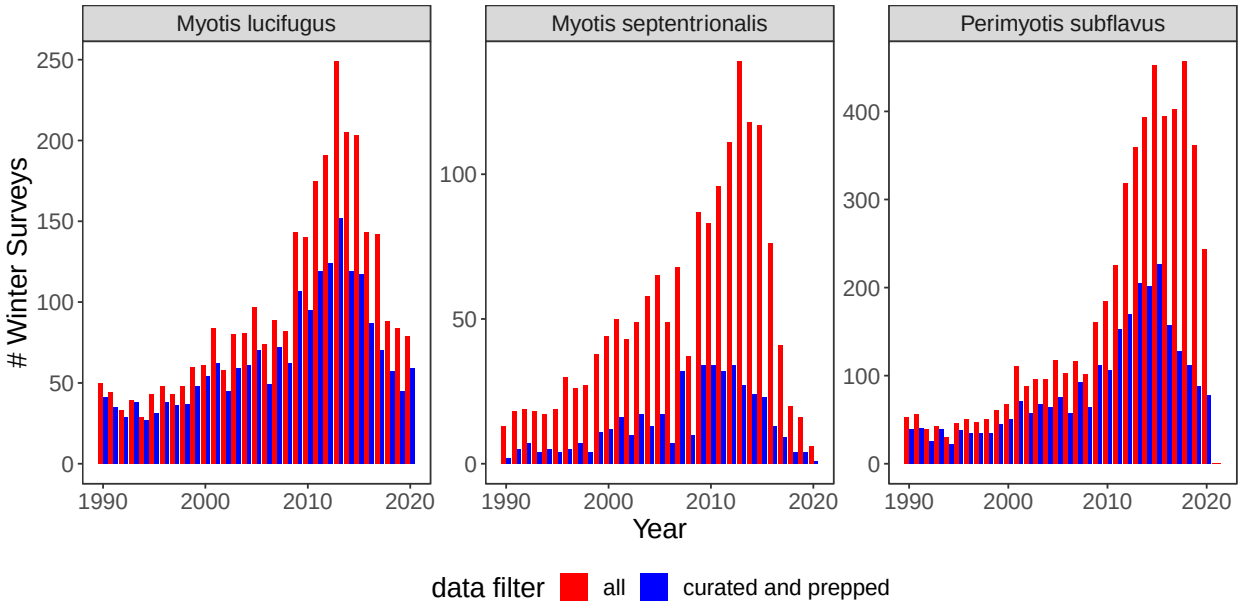

Figure D1. Sample size (number of count surveys for each bat species by year) for curated data (red bars) and data following curation and preparation for analyses (blue bars).

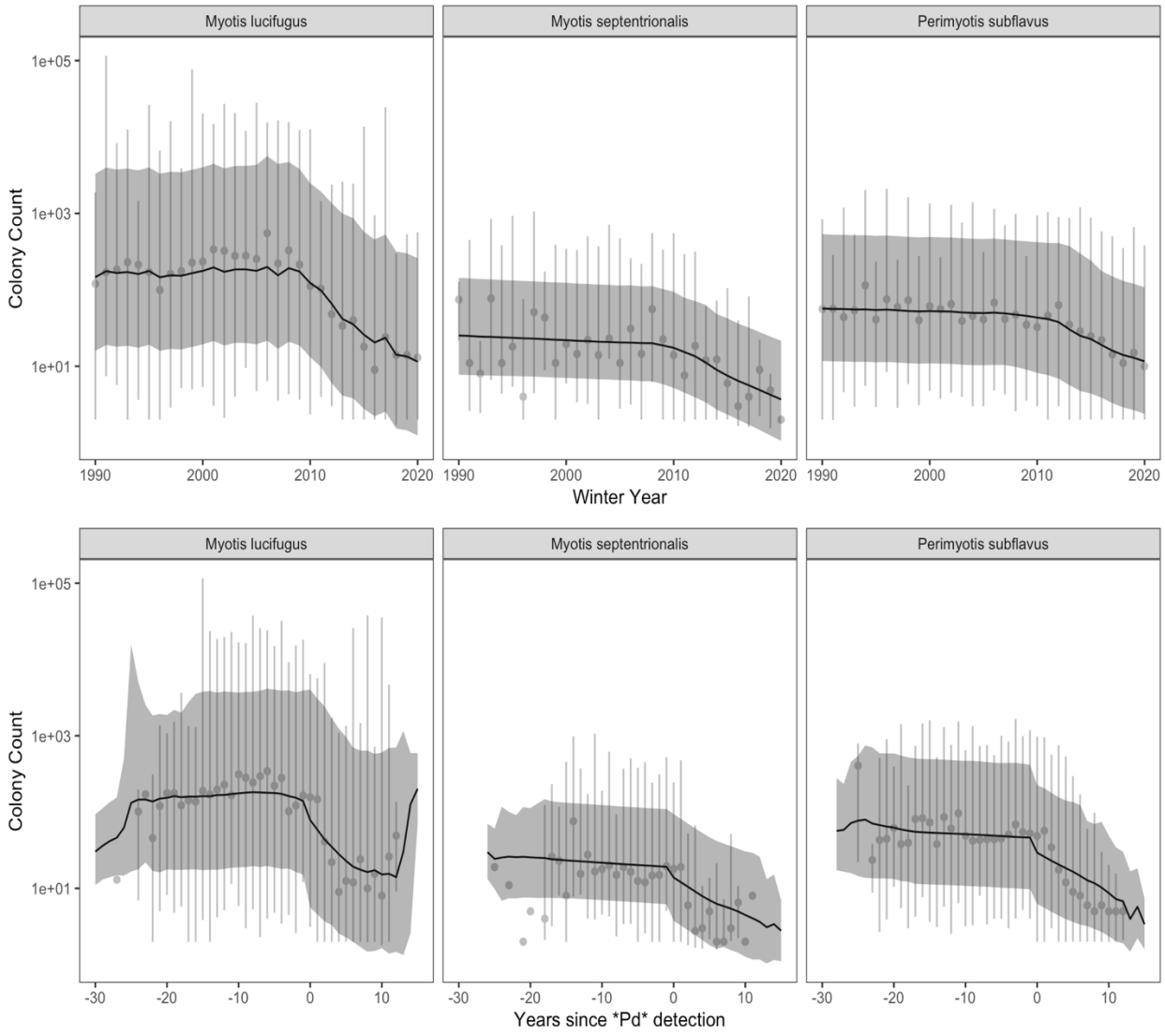

Figure D2. Median predicted counts with 95% confidence interval (line with grey ribbon) and median raw counts with 95% quartiles (points with error bars) by year (top panel) and years since *Pseudogymnoascus destructans (Pd)* detection (bottom panel). Predicted counts were obtained from the best-supported model (Eq. 1).

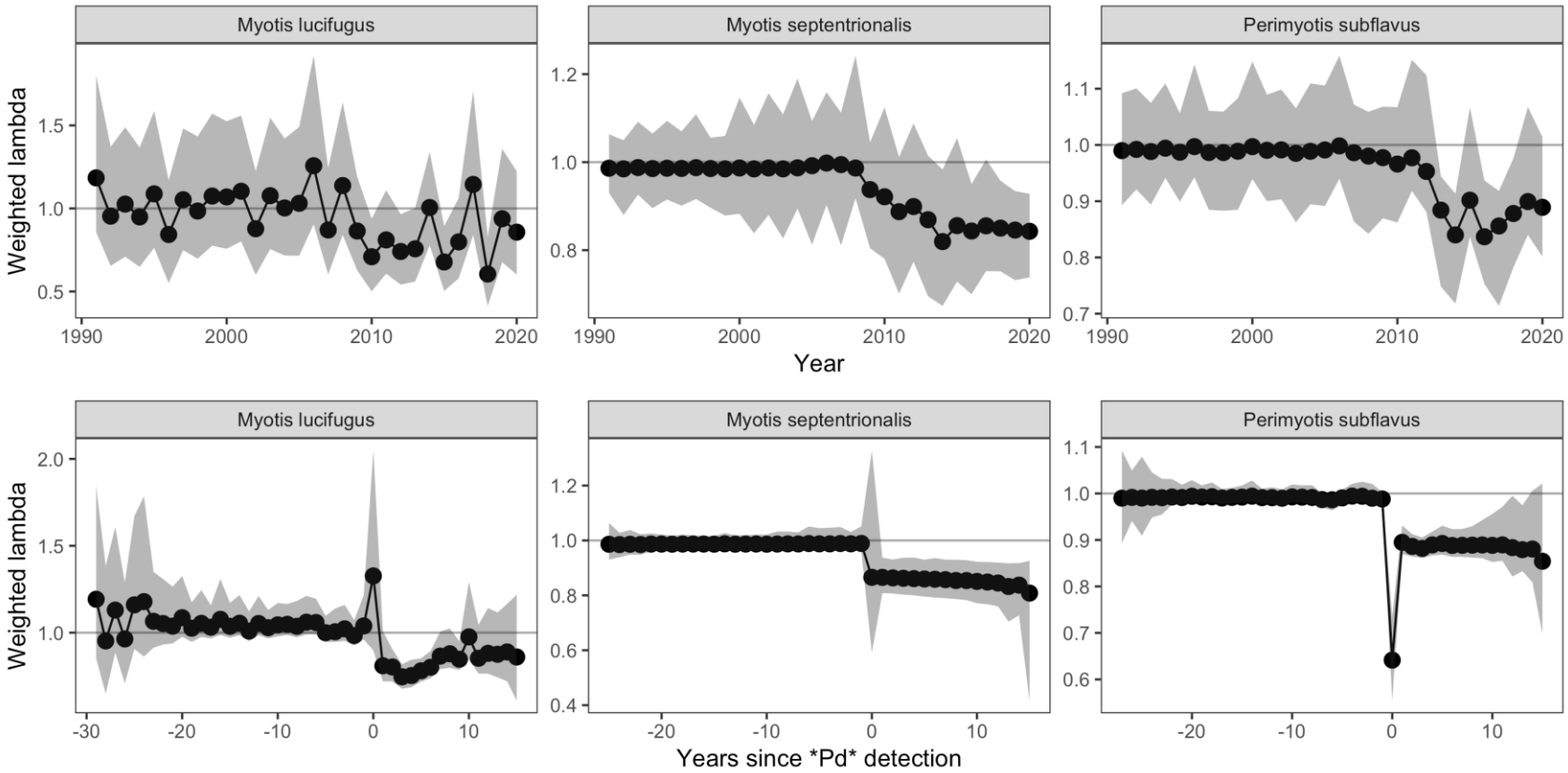

Figure D3. Median estimates of weighted lambda with 95% confidence intervals by year (top panel) and by years since *Pseudogymnoascus destructans* (*Pd)* detection (bottom panel) for *Myotis lucifugus*, *Myotis septentrionalis*, and *Perimyotis subflavus*. Weighted lambda =1 indicates no change in annual population growth rate (horizontal line). Weighted lambda is calculated based on the proportional predicted count of each hibernaculum to the regional total.

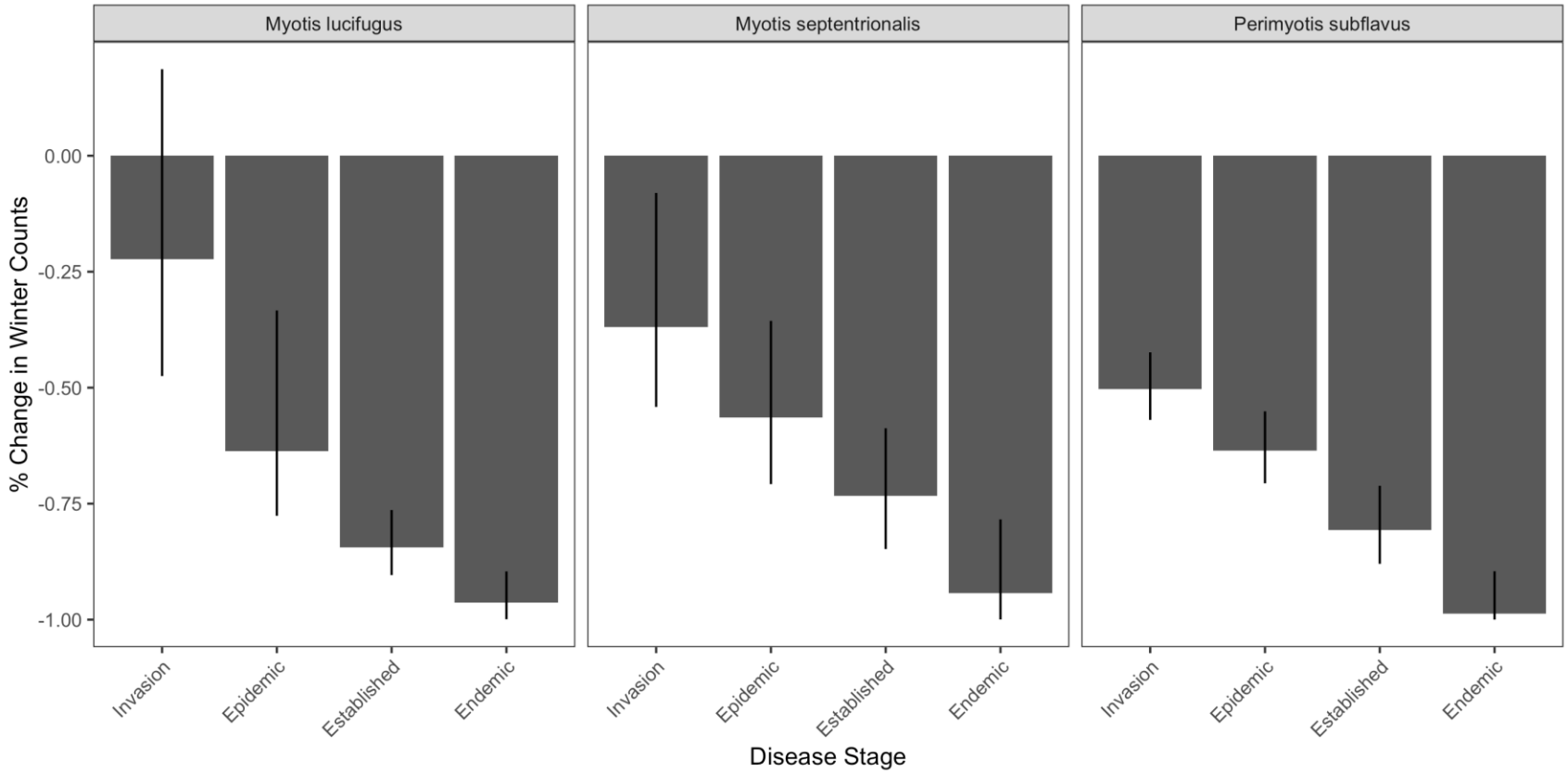

Figure D4. Percent change in winter counts of three bat species by disease stage relative to predicted median counts in pre-arrival of *Pseudogymnoascus destructans* (YSD < 0). Median estimates of percent change in winter counts with 95% confidence intervals are shown for invasion (YSD 0 & 1), epidemic (YSD 2-4), established (YSD 5-7) and endemic (YSD 7+) stages. A negative percent change indicates decline in the population (e.g., -90% = 90% decline). YSD is years since *Pd* arrival.

References Cited

Burnham, K. P., and D. R. Anderson. 2002. Model Selection and Multimodel Inference: A Practical Information-Theoretic Approach, 2nd Ed. Springer. New York. 488 pp.

Cheng T., W. Frick, B.E. Reichert, W.E. Thogmartin, B.J. Udell, A.M. Wiens, M. Whitby, J. Reichard, and J. Szymanski. 2021. In Support of the U.S. Fish and Wildlife Service 3-Bat Species Status Assessment: Winter Colony Count Analysis. U.S. Geological Survey data release, https://doi.org/10.5066/P9YG45TG.

Frick, W.F., T.L. Cheng, K.E. Langwig, J.R. Hoyt, A.F. Janicki, K.L. Parise, J.T. Foster, and A. M. Kilpatrick. 2017. Pathogen dynamics during invasion and establishment of white-nose syndrome explain mechanisms of host persistence. Ecology 98(3): 624-631.

North American Bat Monitoring Program (NABat) Database v6.0.12 (Provisional Release): U.S. Geological Survey. Accessed 2021-02-10. NABat Request Number 12. https://doi.org/10.5066/P9UXA6CF.

Glossary

admin1 Administrative level 1, equivalent to state in the United States.

admin2 Administrative level 2, equivalent to county in the United States.

colony We use the word colony to describe an aggregation of bats at winter hibernacula. We also use the word “population” interchangeably with colony throughout the text. We do not imply social behavior or interactions among individuals with use of the word ‘colony’. Our use of the word population refers to the individuals present at the site during the time of survey and does not represent the entire regional or local population.

grid cell/id 10 km^2 cell based on generalized random tessellation stratified (GRTS) sampling generated by the NABat sampling protocol.

winter The winter season is defined as the period from Nov to March within a survey year.

year Because winter surveys occur over a time period that includes a change in the numerical year (e.g., 2007 to 2008), we use a convention of using the year corresponding to January since the majority of surveys happen after January 1. Therefore, surveys conducted from Nov 2007 to March 2008, would be attributed as year = 2008.

YOA Year of *Pd* arrival (YOA) is defined as the year of first *Pd* detection at a site by quantitative polymerase chain reaction (qPCR). *Pd* detection by qPCR often precedes onset of WNS diagnostic symptoms in an individual and mortality by at least one year. Thus, for sites with a year of WNS confirmation, we equate year of WNS confirmation to YOA by offsetting by one year (year - 1). For these analyses, we used an interpolated YOA calculated by NABat 10 km^2 grid cell.

YSD Year since *Pd* detection (YSD) is defined as the number of years between the year and YOA.

Chapter E. Winter Colony Count Data Assessment and Future Scenarios for the Little Brown, Northern Long-eared and Tricolored Bat Species Status Assessment

By Ashton M. Wiens[1], Jennifer Szymanski[2], Bradley J. Udell[3], and Wayne E. Thogmartin[1]

Disclaimers

Scales on some maps vary by more than 10% and may be inaccurate.

Introduction

Hibernating bats in North America are experiencing local and regional declines caused by multiple environmental stressors, necessitating analysis of the current and future health and population viability of three species, the little brown bat (*Myotis lucifugus*), northern long-eared bat (*Myotis septentrionalis*) and tricolored bat (*Perimyotis subflavus*), under consideration of federal listing through the U.S. Fish and Wildlife Service (USFWS) Species Status assessment (SSA) (Cheng et al. 2021, Frick et al. 2010, Thogmartin et al. 2012, 2013, McGuire et al. 2016, Frick et al. 2015, Turner et al. 2011, Langwig et al. 2012).

White-nose syndrome (WNS), caused by the fungal pathogen *Pseudogymnoascus destructans* (*Pd*), has caused high mortality rates among several bat species since its first documentation in North America in winter 2006-2007. The disease, monitored collectively through the collaboration of many organizations, has decimated populations as it has spread across the continental United States (Frick et al. 2010, Turner et al. 2011, Langwig et al. 2012, Maher et al. 2012, Hefley et al. 2020, Thapa et al. 2021, White-nose Syndrome Response Team 2020, Kramer et al. 2021). In addition, wind turbines located in bat home ranges or migratory

[1] U.S. Geological Survey, Upper Midwest Environmental Sciences Center, La Crosse, WI 54603
[2] Division of Endangered Species, U.S. Fish and Wildlife Service, USGS - Upper Mississippi River Science Center, La Crosse, WI 54603, USA
[3] U.S. Geological Survey, Fort Collins Science Center, Fort Collins, CO 80526

pathways pose a threat to the longevity of bat populations (Erickson et al. 2016, Diffendorfer et al. 2017, Arnett et al. 2010, Diffendorfer et al. 2021, Arnett & Baerwald 2013, Choi et al. 2020, Cryan et al. 2014, Maurer et al. 2020).

We assessed bat population dynamics in winter hibernacula using count data stored in the North American Bat Monitoring Program database (NABat 2021). We modeled counts of bats with log-linear models to estimate the historical and current population status and trends for each of the three species included in the SSA. The *year of arrival* (YOA) of WNS is a key covariate in our modeling framework. We used WNS surveillance data to fit a Gaussian process model, which we then used to predict YOA at unmonitored hibernacula. Next, we incorporated site-level predictions of abundance and growth rates from the log-linear models as input parameters in a demographic matrix projection model to forecast population abundance under several different scenarios. Future scenarios help quantify uncertainties in population vital rates and potential effects of stressors in the model over time. These statistical models provide a quantitative tool for scientists, decision makers, and conservation managers to make informed decisions.

Methods

The following is a summary of the steps taken for the analysis in support of the SSA. Sections that follow describe specific methods in detail.

- Step 1: Download all colony count observations from the NABat database for *Myotis lucifugus*, *Myotis septentrionalis*, and *Perimyotis subflavus* (NABat 2021). Process data to give annual winter year counts.
- Step 2: Calculate historical statistics from colony count observations, including using a piecewise constant annual interpolation of the observations.

This interpolation method assumes the count at a site remains constant at the last observed count until a new count is observed.

- Step 3: Calculate and process WNS spread model covariate data for input into population models.
- Step 4: Calculate expected wind energy related bat mortality. Allocate the expected number of bat fatalities to each site (also referred to as "wind take") based on last observed count at each site.
- Step 5: Fit log-linear generalized additive mixed models to assess the status and trends of the three species. Let the response variable be *log(count+1)*; let the only fixed effect predictor be time, recorded as a winter year, but transformed into the *year since detection* of white-nose syndrome (YSD, identical to *year since arrival* or YSA in other chapters) at a given site using the WNS covariate. The model included a piecewise linear spline on YSD to reflect changing abundance trajectories upon the arrival of WNS at a site. The model additionally included site-level random effects on the spline coefficients to help capture heterogeneity in site trends. Log-linear models provided estimates of current population abundance and growth rate λ for each site modeled.
- Step 6: Summarize white-nose syndrome impacts for each log-linear model from estimated site-level annual median λ values. Group λ values by *year since detection* of *Pd*/WNS at each site. Working under the assumption that the site-level λ values for each year post WNS arrival were due to decreases in the adult winter survival rate (AWS), translate λ values into AWS reductions

by setting all λ values greater than one equal to one. This resulted in a set of site-level λ values for each YSD bounded within the interval [0, 1]. Use these annual sets of λ values as a discrete distribution to be drawn from when applying the impacts of WNS in the demographic model.

- Step 7: Inspect site-level observations and fitted models for anomalies (for largest 90% of total observed population) using an R Shiny visualization application (Chang et al. 2021). We identified a set of "anomalous sites" for which the log-linear model estimates after the arrival of WNS do not properly capture the observed population trajectory. For these sites, we used the last observed count and the pre-WNS λ estimates instead of the log-linear model estimates. In addition, anomalous sites did not receive WNS impacts in the demographic model, necessitated by the limitations of the statistical models used in this analysis.
- Step 8: Define projection scenarios.
- Step 9: Run projection scenarios at the site level using the demographic model, using starting abundances and growth rates, allocated wind related mortality, WNS impacts, and demographic stochasticity and environmental stochasticity.
- Step 10: Process simulations into statistical summaries of population trajectories at several spatial scales. Output included abundance and growth rates over time, as well as probability of growth, persistence, and extinction.

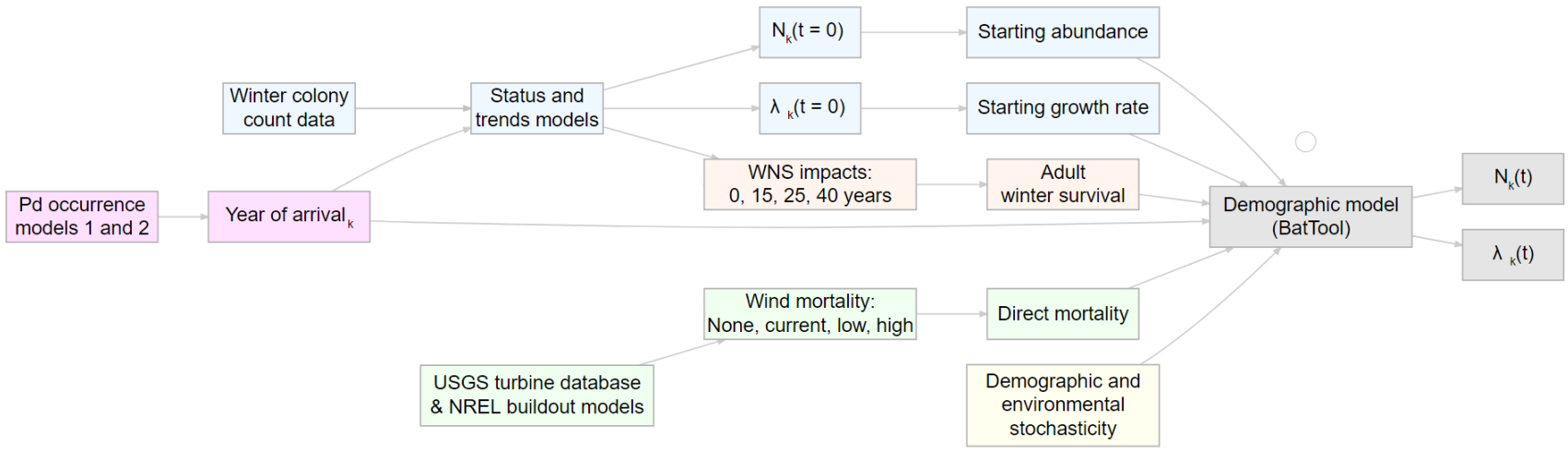

Figure E1. Diagram of model inputs and outputs, sources of data, and basic parameters. WNS=white-nose syndrome, "Pd"=*Pseudogymnoascus destructans*, USGS=U.S. Geological Survey, NREL=National Renewable Energy Laboratory, and $N_k(t)$ and $\lambda_k(t)$ are the population abundance and growth rate for population k at time t.

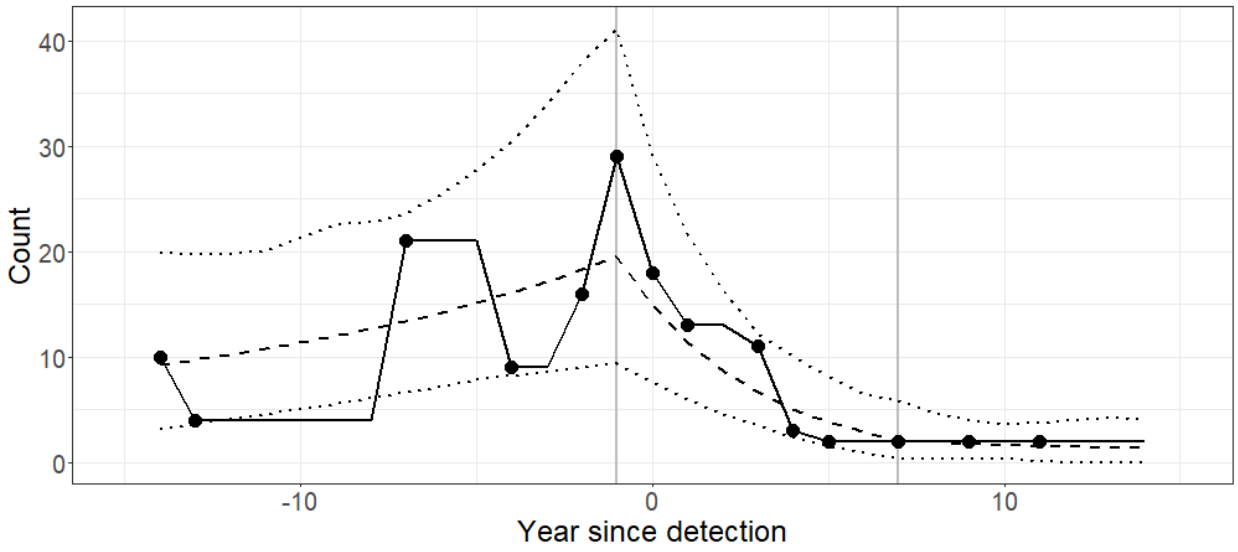

Figure E2. Observed and modeled bat abundance depicting example observations (dots), piecewise constant interpolation of observations (solid line), and fitted spline regression model median predictions (dashed line) with uncertainty bounds (dotted lines) for three bat species. The log-linear model has two cusps at year since detection YSD -1 and 7 indicated by the thick grey vertical lines, dividing the model into three time periods: pre-white-nose syndrome (WNS; left), WNS invasion (middle), and WNS endemic (right).

Data

We obtained winter colony count data from the NABat database (NABat 2021) for *Myotis lucifugus*, *Myotis septentrionalis*, and *Perimyotis subflavus* collected between 1990 and 2020. In addition, general *Myotis* counts from Michigan were obtained and split into *Myotis lucifugus* and *Myotis septentrionalis* counts using ratios 9:1 pre-WNS and 99:1 post-WNS.

We processed colony count data to obtain annual counts at sites collected between November and March for each winter year. For each species, we included any site with at least

one nonzero count. This resulted in a data set for each species comprised of historical winter colony counts from 1990-2020 for the unique sites in which we have at least one record of a nonzero count. We processed colony count data using the following criteria. We summed multiple counts on the same day at the same site. If multiple counts in the same month or year existed, we took the maximum of these counts. If there were counts in multiple months in one winter year, we took the maximum of these counts. We added spatial site-level information such as *year of arrival* (YOA), Representation Unit (RPU, see Figs E4, E6, E8), and hibernaculum complex to the data by joining to the NABat Master Sample Frame, which consists of a 10×10 km spatial grid encompassing all of North America (Talbert and Reichert 2018). This approach allowed us to track sites without using precise spatial locations. We summarized model results across the extent of the available data and for each Representation unit (RPU). RPU allowed model results to be summarized at a regional spatial scale which is preferable to administrative boundaries in addition the entire species range; RPU was not explicitly included as a covariate in any models.

Summary Statistics

Table E1. Number of hibernacula per bat species, tallied by data completeness: whether a hibernaculum has at least three historical counts, whether there are counts before and after the arrival of white-nose syndrome (WNS), and a minimum count of ten bats.

Species	Total no. of hibernacula	Pre-wns count >10	Pre- and post-wns count	>10 pre-count and post-wns count	>10 pre-count and post-wns count and >3 counts
Myotis lucifugus	889	425	482	361	295
Myotis septentrionalis	737	189	416	147	118
Perimyotis subflavus	1,951	658	672	483	388

Table E2. Maximum bat species abundance by year attained from piecewise constant interpolation of the observations.

Species	Year	Abundance
Myotis lucifugus	2001	1,278,126
Myotis septentrionalis	1996	38,131
Perimyotis subflavus	2007	140,547

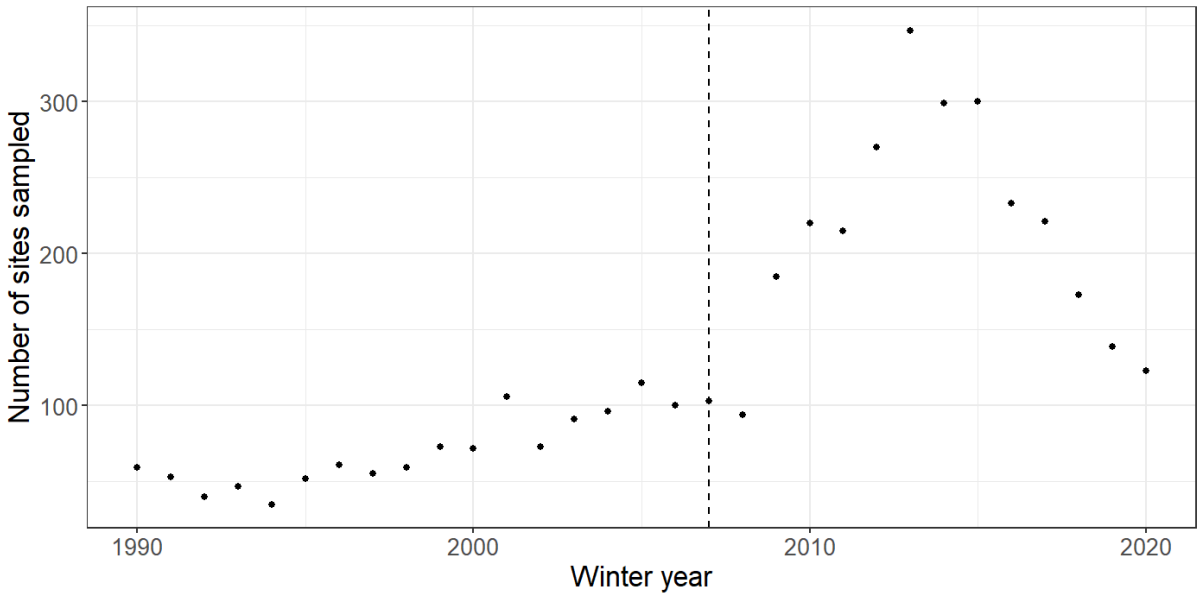

Figure E3. Number of sites (winter colonies) sampled per year for *Myotis lucifugus* (MYLU), from 1990 through 2020. The black dashed line on 2007 indicates the year of presumed arrival of white-nose syndrome (WNS) in North America, after which colony count sampling greatly increased.

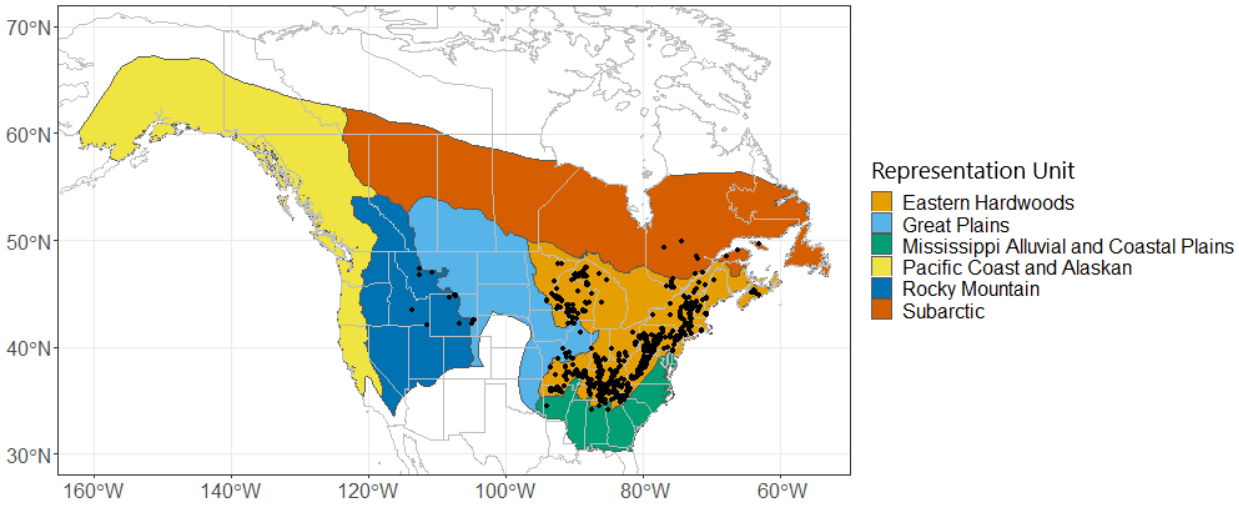

Figure E4. Representation Units for *Myotis lucifugus* as defined by the U.S. Fish and Wildlife Service . Black dots represent approximate locations of winter colonies used to model population dynamics.

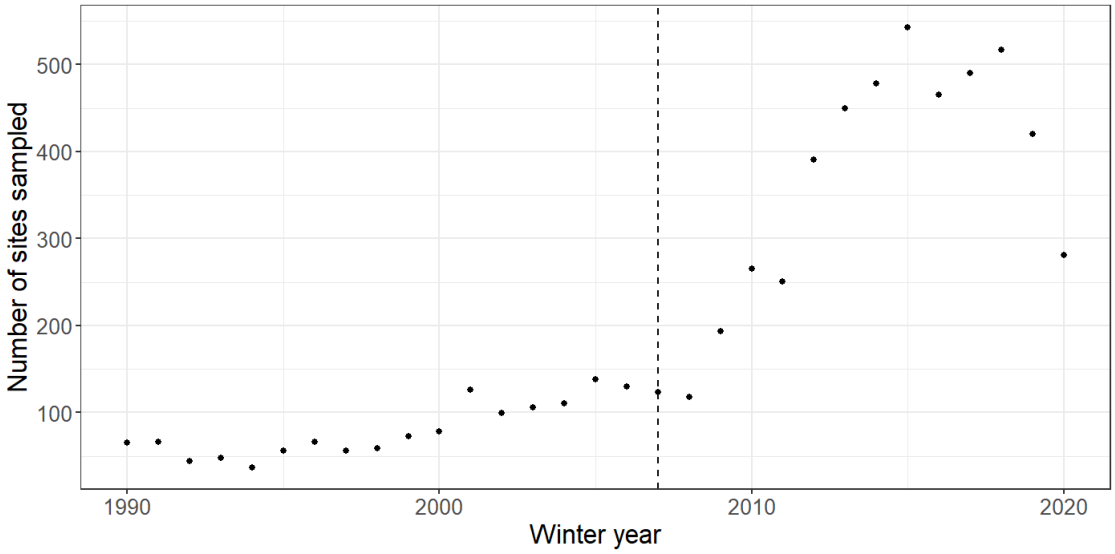

Figure E5. Number of sites (winter colonies) sampled per year for *Perimyotis subflavus* (PESU), from 1990 through 2020. The black dashed line on 2007 indicates the year of presumed arrival of white nose-syndrome (WNS) in North America, after which colony count sampling greatly increased.

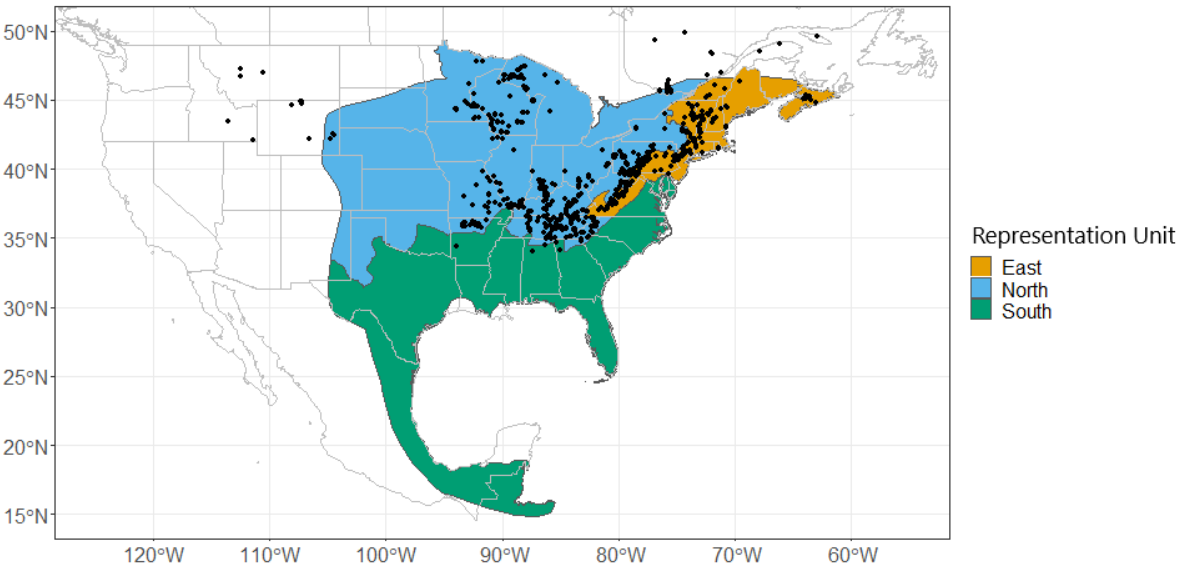

Figure E6. Representation Units for *Perimyotis subflavus* as defined by the U.S. Fish and Wildlife Service. Black dots represent approximate locations of winter colonies used to model population dynamics.

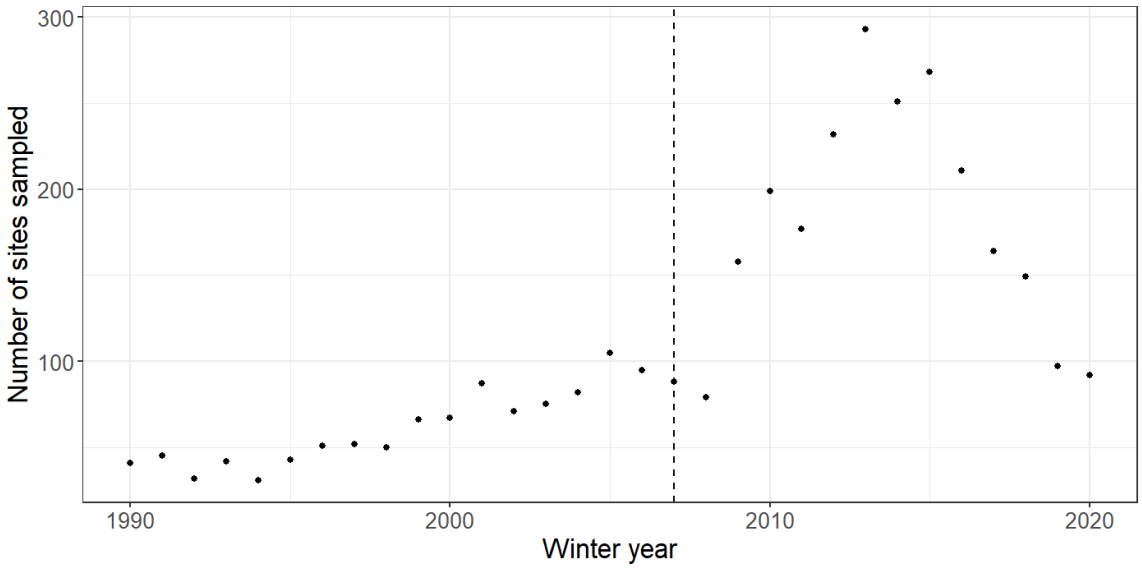

Figure E7. Number of sites (winter colonies) sampled per year for *Myotis septentrionalis* (MYSE), from 1990 through 2020. The black dashed line on 2007 indicates the year of presumed arrival of white-nose syndrome (WNS) in North America, after which colony count sampling greatly increased.

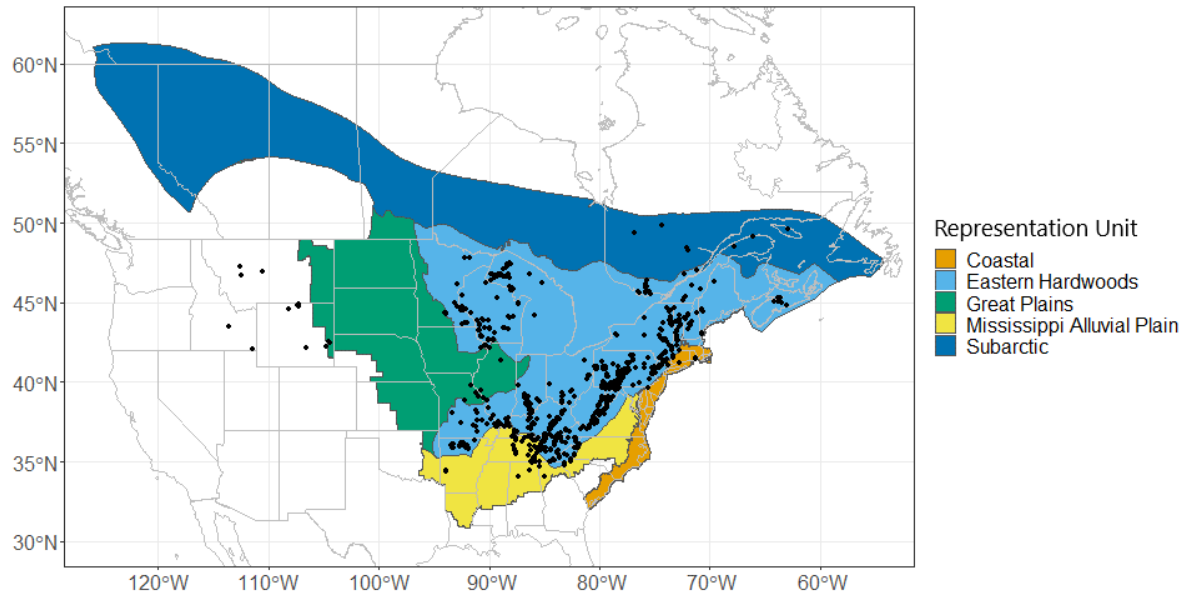

Figure E8. Representation Units for *Myotis septentrionalis* as defined by the U.S. Fish and Wildlife Service. Black dots represent approximate locations of winter colonies used to model population dynamics.

Environmental stressors

When using statistical models for historical and future abundance, covariates can greatly improve model fit and potential for meaningful inference. The USFWS identified WNS and wind energy-related fatality as two important environmental stressors affecting the three bat species; other stressors such as habitat loss and fragmentation and climate change may be affecting bats but were not considered in this work.

Wind energy-related mortality

Wind energy-related mortality was calculated using estimates of bat fatality rates found in the literature and based on reports submitted to U. S. Fish and Wildlife Service. Bat carcasses are collected in proximity to wind turbines, and calculated fatality rates allow for predictions of the expected bat take per megawatt of installed wind energy capacity for bat populations of interest. Given predictions of total wind energy-related bat take in each grid cell (given current or projected installed wind capacity), we allocated predicted bat take among all hibernacula within the maximum dispersal distance of each species based on distance between hibernacula and grid cells with wind turbines, weighted by population abundances (last observed count at each site). Complete methods for predicting and allocating wind energy related mortality are documented in Appendix E-1 and Udell et al. (2021).

White-nose syndrome spread models

Pd occurrence model 1

We fit a spatial Gaussian process model to estimate the *year of arrival* of WNS across North America. We modeled observed county-level YOA (White-nose Syndrome Response Team 2020) using *distance* from the center of Schoharie County in New York as a predictor,

which is where the disease was first documented in North America. We chose to fix the intercept at the year 2007 so that we can interpret the effect of distance from Schoharie County as the radial spread rate, since this is the presumed year and site of introduction of the disease. In addition to the uncorrelated residual error process included in linear models, the Gaussian process included a spatially autocorrelated stochastic process, which allowed the model to identify regions where the year of arrival was observed either sooner or later than expected based on the concentric spread predicted from the effect of *distance*. We specified the spatially autocorrelated process using the Matérn covariance function with smoothness parameter fixed at one. We used restricted maximum likelihood to estimate the *distance* fixed effect in addition to the Matérn range and variance parameters and the residual variance parameter (Cressie 1993). The estimate of the *distance* fixed effect was 135 miles per year (102-199 miles per year 95% confidence interval (CI)) or 217 km per year (164-320 km per year 95% CI). These results can be found in Wiens et al. (2021d).

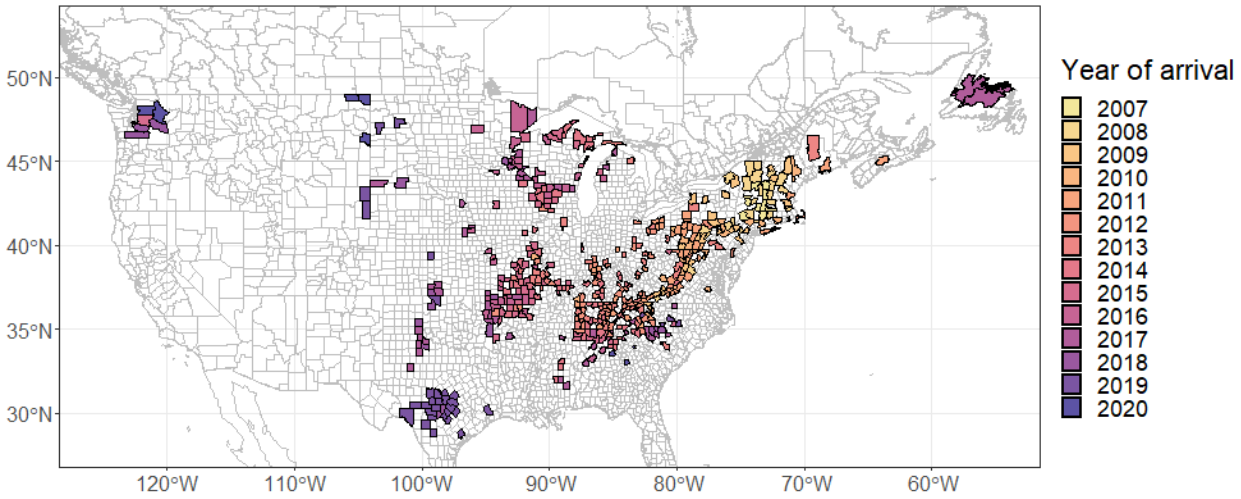

Figure E9. County-level determination of the *year of arrival* of white-nose syndrome (White-Nose Syndrome (whitenosesyndrome.org), accessed 2021-02-10.

Gaussian random fields are continuously indexed in space, meaning predictions of the response YOA can be made at arbitrary spatial locations. We predicted the expected *year of arrival* and uncertainty using the universal kriging estimator equations Cressie 1993) 10×10km grid, a subset of the NABat Master Sample covering the continental United States and Canada. The Gaussian process model provided a fast method for producing predictions of YOA with uncertainty at unobserved locations.

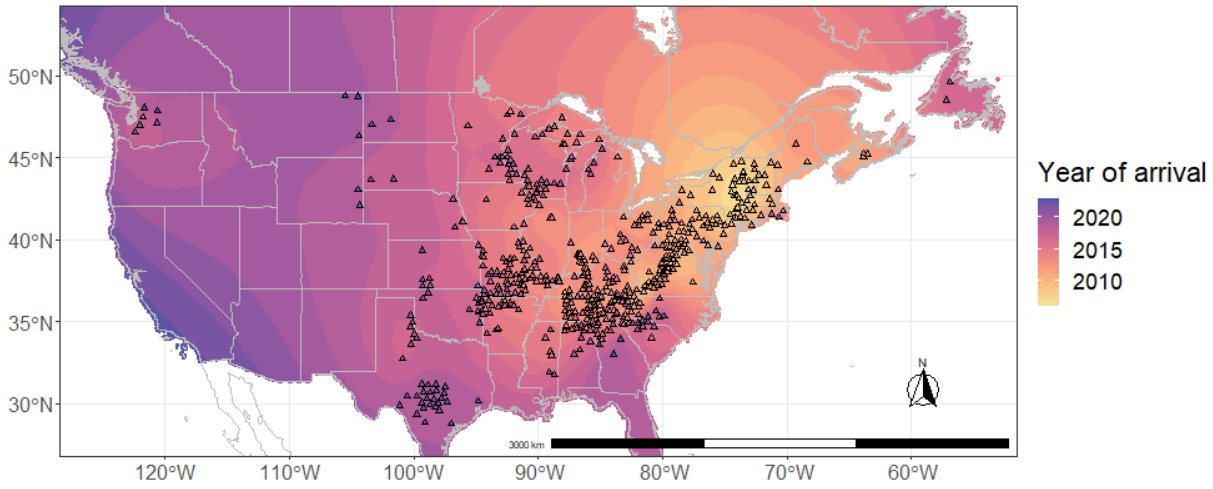

Figure E10. Gaussian process predictions of year of arrival (YOA) of white-nose syndrome (WNS) from 2007 through 2024. Triangles represent county-level WNS year of arrival observations from Figure E9 used to fit the model.

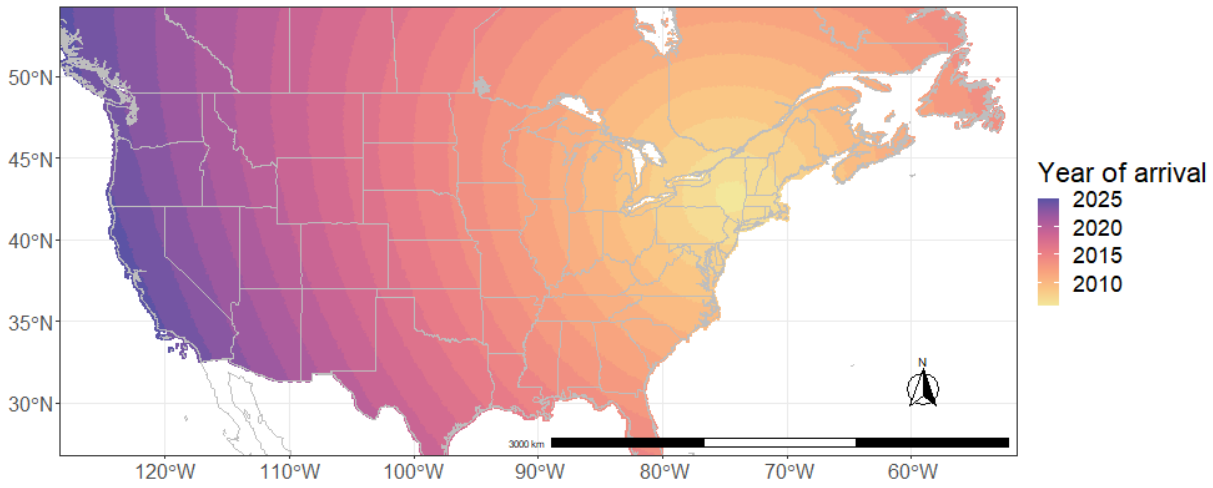

Figure E11. Year of arrival (YOA) predictions including only the distance from Schoharie county fixed effect and intercept from the Gaussian process spread model. The fixed effects imply a concentric spread of white-nose syndrome from 2007 through 2025.

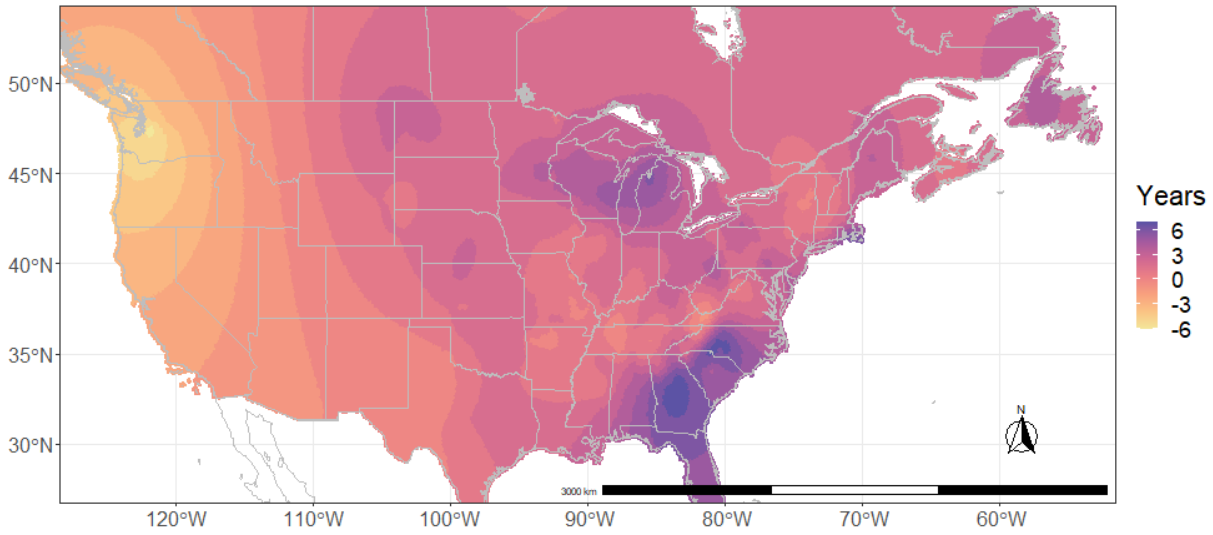

Figure E12. Predictions including only the spatially autocorrelated variation component from the Gaussian process spread model. Spatially autocorrelated variation is in units of years and indicates regions where white-nose syndrome (WNS) arrived sooner or later than expected based on the concentric spread in Figure E11.

Pd occurrence model 2

Hefley et al. (2020) modeled the probability of *Pd* occurrence, producing spatially located probability predictions from 2007 through 2042. Using these data, we derived a *year of arrival* of WNS (Figure E13) by assigning to each NABat grid cell the first year the probability of *Pd* occurrence was greater than 0.25; this threshold was chosen because it has been used to identify the disease front in monitoring efforts (USGS National Wildlife Health Center 2021). Figure E14 shows site-level predictions from *Pd* occurrence model 1 and model 2 were highly correlated ($\rho = 0.81, n = 1{,}158$).

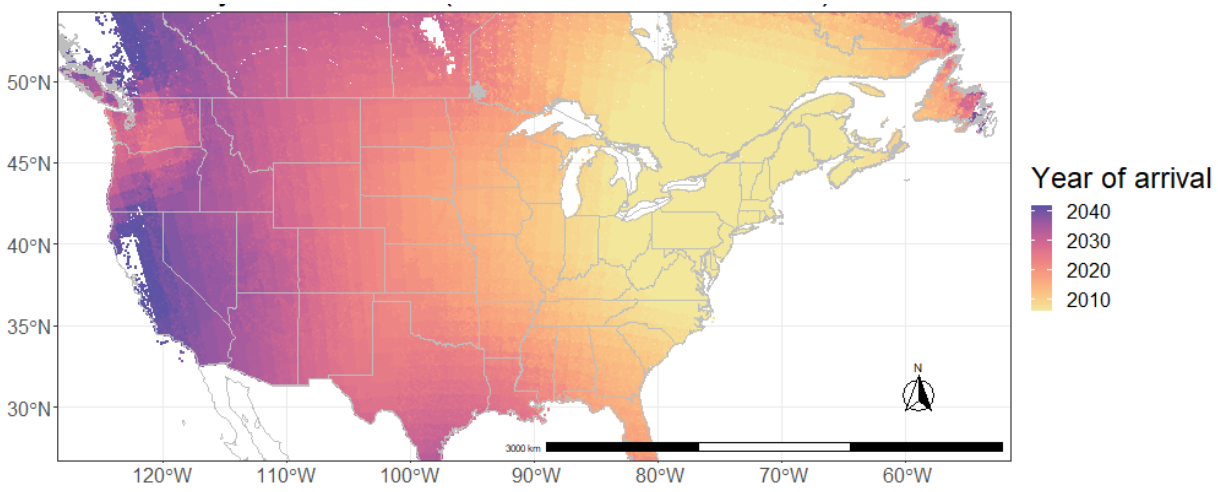

Figure E13. Predicted *year of arrival* of *Pseudogymnoascus destructans*/white-nose syndrome (*Pd*/WNS) across the North American Bat Monitoring Program (NABat) grid cells from 2007 through 2042 obtained using *Pd occurrence model 2*, based on the mechanism of ecological diffusion.

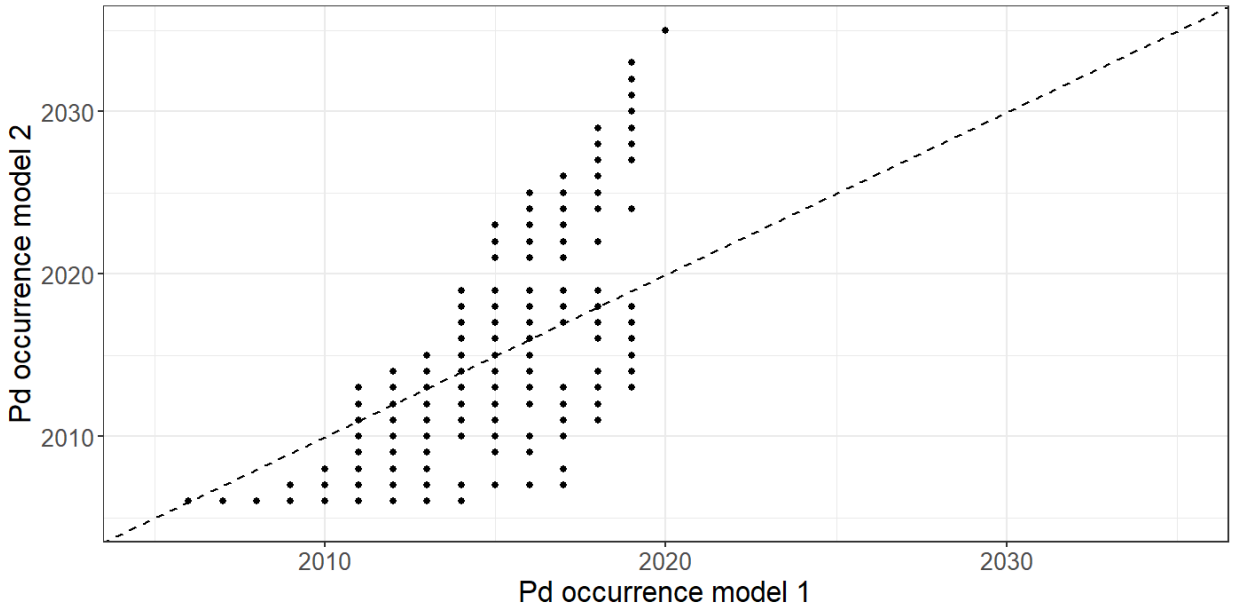

Figure E14. A comparison of model predictions for the year of arrival (YOA) of *Pseudogymnoascus destructans*/white-nose syndrome (*Pd*/WNS) for all sites (*Pd* occurrence model 1 vs *Pd* occurrence model 2). The 1:1 line indicates sites where the spread models agree on the expected YOA; the correlation coefficient between the two sets of predictions is $\rho = 0.81$.

Status and trends estimation

The BatTool (Erickson et al. 2014, Wiens et al. 2021b) is a demographic matrix model used to project a population into the future incorporating uncertainty and environmental stressors. The model uses, as inputs, estimates of the current abundance, population rates of change (Wiens et al. 2021db), and estimates of environmental stressors. We refer to generating these values as status and trends estimation.

Log-linear mixed effects model

To estimate status and trends for each species, we modeled *log(count+1)* using a log-linear mixed effects model (Zuur 2009). The predictors in the model included an intercept and

piecewise linear splines in the time variable. We included random effects (variation) in spline coefficients by site. We fit the model using the `lmer` function in the `lme4` package (Bates et al. 2015) and the `bs` function in the `splines` package in `R`, version 4.1.0 (R Core Team 2021). We included *year since detection* of WNS for each site as a continuous covariate. We placed knots at YSD equal to -1 and 7 for all splines to represent the pre-arrival, invasion, and epidemic stages of WNS. Data were available until *year since detection* of +12 for at least one site. Using *year since detection* requires a *year of arrival* covariate as described in Chapter C. For each species, we fit two log-linear models. The first model incorporated *year of arrival* informed by *Pd* occurrence model 1, while the second model incorporated *year of arrival* informed by *Pd* occurrence model 2.

We subsetted the input data set to the log-linear models to include only sites with a minimum of five colony counts to avoid numerical instability issues caused by a singular covariance matrix when fitting random effects. Table E3 shows the numbers of sites and observations included and excluded from the log-linear models. We used the two log-linear models to simulate 100 realizations of the population trajectory for each site over the historical period 1990-2020. For each site, we summarized population trajectories by calculating the median abundance over time. We denoted the median abundance $n_{i,t}$ for site i at time t, and then defined the population growth rate $\lambda_{i,t} = n_{i,t+1}/n_{i,t}$. Thus, for each site we obtained predictions of median abundance and population growth rate over time.

Table E3. Number of sites and observations included (modeled) and excluded (unmodeled) in the log-linear models for each bat species.

Species	Number of sites included	Number of sites excluded	Number of observations excluded	Number of observations included
Myotis lucifugus	545	344	1,181	2,928
Myotis septentrionalis	440	297	958	2,535
Perimyotis subflavus	1,489	462	2,631	3,711

For sites with less than or equal to four colony counts, we assumed abundance was equal to the last observed count, and we derived an estimate for the population growth rate λ from the closest hibernaculum or hibernacula complex. A hibernacula complex is defined as a group of sites where the distance between sites is less than or equal to ten miles (Thogmartin et al. 2012). We weighted values of λ by abundance within a site complex using the formula $\overline{\lambda_{k,t}} = \sum_{i \in N(k)} \lambda_{i,t}$ for site k where $N(k)$ contains the indices of all sites within the complex to which site k belongs that were included in the log-linear model. For these sites, we made the necessary assumption that local populations remained stable after their last observation and that sites in close proximity exhibit similar dynamics.

WNS impacts

To account for the potential impacts of WNS on population level survival rates, we developed species-specific WNS impacts schedules using annual population growth rates derived from the log-linear mixed effects model. We based the WNS impacts schedules on the distribution of aggregated site-specific λ estimates grouped by YSD.

We assumed fecundity rates for *Myotis lucifugus* and *Myotis septentrionalis* equal to one pup per year and two pups per year for *Perimyotis subflavus* (Wimsatt 1945, Caceres and Barclay 2000, Fujita and Kunz 1984). Given these relatively low fecundity rates, we also assumed that values of λ greater than four were indicative of unmodeled immigration. We were interested in characterizing the population effects of WNS survival only, so we removed these large λ values. The WNS decline estimates may be biased low in this case because of our inability to disentangle emigration from the effects of WNS on local survival in the same way, a limitation of this methodology for assessing the impacts of WNS.

In addition, we set estimated values of λ greater than one equal to one, indicating no declines due to WNS. This decrease in population growth rate was attributed to the effects of WNS, which we characterized through the adult winter survival rates in the demographic model. When WNS is projected at a site using the demographic model during post-WNS years (specific to each site), the vital rates, specifically adult winter survival, which define the demographic model, are altered accordingly. We assumed we had a sufficient number of sites to reliably estimate WNS impacts for at least six years after invasion, a time period chosen based on exploratory analyses of the number of counts for each positive year since detection. One year of data was used for each year YSD one through six to estimate the WNS impacts schedule, and in addition, for all subsequent years (where YSD is greater than six) the estimated λ values were pooled into one distribution defining a 'post-WNS regime', which can be applied to project bat population abundance into the future for longer time horizons. Using *Pd* occurrence model 1 and *Pd* occurrence model 2 we fit two log-linear models for each species. The differences in model λ estimates are apparent in Figures E15 and E16 by the differing densities of points near unity, especially for *Myotis septentrionalis*. The WNS impacts schedule shows separation of most λ

values from one for the log-linear model corresponding to *Pd* occurrence model 1, but this separation is not evident for model 2.

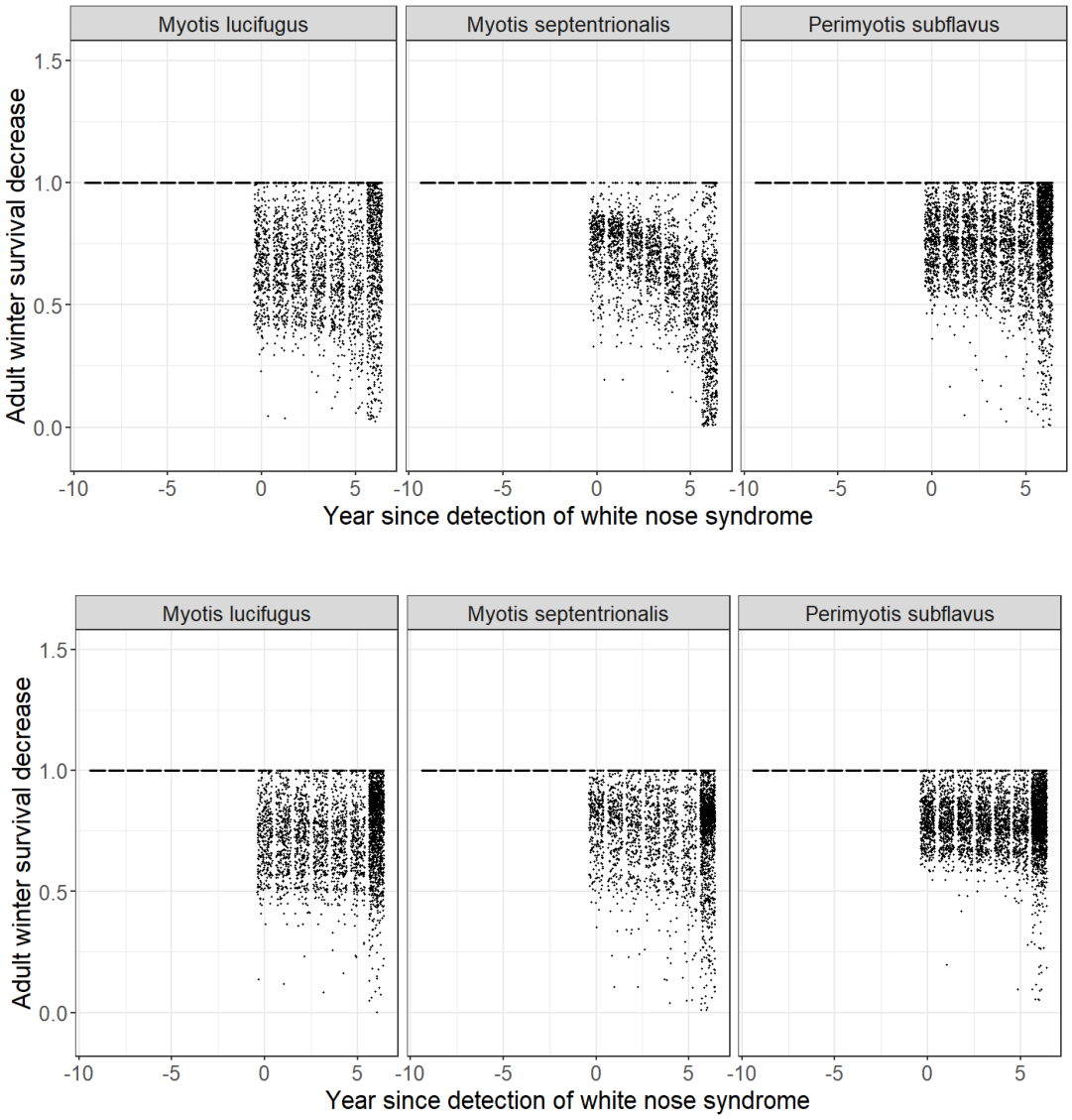

Figures E15 and E16. Species-level white-nose syndrome (WNS) impacts for *Pseudogymnoascus destructans (Pd)* occurrence models 1 (top panel) and 2 (bottom panel) for three bat species. Yearly discrete distributions for both WNS spread models summarize estimates of adult winter survival decreases caused by WNS for all sites. Each dot represents one site's modeled population growth rate λ value in the given year since detection of WNS; sites not suffering declines are the dots on the line y = 1.

Future population projections

For all three species, the population abundance at each site was projected 40 years into the future, from 2020 to 2060, using a demographic matrix projection model and the BatTool R package (Erickson et al. 2014, Wiens et al. 2021). The demographic model projects abundance into the future for each population, under various WNS survival and wind energy mortality scenarios. The inputs to the BatTool are site-specific starting abundance, population growth rate λ, annual WNS schedule, annual (seasonal) expected number of wind energy related bat fatalities, and magnitude of stochasticity. The model produces an ensemble of simulations, projecting the population into the future based on reproductive and survival rates.

We used the BatTool to run 100 simulations of the population trajectory for each site from 2020 to 2060. Each population's starting abundance was split using an 80:20 adult-to-first year ratio (Thogmartin et al. 2013). All simulations included demographic stochasticity and uniform environmental stochasticity of magnitude 0.04 on each vital rate. The differing number of pups per annual litter of the three bat species is accounted for when translating between λ and the fecundity vital rates defining the demographic model.

We used the 2020 predicted abundance (or last observed count) and estimated population growth rate (or population weighted spatial average) as starting values for each site. The estimated population growth rate was the λ value from 3 years before the arrival of WNS (YSD = -3). This was chosen to reflect the state of the population trajectory before the arrival of WNS because the effects of WNS are accounted for when applying decreases to adult winter survival rates in the model using the WNS impacts schedule. If three or more counts were available for the period after six years post-WNS arrival, the λ averaged from this period was used instead of the pre-WNS arrival λ and WNS impacts schedule. Finally, we identified a set of six anomalous

sites which clearly show sustained stability or growth after the arrival of WNS. These sites include (1) for *Myotis lucifugus*, Tippy Dam and Maiden Rock in Michigan, Walter Williams Preserve and Haile's Cave in New York; and (2) for *Perimyotis subflavus*, Louisville Culvert in Mississippi and Frick's Cave in Georgia. The log-linear model did not estimate reliable λ values post-WNS for these sites, so pre-WNS arrival λ was used with no WNS impacts.

Future scenarios differed by varying the *Pd* occurrence model, the length of WNS impacts, and the severity of wind energy related mortality. Wind energy-related mortality was applied in the demographic model by directly subtracting bats from site populations during specific seasons. Future wind scenarios included the current scenario, as if there will be no further wind energy development in the future, and the low impact and high impact future development scenarios which encompass our uncertainty about these estimates.

SSA scenario definitions

A variety of future projection scenarios were explored, characterizing both current and plausible future scenarios, as well as baseline scenarios with no environmental stressors for comparison. Each scenario investigated was a unique combination with one selection from the following options.

Wind scenarios:

- No wind mortality
- Estimated mortality from current wind buildout
- Estimated mortality from low-impact wind buildout
- Estimated mortality from high-impact wind buildout

WNS spread scenarios:

- *Pd* occurrence model 1
- *Pd* occurrence model 2

WNS impacts duration:

- 0-year impacts
- 15-year impacts
- 25-year impacts
- 40-year impacts

Results

The following species-level projected abundance plots show historical trends and future projections. Historical trends pre-2020 include predictions from two log-linear mixed effects models and a piecewise constant interpolation model. For each species, the first plot characterizes future projections under current conditions. The second plot characterizes future projections under possible future wind energy and WNS scenarios. The third plot compares projections under both current conditions and future scenarios. Projected future and current scenarios are combinations of simulations with 80% uncertainty coverage shaded. The results and model predictions used to generate these plots are available through a USGS data release (Wiens et al 2021a; Wiens, Szymanski, and Thogmartin 2021c,d).

Myotis lucifugus

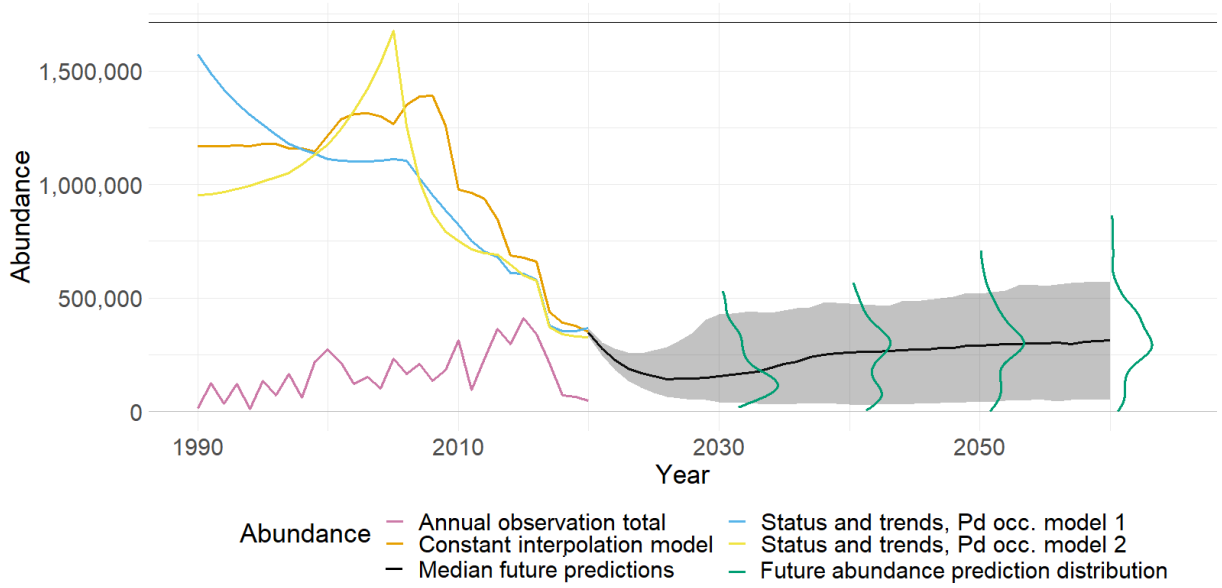

Figure E17. *Myotis lucifugus* species-level abundance projections for current conditions. The pink line shows the annual total observed counts, and the orange line shows the piecewise constant interpolation of the observations. Predictions from the two log-linear models are shown in blue and yellow. The black line is the future median projection with 80% uncertainty coverage (grey shaded region). The vertical green lines show the distribution in future projected abundance at times 2030, 2040, 2050, and 2060. The black horizontal line at the top is the sum of the maximum observed count at each site.

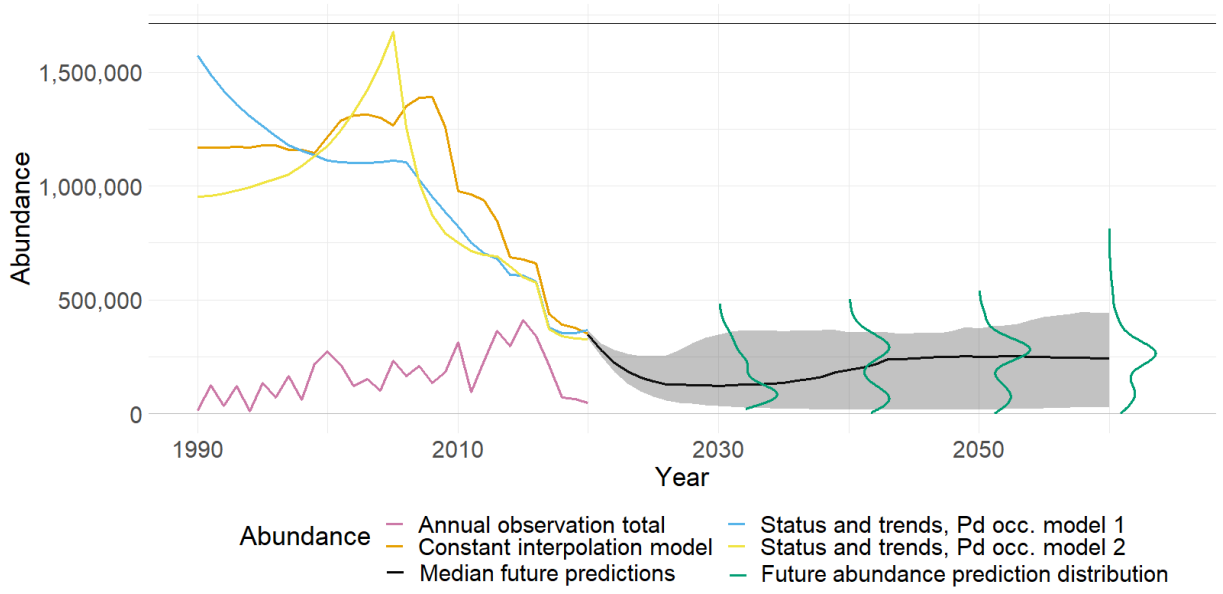

Figure E18. *Myotis lucifugus* species-level abundance projections for future conditions. The pink line shows the annual total observed counts, and the orange line shows the piecewise constant interpolation of the observations. Predictions from the two log-linear models are shown in blue and yellow. The black line is the future median projection with 80% uncertainty coverage (grey shaded region). The vertical green lines show the distribution in future projected abundance at times 2030, 2040, 2050, and 2060. The black horizontal line at the top is the sum of the maximum observed count at each site.

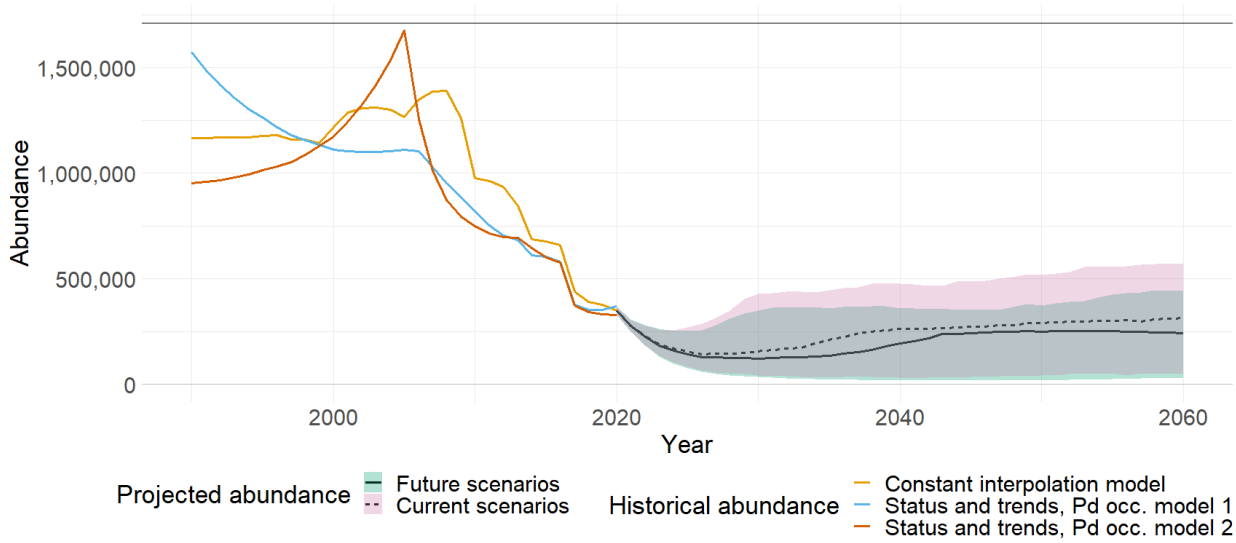

Figure E19. *Myotis lucifugus* species-level abundance projections for current and future conditions. Predictions from the two log-linear models are shown in blue and red lines, and piecewise constant interpolation of the observations is shown as an orange line. The median projection for current scenarios is the black dashed line with uncertainty indicated by the green shaded region, and the future scenario median is the solid black line with uncertainty in the pink shaded region (the grey shaded area is the overlap between the green and pink shaded regions).

Perimyotis subflavus

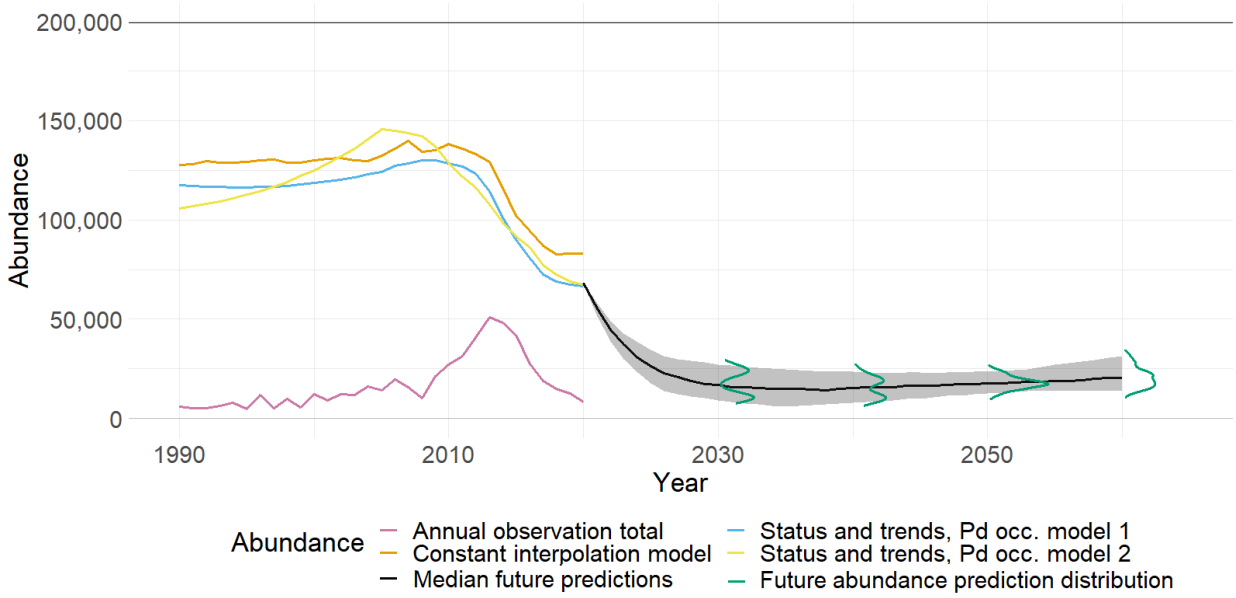

Figure E20. *Perimyotis subflavus* species-level abundance projections for current conditions. The pink line shows the annual total observed counts, and the orange line shows the piecewise constant interpolation of the observations. Predictions from the two log-linear models are shown in blue and yellow. The black line is the future median projection with 80% uncertainty coverage (grey shaded region). The vertical green lines show the distribution in future projected abundance at times 2030, 2040, 2050, and 2060. The black horizontal line at the top is the sum of the maximum observed count at each site.

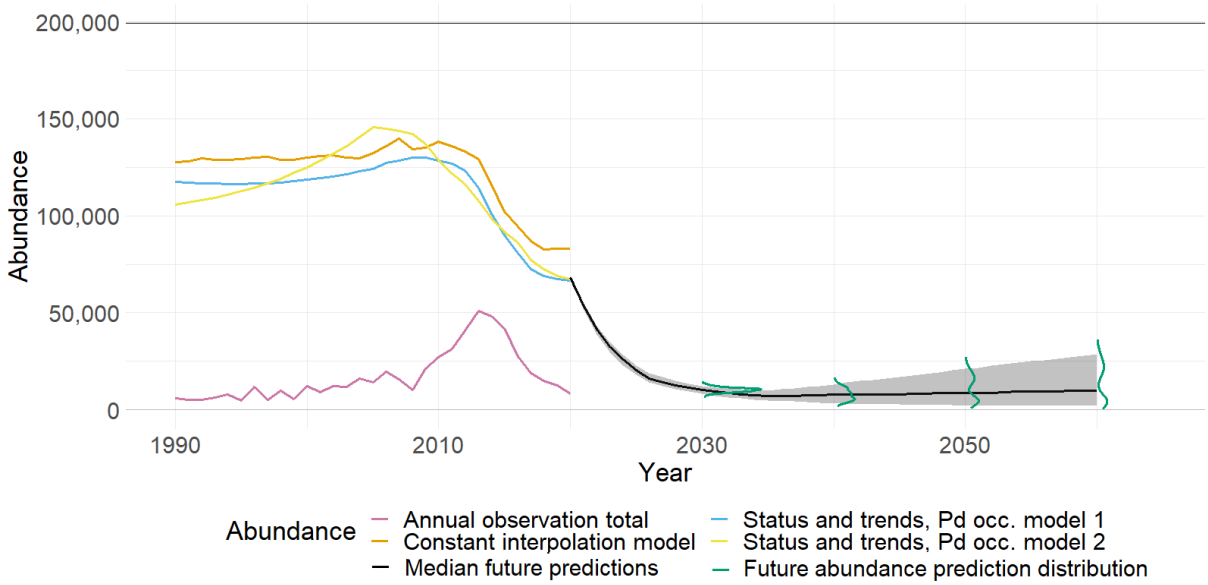

Figure E21. *Perimyotis subflavus* species-level abundance projections for future conditions. The pink line shows the annual total observed counts, and the orange line shows the piecewise constant interpolation of the observations. Predictions from the two log-linear models are shown in blue and yellow. The black line is the future median projection with 80% uncertainty coverage (grey shaded region). The vertical green lines show the distribution in future projected abundance at times 2030, 2040, 2050, and 2060. The black horizontal line at the top is the sum of the maximum observed count at each site.

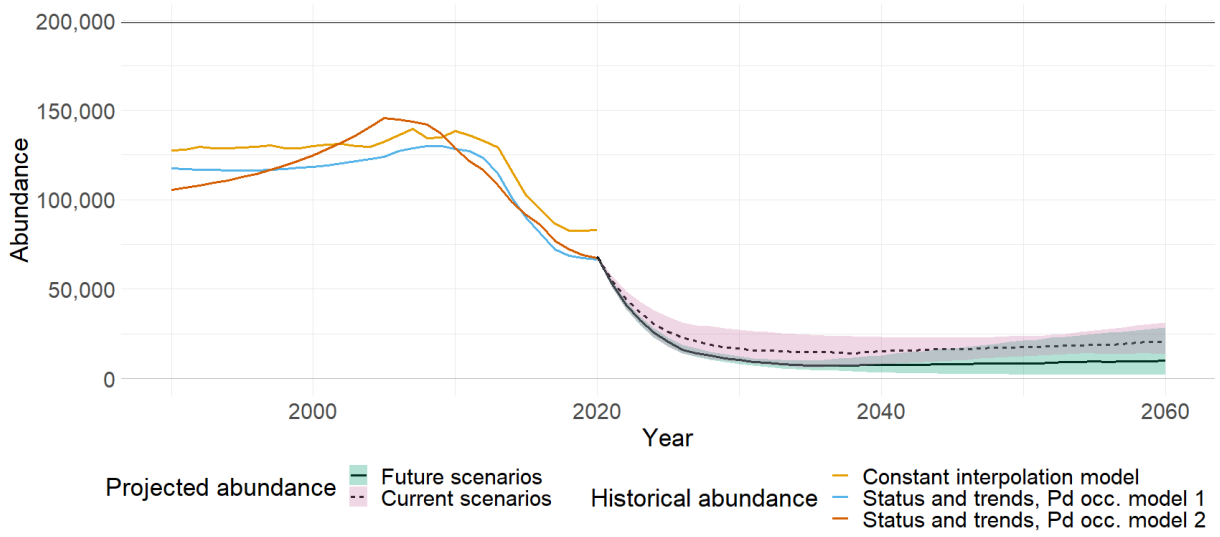

Figure E22. *Perimyotis subflavus* species-level abundance projections for current and future conditions. Predictions from the two log-linear models are shown in blue and red lines, and piecewise constant interpolation of the observations is shown as an orange line. The median projection for current scenarios is the black dashed line with uncertainty indicated by the green shaded region, and the future scenario median is the solid black line with uncertainty in the pink shaded region (the grey shaded area is the overlap between the green and pink shaded regions).

Myotis septentrionalis

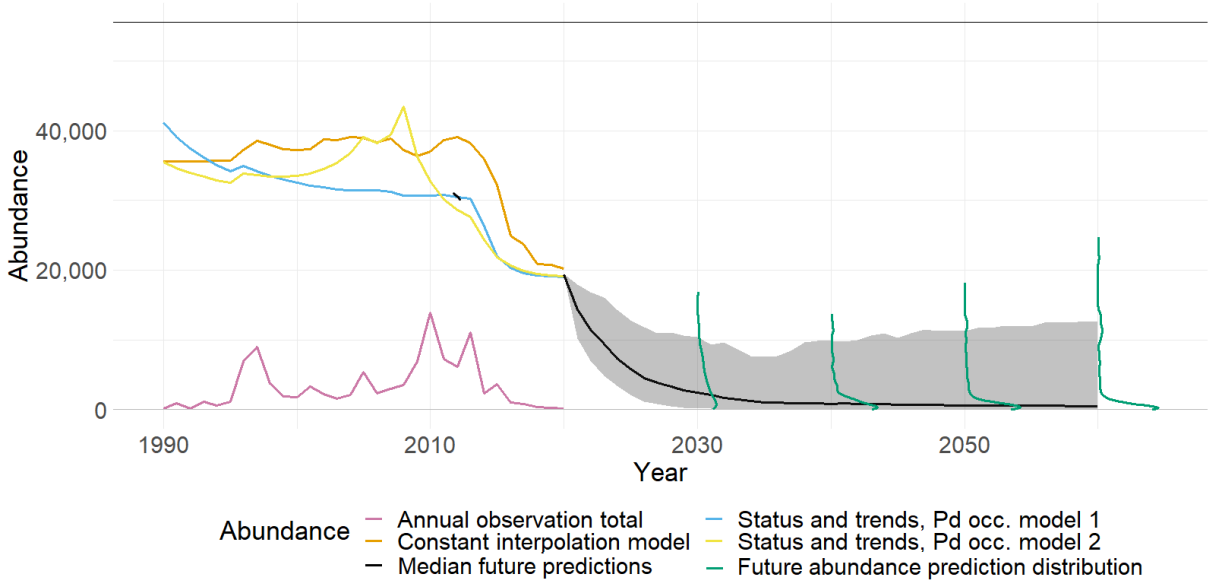

Figure E23. *Myotis septentrionalis* species-level abundance projections for current conditions. The pink line shows the annual total observed counts, and the orange line shows the piecewise constant interpolation of the observations. Predictions from the two log-linear models are shown in blue and yellow. The black line is the future median projection with 80% uncertainty coverage (grey shaded region). The vertical green lines show the distribution in future projected abundance at times 2030, 2040, 2050, and 2060. The black horizontal line at the top is the sum of the maximum observed count at each site.

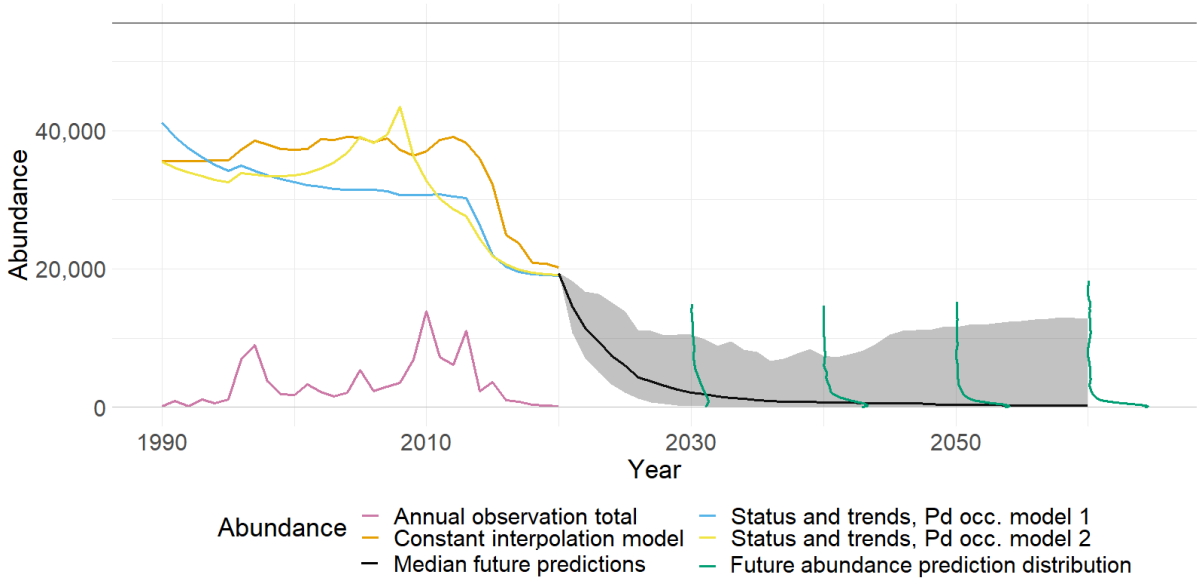

Figure E24. *Myotis septentrionalis* species-level abundance projections for future conditions. The pink line shows the annual total observed counts, and the orange line shows the piecewise constant interpolation of the observations. Predictions from the two log-linear models are shown in blue and yellow. The black line is the future median projection with 80% uncertainty coverage (grey shaded region). The vertical green lines show the distribution in future projected abundance at times 2030, 2040, 2050, and 2060. The black horizontal line at the top is the sum of the maximum observed count at each site.

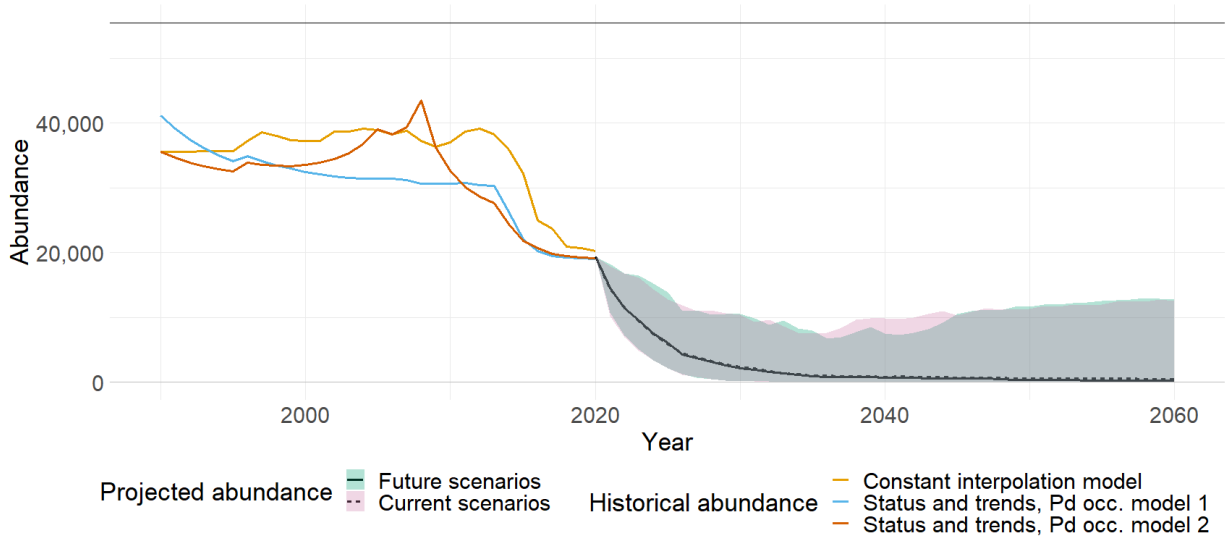

Figure E25. *Myotis septentrionalis* species-level abundance projections for current and future conditions. Predictions from the two log-linear models are shown in blue and red lines, and piecewise constant interpolation of the observations is shown as an orange line. The median projection for current scenarios is the black dashed line with uncertainty indicated by the green shaded region, and the future scenario median is the solid black line with uncertainty in the pink shaded region(the grey shaded area is the overlap between the green and pink shaded regions).

Continued application of WNS impacts caused the sharp declines in all future abundance projections in Figures E17-E25 as WNS reached all known winter colonies based on the *Pd* occurrence models. All species show similar trajectories, but the decline in the smaller known total abundance of *Myotis septentrionalis* suggests the populations of the species face extirpation in the future should our modeling assumptions prove true. The proportion of the total population we are monitoring is an unknown but crucial question NABat will continue to investigate, as the sample of known bat populations for these three species in our data set are almost certainly not a census.

References Cited

Arnett, E. B., and E. F. Baerwald. 2013. Impacts of Wind Energy Development on Bats: Implications for Conservation. Springer New York, New York, NY, pp. 435–456. https://doi.org/10.1007/978-1-4614-7397-821.

Arnett, E. B., M. M. Huso, M. R. Schirmacher, and J. P. Hayes. 2010. Altering turbine speed reduces bat mortality at wind-energy facilities. Frontiers in Ecology and the Environment 9:209–214.

Bates, D., M. Maechler, B. Bolker, and S. Walker (2015). Fitting Linear Mixed-Effects Models Using lme4. Journal of Statistical Software, 67(1), 1-48. doi:10.18637/jss.v067.i01.

Caceres, M. C. and R. M. Barclay. 2000. *Myotis septentrionalis*. Mammalian Species 634: 1-4

Chang, W., J. Cheng, J. Allaire, C. Sievert, B Schloerke, Y. Xie, J. Allen, J. McPherson, A. Dipert and B. Borges. 2021. shiny: Web Application Framework for R. R package version 1.6.0.

Cheng, T. L., J. D. Reichard, J. T. H. Coleman, T. J. Weller, W. E. Thogmartin, B. E. Reichert, A. B. Bennett, H. G. Broders, J. Campbell, K. Etchi-son, D. J. Feller, R. Geboy, T. Hemberger, C. Herzog, A. C. Hicks, S. Houghton, J. Humber, J. A. Kath, R. A. King, S. C. Loeb, A. Mass´e, K. M. Morris, H. Niederriter, G. Nordquist, R. W. Perry, R. J. Reynolds, D. B. Sasse, M. R. Scafini, R. C. Stark, C. W. Stihler, S. C. Thomas, G. G. Turner, S. Webb, B. J. Westrich, and W. F. Frick. 2021. The scope and severity of white-nose syndrome on hibernating bats in North America. Conservation Biology. https://conbio.onlinelibrary.wiley.com/doi/abs/10.1111/cobi.13739

Choi, D. Y., T. W. Wittig, and B. M. Kluever. 2020. An evaluation of bird and bat mortality at wind turbines in the Northeastern United States. PLOSONE 15(8):1–22. https://doi.org/10.1371/journal.pone.0238034.

Cressie, N. A. C. 1993. Statistics for spatial data. John Wiley & Sons. https://doi.org/10.1002/9781119115151.

Cryan, P. M., P. M. Gorresen, C. D. Hein, M. R. Schirmacher, R. H. Diehl, M. M. Huso, D. T. S. Hayman, P. D. Fricker, F. J. Bonaccorso, D. H. Johnson, K. Heist, and D. C. Dalton. 2014. Behavior of bats at wind turbines. Proceedings of the National Academy of Sciences 111(42):15126–15131. https://www.pnas.org/content/111/42/151261.

Diffendorfer, J. E., J. A. Beston, M. D. Merrill, J. C. Stanton, M. D. Corum, S. R. Loss, W. E. Thogmartin, D. H. Johnson, R. A. Erickson, and K. W. Heist. 2017. A method to assess the population-level consequences of wind energy facilities on bird and bat species. Wind Energy and Wildlife Interactions pp. 65–76.

Diffendorfer, J. E., J. C. Stanton, J. A. Beston, W. E. Thogmartin, S. R. Loss, T. E. Katzner, D. H. Johnson, R. A. Erickson, M. D. Merrill, and M. D. Corum. 2021. Demographic and potential biological removal models identify raptor species sensitive to current and future

wind energy. Ecosphere 12(6):e03531. https://esajournals.onlinelibrary.wiley.com/doi/abs/10.1002/ecs2.3531.

Erickson, R. A., W. E. Thogmartin, J. E. Diffendorfer, R. E. Russell, and J. A. Szymanski. 2016. Effects of wind energy generation and white-nose syndrome on the viability of the Indiana bat. PeerJ pp. 1–19.

Erickson, R. A., W. E. Thogmartin, and J. A. Szymanski. 2014. BatTool: an R package with GUI for assessing the effect of white-nose syndrome and other take events on *Myotis* spp. of bats. Source Code for Biology and Medicine 9(9):1–10.

Frick, W. F., J. F. Pollack, A. C. Hicks, K. E. Langwig, S. D. Reynolds, G. G. Turner, C. M. Butchkoski, and T. H. Kunz. 2010. An emerging disease causes regional population collapse of a common North American bat species. Science 329:678–682.

Frick, W. F., S. J. Puechmaille, J. R. Hoyt, B. A. Nickel, K. E. Langwig, J. T. Foster, K. E. Barlow, T. Bartonicka, D. Feller, A. J. Haarsma, C. Herzog, I. Horacek, J. van der Kooij, B. Mulkens, B. Petrov, R. Reynolds, L. Rodrigues, C. W. Stihler, G. G. Turner, and A. M. Kilpatrick. 2015. Disease alters macroecological patterns of North American bats. Global Ecology and Biogeography 24(7):741–749. https://onlinelibrary.wiley.com/doi/abs/10.1111/geb.12290.

Fujita, M. and T. Kunz. 1984. *Pipistrellus subflavus*. Mammalian Species 228: 1-6.

Hefley, T. J., R. E. Russell, A. E. Ballmann, and H. Zhang. 2020. When and where: estimating the date and location of introduction for exotic pests and pathogens. arXiv stat.AP.

Kramer, A. M., A. Mercier, S. Maher, Y. Kumi-Ansu, S. Bowden, and J. M. Drake. 2021. Spatial spread of white-nose syndrome in North America, 2006-2018. bioRxiv. https://www.biorxiv.org/content/early/2021/01/30/2021.01.28.4285262.

Langwig, K. E., W. F. Frick, J. T. Bried, A. C. Hicks, T. H. Kunz, and A. Marm Kilpatrick. 2012. Sociality, density-dependence and microclimates determine the persistence of populations suffering from a novel fungal disease, white-nose syndrome. Ecology Letters 15(9):1050–1057. https://onlinelibrary.wiley.com/doi/abs/10.1111/j.1461-0248.2012.01829.x.

Maher, S., A. Kramer, J. Pulliam, M. Zokan, S. Bowden, H. Barton, K. Magori, and J. Drake. 2012. Spread of white-nose syndrome on a network regulated by geography and climate. Nature Communications 1306.

Maurer, J., M. Huso, D. Dalthorp, L. Madsen, and C. Fuentes. 2020. Comparing methods to estimate the proportion of turbine-induced bird and bat mortality in the search area under a road and pad search protocol. Environmental and Ecological Statistics 27:769–801.

McGuire, L. P., J. M. Turner, L. Warnecke, G. McGregor, T. K. Bollinger, V. Misra, J. T. Foster, W. F. Frick, A. M. Kilpatrick, and C. K. R. Willis. 2016. White-nose syndrome disease severity and a comparison of diagnostic methods. EcoHealth 13:60–71.

North American Bat Monitoring Program (NABat) Database v6.0.12 (Provisional Release): U.S. Geological Survey. Accessed 2021-02-10. NABat Request Number 12. https://doi.org/10.5066/P9UXA6CF.

R Core Team. 2021. R: A language and environment for statistical computing. R Foundation for Statistical Computing,Vienna, Austria. https://www.R-project.org/.

Talbert, C., and B. E. Reichert. 2018. North American Bat Monitoring Program (NABat) Master Sample and Grid-Based Sampling Frame [Data set].

Thapa, V., G. G. Turner, and M. J. Roossinck. 2021. Phylogeographic analysis of Pseudogymnoascus destructans partitivirus-pa explains the spread dynamics of white-nose syndrome in North America. PLOS Pathogens 17(3):1–21. https://doi.org/10.1371/journal.ppat.1009236.

Thogmartin, W. E., R. A. King, P. C. McKann, J. A. Szymanski, and L. Pruitt. 2012. Population-level impact of white-nose syndrome on the endangered Indiana bat. Journal of Mammalogy 93(4):1086–1098.

Thogmartin, W. E., C. A. Sanders-Reed, J. A. Szymanski, P. C. McKann, L. Pruitt, R. A. King, M. C. Runge, and R. E. Russell. 2013. White-nose syndrome is likely to extirpate the endangered Indiana bat over large parts of its range. Biological Conservation 160: 162–172.

Turner, G., D. Reeder, and J. Coleman. 2011. A five-year assessment of mortality and geographic spread of white-nose syndrome in North American bats, with a look at the future. Update of white-nose syndrome in bats. Bat Research News 52:13–27.3

Udell, B.J., B. Straw, J. Szymanski, M. Seymor, J. Wong, A. Wiens, B.E. Reichert, J.E. Diffendorfer, and L. Kramer. 2021. In Support of the U.S. Fish and Wildlife Service 3-Bat Species Status Assessment: Predicted Wind Take Allocated To Hibernacula Each Year Under Current and Future Scenarios: U.S. Geological Survey data release, https://doi.org/10.5066/P97XVX22.

USGS National Wildlife Health Center. 2021. Update for the Association of Fish and Wildlife Agencies from the USGS National Wildlife Health Center. Accessed on September 28, 2021. https://prd-wret.s3.us-west-2.amazonaws.com/assets/palladium/production/atoms/files/AFWA%20report%20Sept2021_final.pdf

White-nose Syndrome Response Team. 2020. White-nose syndrome spread map. Accessed: 2020-02-10. www.whitenosesyndrome.org

Wiens, A.M., Cheng, T.L., Reichard, J.D., and Thogmartin, W.E. 2021a. In Support of the U.S. Fish and Wildlife Service 3-Bat Species Status Assessment: Gaussian Process Model Predictions for the Spread of White-Nose Syndrome across North America, https://doi.org/10.5066/P9QUARC0.

Wiens, A., A. Schorg, J. Szymanski, and W. E. Thogmartin. 2021b. BatTool: projecting bat populations facing multiple stressors using a demographic model. In press.

Wiens, A., J. Szymanski, and W.E. Thogmartin. 2021c. In Support of the U.S. Fish and Wildlife Service 3-Bat Species Status Assessment: Future Projections of Known North American Bat Populations for 3 Species (2020-2060), Processed from NABat Database Winter Colony Counts from 1990-2020, https://doi.org/10.5066/P9NDMY47.

Wiens, A., J. Szymanski, and W.E. Thogmartin. 2021d. In Support of the U.S. Fish and Wildlife Service 3-Bat Species Status Assessment: Status and Trends of Known North American Bat Populations for 3 Species from 1990-2020, Processed from NABat Database Winter Colony Counts, https://doi.org/10.5066/P9AVS764.

Wimsatt, W.A. 1945. Notes on breeding behavior, pregnancy, and parturition in some Vespertilionid bats of the Eastern United States. Journal of Mammalogy 26:23-33.

Zuur A. F. 2009. Mixed effects models and extensions in ecology with R. New York: Springer. https://doi.org/10.1007/978-0-387-87458-6.

Appendix E-1. Spatially explicit method of predicting bat wind take at wind facilities and allocating it among winter hibernacula populations

By Brad J. Udell[1], Bethany R. Straw[1], Jennifer Szymanski[2], Megan Seymour[3], Jennifer Wong[4], Ashton M. Wiens[5], Brian E. Reichert[1], James E. Diffendorfer[6], Luisa Kramer[6], and Zachary Ancona[6]

Part 1: Spatially explicit forecasts of future wind energy development scenarios

Here we describe the workflow and methods associated with the spatial forecasts of installed wind capacity to enable estimation of potential future wind take (the expected number of bat fatalities) in a spatially relevant manner. Additional descriptions of the methods, along with the resulting data files for take predictions under different scenarios is available in Udell et al. (2021).

Original data

The National Renewable Energy Laboratory (NREL) provided three original files:

1. A shape file for the regions (https://www.nrel.gov/analysis/assets/pdfs/reeds-model-regions-map.pdf) used in the Regional Energy Deployment System (ReEDS) model (Cohen et al. 2019).
2. The forecasted total megawatts (MW) of installed capacity in 2030, 2040, and 2050 for each of the ReEDS regions for the high and low-cost Standard Scenarios ReEDS simulations (Cole et al. 2020).

[1] U.S. Geological Survey, Fort Collins Science Center, Fort Collins, Colorado, 80526, USA
[2] Division of Endangered Species, U.S. Fish and Wildlife Service, USGS - Upper Mississippi River Science Center, La Crosse, WI 54603, USA
[3] U.S. Fish and Wildlife Service, Ohio Field Office, Columbus, Ohio, 43230, USA
[4] U.S. Fish and Wildlife Service, Michigan Field Office, East Lansing, Michigan, 48823, USA
[5] U.S. Geological Survey, Upper Midwest Environmental Sciences Center, La Crosse, WI 54603, USA
[6] U.S. Geological Survey, Geosciences and Environmental Change Science Center, Denver, Colorado, 80225, USA

3. The point locations used in NRELs Renewable Energy Potential (reV) Model (Maclaurin et al. 2019). These points represent the center of an 11.5 x 11.5 km nationwide grid used in the simulation. At each point, the reV model estimates:
    - The amount of wind energy capacity (in MW) available to build if full wind buildout occurred in the area.
    - Capacity: maximum electric output that can be produced operating at continuous full power.
    - Capacity factor: ratio between what a generation unit is capable of generating at maximum output versus the unit's actual generation output over a period of time.
    - Average wind speed.
    - Distance to transmission.

Methods

ArcMap spatial join

The following steps were taken to join the ReEDS Regions shapefile and the supply curve points shapefile.

1. Perform a spatial join between the supply curve points and the ReEDS Regions shapefile. The "DEMREG" attribute was carried over to provide the ReEDS region by supply curve point.
2. Remove any supply curve points with <20 MW of capacity as these are not modeled under NREL Standard Scenarios.
3. Select a year and scenario of interest from the Standard Scenarios results.

4. Fill capacity in each 11.5 x11.5 km cell to satisfy the megawatt (MW) buildout for the scenario and year without exceeding supply curve capacity (i.e., what is available to build) for that area.

The supply curve originally had 57,123 points and was filtered to 49,736 through the removal of the points less than 20 megawatts. To complete the spatial join, the ReEDS regions file was sectioned into regional power authorities due to the limits ArcMap puts on shapefiles when using the spatial join tool. The eight regional power authorities in the ReEDS regions file include: MISO, N_ENG, NY_ISO, NoAssigned, PJM, SERC, SPP and TVA and were only used for this initial spatial join to carryover the DEMREG attribute.

Excel cleaning and formulas

The eight regional files were exported to ".csv's" and converted to Excel files where we modelled the forecasted buildout for each NREL region (DEMREG) across the reference points. The goal was to 'build up' each DEMREG region using the megawatts assigned to the supply curve capacity points. Capacity factor and distance to transmission line were used to prioritize buildout. Capacity factor is defined as the ratio between what a generation unit is capable of generating at maximum output versus the unit's actual generation output over a period of time. So, the higher the capacity factor, the more 'appealing' it is to construct a new wind facility. Because the cost of deployment increases with distance to transmission, the lower the distance to transmission the greater the 'appeal' for new wind development. While distance to transmission is a one-time cost of installation, capacity factor is an indication of Annual Energy Production and therefore potential revenue that can be generated year over year. Therefore, we decided to weight distance to transmission lower than capacity factor in our models at weights of 10% and 90%, respectively.

We first sorted the supply curve capacity spreadsheet by DEMREG region, then Capacity_Distance_Ratio (highest to lowest) so that the capacity of megawatts for each DEMREG region would be built up (i.e., begin to accumulate) first from the highest Capacity_Distance_Ratio. A VLOOKUP formula was used to pull the Capacity_MW values from the standard scenario spreadsheets and assign them to the associated DEMREG region present in the supply curve capacity spreadsheets. This is the megawatt value each DEMREG region would build up until capacity was reached. A final field was included to conduct another spatial join back to the supply curve point shapefile for only those points that were selected for buildout in each region to fill the total capacity. This formula simply looked at the new Forecast_MW field and selected the Field1 unique ID if the value was greater than 0, thus only selecting the points that were used to fill the Capacity_MW value from the Standard Scenario spreadsheets. This process was repeated six times for each of the low and high (2030, 2040 and 2050) scenarios.

The final spatial join was conducted between the six spreadsheets and the original filtered supply curve capacity by linking the Field1 unique values and only keeping those that match. The final shapefiles range from an original point count of 49,736 to around 1,700~ points (depending on the scenario) when building up these DEMREG regions.

Part 2: Predicted take at each current wind energy location given capacity (megawatts) and curtailment protocols

Megawatts (MW) in each curtailment category at each wind energy location were converted to predicted take given regional rates for: the fatality rate (take/MW) given curtailment, species composition given region, and *Pd* status. The following assumptions and rates were developed based on data provided by United States Fish and Wildlife Service

(USFWS), published studies in the academic literature, and feedback from the United States Fish and Wildlife Service 3-Bat SSA Wind Core Team.

Assumptions

1. Let total rated capacity in megawatts (MW) in each grid cell serve as a proxy for mortality risk as related to the size and density of wind turbines in each cell) which correlates with the expected area of potential collision space.
2. The species proportional composition of take varies by region, and is also different pre-*Pd* (before the arrival of the causative vector of White Nose Syndrome) and post-*Pd*.
3. Species composition was assigned to each wind energy location based on the USFWS region and the predicted year of arrival, 'YOA,' of *Pd* (*Pseudogymnoascus destructans*), the vector of White Nose Syndrome. Two separate YOA scenarios are implemented, based on different models.
4. We assume curtailment reduces fatality rates by 50%. Previous studies show that increases wind turbine cut-in speed by 1.5 meters/second reduces take by approximately 50% (Arnett et al. 2013). Because incidence of fatality varies between seasons (i.e., fatality is highest in late summer and early fall; Arnett et al. 2008; AWWI 2020), the proportion of annual mortality that is reduced by curtailment is dependent upon the season(s) in which it is applied. We assume fall only curtailment reduces annual take by 34%. This estimate was provided by the USFWS 3-Bat SSA Core Team who calculated it using post-construction mortality monitoring data and reports provided to the USFWS.

5. MW and predicted bat take were tracked for each curtailment category and NREL grid cell.
6. Species take in each curtailment category was calculated as: MW * species prop. * take/MW * (1-curtailment reduction).
7. Total species take in each grid cell equals the sum of take across all curtailment categories.
8. Wind energy locations greater than the maximum migration distance of a species from every known hibernaculum are dropped from that species' analysis (i.e., they do not contribute to bat take at known hibernacula).
9. Because spatially explicit future scenarios for Canada do not exist, providence centroids were used as proxies for Canadian wind energy locations, total MW for each providence was included, and all MW were assumed to be non-curtailment.

Steps

1. Determine current MW in each curtailment category and the total for each NREL cell and assign curtailment reduction in fatality (Table E1.1)
    A. Fall and summer
    B. Fall only
    C. No curtailment
2. Determine fatality rates for each curtailment category for each location
    A. USFWS Region
        i. Intersect USFWS regions
        ii. Assign take/MW given region (Table E1.3)

iii. Left join table with pre and post species composition rates by region (Table E1.2)

B. YOA scenario (pre or post)

i. Intersect with YOA layer

ii. If year is before YOA, assign pre *Pd* species composition rate, else post *Pd* species composition rate (Table E1.2)

C. Calculate take rate (per MW) and take for each curtailment category

i. Take_rate = Species comp * take/MW * Curtailment_reduction

a. Mean, lower confidence interval (LCI) (25%), and upper confidence interval (UCI) (75%)

ii. Take = take_rate * MW

a. Mean, LCI (25%), and UCI (75%)

D. Calculate total take across all curtailment categories

i. Mean, LCI (25%), and UCI (75%)

Limitations

The last observed count for each hibernaculum was used in place of abundance since abundance estimates are not available.

Part 3: Predicted future take for each wind energy location under each future scenario

Under each spatially explicit future wind energy deployment scenario, convert MW in each curtailment category at each wind energy location to predict take given regional rates for: take/MW given curtailment, species composition given region and *Pd* status.

Assumptions

1. Take/MW rates, after accounting for region and pre vs post white-nose syndrome species compositions, is constant over time.
2. Future wind scenarios were obtained from NREL for spatially explicit predictions each decade (2030, 2040, and 2050) under two different scenarios, assuming low cost of development, or assuming high cost of development.
3. This methodology assumes these scenarios are representative of the potential future bounds of upper and lower bounds of potential wind energy development.
4. All future wind energy that is added assumes no-curtailment.
5. If wind energy decreases in an NREL grid cell in the future, MW are subtracted from the historic curtailment categories in the same proportion they existed prior (i.e., assuming random loss of wind energy).

Steps

1. Determine current MW in each curtailment category and the total for each NREL cell and assign curtailment reduction in fatality (Table E1.1).
    A. Fall and summer
    B. Fall only
    C. No curtailment
2. For 2030 USA scenarios
    A. Join 2030 wind to current wind to keep track of historic MW in each category
        i. Left join current data to future data based on NREL cell ID

B. Based on the difference in total MW across all curtailment categories, assign the change in take to each MW category
    i. If change in total MW is positive (new wind is added) it is added to no curtailment MW
    ii. If change in total MW is not applicable (NA) (new wind added) new wind is added to no curtailment MW
    iii. If change is negative, it is subtracted from each category in the same proportion as that which previously occurred (assuming random loss).
C. Determine fatality rates for each curtailment category for each location
    i. USFWS Region
        a. Intersect USFWS regions
        b. Assign take per MW given region (Table E1.3)
        c. Left join table with pre and post species composition rates by region (Table E1.2)
    ii. YOA scenario (pre or post)
        a. Intersect with YOA layer
        b. If year is before YOA, pre composition rate, else post composition rate (Table E1.2)
    iii. Calculate take rate (per MW) and take for each curtailment category
        a. Take_rate = Species comp * take/MW * Curtaillment_reduction

- Mean, LCI (25%), and UCI (75%)

b. Take = take_rate * MW

- Mean, LCI (25%), and UCI (75%)

iv. Calculate total take across all curtailment categories

- Mean, LCI (25%), and UCI (75%)

3. For 2040 and 2050 USA scenarios

A. Same procedure as 2030, only using the decade prior (within a wind energy cost scenario) as the historical MWs to reconcile with new wind development.

i. 2040 with 2030 as historic

ii. 2050 with 2040 as historic

Limitations

1. Assumes take/MW is constant over time. In reality, this is likely to change with changing technology, and due to changing abundances and spatial distributions of bats and wind facilities.

Part 4: Allocating take from wind energy locations to winter hibernacula populations

For each wind energy deployment and year scenario, allocate take from all United States and Canada wind energy locations among all hibernacula within maximum dispersal distance.

Assumptions

1. The total take from each wind facility is allocated among all hibernacula that lie within the maximum migration distance of the wind energy location.
2. Take is allocated according to a weighting scheme based on proximity and abundance of each hibernaculum (see equations below).

3. Proximity weights are based on the distance between hibernacula and wind energy, given the average migration distance of each species and the exponential dispersal kernel as a distance decay function (Equation 1).
4. Assumed average migration distances, and maximum migration distance for each species are recorded in Table E1.4.
5. Proximity weights are multiplied by hibernacula abundance to yield the expected relative number of individuals to encounter the wind facility, then rescaled by the sum so that all weights add up to one (Equation 1).
6. If a wind energy location has no hibernacula within the maximum migration distance, it is dropped from the analysis.
7. Hibernacula locations are assumed to be constant.
8. Because abundance estimates are not available for every hibernaculum, the last observed colony count of each hibernaculum was used as a proxy for abundance.
9. Hibernacula abundance is assumed to remain constant.
10. The total take for each hibernaculum is the sum of contributions from each wind facility (Equation 3 and Equation 4).

Weighting scheme

For each hibernaculum i and wind energy location j, the unscaled proximity weight p_{ij} is calculated based on the distance between hibernacula, the average migration distance (where $\alpha = \frac{1}{\text{mean dispersal distance}}$), and the exponential migration kernel (distance decay function) (Equation 1). This also yields the relative per animal probability of encountering a wind facility given the distance from the hibernacula.

$$\text{Eq.1: } p_{ij} = \exp\left(-\alpha * distance_{ij}\right)$$

These proximity weights (p_{ij}), are multiplied by the abundance (A_i) of each hibernaculum i, yielding the relative number of individuals at risk of encountering the wind facility given distance. These values are used to weight and allocate take from a wind energy location to each hibernaculum based on relative risk $(A_i * p_{ij})$. These values are divided by the sum across hibernacula for each wind energy location, so that the scaled weights sum to one for each wind energy location j (Equation 2).

$$\text{Eq.2: } w_{ij} = \frac{A_i * p_{ij}}{\sum_i (A_{ij} * p_{ij})}$$

Therefore, weights (w_{ij}) are the proportion of take at a wind facility j that gets allocated to each hibernaculum i. Take from each wind energy location $\left(Take_{Facility_j}\right)$ was allocated among all hibernacula within the maximum migration distance by multiplying expected take at the wind energy location by the scaled proximity weight (w_{ij}) of each corresponding hibernaculum.

$$\text{Eq.3: } Take_{ij} = Take_{Facility_j} * w_{ij}$$

Where $Take_{ij}$ is the expected take at each hibernaculum i from each wind energy location j. Using this formulation, the exact amount of take from each wind facility gets redistributed among all hibernacula withing the maximum migration distance.

Finally, the total take for each hibernaculum i is the sum across take from all corresponding wind facilities j.

$$\text{Eq.4: } Take_i = \sum_j Take_{ij}$$

See Udell et al. (2021) for detailed predictions.

Limitations

1. Does not account for the full seasonal cycle (take occurs in the spring through fall). Uses the winter locations and distance decay scheme because these are the best-known locations of each population.
2. Assumes symmetric dispersal in every direction, does not account for asymmetric dispersal directions for migration
3. If there is only one far away hibernaculum within the maximum migration distance of a wind facility, it will receive all of the take, even if is very far away or has a low abundance of bats.

Part 5: Linear interpolation of take for years between 10-year data points

1. For each species, hibernaculum, wind scenario, and YOA scenario, interpolate take for years between data points at 2020, 2030, 2040, and 2050.
    A. Within each scenario, join all 3 decadal data points to each hibernaculum.
    B. Calculate the slope (rise/run) between decadal data points for each hibernaculum.
    C. Use linear interpolation to make a prediction for every year between decades.
    D. One prediction each for the mean, LCI, and UCI estimates of take.

Tables and Figures

Table E1.1. Reduction in bat fatality rate, compared to no curtailment, given curtailment status.

Curtailment	% reduction	Proportion fatality	Take reduction
Summer only	0.5	0.252	0.126
Fall only	0.5	0.68	0.34
Summer + Fall	0.5	1	0.5

Table E1.2. Species proportion (SpComp) of take by the U.S. Fish and Wildlife Service region and Canadian Providence for three species of bats, before and after the arrival of *Pseudogymnoascus destructans* (*Pd*), the fungus that causes White-Nose Syndrome. MYLU, *Myotis lucifugus*; MYSE, *Myotis septentrionalis*; PESU, *Perimyotis subflavus*

		MYLU		MYSE		PESU	
Region Name	**Region**	**Pre-*Pd* Sp. Comp**	**Post-*Pd* SpComp**	**Pre-*Pd* Sp. Comp**	**Post-*Pd* Sp Comp**	**Pre-*Pd* Sp. Comp**	**Post-*Pd* Sp Comp**
Pacific Region	1	2.50%	2.50%				
Southwest Region	2	0.70%	0.70%	0.19%	0.19%	0.40%	0.40%
Midwest Region	3	9.38%	0.19%	0.19%	0.19%	0.44%	0.29%
Southeast Region	4	7.74%	4.98%	0.19%	0.19%	17.00%	5.41%
Northeast Region	5	7.74%	4.98%	0.19%	0.19%		
Northeast Region (South)	5S					17.00%	5.41%
Northeast Region (North)	5N					0.47%	0.09%
Mountain Prairie Region	6	1.30%	1.30%	0.19%	0.19%	0.44%	0.29%
Pacific Southwest Region	8	2.50%	2.50%				
British Columbia	9	0.46%	0.46%	0.00%	0.00%	0.00%	0.00%
Alberta	10	0.46%	0.46%	0.00%	0.00%	0.00%	0.00%
Saskatchewan	11	0.46%	0.46%	0.00%	0.00%	0.00%	0.00%
Manitoba	12	0.09%	0.09%	0.002%	0.002%	0.0013%	0.0013%
Ontario	13	0.09%	0.09%	0.002%	0.002%	0.0013%	0.0013%
Quebec	14	0.09%	0.09%	0.002%	0.002%	0.0013%	0.0013%
Atlantic Canada	15	0.67%	0.67%	0	0	0.00%	0.00%

Table E1.3. Bat fatality rates per megawatt (take/MW) for each U.S. Fish and Wildlife Service region and Canadian providence.

Region Name	Region	Mean	25th%	75th%
Pacific Region	1	1.11	0.39	1.88
Southwest Region	2	6.01	1.98	6.12
Midwest Region	3	14.59	4.7	17.79
Southeast Region	4	11.61	3.5	14.45
Northeast Region	5	11.61	3.5	14.45
Mountain Prairie Region	6	3.66	1.49	3.78
Pacific Southwest Region	8	1.99	0.82	3.22
British Columbia	9	5.03	4.07	5.98
Alberta	10	5.03	4.07	5.98
Saskatchewan	11	5.03	4.07	5.98
Manitoba	12	7.199	7.109	7.289
Ontario	13	7.199	7.109	7.289
Quebec	14	7.199	7.109	7.289
Atlantic Canada	15	0.1377	0.107	0.168

Table E1.4. Mean and maximum dispersal distances (in kilometers) for each species, as determined by the U.S. Fish and Wildlife Service. MYLU, *Myotis lucifugus*; MYSE, *Myotis septentrionalis*; PESU, *Perimyotis subflavus*

Species	Mean	Maximum
MYLU	100	500
MYSE	75	90
PESU	126	245

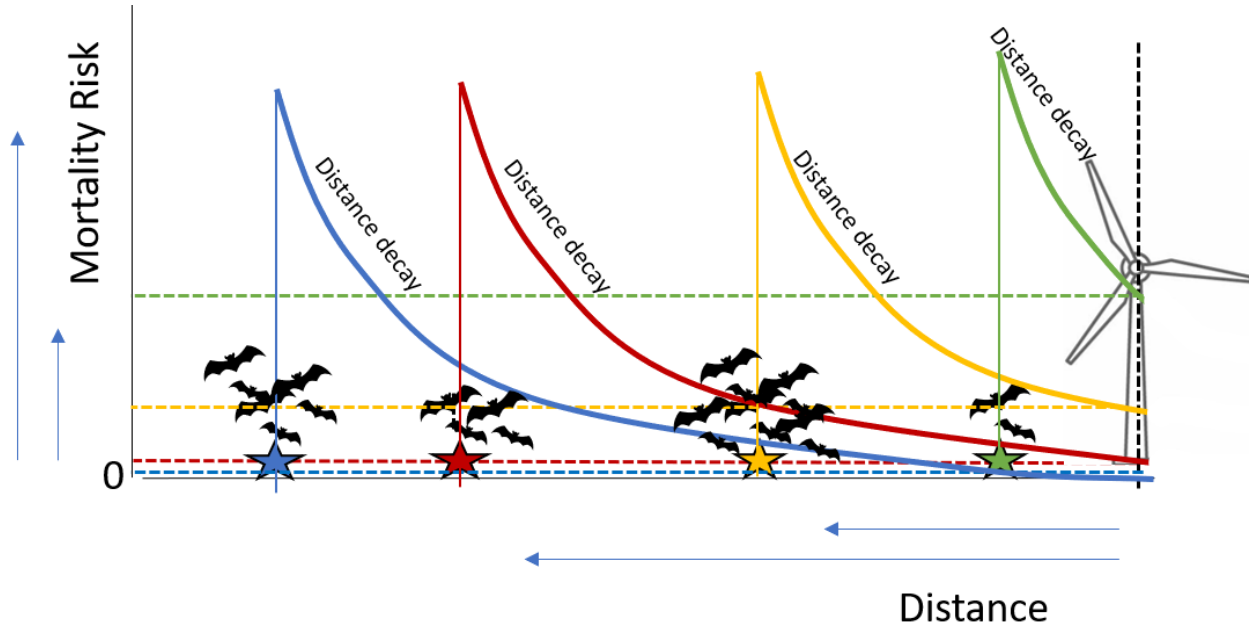

Figure E1.1. A depiction of risk to bats of wind facility associated mortalities according to exponential distance decay (exponential dispersal kernel) and abundance effects. Relative risk to hibernacula is higher at shorter distances to wind facilities, and also at higher bat abundances.

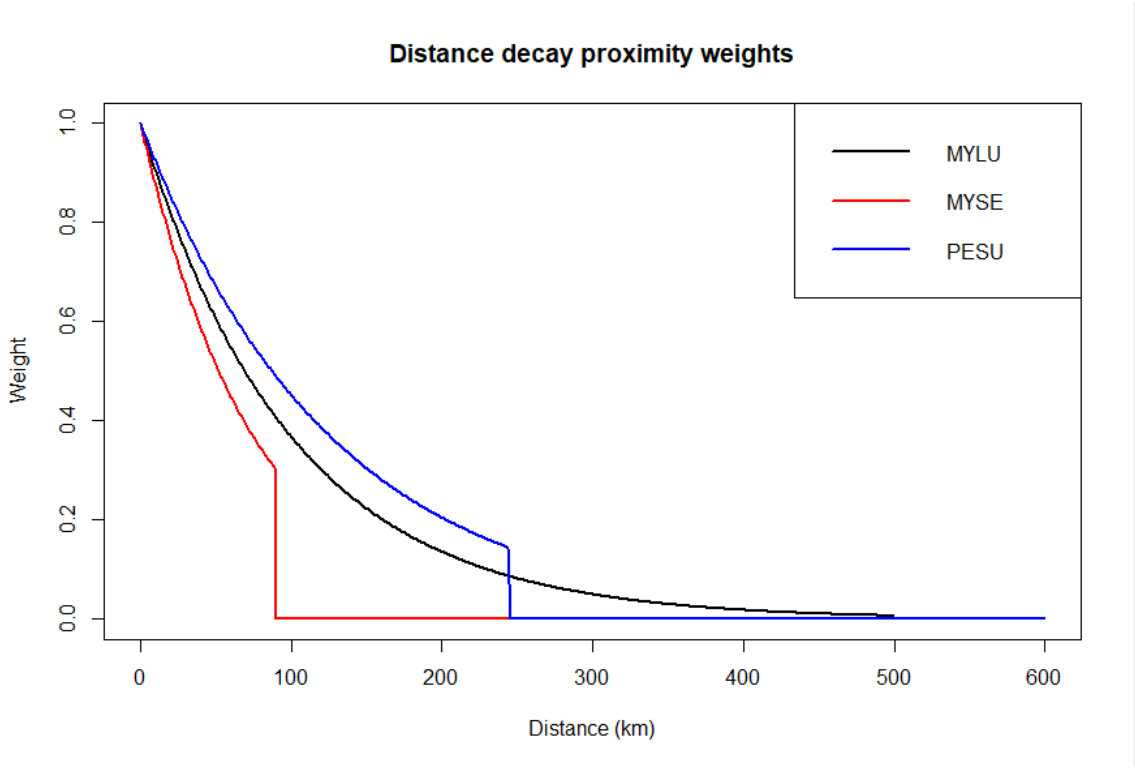

Figure E1.2. Unscaled proximity weights of each bat species given distance of hibernacula from wind facilities and the exponential distance decay function for each species, before including abundance and rescaling to sum to one. MYLU, *Myotis lucifugus*; MYSE, *Myotis septentrionalis*; PESU, *Perimyotis subflavus*

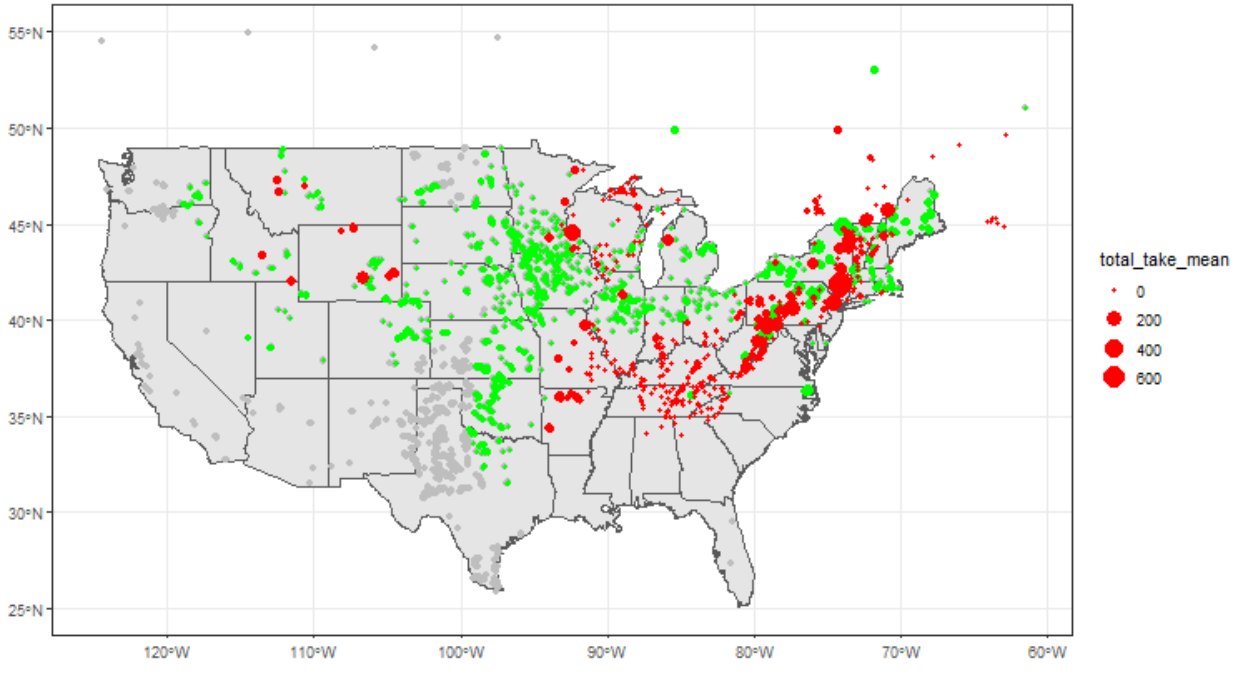

Figure E1.3. Map depicting an example of allocated take (bat fatalities) at wind energy locations (grey = unallocated, green = allocated) and hibernacula (red) for the bat *Myotis lucifugus* (MYLU) under current wind energy deployment. The size of circles is proportional to take.

References Cited

American Wind Wildlife Institute (AWWI). 2020. AWWI Technical Report: 2nd Edition: Summary of Bat Fatality Monitoring Data Contained in AWWIC. Washington, DC. Available at www.awwi.org. © 2020 American Wind Wildlife Institute.

Arnett, E. B., W. K. Brown, W. P. Erickson, J. K. Fielder, B. L. Hamilton, T. H. Henry, A. Jain, G.D. Johnson, J. Kerns, R. R. Koford, C. P. Nicholson, T. J. O'Connell, M. D. Piorkowski, and R. D. Tankersley, Jr. 2008. Patterns of Bat Fatalities at Wind Energy Facilities in North America. The Journal of Wildlife Management. 72: 61-78. Doi:10.2193/2007-221. https://wildlife.onlinelibrary.wiley.com/doi/Pdf/10.2193/2007-221.

Arnett, E. B., G. D. Johnson, W. P. Erickson, and C. D. Hein. 2013. A Synthesis of Operational Mitigation Studies to Reduce Bat Fatalities at Wind Energy Facilities in North America. A report submitted to the National Renewable Energy Laboratory. Bat Conservation International. Austin, Texas. https://www.energy.gov/sites/prod/files/2015/03/f20/Operational-Mitigation-SynthesisFINAL-REPORT-UPDATED.Pdf

Cohen, Stuart, Jon Becker, Dave Bielen, Maxwell Brown, Wesley Cole, Kelly Eurek, Will Frazier, et al. 2019. Regional Energy Deployment System (ReEDS) Model Documentation: Version 2018. Golden, CO: National Renewable Energy Laboratory. NREL/T *P*-6A20-72023. https://www.nrel.gov/docs/fy19osti/72023.Pdf.

Cole, Wesley, Sean Corcoran, Nathaniel Gates, Trieu Mai, and Paritosh Das. 2020. 2020 Standard Scenarios Report: A U.S. Electricity Sector Outlook. Golden, CO: National Renewable Energy Laboratory. NREL/T P-6A20-77442. https://www.nrel.gov/docs/fy21osti/77442.Pdf.

Maclaurin, Galen, Nick Grue, Anthony Lopez, Donna Heimiller, Michael Rossol, Grant Buster, and Travis Williams. 2019. The Renewable Energy Potential (reV) Model: A Geospatial Platform for Technical Potential and Supply Curve Modeling. Golden, CO: National Renewable Energy Laboratory. NREL/T P-6A20-73067. https://www.nrel.gov/docs/fy19osti/73067.Pdf.

Udell, B.J., B. Straw, J. Szymanski, M. Seymour, J. Wong, A. Wiens, B.E. Reichert, J.E. Diffendorfer, and L. Kramer. 2021. In Support of the U.S. Fish and Wildlife Service 3-Bat Species Status Assessment: Predicted Wind Take Allocated To Hibernacula Each Year Under Current and Future Scenarios: U.S. Geological Survey data release, https://doi.org/10.5066/P97XVX22

Glossary

grid cell 10km x 10km grid cell within the grid-based sampling frame of the NABat Master Sample for the continental United States (Talbert and Reichert 2018).

MW Current (or predicted future scenario) megawatt capacity at each 11 x 11 m grid cell with wind facilities.

National Renewable Energy Laboratory (NREL) wind energy scenarios Spatially explicit future projection scenarios for wind energy development, forecasting the megawatt capacity across the continental United States each decade (2030-2050) under low cost or high-cost assumptions.

Curtailment A wind facility protocol whereby turbine blades are feathered (or rotated) to slow the rotation of the rotor under a threshold wind speed. This protocol reduces the take rate of bats when in effect. Three different curtailment categories in the United States data include, Fall and Summer, Fall only, and No curtailment.

Species proportion composition: The proportion of take of each species summarized within in each USFWS region given pre or post arrival of Pseudogymnoascus destructans.

YOA Year of arrival of Pseudogymnoascus destructans, the fungi that causes white nose syndrome. Two different models of YOA are used: Yoa (Wein's model) and yoa_prev (Russel's model).

Fatality rate The per MW rate of bat take (bats/MW) across all species for each region.

Curtailment reduction The percent reduction in the bat fatality rate in each region under each curtailment category.

Take Expected bat mortality (number of animals) at each wind energy location (grid cell with wind energy) given the current (or forecasted) MW capacity, curtailment protocol, and the take/MW estimate.

Hibernacula Winter hibernation locations of bat populations.

Hibernacula abundance The abundance of the population in each hibernaculum for each species.

Dispersal kernel A type of distance decay function that models the relative probability of animals dispersing to some location given the distance from the starting location.

Exponential kernel A commonly used dispersal kernel and distance decay function with a single parameter, the average migration distance.

Maximum migration distance The maximum seasonal migration distance of each species.

Mean migration distance The mean seasonal migration distance of each species.